Approaches to Tailoring the Structure and Properties of Polyethylene

by

Colin Li Pi Shan

A thesis

presented to the University of Waterloo

in fulfilment of the

thesis requirement for the degree of

Doctor of Philosophy

in

Chemical Engineering

Waterloo, Ontario, Canada, 2002

I hereby declare that I am the sole author of this thesis. This is a true copy of the thesis, including any required final revisions, as accepted by my examiners.

I understand that my thesis may be made electronically available to the public.

Abstract

Alternative methods to control the molecular weight and short chain branching distribution of polyethylene were investigated. The ability to produce polyolefins with multimodal microstructural distributions using single catalyst/single reactor set-up is very attractive and could, in principle, be used to produce polyolefin resins with advanced molecular architecture. In this thesis, resins with controlled microstructures were produced, characterized and properties tested in order to develop a better understanding of polymerization structure-property relationships.

Copolymerizations of ethylene and 1-hexene were carried out with an in-situ supported metallocene catalyst. Copolymers were produced with different alkylaluminum activators and the effect on molecular weight and short chain branching distributions was examined. It was found that different activator types produce polymer with unimodal and narrow molecular weight distributions but with very different short chain branching distributions. Each activator exhibits unique comonomer incorporation characteristics to produce bimodal short chain branching distributions with the use of a single activator. By using individual and mixed activator systems, it is possible to control the short chain branching distributions of the resulting copolymers while maintaining narrow molecular weight distributions.

To further investigate the capabilities of this in-situ supported catalyst system, an experimental design was carried out to study the effect of polymerization conditions on the catalyst activity and microstructure of poly(ethylene-*co*-1-octene). The parameters investigated were: polymerization temperature, monomer pressure, chain transfer to hydrogen, comonomer/ethylene feed ratio and concentration of alkylaluminum. The effect of each parameter on the catalyst activity, comonomer incorporation and molecular weight distribution

was investigated. The results obtained were not typical of a conventional single-site catalyst. The copolymerization system was sensitive to all of the parameters and many interactions were evident. The most prominent effect was the catalyst response to temperature. As the temperature was decreased, the short chain branching distributions of the copolymers became broad and bimodal. Overall, it was found that a wide range of microstructures could be produced, ranging from copolymers with low and high 1-octene content with unimodal to broad short chain branching distributions, and from low to high molecular weight with narrow to broad molecular weight distributions.

To examine the effect of these broad short chain branching distributions on the polymer properties, a series of poly(ethylene-*co*-1-hexene) resins with very distinct, and in some cases bimodal crystalline distributions, were synthesized. The attractive feature of the resins in this study is that their molecular weight distributions are similar but each possesses a different short chain branching distribution, thus effectively minimizing the effect of molecular weight on the properties investigated. It was found that the tensile properties of a copolymer could be controlled by the ratio of the crystalline species present in the sample. In this study, a balance of stiffness and toughness was exhibited by a copolymer containing a large proportion of crystalline material and a small fraction of material of lower crystallinity.

A series of poly(ethylene-*co*-1-octene) resins with tailored molecular weight and short chain branching distributions were synthesized with a heterogeneous metallocene catalyst in a two-stage polymerization process. Blends of high molecular weight copolymer and low molecular weight homopolymer and reverse blends of low molecular weight copolymer and high molecular weight homopolymer were produced. The physical properties of these resins were tested for their dynamic mechanical (tensile) and rheological properties. Increasing the

copolymer content in the blend resulted in a decrease in stiffness. However, the energy dampening properties of these blends benefit from the presence of the copolymer. It was also confirmed that the melt flow properties of polymers mostly depend on their molecular weight distribution. Regardless of the comonomer content, the melt viscosities decreased with the addition of low molecular weight polymer.

Acknowledgements

I would like to thank my supervisors, Joao Soares and Alexander Penlidis for their guidance, support, and wisdom throughout my work; for trusting my decisions and allowing me the flexibility to achieve my project goals.

My sincere gratitude goes out to my friends and colleagues who I have shared in my work and my life, making my graduate experience at Waterloo a memorable one (as evidenced below).
My thanks goes to KJ Chu for his mentorship, Rosemary Anderson for taking care of the little things, my colleagues JD, Uncle Daryoosh, Luigi, Catherine, Will & Deborah, Leo and Neil. Special thanks also goes to Karen, a polymer pelletization expert (polymer processor) but we won't hold that against her. :)

Dedication

To my family, yes, I'm finally done school!!!

To Sensei Bill Bickford and my Aikido friends who have taught me to extend Ki.

Table of Contents

Abstract	iii
Acknowledgements	vi
Table of Contents	viii
List of Figures and Tables	xi
Nomenclature and Symbols	xv
Chapter 1 – Introduction and background	1
1.1 Polyolefins	2
1.2 Types of Polyethylene	2
1.3 Importance of MWD and Comonomer Distribution on Physical Properties	4
1.4 Catalyst Selection	8
1.5 Methods to Tailor the MWD and SCBD	10
Chapter 2 – Research objectives	13
2.1 Using Alkylaluminum Activators to Tailor the Short Chain Branching Distribution of Ethylene/1-Hexene Copolymers Using In-Situ Supported Metallocene Catalysts	14
2.2 Mechanical Properties of Ethylene/1-Hexene Copolymers with Tailored Short Chain Branching Distributions	14
2.3 Effect of Reaction Parameters on the Microstructure of Poly(Ethylene-*co*-1-Octene) Copolymers	15
2.4 Mechanical and Rheological Properties of HDPE/LLDPE Reactor Blends with Bimodal Microstructures	15
Chapter 3 – Experimental	16
3.1 Materials	17
3.2 Procedures	17
3.2.1 Equipment	17
3.3.2 In-Situ Supported Metallocene Polymerization Method	18
3.3.3 Vapour-Liquid Equilibrium Estimation of α-Olefin Comonomer Concentration	20
3.3 Characterization Methods	20
3.3.1 Gel Permeation Chromatography	20
3.3.2 Crystallization Analysis Fractionation	21
3.3.3 Differential Scanning Calorimetry	22
3.3.4 Fourier Transform Infrared Spectroscopy	23
3.4 Physical Property Testing	23
3.4.1 Tensile Testing	23
3.4.2 Dynamic Mechanical Thermal Analysis	25
3.4.3 Small Amplitude Oscillatory Shear Analysis	27
Chapter 4 - Using Alkylaluminum activators to tailor the short chain branching distribution of ethylene/1-hexene copolymers using in-situ supported metallocene catalysts	29
4.1 Introduction	30
4.2 Experimental	32

4.2.1 Polymerization 32
4.2.2 Characterization 33
4.3 Results and Discussion 34
4.4 Conclusions 54
4.5 References 55

Chapter 5 - Mechanical properties of ethylene/1-hexene copolymers with tailored short chain branching distributions 57
5.1 Introduction 58
5.2 Experimental 60
5.2.1 Sample Production 60
5.2.2 Microstructural Characterization 60
5.2.3 Mechanical Testing 61
5.2.3.1 Tensile Testing 61
5.2.3.2 Dynamic Mechanical Analysis 61
5.3 Results and Discussion 62
5.4 Conclusions 80
5.5 References 81

Chapter 6 – Ethylene/1-octene copolymerization studies with in-situ supported metallocene catalysts: effect of reaction parameters on catalyst activity and polymer microstructure 83
6.1 Introduction 84
6.2 Experimental 90
6.2.1 Polymerization 90
6.2.2 Characterization 91
6.2.3 Experimental Design Procedure 93
6.2.4 Response Analysis 96
6.3 Results and Discussion 97
6.3.1 Activity 97
6.3.2 Short Chain Branching Distributions 108
6.3.4 Molecular Weight 121
6.3.5 Single Factor Experiments 128
6.4 Conclusions 133
6.5 References 134

Chapter 7 - Mechanical and rheological properties of HDPE/LLDPE reactor blends with bimodal microstructures 137
7.1 Introduction 138
7.2 Experimental 144
7.2.1 Sample Production 144
7.2.2 Microstructural Characterization 146
7.2.3 Mechanical Testing 147
7.2.3.1 Tensile Testing 147
7.2.3.2 Dynamic Mechanical Analysis 147
7.2.3.3 Small Amplitude Oscillatory Shear Experiments 148

7.3 Results and Discussion 149
7.3.1 Microstructural Characterization 152
7.3.2 Mechanical Properties 164
7.3.2.1 Tensile Testing 165
7.3.2.2 Dynamic Mechanical Properties 177
7.3.2.3 Melt Rheology 194
7.4 Conclusions 210
7.5 References 212

Chapter 8 – Contributions to research 216

Bibliography 219

Appendix 228

Appendix A1 - Estimation of Monomer/Comonomer Liquid Concentrations 229
Appendix A2 - Fortran 77 Program: Vapour Liquid Equilibrium Ethylene α-Olefin Composition Estimation 230
Appendix A3 - Thermodynamic Property Data for Common Olefins and Solvents 234

List of Figures and Tables

Chapter 1 -Introduction and background
Figure 1.1 – Structures of Polyethylene 3
Figure 1.2 – Crystal Structures of Polyethylene 6
Figure 1.3 – Initial Deformation of Polyethylene 6
Figure 1.4 – Typical Molecular Weight and Comonomer Distributions of PE 7
Figure 1.5 – Metallocene Catalyst Structures 8
Figure 1.6 – Comparison of the MWDS of Z-N and Metallocene Polyolefins 12
Figure 1.7 – Comparison of the SCBDs of Z-N and Metallocene LLDPE Resins 12

Chapter 3 – Experimental
Figure 3.1 – Experimental Setup for Polymerization 19
Figure 3.2 – Cumulative and Derivative CRYSTAF Profiles of an LLDPE Resin 22
Figure 3.3 - Stress-Strain Deformation of Semicrystalline Polymer 24
Figure 3.4 – Viscoelastic Characteristics of Polymers 26
Figure 3.5 – Dynamic Mechanical Responses of a Polymer 26
Figure 3.6 – Typical Dynamic Mechanical Responses of Polyethylene 27
Figure 3.7 – Typical Oscillatory Shear Responses of Polyethylene 28

Table 3.1 – Available Reactors for this Study 18
Table 3.2 – Percentage Errors Associated with Dynamic Mechanical Responses of Polyethylene 27
Table 3.3 – Percentage Errors Associated with Oscillatory Shear Responses 28

Chapter 4 –Using alkylaluminum activators to tailor the short chain branching distribution of ethylene/1-hexene copolymers using in-situ supported metallocene catalysts
Figure 4.1 – Molecular Weight Distributions of Ethylene/1-Hexene Copolymers Produced with Different Activators 38
Figure 4.2 – Short Chain Branching Distributions of Ethylene/1-Hexene Copolymers Produced with Different Activators 38
Figure 4.3 – Melting Endotherms of Ethylene/1-Hexene Copolymers Produced with Different Activators 39
Figure 4.4 – SCBDs of Ethylene/1-Hexene Copolymers Produced with Different Activators Under Homogeneous Polymerization Conditions 41
Figure 4.5 – Effect of Polymerization Time on SCBDs of Ethylene/1-Hexene Copolymers Produced with TEA 42
Figure 4.6 – Effect of H_2 on the SCBDs of Ethylene/1-Hexene Copolymers Produced with Different Activators 42
Figure 4.7 – SCBDs of Ethylene/1-Hexene Copolymers Produced with Mixtures of TMA and TEA Activators 44
Figure 4.8 – SCBDs of Ethylene/1-Hexene Copolymers Produced with Mixtures of TMA and TIBA Activators 44
Figure 4.9 – Polymerization Activity of Ethylene/1-Hexene Copolymers Produced with Mixtures of TMA/TEA and TMA/TIBA Activators 45

Figure 4.10 – Comparison of Actual and Predicted SCBDs of Ethylene/1-Hexene Copolymers Produced with Mixtures of TMA and TEA Activators 49
Figure 4.11 – Comparison of Actual and Predicted SCBDs of Ethylene/1-Hexene Copolymers Produced with Mixtures of TMA and TIBA Activators 49
Figure 4.12 – Comparison of Actual and Predicted Polymerization Activity of Ethylene/1-Hexene Copolymers Produced with Mixtures of Activators 50
Figure 4.13 – Comparison of Actual and Fitted SCBDs of Ethylene/1-Hexene Copolymers Produced with Mixtures of TMA and TEA Activators 52
Figure 4.14 – Comparison of Actual and Fitted SCBDs of Ethylene/1-Hexene Copolymers Produced with Mixtures of TMA and TIBA Activators 52
Figure 4.15 – Comparison of Actual and Fitted Polymerization Activity of Ethylene/1-Hexene Copolymers Produced with Mixtures of Activators 53

Table 4.1 – Ethylene/1-Hexene Copolymerizations with $Et[Ind]_2ZrCl_2$ and Different Activators 36
Table 4.2 – Summary of Results of Ethylene/1-Hexene Copolymerizations with $Et[Ind]_2ZrCl_2$ and Different Activators 37
Table 4.3 – Comparison of Experimental and Calculated Mixing Ratios of Mixed Activated Systems 47

Chapter 5 –Mechanical properties of ethylene/1-hexene copolymers with tailored short chain branching distributions
Figure 5.1 – Comparison of CRYSTAF Profiles of Tailored Ethylene/1-Hexene Copolymers 65
Figure 5.2 – Calibration Curve Relating the CRYSTAF Crystallization Temperature and 1-Hexene Incorporation in the Copolymer 66
Figure 5.3 – Comparison of MWDs of Tailored Ethylene/1-Hexene Copolymers 67
Figure 5.4 – DSC Melting Profiles of Tailored Ethylene/1-Hexene 69
Figure 5.5 – Tensile Deformation Comparison of Tailored Ethylene/1-Hexene Resins 70
Figure 5.6 – Tan Delta Comparison of Tailored Ethylene/1-Hexene Copolymers Carried Out at 1 Hz 75
Figure 5.7 – Elastic Response Comparison of Tailored Ethylene/1-Hexene Copolymers Carried Out at 1 Hz 77
Figure 5.8 – Loss Response Comparison of Tailored Ethylene/1-Hexene Copolymers Carried Out at 1 Hz 77
Figure 5.9 **–** Frequency Dependence of E'' (Loss Modulus) of Tailored Ethylene/1-Hexene Copolymers at Room Temperature 79

Table 5.1 – Microstructural Properties of Ethylene/1-Hexene Resins 64
Table 5.2 – Tensile Property Data of Ethylene/1-Hexene Copolymers 72

Chapter 6 – Ethylene/1-octene copolymerization studies with in-situ supported metallocene catalysts: effect of reaction parameters on catalyst activity and polymer microstructure
Figure 6.1 – Polymerization Mechanisms 88
Figure 6.2 – CRYSTAF Calibration Curve - 1-Octene Comonomer Incorporation 92

Figure 6.3 – Effect of Polymerization Conditions on Catalyst Activity 104
Figure 6.4 – Interaction of Polymerization Conditions on Catalyst Activity 107
Figure 6.5 – SCBD Comparison of Replicate Center Points 109
Figure 6.6 – Effect of Temperature Without Hydrogen on the SCBD 111
Figure 6.7 – Effect of Temperature With Hydrogen on the SCBD 112
Figure 6.8 – Effect of Temperature at the Low Comonomer Level Without Hydrogen on the SCBD 113
Figure 6.9 – Effect of Polymerization Conditions on Comonomer Incorporation 114
Figure 6.10 – Effect of Polymerization Conditions on Homopolymer/Copolymer Temperature Difference (Peak Separation) 115
Figure 6.11 – Interaction of Polymerization Conditions on Comonomer Incorporation 118
Figure 6.12 – Interaction of Polymerization Conditions on Homopolymer/Copolymer Temperature Difference (Peak Separation) 119
Figure 6.13 – Effect of Polymerization Conditions on Molecular Weight 122
Figure 6.14 – Effect of Polymerization Conditions on MWD 123
Figure 6.15 – Interaction of Polymerization Conditions on Molecular Weight 126
Figure 6.16 – Interaction of Polymerization Conditions on MWD 127
Figure 6.17 – Single Factor: Effect of Temperature on SCBD 129
Figure 6.18 – Single Factor: Effect of Pressure on SCBDs 129
Figure 6.19 – Single Factor: Effect of Hydrogen on SCBDs 130
Figure 6.20 – Single Factor: Effect of Comonomer/Ethylene (C/E) Ratio on SCBDs 132
Figure 6.21 – Single Factor: Effect of Aluminium/Support (A/S) Ratio on SCBDs 132

Table 6.1 – Effect of Polymerization Conditions on Catalyst Activity and Polymer Microstructure 86
Table 6.2 – Experimental Conditions for the Experimental Design Levels 94
Table 6.3 – Estimates of the 1-Octene and Ethylene Concentrations in Hexane at the Experimental Design Levels 95
Table 6.4 – ½ Fractional Design Responses: Activity 98
Table 6.5 – ½ Fractional Design Responses: CRYSTAF Analysis 99
Table 6.6 – ½ Fractional Design Responses: Molecular Weight Analysis 100
Table 6.7 – Central Composite Design Responses: Activity 101
Table 6.8 – Central Composite Design Responses: CRYSTAF Analysis 102
Table 6.9 – Central Composite Design Responses: Molecular Weight Analysis 103

Chapter 7 – Mechanical and rheological properties of HDPE/LLDPE reactor blends with bimodal microstructures

Figure 7.1 – Typical Molecular Weight and comonomer distributions of polyethylene 140
Figure 7.2 – Ethylene Flow Profiles from Two-step Polymerizations 150
Figure 7.3 – Set #1: Comonomer Distribution Comparison of Reactor Blends 153
Figure 7.4 – Set #2: Comonomer Distribution Comparison of Reactor Blends 154
Figure 7.5 – Set #3: Comonomer Distribution Comparison of Reactor Blends 155
Figure 7.6 – Set #1: Molecular Weight Distribution Comparison of Reactor Blends 160
Figure 7.7 – Set #2: Molecular Weight Distribution Comparison of Reactor Blends 161
Figure 7.8 – Set #3: Molecular Weight Distribution Comparison of Reactor Blends 162

Figure 7.9 – Set #1: Comparison of Tensile Properties of Reactor Blends 167
Figure 7.10 – Set #2: Comparison of Tensile Properties of Reactor Blends 168
Figure 7.11 – Set #3: Comparison of Tensile Properties of Reactor Blends 169
Figure 7.12 – Set #1: Comparison of Initial Tensile Yielding Behaviour 172
Figure 7.13 – Set #2: Comparison of Initial Tensile Yielding Behaviour 173
Figure 7.14 – Set #3: Comparison of Initial Tensile Yielding Behaviour 174
Figure 7.15 – Effects of Blend Composition and Degree of Crystallinity on Tensile Yield 176
Figure 7.16 – Dynamic Stress-Strain Comparison of Reactor Blends 178
Figure 7.17 – Energy Dampening Comparison of Reactor Blends Under Dynamic Strain 180
Figure 7.18 – Effect of Temperature on Storage Modulus of Reactor Blends 182
Figure 7.19 – Effect of Temperature on Loss Modulus of Reactor Blends 183
Figure 7.20 – Effect of Temperature on the Tan Delta of Reactor Blends 184
Figure 7.21 – Effect of Frequency on the Storage Modulus of Reactor Blends 187
Figure 7.22 – Effect of Frequency on the Loss Modulus of Reactor Blends 188
Figure 7.23 – Effect of Frequency on the Energy Dampening of Reactor Blends 189
Figure 7.24 – Elastic Property Comparison of Reactor Blends at Room Temperature and a Testing Frequency of 10 Hz 193
Figure 7.25 – Energy Dampening Comparison of Reactor Blends at a Room Temperature and a Testing Frequency of 10 Hz 193
Figure 7.26 – Melt Viscosity (Complex) Comparison of Reactor Blends 196
Figure 7.27 – Molecular Weight Dependence of Zero-Shear Viscosity of Reactor Blends 202
Figure 7.28 – Log Additivity of Viscosity and Blend Composition 203
Figure 7.29 – Melt Elasticity Comparison of Reactor Blends 205
Figure 7.30 – G'' versus G' Plot Comparison 207
Figure 7.31 – Flow Recovery Comparison of Reactor Blends 208

Table 7.1 – Reaction Conditions for the Two-Step Polymerizations 145
Table 7.2 – Microstructural Properties of LMW Homopolymer/HMW Copolymer Blends 157
Table 7.3 – Tensile Property Data of Ethylene/1-Hexene Copolymers 166
Table 7.4 – Rheological Property Comparison of Reactor Blends 197

Appendix

Figure A1.1 – Algorithm Used for Estimation of Monomer/Comonomer Liquid Concentrations 229

Nomenclature

ASTM – American Standards Testing Method
CRYSTAF – Crystallization Analysis Fractionation
DMTA – Dynamic Mechanical Thermal Analysis
DSC – Differential Scanning Calorimetry
GPC – Gel Permeation Chromatography
HDPE – High Density Polyethylene
HMW – High Molecular Weight
LCB – Long Chain Branch
LDPE – Low Density Polyethylene
LLDPE – Linear Low Density Polyethylene
LMW – Low Molecular Weight
MAO - Methylaluminoxane
MW – Molecular Weight
MWD – Molecular Weight Distribution
NMR – Nuclear Magnetic Resonance
PDI – Polydispersity Index
PE – Polyethylene
PP - Polypropylene
SCB – Short Chain Branch
SCBD – Short Chain Branching Distribution
SMAO – Silica Supported Methylaluminoxane
TCB – Trichlorobenzene
TEA – Triethylaluminum
TIBA – Triisobutylaluminum
TMA – Trimethylaluminum
TREF – Temperature Rise Elution Fractionation
VLDPE – Very Low Density Polyethylene
Z-N – Ziegler-Natta

Symbols

α - Alpha Transition
β - Beta Transition
δ - Phase angle delta
ΔH_f – Heat of Fusion (J/g)
γ - Gamma transition
$\dot{\gamma}$ - Shear Rate (s^{-1})
γi – Liquid Phase Activity Coefficient
ϕ_i^l - Liquid Phase Fugacity Coefficient
ϕ_i^v - Vapour Phase Fugacity Coefficient
λ -Characteristic Time of Cross Model

Σ - Summation
τ - Ratio of Transfer to Propagation Rates
A/S – Alkyaluminum to Silica Support Ratio
C/E – Comonomer to Ethylene Ratio
$[Cat^*]$ – Catalyst Concentration (mol/L)
dW/d(LOG(MW) – Derivative Weight Fraction of Molecular Weight
dW/dT – Derivative of Cumulative Weight versus Temperature
E' – Storage Modulus Solid State (Pa)
E'' – Loss Modulus Solid State (Pa)
f(m) – Weight Fraction of Polymer
f(T) – SCBD Data as Values of dW/dT from CRYSTAF
G' – Storage Modulus Melt State (Pa)
G'' – Loss Modulus Melt State (Pa)
H – Hydrogen
k_{act} – Activation Rate Constant
k_i – Initiation Rate Constant
k_p – Propagation Rate Constant
k_t – Termination Rate Constant
k_f – Transfer Rate Constant
k_d – Deactivation Rate Constant
K – Consistency Index from Power-Law Model
m – 1-Octene Concentration (mol %)
[M] – Monomer Concentration (mol/L)
M_N – Number Average Molecular Weight (g/mol)
M_W –Weight Average Molecular Weight (g/mol)
η - Shear Viscosity (Pa s)
η^* - Complex Viscosity (Pa s)
η_0 – Zero-Shear Viscosity (Pa s)
P – Pressure (Pa)
R_N – Number Average of Repeating Units
T – Temperature (°C)
T_c – Crystallization Temperature (°C)
T_n – Number Average Temperature (°C)
TAN DELTA – Ratio of the Loss Modulus (E'' or G'') and Storage Modulus (E' or G')
T_i – Temperature of Polymer Fraction i(°C)
W_i – Weight Fraction of Polymer i
$x^*_{TMA,TEA\ or\ TIBA}$ – Fractional Component of Polymer Produced by TMA,TEA or TIBA
x_i – Fraction of Liquid Component
y_i – Fraction of Vapour Component

Chapter 1

Introduction and Background

1.0 Introduction and Background

1.1 Polyolefins

Polyolefins are the most widely produced plastics in the world and are found in numerous applications. Polyolefins are considered 'commodity polymers' consisting mostly of polyethylene (PE) and polypropylene (PP) and their copolymers with alpha olefins such as 1-butene, 1-hexene and 1-octene. Microstructural properties such as molecular weight distribution (MWD), branching structure and stereoregularity determine the applications of polyolefins (Manders, 1995). In turn, the polymer microstructure controls the end-use applications. The choice of polymer depends on the desired properties such as its stiffness, toughness, stress-crack resistance, optical clarity etc. and the polymer processing operation to be used.

1.2 Types of Polyethylene (Elvers et al., 1992)

The most common polyolefin is polyethylene. PE has the basic structure of $-(CH_2CH_2)_n-$ which consists of a long chain of repeated ethylene units. Even though PE has this simple structure, there are several families of PE with different branching structures. Since polyethylene is a partially crystalline solid, different branching structures affect the crystallinity and density. Commercially, PE is generally classified as high density polyethylene (HDPE), low density polyethylene (LDPE), linear low density polyethylene (LLDPE) and very low density polyethylene (VLDPE). If the polymer backbone is linear and contains no or few short chain branches (as shown in Figure 1.1a), the term HDPE is used. HDPE is a white opaque solid that is rigid and forms films that are crispy to the touch. This polymer is highly crystalline (70-80%) and has a melting point of up to 135 °C. As a measure of crystallinity, density is often used

having a value between 0.96-0.97 g/cm^3 for HDPE. To reduce crystallinity, alkyl substituents such as α-olefins (1-butene, 1-hexene, 1-octene, etc.) are introduced as comonomers during the polymerization to incorporate short chain branches (SCB) along the backbone. These alkyl SCBs are concentrated in the amorphous regions of the copolymer where they are mobile and their effect is to reduce stiffness. This PE is called LLDPE and is shown in Figure 1.1b. LLDPE has branching of almost uniform length to form random copolymers and sometimes "blocky" copolymers. However, the highest concentration of branches is generally found on the shorter chains. This type of PE has a crystallinity of around 40-50% and has a lower melting point of 105-115°C. Depending on the density and comonomer content, these copolymers can be linear low density/medium density PE (0.915 – 0.94 g/cm^3) or very low density PE (VLDPE, ≈ 0.88-0.912 g/cm^3). LLDPE forms translucent films that are fairly flexible and used for packaging with good mechanical properties. A somewhat different type of PE is LDPE, which differs from the others because of its highly branched structure (see Figure 1.1c).

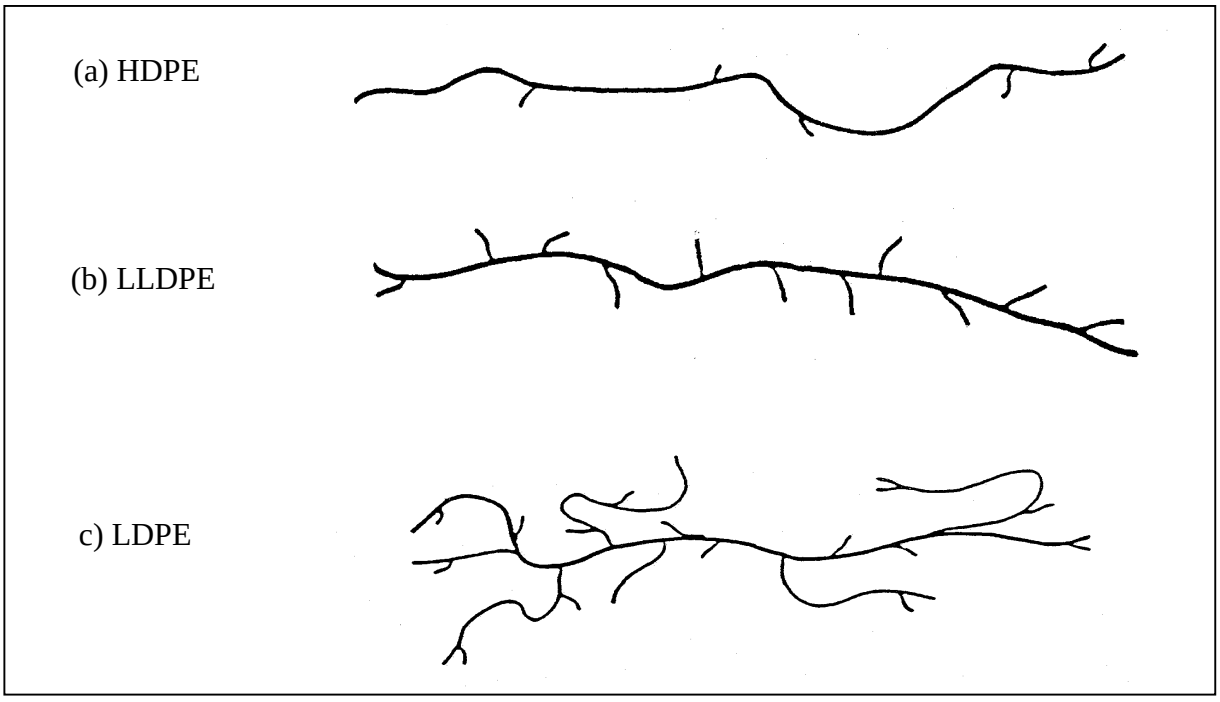

Figure 1.1 – Structures of polyethylene

This type of polymer microstructure is a product of many side reactions during a high temperature and high pressure free radical process. As shown, many SCBs are present as well as long chain branches (LCB) that can be of the same length as the polymer backbone. The density of LDPE is between 0.915 and 0.935 g/cm^3. LDPE finds wide use in wire and cable applications and in the film/packaging industry but it is slowly being replaced by LLDPE resins. However, LDPE is still widely favoured for its good processability and high melt strength due to the entanglement of the branches (Goyal, 1994). Given the importance of these entanglements, a recent trend has been to include controlled amounts of LCB into linear polyolefin resins with the use of single-site catalysts (Schwank, 1993; Chum et al., 1995).

1.3 Importance of MWD and Comonomer Distribution on Physical Properties

The molecular weight distribution of a polymer is a very important factor in determining its mechanical properties and processing behaviour. The mechanical properties of a polymer in the solid-state such as its stiffness, toughness, impact strength and stress-crack resistance depend upon its crystalline structure. Upon cooling a polymer from the melt-state, the disentangled chains will crystallize to form crystal lamellae. The thickness and shape of these lamellae are determined by the ability of the polymer chains to pack together. The degree of crystallinity and melting point of the polymer depends on the length of the chains and the presence of any side branches. Figure 1.2 shows the possible arrangements of the crystal lamellae at different density levels. The stiffness of the polymer depends on its degree of crystallinity. The degree of crystallinity and stiffness decreases with increasing the molecular weight of the chains (Nunes et al., 1982). However, toughness and long-term creep properties such environmental stress crack resistance are highly influenced by the entanglement of the longer chains to increase ‘tie

molecule' concentration and better link the polymer crystallites (Lustiger and Markham, 1983). Figure 1.3 shows the tensile deformation of polymer lamellae. Chain entanglements and tie molecules are located in the amorphous region and are sandwiched between the crystal lamellae.

It is generally found that the mechanical properties of a polymer deteriorate with broadening MWD. Polymers with narrower MWD crystallize more uniformly and exhibit better physical properties such as increased dimensional stability, higher impact resistance, greater toughness at low temperatures and higher resistance to environmental stress cracking (Zucchini and Cecchin, 1983). However, broadening of the MWD enhances the polymer processability. In an extrusion process, resins with broader MWDs exhibit lower viscosities at processing shear rates. Depending on the processing method used such as injection molding, blow molding, extrusion, etc., there is a processability trade-off with regards to the achievable physical properties. This is one of the major reasons why the plastics market contains so many different grades of each polymer, even though the chemical composition may be identical (Rudin, 1982).

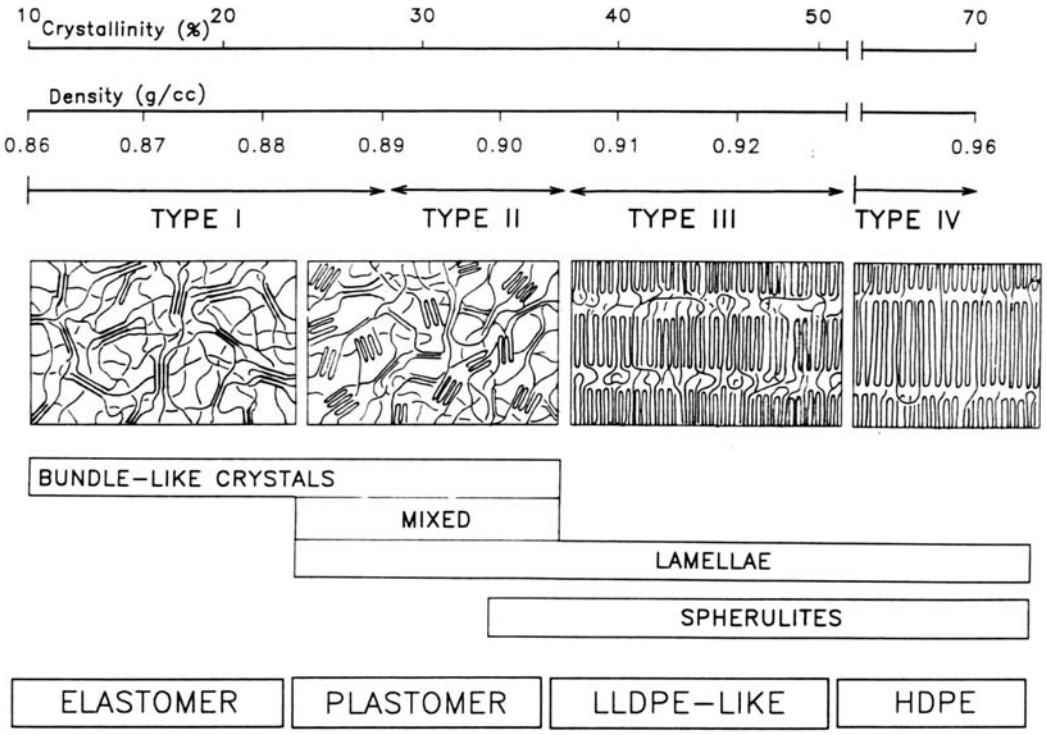

Figure 1.2 – Crystal Structures of Polyethylene (Bensason et al., 1996)

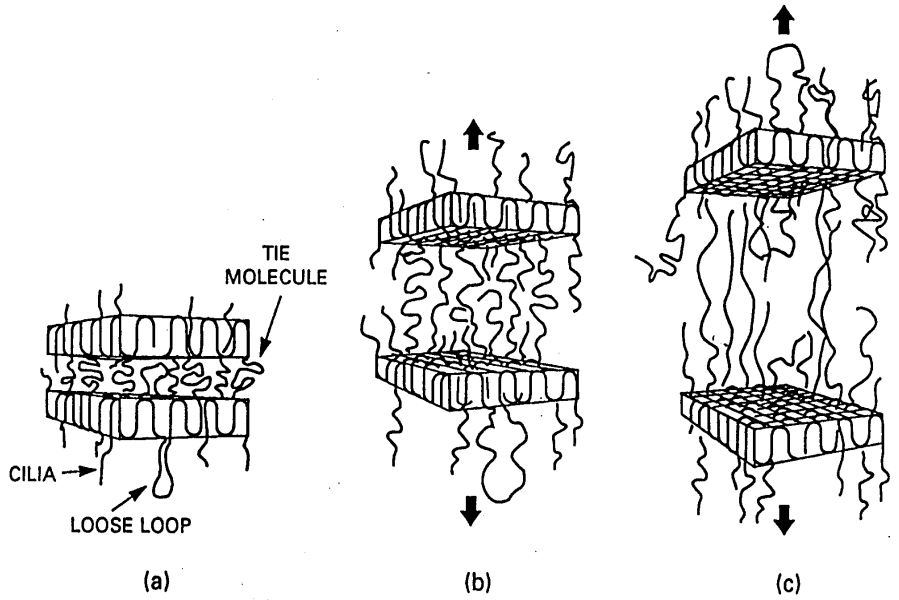

Figure 1.3 – Initial deformation of Polyethylene (Browstow and Corneliussen, 1986)

One method of tailoring the property-processing relationship is to control the shape of the MWD. For many industrial resins, especially for pipe grade PEs, the MWDs are very broad and sometimes bimodal (Figure 1.4b). Bimodal resins have a high molecular weight component to impart strength and toughness and a low molecular weight component to facilitate extrusion (Avela et al., 1998; Berthold et al., 1996; Scheirs et al., 1996).

The comonomer distribution is also an important property that can be tailored for the desired application. For Zielger-Natta LLDPE, it is generally found that the comonomer distribution is broad and uneven. A greater concentration of comonomer is found on the shorter chains. Single-site LLDPE has a narrow and more uniform distribution of comonomer. Figure 1.4a shows examples of these two types of comonomer distributions. A recent trend is to produce resins with 'reverse comonomer distributions' in which the comonomer is placed on the high molecular weight chains. For bimodal PEs made in a series reactor, the addition of high molecular weight copolymer increases the number of entanglements and enhances its toughness and stress crack resistance (Avela et al., 1998; Berthold et al., 1996; Scheirs et al., 1996). Dow has also recently introduced resins with unimodal MWDs with reverse comonomer distributions produced with their Insite© catalysts (Matsushita et al., 1998).

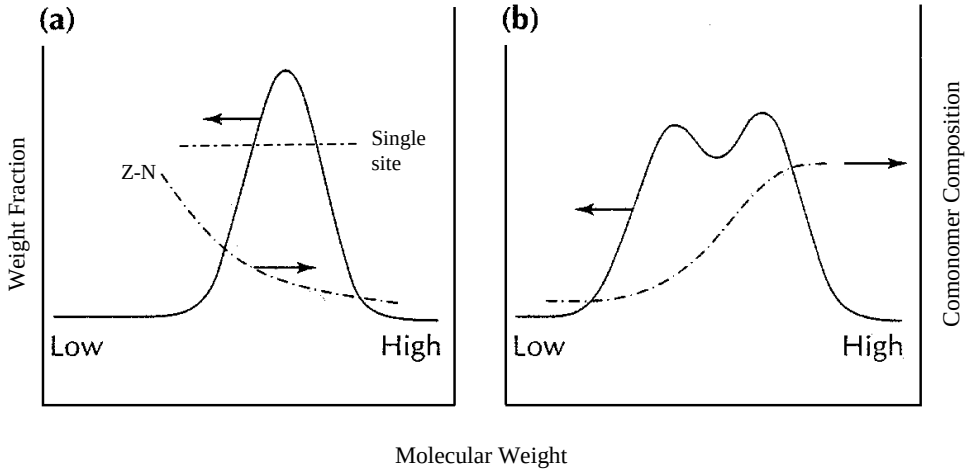

Figure 1.4 – Typical molecular weight and comonomer distributions of PE (Scheirs et al., 1996)
(a) Conventional Ziegler-Natta PE made in a single reactor
(b) Bimodal Ziegler-Natta PE made in a series of reactors

1.4 Catalyst Selection

Metallocene catalysts are very versatile tools in tailoring the properties of polyolefins. By altering the catalyst structure, control over molecular weight, short chain branching and stereoregularity is possible. Metallocenes are considered single-site catalysts and produce polyolefins with narrow MWDs and narrow SCBDs. As a result, many new industrial resins with improved properties are now available. There are two main aspects that affect the polymerization behaviour of these catalysts. Firstly, the properties depend on the catalyst type. Catalysts with different metal centers and ligands produce polymer chains with different average molecular weights and vary in their ability to incorporate comonomer. Secondly, catalyst behaviour can change with the polymerization conditions, such as the catalyst and cocatalyst concentration, polymerization temperature, monomer pressure and type and concentration of chain transfer agents (Huang and Rempel, 1995; Reddy and Sivaram, 1995).

For these studies, two different metallocenes were used, rac-(ethylenebis(indenyl))zirconium dichloride [Et[Ind]$_2$ZrCl$_2$] and rac-(dimethylsilylbis(methyl benzoindenyl)) zirconium dichloride [Me$_2$Si(2-Me-4,5 BenzInd)$_2$ZrCl$_2$]. Figure 1.5 shows that both catalysts are bridged metallocenes, have very open structures, and faciliate the

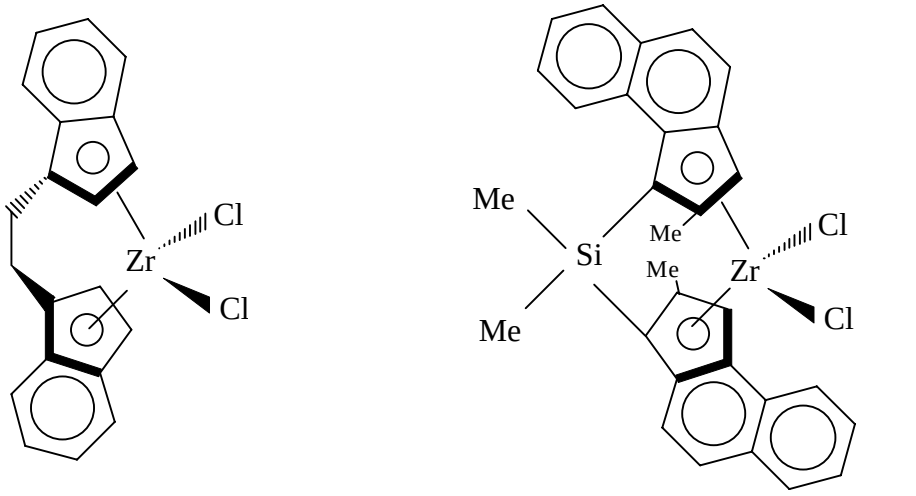

(A) Et[Ind]$_2$ZrCl$_2$ (B) Me$_2$Si(2-Me-4,5 BenzInd)$_2$ZrCl$_2$

Figure 1.5 – Metallocene catalyst structures

incorporation of comonomer. Preliminary screening studies showed that both of these catalysts incorporate α-olefin comonomers to produce ethylene copolymers with high comonomer content. However, the catalysts differ in their sensitivities to temperature, pressure and hydrogen. It was found that $Et[Ind]_2ZrCl_2$ is fairly insensitive to monomer pressure and hydrogen to produce polyethylenes with moderate molecular weights in the range of 30,000 – 100,000 g/mol. $Me_2Si(2\text{-}Me\text{-}4,5\ BenzInd)_2ZrCl_2$ was found to produce polymer with higher molecular weight and was pressure- and hydrogen-sensitive.

For these studies, a heterogeneous catalyst was employed. A heterogeneous catalyst system is important for the production of polymers with high bulk density for use in slurry or gas phase processes (Gali, 1995,1999). Catalyst heterogenization involves the attachment of a catalyst to an inorganic support such as silica or magnesium chloride through a series of preparatory steps (Ribeiro et al., 1997; Hltaky, 2000). The advantage of supporting the catalyst is to control the morphology of the polymer particles. The polymer particles produced replicate the shape of the catalyst supports (replication phenomena) (Hamielec and Soares, 1996). By manipulating the catalyst morphology, it is possible to control the polymer particle size, shape and bulk density. This also eliminates the need for the pelletizing step during the manufacture of the polymer.

For these studies a novel in-situ supported metallocene catalyst, which eliminates the need for a catalyst supporting stage, was used (Chu et al., 2000). This in-situ system combines catalyst supporting and polymerization in one-step and produces polyethylene and ethylene/α-olefin copolymers with high activities, good polymer morphology, and minimal reactor fouling. This in-situ system was selected because of its ease of use, high activity and ability to produce polymer with good morphology.

1.5 Methods to Tailor the MWD and SCBD

Using a single reactor and a single catalyst system, microstructural control of a polymer is generally achieved by altering the polymerization conditions such as the polymerization temperature, monomer pressure, and the addition of chain transfer agents.

It is generally found that the molecular weight of the polymer is inversely proportional to the polymerization temperature. At elevated temperatures, the molecular weight of polymers decreases due to an increase in transfer rates, as compared to the propagation rate. Polymer molecular weight increases with increasing monomer pressure since the rate of propagation is first order in monomer concentration. With the addition of a chain transfer agent such as hydrogen, the molecular weight of polymers can be significantly reduced. The breadth of the molecular weight distribution of polymers produced generally depends on the catalyst type. Multiple-site-type catalysts such as heterogeneous Ziegler-Natta ($TiCl_4/MgCl_2$) produce polymers with broad MWDs with polydispersity indices (PDI) between 4-8, while metallocenes produce narrow MWDs with PDIs around 2. Figure 1.6 compares the molecular weight distribution of a Ziegler-Natta and a metallocene polymer.

The short chain branching distribution (SCBD) of polyethylene is also affected by the polymerization conditions mentioned above, but to a lesser extent. Generally, the level of comonomer incorporation depends on the concentration of comonomer in the feed. The breadth of distribution that results depends on the catalyst type. As mentioned, Ziegler-Natta catalysts produce copolymers with broad and uneven distributions while metallocenes result in higher incorporation (for the same comonomer concentration in the reactor) and narrower distributions. Figure 1.7 compares the short chain branching distribution of a Ziegler-Natta and metallocene LLDPE.

Both the MWD and SCBD can be tailored with a series process that controls the polymerization conditions of each stage. The structure and properties of the resin can be tailored by controlling the polymer's molecular weight, MWD, comonomer content and the location of the comonomer within the MWD. An alternative method is to use a combined catalyst system in a single reactor. A mixture of catalysts will produce polymer chains from each individual catalyst (Soares et al., 1997; Heiland and Kaminsky, 1992). Resins with blended characteristics can result depending on the molecular weight and comonomer content of each polymer component. This method is attractive from an economical point of view (only one reactor is required); however, the design and development of combined catalysts is still under way.

Ultimately, the microstructure of polyethylene depends on the choice of catalyst, the method of polymerization, and the polymerization conditions. The microstructure of the polymer governs the attainable physical properties and determines its end-use application and processing operation.

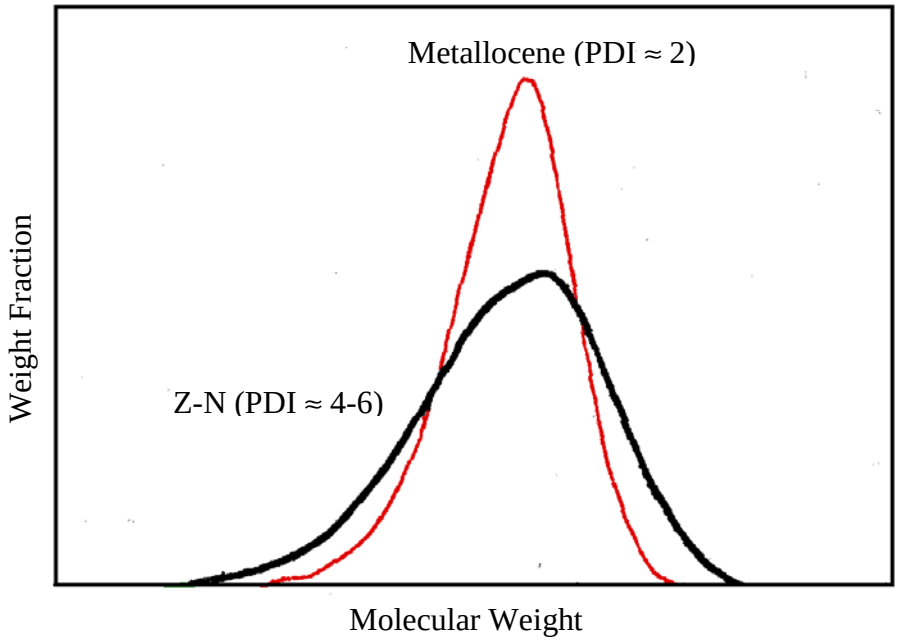

Figure 1.6 – Comparison of the MWDs of Z-N and metallocene polyolefins (Foster and Wasserman, 1997)

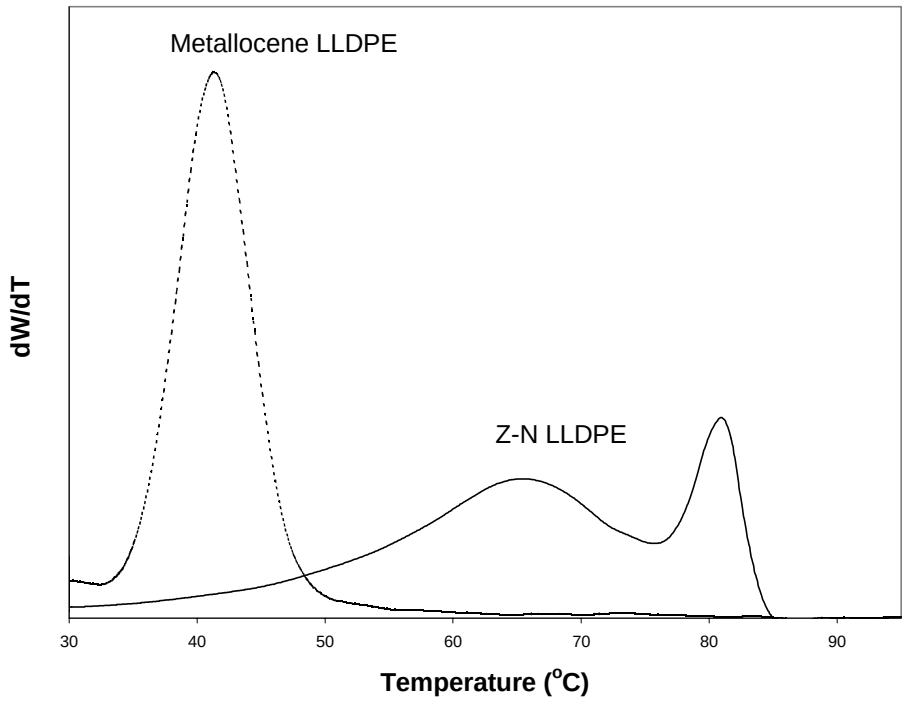

Figure 1.7 – Comparison of the SCBDs of Z-N and metallocene of LLDPE resins

Chapter 2

Research Objectives

2.0 Topics Studied

The focus of this thesis has been to investigate alternative methods to control the molecular weight and short chain branching distribution of polyethylene. Using different polymerization methods, resins with controlled microstructures were characterized and tested to develop structure-property relationships. The thesis is divided into a series of papers that investigate the topics listed below:

2.1 Using alkylaluminum activators to tailor the short chain branching distribution of ethylene/1-hexene copolymers using in-situ supported metallocene catalysts

With a single catalyst and single reactor, it was demonstrated that the comonomer incorporation characteristics of a catalyst could be altered depending on the alkylaluminum activator used. The ethylene copolymers produced exhibited broad and bimodal SCBDs, while maintaining narrow MWDs. This method was used as a simple tool to tailor the SCBDs of ethylene copolymers (Li Pi Shan et al., 2000).

2.2 Mechanical properties of ethylene/1-hexene copolymers with tailored short chain branching distributions

Using the catalyst system mentioned above, a series of poly(ethylene-*co*-1-hexene) resins with distinct SCBDs were produced. These resins were characterized and tested for their tensile and dynamic mechanical properties (Li Pi Shan et al., 2001).

2.3 Effect of reaction parameters on the microstructure of poly(ethylene-*co*-1-octene) copolymers

An experimental design study was carried out to examine the effect of the polymerization conditions on the resulting polymer microstructure. Parameters investigated included polymerization temperature, ethylene pressure, hydrogen concentration, comonomer/ethylene feed ratio and amount of alkylaluminum. It was discovered that a wide range of microstructures could be obtained by varying these parameters (Li Pi Shan et al., 2002).

2.4 Mechanical and rheological properties of HDPE/LLDPE reactor blends with bimodal microstructures

Three series of polyethylene resins with bimodal microstructures were produced using a two-step polymerization method. The polymerization conditions to produce the desired polymer in each stage were obtained from the previous reaction parameter study. Reactor blends of HDPE/LLDPE were produced to determine the effect of the polymer molecular weight, MWD, comonomer content and location of the comonomer within the MWD on the physical properties. The resins were characterized and tested for their mechanical and melt rheological properties (Li Pi Shan et al., 2002).

Chapter 3

Experimental

3.0 Experimental

3.1 Materials

The metallocene catalysts used in these studies were *rac*-(ethylenebis(indenyl))zirconium dichloride [Et[Ind]$_2$ZrCl$_2$] and r*ac*-(dimethylsilylbis(methylbenzoindenyl)) zirconium dichloride [Me$_2$Si(2-Me-4,5 BenzInd)$_2$ZrCl$_2$] obtained from Aldrich Chemical Co. and Boulder Scientific Co. respectively. Silica supported methylaluminoxane (SMAO, 24.4 wt% Al, purchased from Witco) was used as a catalyst support.

Toluene was purified by refluxing over n-butyl lithium/styrene oligomers and by distillation. n-Hexane was dried over a mixture of 3A/4A molecular sieves (purchased from BDH) and used without further purification.

CP grade ethylene and ultra high purity nitrogen (purchased from Praxair) were purified by passing them through molecular sieves and de-oxygenating beds. Ultra high purity hydrogen (Praxair) was used as received. 1-Hexene and 1-octene were obtained from Aldrich Chemicals, dried over molecular sieves and degassed with purified nitrogen. Trimethylaluminum (TMA), triethylaluminum (TEA) and triisobutylaluminum (TIBA) were purchased from Aldrich Chemicals and used without further purification.

3.2 Procedures

3.2.1 Equipment

Table 3.1 lists the reactors used in this study. The 300 mL reactor was used for the exploratory investigations. The 1L reactor was used for the production of larger polymer samples when physical property testing was required.

Table 3.1 – Available reactors for this study

Type	Manufacturer	Details
300 mL Autoclave Reactor	Parr Industries	Equipped with mass flowmeter, temperature controller and rotating stirrer
1 L Autoclave Reactor	Pressure Product Industries	Equipped with flow rotameter, temperature controller and rotating stirrer

3.3.2 In-situ Supported Metallocene Polymerization Method

For these studies, a novel in-situ supported metallocene catalyst which eliminates the need for a catalyst supporting stage, was used (Chu et al., 2000). This method was pioneered in our laboratory to combine catalyst supporting and polymerization in one-step. This in-situ system uses a silica support that has been impregnated with a high concentration of methylaluminoxane (MAO, 24 wt%) and will be referred to herein as SMAO. When SMAO is combined with a homogeneous metallocene solution followed by the addition of an aluminum alkyl such as trimethylaluminum, olefin polymerization active species are generated.

Figure 3.1 shows one of the experimental setups used for polymerization. The air-sensitive technique used to carry out the polymerization is outlined below:

1. Dry and evacuate the reactor at 150°C.
2. Cool the reactor to room temperature.
3. Weigh out the desired catalyst components in the nitrogen glovebox and place them into septum-sealed vials.
4. Transfer the dried solvent (hexane) under positive N_2 pressure with a cannula to the round bottom flask sealed with septa. Add 150 mL for the 300 mL reactor and 750 mL for the 1L reactor.
5. Transfer the desired amount of alkylaluminum from a septum-sealed vial to the solvent present in the flask.
6. Stir the solvent with alkylaluminum for a few minutes.
7. Transfer approximately half of the pre-treated solvent to the reactor.
8. Transfer the solid SMAO to the reactor using a portion of the remaining pre-treated solvent.
9. Transfer the catalyst present as a toluene solution using the remaining pre-treated solvent.

10. If comonomer is necessary, add the pre-dried comonomer to the reactor from a nitrogen-sealed container using a transfer syringe.
11. If hydrogen is necessary, purge the hydrogen bottle to the atmosphere and then measure the required amount using a transfer syringe. Seal all ports to the reactor except the injection port. Inject the hydrogen into the reactor and close the remaining port.
12. Pre-heat the reactor to the desired temperature at a very low stirring speed to promote better heat transfer.
13. Once the desired reaction temperature is reached, increase the stirring speed to the desired level. An acceptable speed is 300 rpm.
14. Pressurize the reactor with ethylene.
15. Monitor the ethylene flowrate and polymerize for the desired reaction time.
16. Depressurize the reactor and quench the reactor medium with acidified ethanol.
17. Filter and dry the polymer.

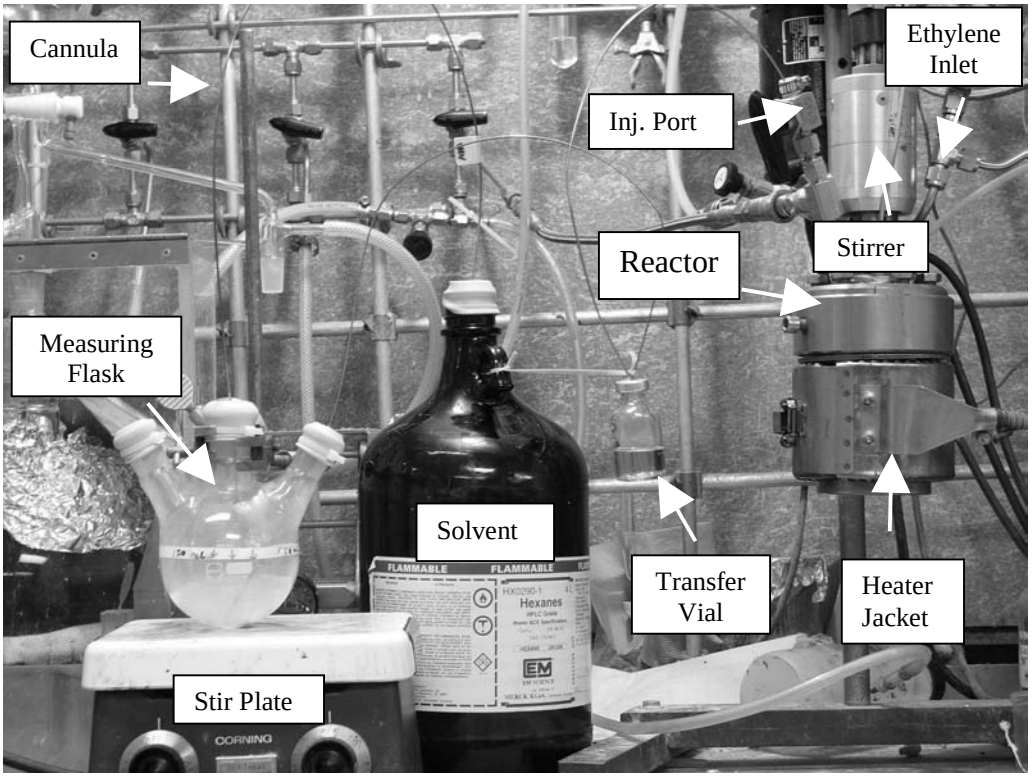

Figure 3.1 – Experimental Setup for Polymerization

3.3.3 Vapour-Liquid Equilibrium Estimation of α-Olefin Comonomer Concentrations

To estimate the amount of α-olefin comonomer required for the different polymerization conditions, bubble point pressure calculations were performed based on the Chao-Seader method and other thermodynamic correlations (Smith and Van Ness, 1975).

A Fortran 77 program was used to estimate the liquid concentrations of ethylene and 1-hexene or 1-octene in hexane at the specified temperature and pressure. Appendix A1 shows the algorithm used. The Fortran 77 program is included in Appendix A2 for archival purposes. Appendix A3 lists the thermodynamic property data for different monomer, comonomer and solvent systems.

3.3 Characterization Methods

In this section the analytical methods used to characterize and test the microstructure and physical properties of the polymers will be introduced. A detailed description of the testing conditions used for each study is included in the results and discussion (Chapt. 4-7).

3.3.1 Gel Permeation Chromatography (GPC)

GPC works on the principle of size exclusion. A polymer solution is passed through a column of cross-linked polymer (such as styrene divinylbenzene). Smaller chains can diffuse into more pore sizes than larger chains and, consequently, smaller chains have a higher retention time in the GPC columns. A calibration curve relating retention time to molecular weight is used to calculate MWD (Styring and Hamielec, 1989). For polyolefins, GPC is carried out in solvents operating at high temperatures because of the difficulty in dissolving the polymers.

A Waters GPCV 150+ instrument equipped with a Viscotek 150R viscometer was used with 1,2,4 trichlorobenzene (TCB) as a solvent operating at 140°C. Number average and weight average molecular weights were calculated using conventional GPC analysis and a universal calibration curve based on narrow polystyrene standards.

The pure error for the GPC instrument used in this study was estimated to be around 5% for the weight average molecular weight (D'Agnillo et al., 1999). For these studies, the molecular weight distributions were fairly reproducible and within this error range.

3.3.2 Crystallization Analysis Fractionation (CRYSTAF)

Short chain branching distributions were determined by crystallization analysis fractionation using a CRYSTAF 200 instrument (Polymer Char, Valencia, Spain). CRYSTAF is a technique similar to temperature rising elution fractionation (TREF), but with significantly shorter analysis time (Monrabal, 1994; Monrabal, 1996). The CRYSTAF method begins with the dissolution of the polymer at high temperature (160°C) in trichlorobenzene followed by slow cooling of the polymer solution to room temperature. During the cooling step, polymer chains crystallize and precipitate, thus decreasing the polymer concentration in solution. The concentration of polymer in solution is monitored by an on-line infra-red detector as a function of crystallization temperature, generating a plot of the cumulative distribution of polymer solution concentration. The first derivative of this cumulative distribution will give the distribution of chain crystallinities (measured as solubility in TCB) as a function of crystallization temperature in TCB. Refer to Figure 3.2 for an example of a CRYSTAF profile.

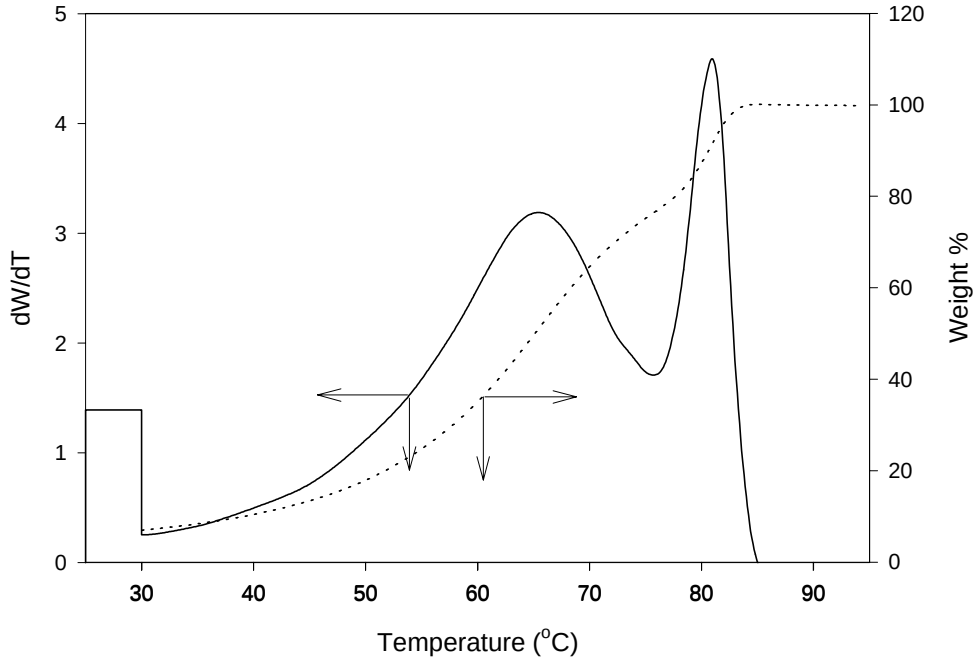

Figure 3.2 – Cumulative and derivative CRYSTAF profiles of an LLDPE resin

A calibration curve can be used to relate this crystallization profile to SCB degree. The least branched chains crystallize first, followed by increasingly branched ones.

Overall, the reproducibility of the CRYSTAF instrument was very good. From an in-house reproducibility study, it was found that the peak positions are repeatable within ± 0.5 °C.

3.3.3 Differential Scanning Calorimetry (DSC)

DSC is a thermal method that is used to measure the enthalpic changes of a sample. By monitoring the changes in supplied energy against the temperature, the thermal transitions of a polymer such as the glass transition and the heat of fusion or crystallization can be observed. For a semi-crystalline polymer, the shape of the DSC curve also gives an indication to the range of crystalline species present. For polyethylene, the degree of crystallinity can be estimated by comparing the measured melting enthalpy to that of a pure polyethylene crystal (Sperling, 1992).

The ΔH_f for a pure polyethylene crystal is estimated to be approximately 289 J/mol (Xu, 1999). The melting transitions of polymers are very sensitive to its thermal history. Different crystalline structures are formed depending on the thermal treatment of the sample either by slow annealing or quenching of the sample. To include the effect of thermal history of the sample, DSC measurements can be obtained from the first temperature scan. A better estimate of the inherent properties of the polymer is to erase the thermal history of the sample by melting it in the first scan and then obtaining the thermal estimates from a second scan.

3.3.4 Fourier Transform Infrared Spectroscopy (FTIR)

In preliminary studies, FTIR was used to estimate the comonomer content of some of the poly(ethylene-*co*-1-hexene) polymers. The comonomer content was determined using a calibration curve constructed based on the ratio of the 1380/1370 cm^{-1} peaks from the polymer as demonstrated in the literature (Nowlin et al., 1988). It was later verified that the estimates of the comonomer content were similar to those determined by CRYSTAF.

3.4 Physical Property Testing

3.4.1 Tensile Testing

Uniaxial tensile testing was performed to examine the deformation behaviour of the resins. Figure 3.3 shows the typical deformation behaviour of a semi-crystalline polymer. Initially, Hookean elastic behaviour is observed until the sample draws and permanent deformation occurs. As the sample draws, the polymer chains orient and recrystallize to form stronger material and eventually the sample breaks. The initial yield stress that is measured is related to modulus of the polymer. The ultimate yield stress and elongation contribute to the

area underneath the stress-strain curve and relates to the toughness of the polymer. The yielding behaviour depends on the crystalline structure of the polymer (Sperling, 1992).

The tensile measurements were performed on an Instron 4465 materials tester. The error in the measured values from the sample depends on preparation of the sample bar. For these studies, difficulties were encountered in the preparation of defect-free sample bars. From replicate testing, the error associated with the tensile stresses at yield was 8 %, from a pooled standard deviation based on a total of 37 tests at a 95% confidence level. For the tensile stresses at break and percentage elongation, the error increased to about 25%.

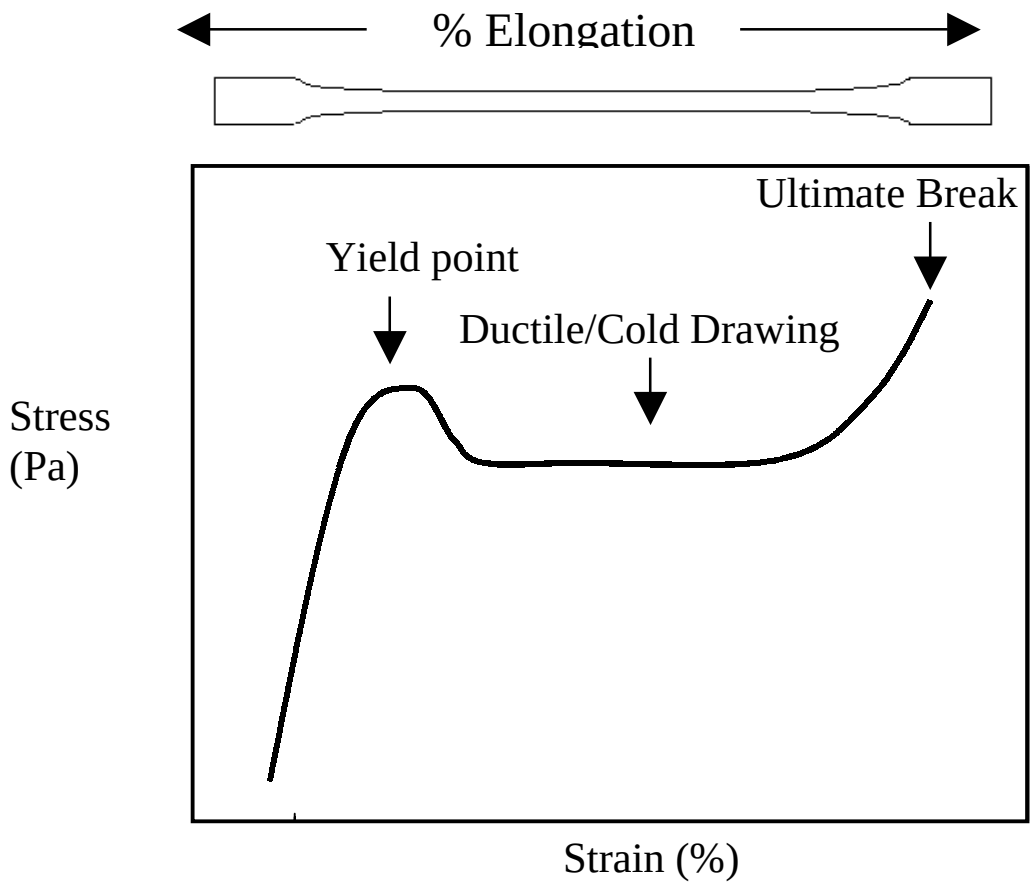

Figure 3.3 - Stress-Strain Deformation of Semicrystalline Polymer

3.4.2 Dynamic Mechanical Thermal Analysis (DMTA)

DMTA is often used to determine the viscoelastic properties of a material in its solid-state. It is well known that polymeric behaviour can be modelled by the individual contributions of elastic and viscous components. Figure 3.4 displays the analogy of dropping a ball to show the role of energy storage (elastic) and energy loss (viscous). A DMTA instrument measures the response of a material to an applied oscillating force. From the measurement of the phase lag and the sample recovery, the storage (E') and loss modulus (E'') can be calculated; the tan delta is the ratio of the E'' and E' (Figure 3.5). Small tan deltas indicate a stiffer more elastic response while large values show greater energy loss. These dynamic mechanical properties are all linked to the relaxation behaviour of the polymer chains.

DMTA analysis should be carried out in the linear viscoelastic region of the polymer in which the imposed deformations are reversible. The linear viscoelastic region is determined by a strain sweep to determine the allowable range of strains. Application-specific testing can be carried out at a desired frequency and temperature. It is well known that the properties of a polymer are frequency and temperature dependent. Both time (frequency) and temperature are related; with an increase in frequency or decrease in temperature, the polymer chains appear stiffer since their relaxation is slowed. The opposite is observed at low frequency or high temperature since a polymer will appear more flexible, given more time to relax. Temperature and frequency studies can reveal insight into polymer characteristics such as its solid-state transitions, chain mobility and microstructure (Menard, 2000).

For these analyses, a Rheometrics DMTA V instrument was used. Figure 3.6 shows the dynamic responses of a polyethylene sample tested five times. The experiments were carried out at room temperature with a frequency range between 0.01 to 100 Hz at a strain level of 0.05 %.

The error increases with an increase in frequency. Table 3.2 lists the associated errors at certain frequencies for the measured values.

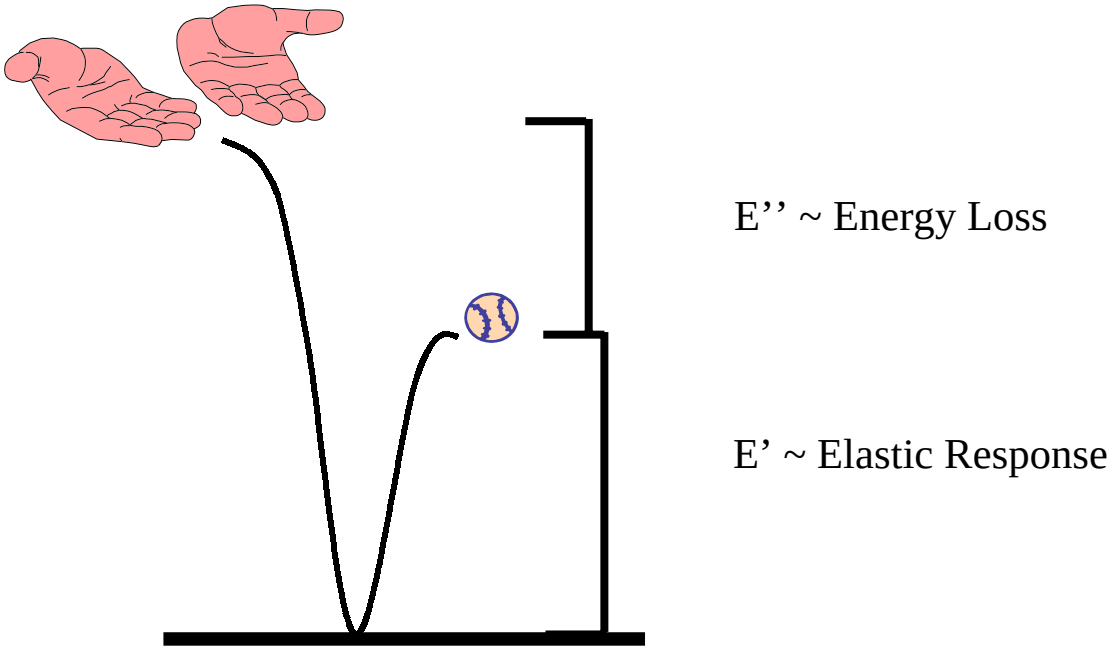

Figure 3.4 Viscoelastic Characteristics of Polymers

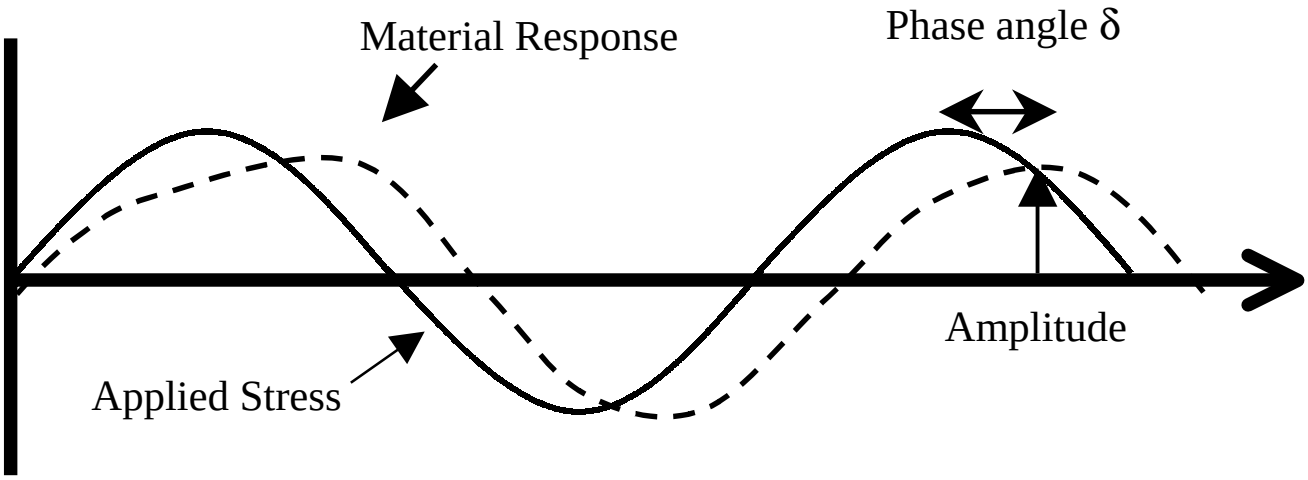

Figure 3.5 – Dynamic Mechanical Responses of a Polymer

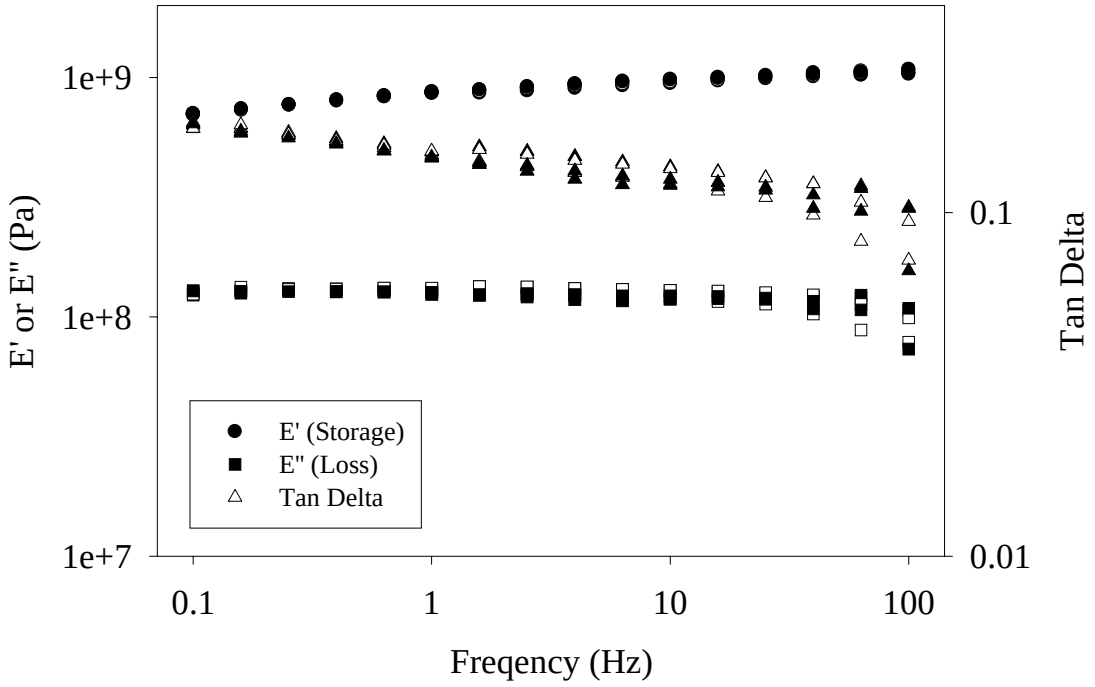

Figure 3.6 – Typical Dynamic Mechanical Responses of Polyethylene

Table 3.2 – Percentage Errors Associated with Dynamic Mechanical Responses of Polyethylene

Frequency	E' (Pa) (± %)*	E'' (Pa) (± %)*	Tan Delta (± %)*
0.1	0.65	2.13	2.34
1	0.73	2.89	2.56
10	1.99	5.28	7.19
100	2.43	21.75	23.88

*Calculated at a 95% confidence level with 5 samples.

3.4.3 Small Amplitude Oscillatory Shear Analysis

The viscoelastic characteristics of the polymers in the melt-state were measured with a rotational rheometer operating in the oscillatory mode. The principles for the estimation of the storage (G') and loss modulus (G'') from such a rheometer are similar to that of DMTA. From these analyses, the flow behaviour of the polymers according to its complex viscosity and shear thinning behaviour were compared. Frequency sweeps were carried out to compare the shear rate dependence of the complex viscosities. Using the Cox-Merz conversion, complex viscosity

versus frequency is similar to shear viscosity versus shear rate data collected by a capillary rheometer or continuous flow measurements. The G' and G'' also give an indication of the elastic and flow recovery behaviour of the material (Dealy and Wissbrun, 1990).

For these analyses, a TA Instruments AR2000 rheometer was used. Figure 3.7 shows the dynamic responses of a high density polyethylene sample tested 3 times. The experiments were carried out at 190°C with a frequency range was 0.1 to 100 Hz at a strain level of 2.5 %. It was observed that the error decreases with an increase in frequency. Table 3.3 lists the associated errors at certain frequencies for the measured values.

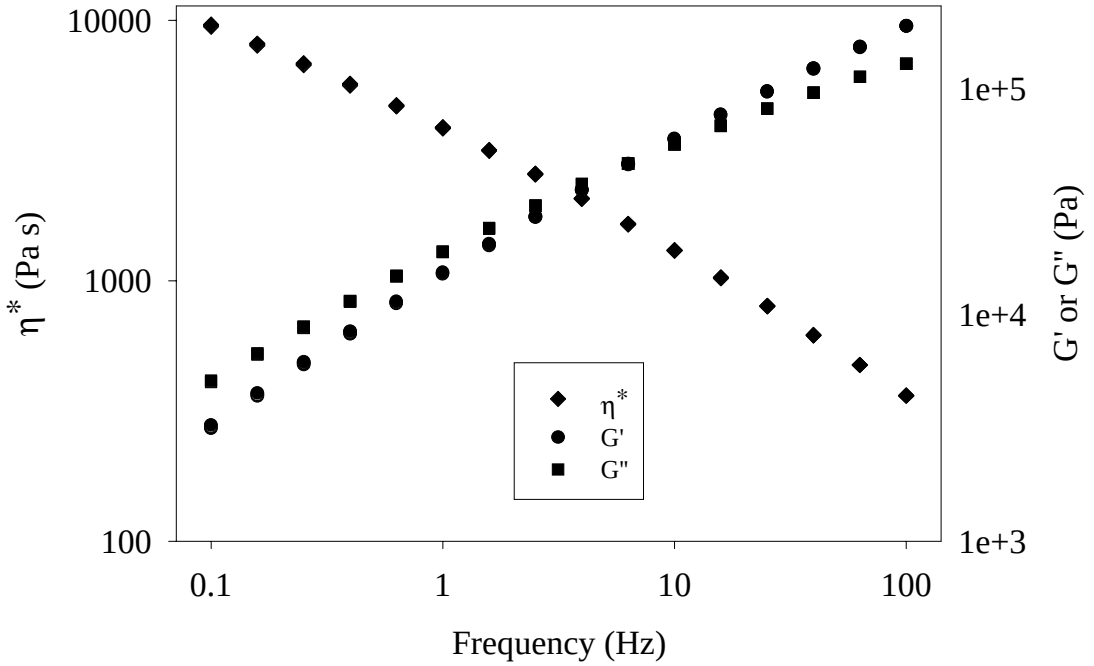

Figure 3.7 – Typical Oscillatory Shear Responses of Polyethylene

Table 3.3 – Percentage Errors Associated with Oscillatory Shear Responses

Frequency	η* (Pa s) (± %)*	G' (Pa) (± %)*	G'' (Pa) (± %)*
0.1	2.64	3.90	2.13
1	1.33	2.06	0.87
10	0.76	1.11	0.63
100	0.56	0.55	0.59

* Calculated at a 95% confidence level with 3 samples.

Chapter 4

Using Alkylaluminum Activators to Tailor Short Chain Branching Distributions of Ethylene/1-Hexene Copolymers Produced with In-Situ Supported Metallocene Catalysts

4.1 Introduction

Olefin copolymerizations with homogeneous and some supported metallocene catalysts can produce copolymers with narrow molecular weight distributions and narrow comonomer distributions (1). Industrial methods to tailor molecular weight distribution (MWD) and short chain branching distribution (SCBD) typically involve tandem or cascade reactors that produce the desired polymer depending on the polymerization conditions in each reactor (2). Another method includes the use of combined catalyst systems where each catalyst produces polymer with different properties (3-4). With either method, the idea is to design polymer resins with controlled MWD and SCBD for the desired end-use (5).

We have recently illustrated the use of an in-situ supported metallocene catalyst that eliminates the need for a metallocene supporting stage. This catalyst system is prepared directly in the polymerization reactor by the simultaneous addition of a homogeneous metallocene solution, a pretreated silica support with impregnated MAO (supplied from Witco), and an alkylaluminum activator such as trimethylaluminum (TMA), followed by the addition of ethylene. Note that no other preparation steps are involved and no aging is required. This in-situ system combines metallocene supporting and polymerization in one step and produces polyethylene and ethylene/α-olefin copolymers with high activities, good polymer morphology and minimal reactor fouling (6-7).

In this study, ethylene/1-hexene copolymerizations were carried out with in-situ supported rac-(ethylenebis(indenyl))zirconium dichloride. The effect of different alkylaluminum activators on the copolymerization characteristics and resulting copolymer microstructure (MWD and SCBD) was examined. The exact role of activators such as trimethylaluminum (TMA), triethylaluminum (TEA) and triisobutylaluminum (TIBA) in catalytic systems is unclear

in the literature. It has been suggested that TMA is the actual cocatalyst since methylaluminoxane (MAO) formulations always contain varying amounts of residual TMA (8). Others have reported that these activators can affect molecular weight, activity, stereoregularity and comonomer incorporation (9-14). With the in-situ supported catalyst mentioned above, it has been suggested that TMA acts as scavenger, alkylating agent and catalyst activator (6).

With this in-situ supported system, we have observed some unique effects of different activators on the microstructures of the polymers formed. By mixing different activators we illustrate a method to modify this catalyst system to produce ethylene/1-hexene copolymers with tailored SCBDs while maintaining narrow MWDs.

4.2 Experimental

Rac-(ethylenebis(indenyl))zirconium dichloride ($Et[Ind]_2ZrCl_2$) was purchased from Aldrich Chemicals. Silica supported methylaluminoxane (SMAO, 24.4 wt% Al, purchased from Witco) was used as a catalyst support. CP grade ethylene and ultra high purity nitrogen (purchased from Linde) were purified by passing through molecular sieves and de-oxygenating beds. Ultra high purity hydrogen was used without further purification. 1-hexene was dried over 3A/4A molecular sieves and used without further purification.

Toluene was purified by refluxing over n-butyl lithium/styrene oligomers and by distillation. n-Hexane was dried over a mixture of 3A/4A molecular sieves (purchased from BDH) and degassed by bubbling with nitrogen.

Trimethylaluminum (TMA), triethylaluminum (TEA) and triisobutylaluminum (TIBA) were purchased from Aldrich Chemicals and used without further purification.

4.2.1 Polymerization

Polymerizations were performed in a 300 mL Parr semi-batch autoclave reactor equipped with a temperature control unit comprising of a cooling coil and electric heater. 150 mL of hexane was pretreated with 2.46 mmol of TMA, TEA, TIBA or mixtures of each, to scavenge impurities and activate the catalyst. After evacuation of the reactor and backfilling with nitrogen, approximately 50 mL of hexane was added. This was followed by the addition of 0.3 g SMAO and 6μmol of $Et[Ind]_2ZrCl_2$ (solution in toluene). 5 mL 1-hexene (30 mol % feed in hexane) was added to the reactor via a transfer syringe. The reactor was then heated to the polymerization temperature of 60°C. Once the reaction temperature was reached, a stirring rate of 400 rpm was set and the reactor was pressurized with ethylene to begin the polymerization.

After 20 min, the polymerization was quenched with an excess of ethanol. The resulting polymer was then filtered, washed and dried at 60°C under vacuum.

4.2.2 Characterization

Molecular weight distributions were determined by high temperature gel permeation chromatography (GPC). A Waters GPCV 150+ instrument with a Viscotek 150R viscometer was used with 1,2,4-trichlorobenzene as a mobile phase operating at 140°C. Short chain branching distributions were determined by crystallization analysis fractionation using a CRYSTAF 200 instrument (Polymer Char, Valencia, Spain). CRYSTAF is a technique similar to temperature rising elution fractionation (TREF), but with significantly shorter analysis time (15,16). 1-hexene comonomer compositions were determined using FTIR (Bomem 102) and a calibration curve constructed based on the ratio of the 1380/1370 cm^{-1} peaks from the polymer as demonstrated in the literature (17). Melting endotherms were determined using a TA 2100 differential scanning calorimeter (DSC). Two scans were performed. The first scan was to erase the thermal history of the sample by the DSC cycle of melting followed by cooling with air. The second scan was at a heating rate of 10°C/min and from this scan the temperatures were recorded.

4.3 Results and Discussion

Results from the polymerizations with the three different activators are shown in Tab. 4.1 (runs 1a-3a) and a summary of all runs performed is shown in Tab. 4.2. These runs were carried out under similar polymerization conditions and limited to low polymer yields to minimize the drift in comonomer concentration. The polymerizations only differed in the type of activator (unless indicated otherwise). Under these polymerization conditions, the copolymers were produced with reasonable activities and exhibited good powder morphology with minimal fouling of the reactor. As reported previously, these are some of the major benefits of in-situ supported metallocene catalysts (6,7).

From the GPC analysis, it was found that the molecular weight distributions of the copolymers were fairly narrow and within a moderate range (refer to Tab. 4.1). The molecular weight distributions for these copolymers are shown in Fig. 4.1. It can be seen that the molecular weight distributions are unimodal and similar in shape. The polymer produced by TIBA seemed to result in the highest molecular weight followed by TMA and then by TEA. This same trend has been observed by Michiels et al. and it was suggested that bulkier alkyl ligands in the aluminum compound reduce the termination by chain transfer to aluminium (10). Others have also observed that TIBA produces higher molecular weight polymer when used with homogeneous metallocenes (12-14) and supported metallocene catalysts (9,11).

Upon comparison of the polymer yields from these activators, it seems that TMA exhibited the highest activity while TEA and TIBA had significantly lower activities. The explanation for the observed decrease in activity is unclear but it may be linked to the reduction in alkylation ability of the activators or steric hindrance due to increasing molecular size. Due to the increasing bulkiness of these activators it is possible that access to the catalyst on the support

is limited reducing the number of active sites. These polymerizations have been replicated and are also shown in Tab. 4.2 (runs 1b, 2b). A plausible polymerization mechanism explaining the role of the alkylaluminum activator as a scavenger, alkylating agent and catalyst activator with in-situ supported metallocenes has been reported by Chu et al. (6).

CRYSTAF results for these copolymers are shown in Fig. 4.2. The results shown are remarkable, since the SCBDs of copolymers produced with different activators exhibit rather broad and very different distributions. One would expect copolymers produced with homogeneous or supported single site metallocenes to have narrow SCBDs (18). This is clearly not the case for in-situ supported metallocenes. TMA-activated $Et[Ind]_2ZrCl_2$ shows a broad unimodal SCBD with a small shoulder in the high crystalline region. For the TEA and TIBA cases, the SCBDs are bimodal and similar in shape; both show polymer chains in the medium (~40-70°C) and high crystalline regions (>70°C). It seems that 1-hexene incorporation is higher when an activator with greater acidity or smaller molecular size (i.e. TMA) is used with $Et[Ind]_2ZrCl_2$. This observation is also confirmed by the FTIR and DSC results in Tab. 4.1. The corresponding melting endotherms are shown in Fig. 4.3 for comparison. As seen, the polymers exhibited broad melting distributions but the broad SCBD samples (TEA and TIBA) had both a distinct melting peak and a plateau indicating a very nonuniform crystallite distribution. Broad distributions were observed for both the TEA and TIBA cases. Since MAO is known to contain residual amounts of TMA (8), it is quite possible that these broad SCBDs are due to the presence of both TMA and TEA, or TMA and TIBA, which individually possess different comonomer incorporation characteristics.

For comparison, conventional homogeneous polymerizations were carried out with $Et[Ind]_2ZrCl_2$, methylaluminoxane and the different activators. The SCBDs of these polymers

Table 4.1. Ethylene/1-hexene copolymerizations with Et-$[Ind]_2ZrCl_2$ and different activators

Run	Activator	Activity[a] (kg PE/ mol·cat·atm·hr)	$\overline{M}_w$[b] (g/mol)	$\overline{M}_w/\overline{M}_n$	1-hexene composition[c] (mol % in copolymer)	Melting Peak (°C)[d]
1a	TMA	795.5	113,300	3.5	3.7	112.9
2a	TEA	163.8	85,000	2.4	3.0	120.6
3a	TIBA	63.5	146,100	2.2	2.9	118.3

[a] Polymerization conditions: $[Et(Ind)_2ZrCl_2]$ = 40 μmol/L, Al/Zr = 500, activator amt. = 2.46 mmol, ethylene pressure = 100 psig, [1-hexene] = 30 mol % feed (5 mL), temperature = 60°C, time= 20-30 min, stirring rate = 350 rpm

[b] As determined by GPC using narrow polystyrene standards and the universal calibration curve

[c] As determined by FTIR from 1-hexene calibration curve based on 1380/1370 cm^{-1} peak ratios (17)

[d] As determined by DSC. Note that these samples exhibited very broad melting distributions.

Table 4.2. Summary of results of ethylene/1-hexene copolymerizations with Et-[Ind]$_2$ZrCl$_2$ and different activators

Run	Conditions	Activator	Activity[a] (kg PE/ mol cat atm hr)	$\overline{M}_w$[b] (g/mol)	$\overline{M}_w/\overline{M}_n$
1a	In-situ	TMA	795.5	113,300	3.5
2a	In-situ	TEA	163.8	85,000	2.4
3a	In-situ	TIBA	63.5	146,100	2.2
1b	In-situ	TMA	745.9	112,100	3.7
2b	In-situ	TEA	183.8	55,600	1.9
4[c]	In-situ (1hr)	TEA	156.6	69,500	2.2
4[d]	Homo	TMA	2994.1	99,900	1.9
5[d]	Homo	TEA	4341.7	80,200	1.8
6[d]	Homo	TIBA	3000.0	105,800	2.2
7[e]	In-situ (w/ 50 ml H_2)	TMA	804.3	65,700	3.3
8[e]	In-situ (w/ 50 mL H_2)	TEA	57.2	67,700	3.2
9[e]	In-situ (w/ 50 mL H_2)	TIBA	67.2	74,900	3.0
10	In-situ	50 % TMA/ 50% TEA	446.1	91,400	2.6
11	In-situ	25% TMA/ 75%TEA	227.9	58,400	2.1
12	In-situ	50% TMA/ 50% TIBA	204.9	90,900	2.3
13	In-situ	10% TMA/ 90 % TIBA	118.1	103,700	2.2

[a] Polymerization conditions: [Et(Ind)$_2$ZrCl$_2$] = 40 μmol/L, Al/Zr = 500, activator amt. = 2.46 mmol, ethylene pressure = 100 psig, [1-hexene] = 30 mol % feed (5 mL), temperature = 60°C, time= 20-30 min, stirring rate = 350 rpm

[b] As determined by GPC using narrow polystyrene standards and the universal calibration curve

[c] Copolymerization with TEA activator for 60 min

[d] Homogeneous polymerization conditions: [Et(Ind)$_2$ZrCl$_2$] = 2 μmol/L, MAO/Zr = 500, activator amt. = 0.123 mmol, ethylene pressure = 100 psig, temperature = 60°C, time = 20 min, stirring rate 350 rpm

[e] Copolymerization with the addition of 50 mL H_2

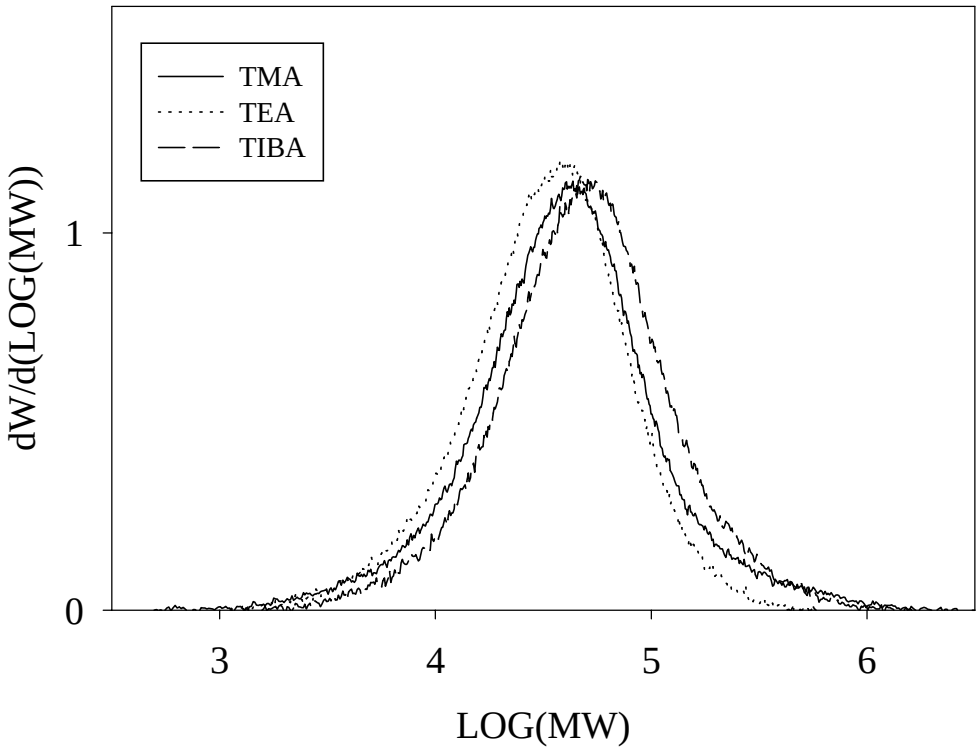

Figure 4.1 – Molecular weight distributions of ethylene/1-hexene copolymers produced with different activators

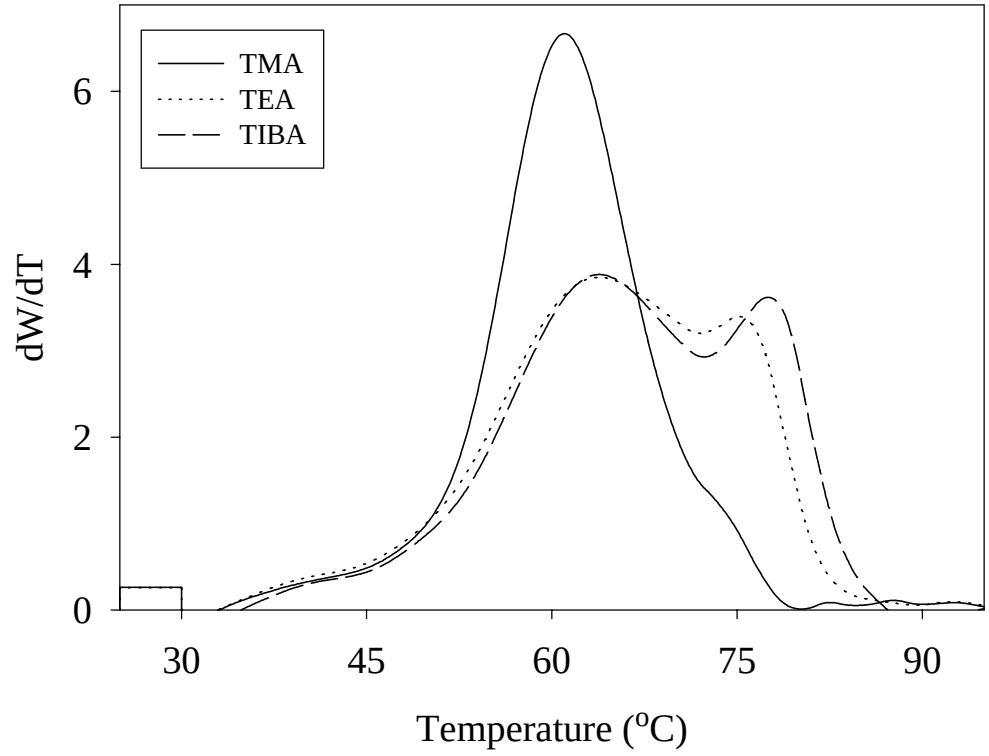

Figure 4.2 – Short chain branching distributions of ethylene/1-hexene copolymers produced with different activators

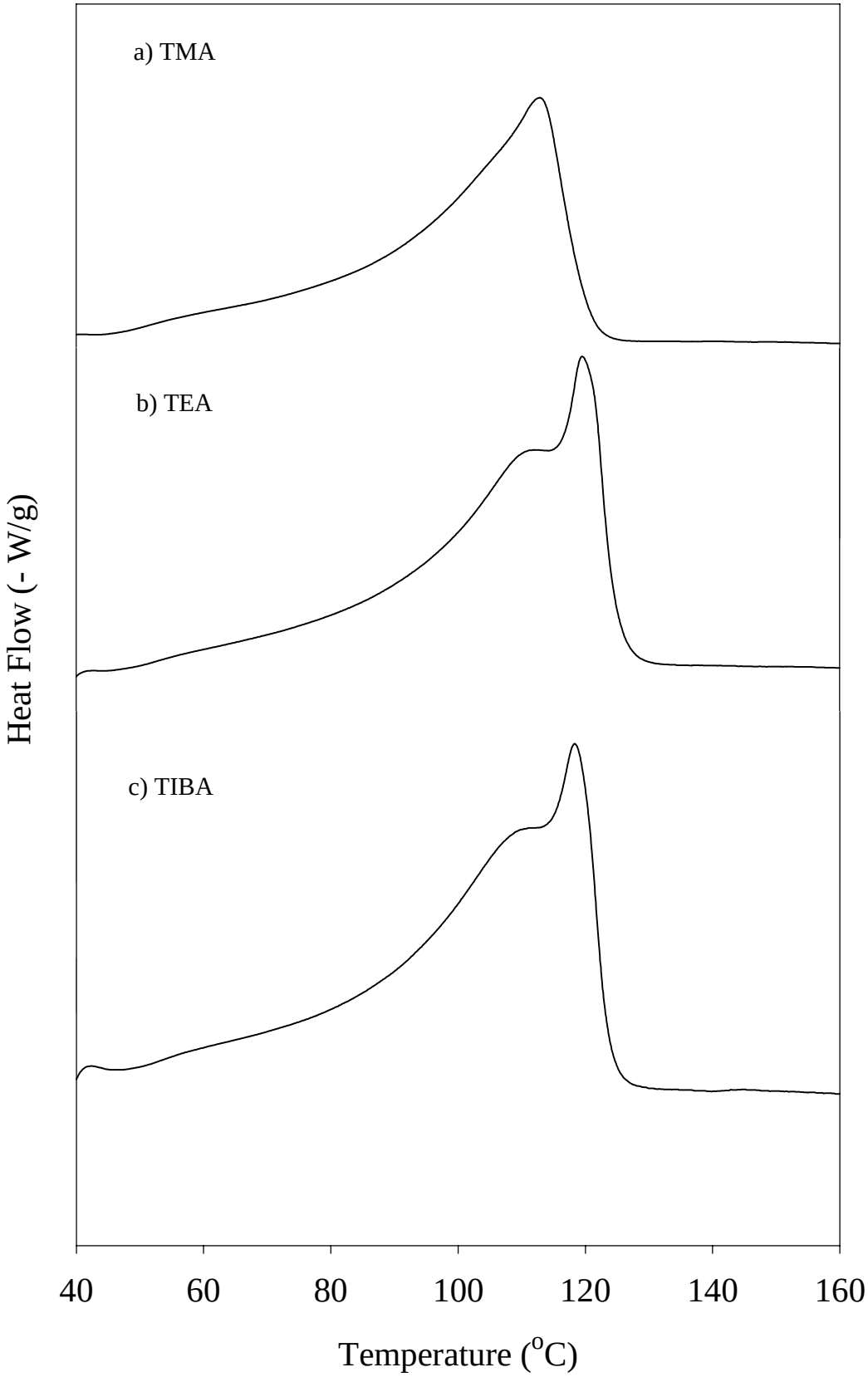

Figure 4.3 – Melting endotherms of ethylene/1-hexene copolymers produced with different activators

are shown in Fig 4.4 (6). As expected from homogeneous copolymerization with single-site-type catalysts, the resulting distributions are unimodal and narrow. In comparison with the bimodal SCBDs produced with the in-situ supported catalysts, the comonomer incorporation did not vary with activator type. The comparison of these two systems may be hinting that the bulkiness of the alkylaluminum activator can interact with the catalyst support to affect the comonomer incorporation and polymerization activity. Homogeneous systems would be less susceptible to effects of diffusion due to steric hindrances.

To examine the effect of time on the polymerization, a comparison of run 2a (20 min) with run 4 (1 hr) with TEA as an activator is shown in Fig 4.5. As shown, the resulting SCBDs are similar and vary slightly with time. The variation of SCBD with time may be due to a slight drift in comonomer concentration, since 1-hexene concentration decreases with polymerization time.

To examine the effect of hydrogen on the copolymerization characteristics of the in-situ system, polymerizations were carried out with the different activators in the presence of some hydrogen. As can be seen in Tab. 4.2 (runs 7,8,9), the addition of hydrogen lowered the molecular weights of the copolymer formed, as usual with these catalysts. More remarkably, hydrogen affects the SCBDs of the resulting copolymers as shown in Fig 4.6. The SCBDs produced were broad but no longer bimodal (compare with Fig. 4.2.). This indicates that hydrogen can alter the nature of the active sites of the catalyst, affecting their comonomer incorporation characteristics.

These results are quite unusual for copolymers made with metallocene catalysts. Notice that the SCBDs obtained with TEA and TIBA in absence of hydrogen are similar to the ones of

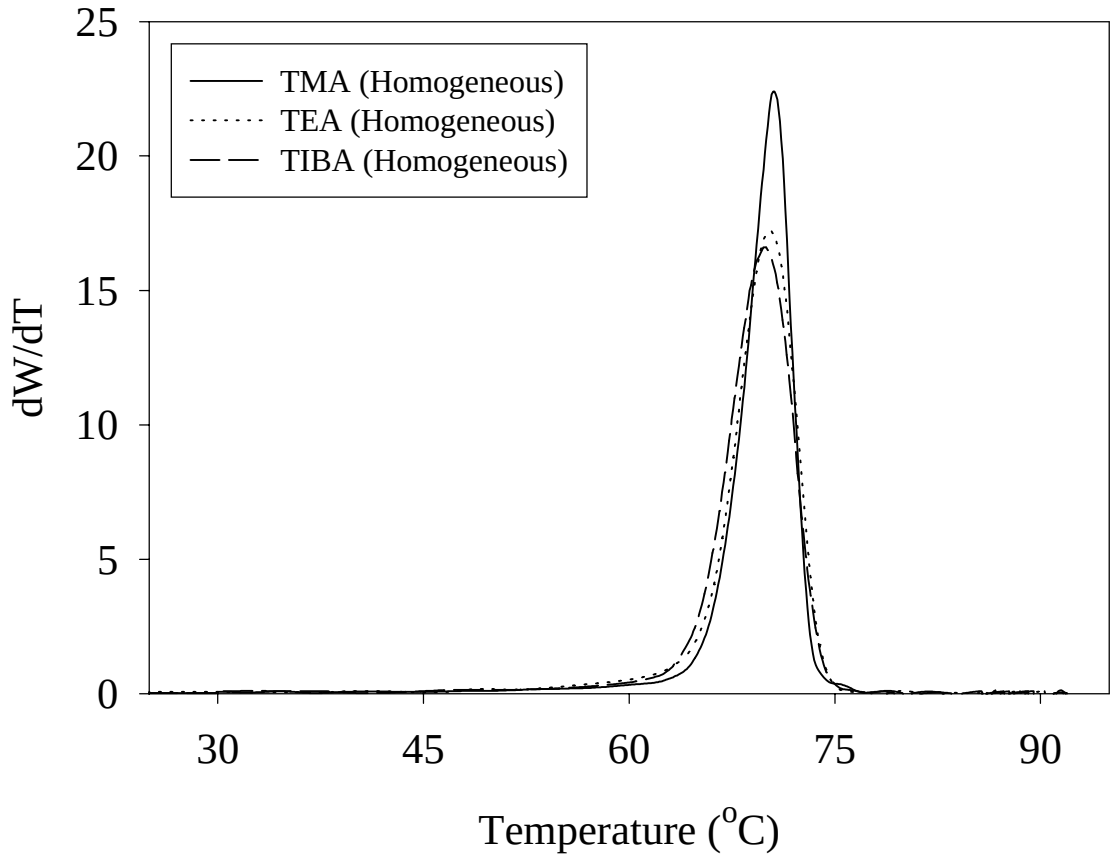

Figure 4.4 – SCBDs of ethylene/1-hexene copolymers produced with different activators under homogeneous polymerization conditions

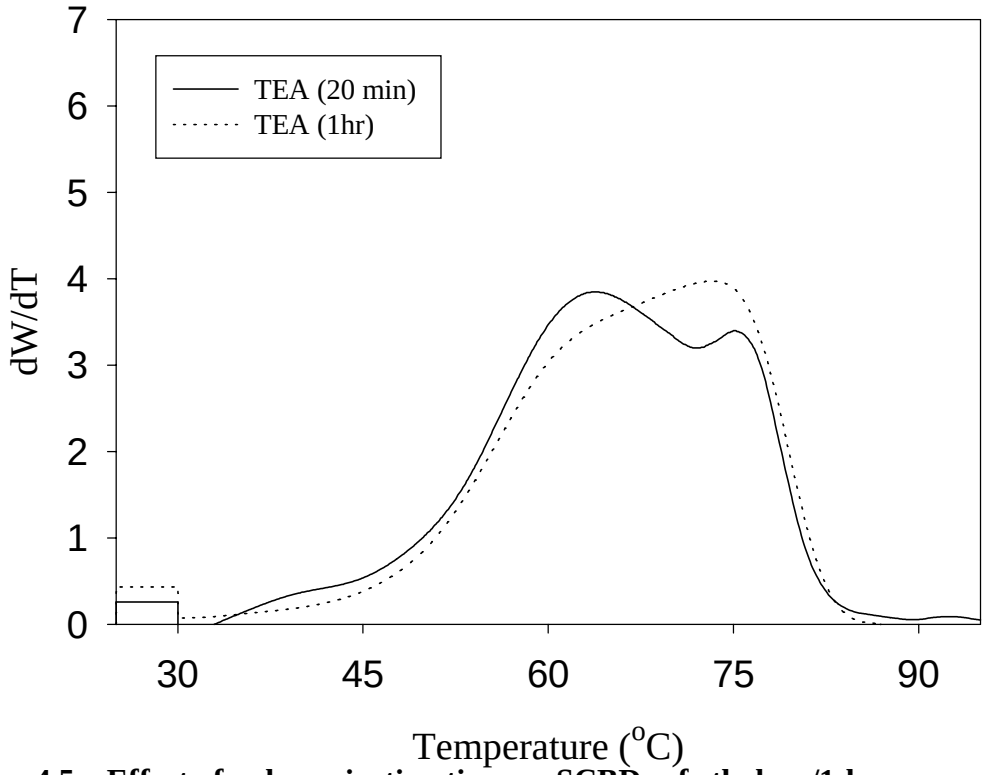

Figure 4.5 – Effect of polymerization time on SCBDs of ethylene/1-hexene copolymers produced with TEA

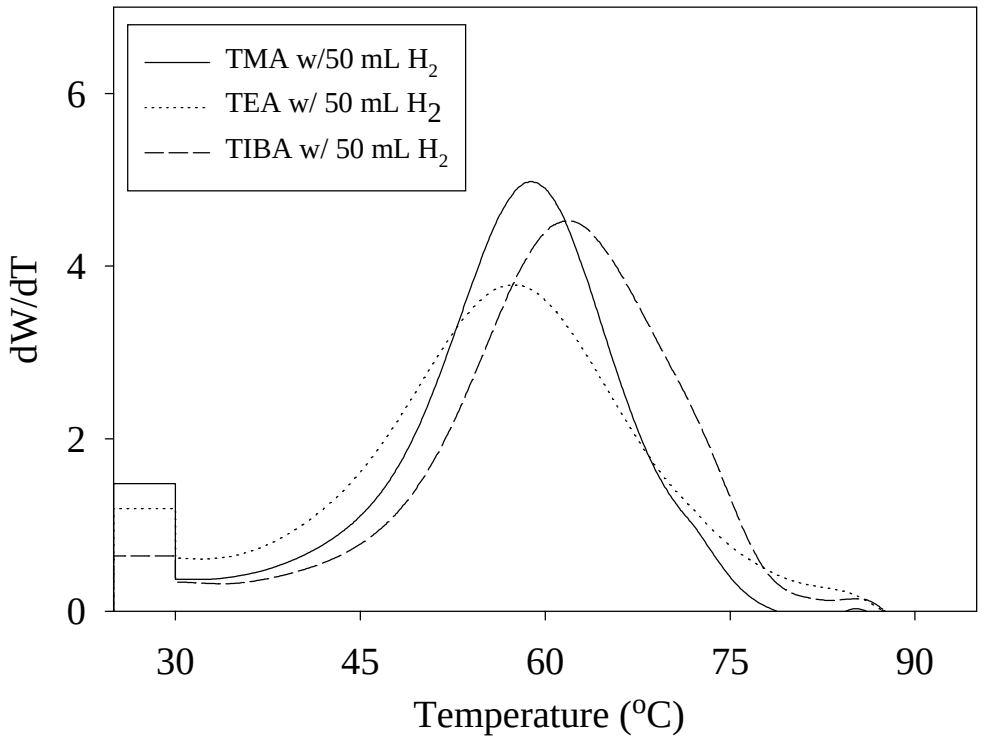

Figure 4.6 – Effect of H_2 on the SCBDs of ethylene/1-hexene copolymers produced with different activators

LLDPE resins produced with Ziegler-Natta catalysts. This would indicate that multiple active sites are being formed. The formation of multiple active sites with a single activator that exhibits different comonomer incorporation characteristics is unreported to our knowledge for a MAO-treated silica support. However, Soga et al. has reported the synthesis of ethylene/propylene/1-hexene copolymers with appreciable amounts of homopolymer with a $Et[IndH_4]_2ZrCl_2$/MAO/$MgCl_2$-TIBA system and have suggested possible interaction between TIBA and $MgCl_2$ (9). Another remarkable feature of these results is that the molecular weight distributions are unimodal, relatively narrow and only slightly varying with activator type. These different activators can be used to tailor SCBDs of the copolymers while maintaining similar MWDs. By mixing different activators, it may be possible to control the SCBDs of the resulting copolymers. Copolymerizations were carried out with mixtures of each activator with varying amounts of TMA and TEA, or TMA and TIBA. The total molar amount of alkylaluminum added was kept constant and consisted of mixtures of TMA and TEA (runs 10-11) or TMA and TIBA (runs 12-13). The SCBDs of copolymers made with these mixed activator systems are shown in Fig. 4.7 for the TMA/TEA system and Fig. 4.8 for the TMA/TIBA system. As shown, the mixing of activators produces SCBDs that are consistent based on the observations with single activators. By increasing the level of either TEA or TIBA with TMA, the proportion of the high crystalline material can also be increased while retaining a large portion of lower crystalline material. The activities of these polymerizations are plotted in Fig. 4.9. As shown, the activity decreased with increasing amount of either TEA or TIBA, confirming the previous observations in Tab. 4.1. The corresponding MWDs for the mixed activated copolymers were similar and narrow (see Tab. 4.2.). For the TMA/TEA case, a decrease in MW was observed with an increase in TEA in the mixture which is consistent with

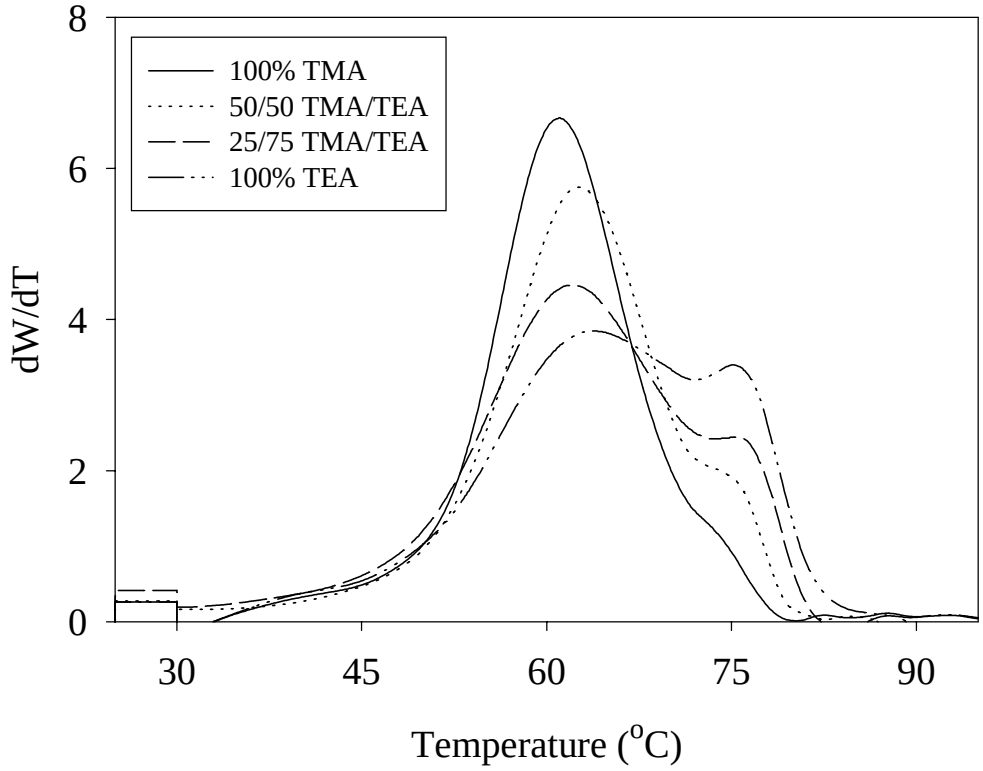

Figure 4.7 – SCBDs of ethylene/1-hexene copolymers produced with mixtures of TMA and TEA activators

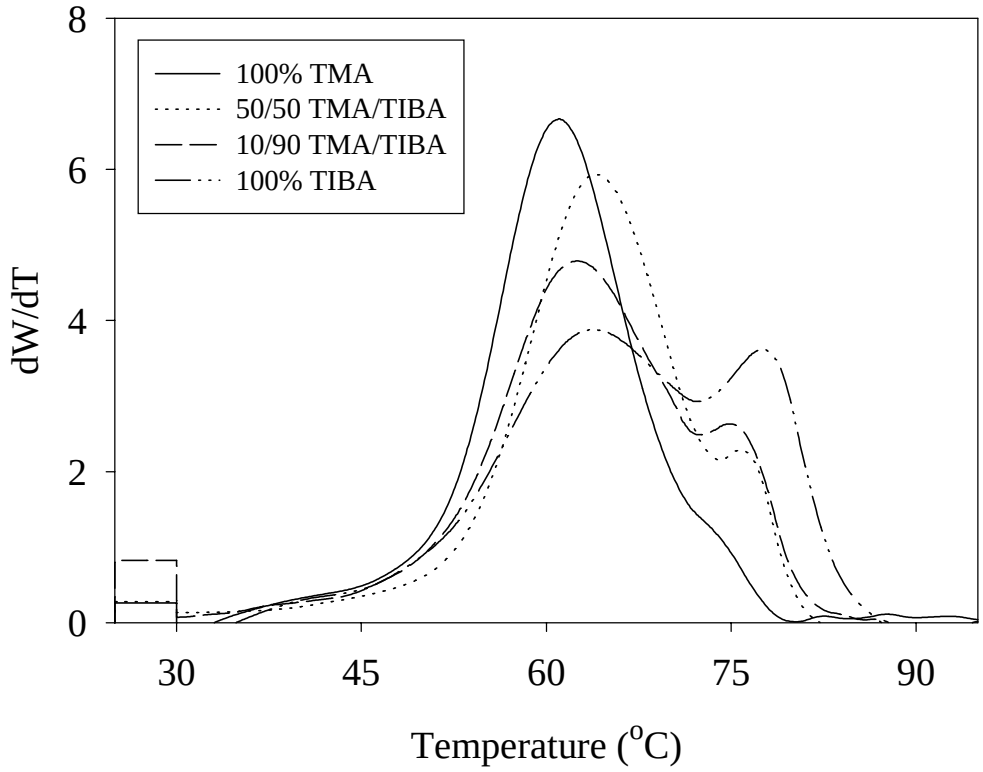

Figure 4.8 – SCBDs of ethylene/1-hexene copolymers produced with mixtures of TMA and TIBA activators

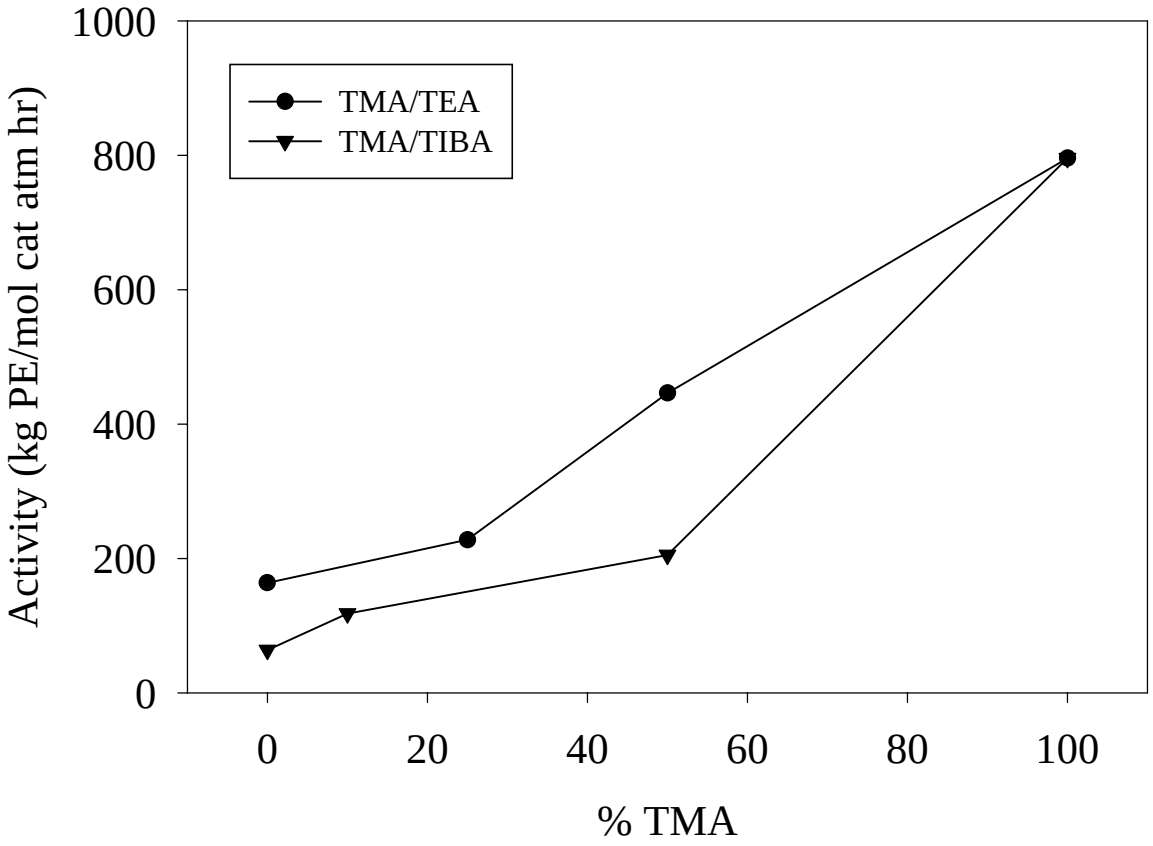

Figure 4.9 – Polymerization activity of ethylene/1-hexene copolymers produced with mixtures of TMA/TEA and TMA/TIBA activators

the earlier findings that TEA produces lower MW polymer than TMA. Similarly, for the TMA/TIBA case, an increase in MW was observed with increasing TIBA in the mixture, which is also consistent in that TIBA produces higher MW polymer.

To examine whether the sites created by the different activators are independent of each other, predictions of the resulting SCBDs were calculated from the data available for polymerizations with each individual activator. If each active site generated by each activator behaves independently from the other activators present in the reactor, then the activities reported in Tab. 4.1 for each activator and the mixing molar fraction can be used to estimate the fraction of polymer produced by each site (activator) type:

$$x^{*}_{TEA\ \text{or TIBA}} = \frac{x_{TEA\,\text{or}\,TIBA}(Activity_{TEA\,\text{or}\,TIBA})}{x_{TEA\,\text{or}\,TIBA}(Activity_{TEA\,\text{or}\,TIBA}) + x_{TMA}(Activity_{TMA})} \qquad (1)$$

As an example for a 50/50 TMA/TEA mixture:

$$x^{*}_{TEA} = \frac{0.5(163.8)}{0.5(163.8) + 0.5(795.5)}$$
$$= 0.17$$
$$x^{*}_{TMA} = 1 - x^{*}_{TEA}$$
$$= 0.83$$

where $x^{*}_{TEA,TMA}$ is the estimated fraction of polymer produced by each activator.

The predicted fractions for the mixing experiments are listed in Tab. 4.3. Using the fractions determined from equation (1), predictions of the resulting SCBDs were made. These predicted SCBDs were calculated as the summation of the individual SCBDs with the appropriate weighting fraction x_{TMA} as shown in equation 2. Note that the f(T) represents the SCBD data as values of dW/dT as a function of temperature (T).

$$f_{predicted}(T) = x^{*}_{TMA}\ f_{TMA}(T) + (1 - x^{*}_{TMA})\ f_{TEA\,\text{or}\,TIBA}(T) \qquad (2)$$

Table 4.3. Comparison of Experimental and Calculated Mixing Ratios of Mixed Activated Systems

Actual Mixing Ratio	Predicted[a]		Fitted[b]	
	% TMA	% TEA,TIBA	% TMA	% TEA,TIBA
50/50 TMA/TEA	83	17	62	38
25/75 TMA/TEA	62	38	33	67
50/50 TMA/TIBA	93	7	49	51
10/90 TMA/TIBA	58	42	43	57

[a] Predicted mixing ratio taking into account activity of each activator calculated from equation (1)
[b] Fitted mixing ratio determined from the minimization of equation (4)

A comparison of the predicted and experimental SCBDs for the TMA/TEA mixtures is shown in Fig. 4.10, and for the TMA/TIBA mixtures in Fig. 4.11. As shown in the TMA/TEA and TMA/TIBA cases, the calculated SCBDs under predict the experimental SCBDs. It is seen that the peak at 60°C, presumably produced mostly by the TMA activator, clearly dominates. As shown in Tab. 4.3, the predicted fraction produced by TMA is quite large and is heavily weighted in the predicted SCBD. This heavy weighting is due to the high polymerization activity of the individual TMA activator. In Fig. 4.12, the predicted polymerization activities are compared with the experimental activities of the mixed activated copolymerizations. The predicted polymerization activity was calculated based on the activities of the individual activators and the actual mixing ratio:

$$activity_{predicted} = x_{TMA}(activity_{TMA,100\%}) + x_{TEA\ or\ TIBA}(activity_{TEA\ or\ TIBA,100\%}) \quad (3)$$

It was observed that, in all the mixed activator experiments, the resulting polymerization activity was lower than the predicted ones. This indicates that the two site types do not behave independently of each other.

To obtain a better estimate of the fraction of polymer produced by each site, each of the mixed SCBDs were fitted with a summation of the two individual SCBDs. The fitted fraction was determined by minimizing the squared difference between the actual distribution and the summed distribution of individual SCBDs of TMA and TEA or TMA and TIBA. Using the Generalized Reduced Gradient (GRG2) nonlinear optimization method located in Microsoft Excel Software package, estimates of the polymer fractions X_{TMA} and $X_{TEA\ or\ TIBA}$ that would best describe the experimental SCBDs were determined. These were obtained with iterations of values for X_{TMA}, equation (2), to calculate the predicted SCBD and the minimization of the squared difference of the experimental and predicted SCBD with equation (4).

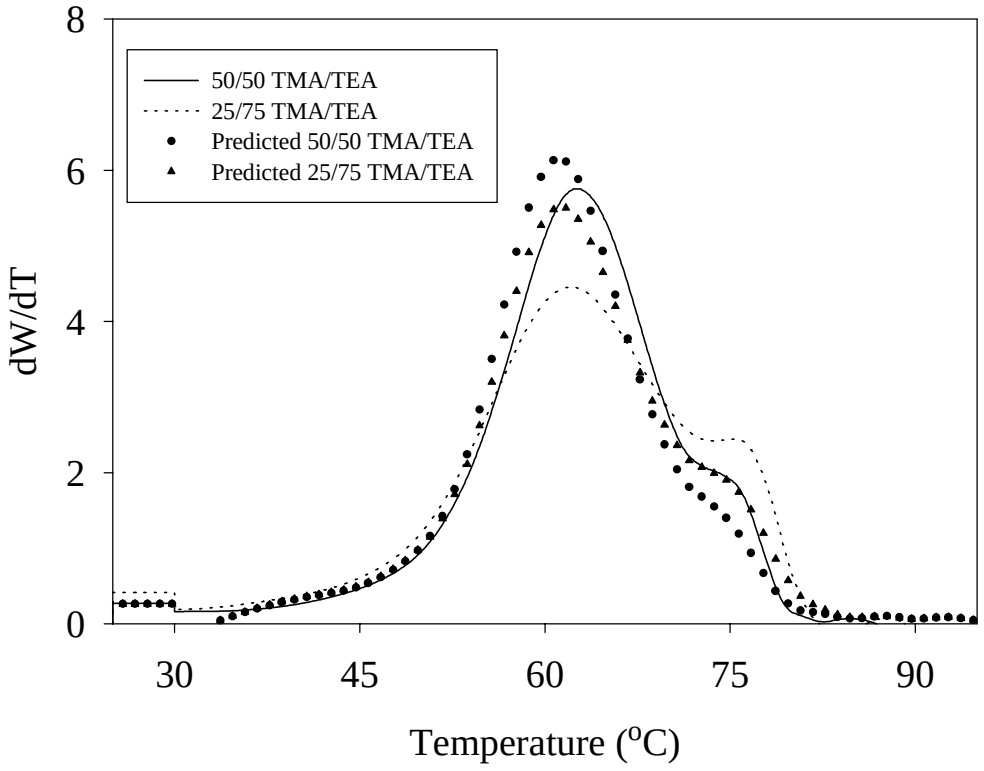

Figure 4.10 – Comparison of actual and predicted SCBDs of ethylene/1-hexene copolymers produced with mixtures of TMA and TEA activators

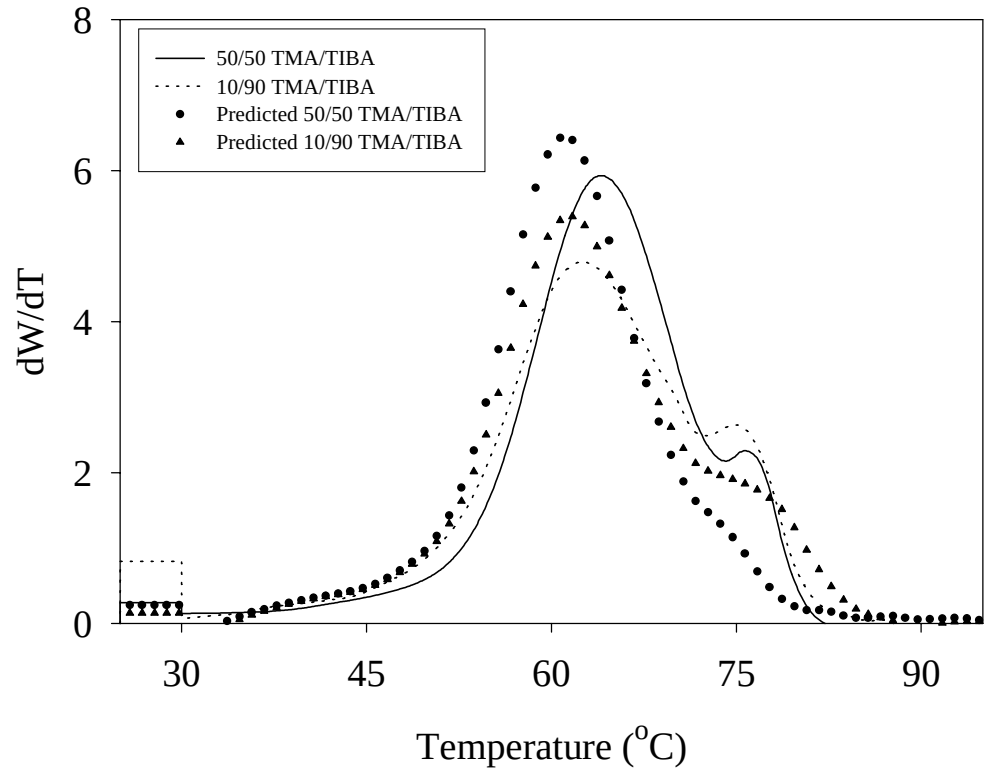

Figure 4.11 – Comparison of actual and predicted SCBDs of ethylene/1-hexene copolymers produced with mixtures of TMA and TIBA activators

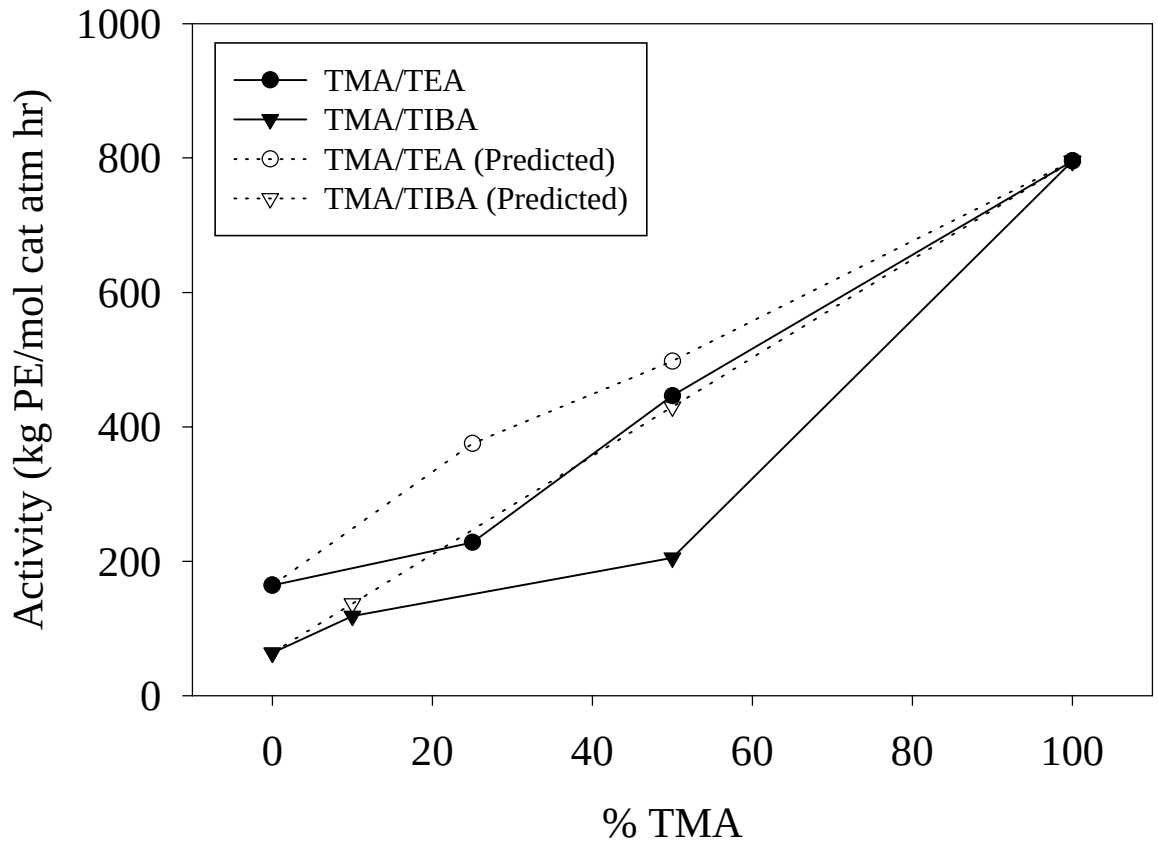

Figure 4.12 – Comparison of actual and predicted polymerization activity of ethylene/1-hexene copolymers produced with mixtures of activators

$$\sum (f_{\text{exp erimental}}(T) - f_{predicted}(T))^2 \quad (4)$$

A comparison of the experimental SCBDs and fitted SCBDs is shown in Fig. 4.13 and Fig. 4.14 for TMA/TEA and TMA/TIBA, respectively. For the TMA/TEA and TMA/TIBA cases, the calculated SCBDs represent the experimental mixed SCBDs better but there is some evidence of lack of fit in the region of the high crystalline tail. As shown in Tab. 4.3, the fitted fraction of polymer produced by the TMA activator is clearly less than the fraction estimated from the catalyst activity data alone. These fitted fractions are more representative of the actual polymer produced by each activator site since they were estimated from the SCBD of the polymer sample. A plot comparing the experimental activities (calculated with equation 3) and the estimated activities using the fitted fractions is shown in Fig. 4.15. As seen, the estimated activities are much higher than the experimental ones. Once again, this indicates that sites activated by mixtures of activators can interact with each other to behave differently than the ones activated by individual activators. The nature of this interaction may be linked to the electronic environment that is present around the active site which is probably altered by the presence of different activators. To account for the experimental SCBDs, a comparison of the predicted fractions to the fitted fractions in Tab. 4.3 indicates that the active sites generated in the mixed system exhibit different activities from the individual ones. It can be inferred that the polymerization activity of the TMA activated sites was supressed and the TEA or TIBA activated sites enhanced by the presence of each other. Therefore, it is evident that the active sites produced by each activator are not independent of each other and the interaction between the sites can alter the comonomer incorporation characteristics of the catalyst.

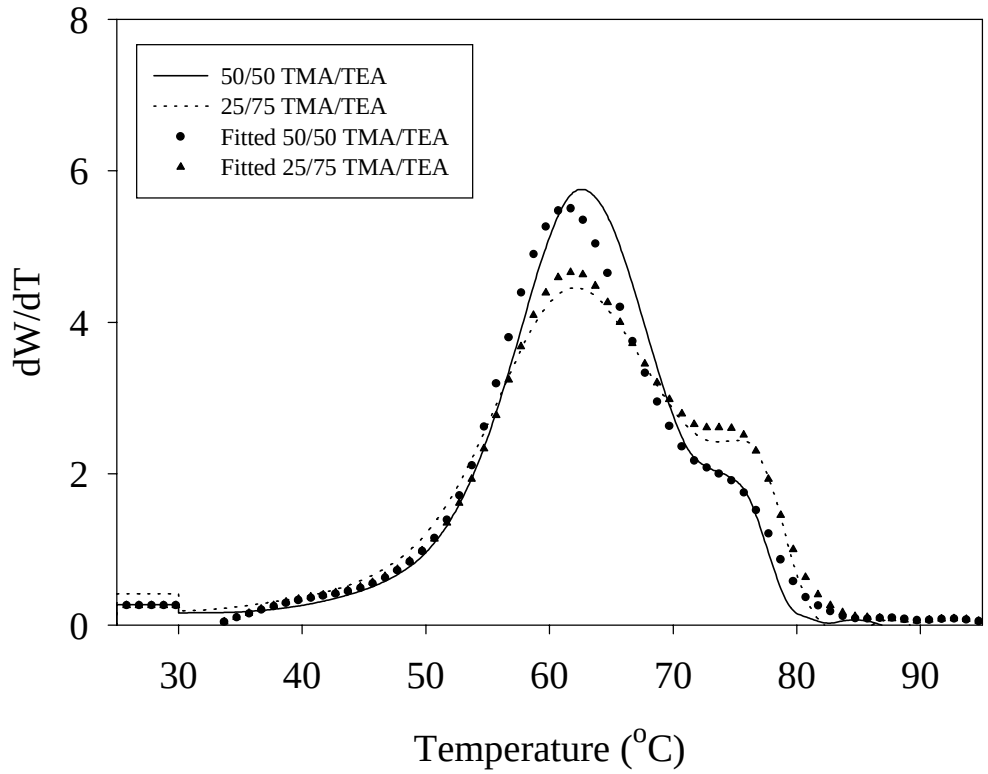

Figure 4.13 – Comparison of actual and fitted SCBDs of ethylene/1-hexene copolymers produced with mixtures of TMA and TEA activators

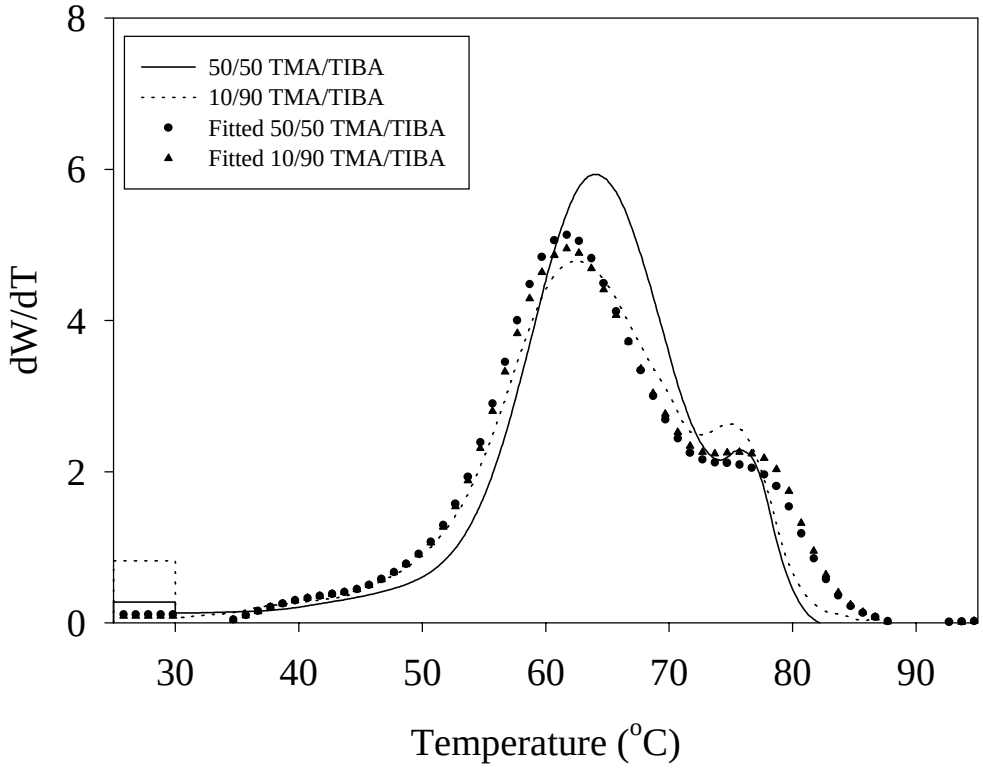

Figure 4.14 – Comparison of actual and fitted SCBDs of ethylene/1-hexene copolymers produced with mixtures of TMA and TIBA activators

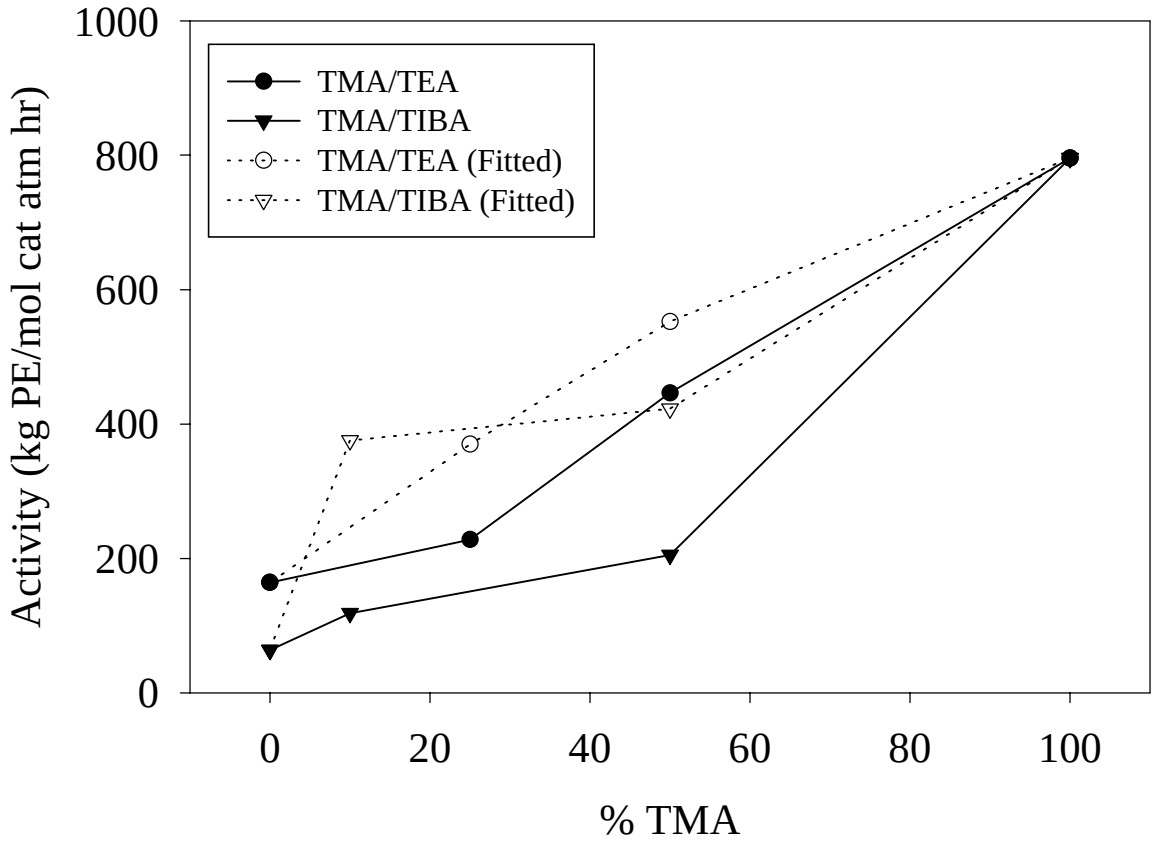

Figure 4.15 – Comparison of actual and fitted polymerization activity of ethylene/1-hexene copolymers produced with mixtures of activators

4.4 Conclusions

In-situ supported $Et[Ind]_2ZrCl_2$ can be used with different alkylaluminum activators to produce poly(ethylene-1-hexene) with narrow MWD, yet broad and bimodal SCBD. These findings are different from the ones observed with homogeneous systems and not previously reported for supported systems. It has been shown that, with the use of individual and mixed activator systems, it is possible to manipulate the SCBDs of the resulting copolymers while maintaining similar MWDs. Attempts to make predictions of the resulting SCBDs *a priori* for a mixed activated system is difficult to quantify, since the behaviour of the sites can be altered in the presence of mixtures of activators. However, this method lends itself as a simple tool in tailoring SCBDs of ethylene/α-olefin copolymers made with in-situ supported metallocenes.

4.5 References

1) Brintzinger, H.;Fischer, D.;Mulhaupt, R.;Rieger,B.;Waymouth, R.M.; *Angew. Chem. Int. Ed. Engl.*, 34, 1143-1170 (1995).

2) Scheirs, J.;Bohm, L.L.; Bout, J.;Leevers, P.S.; *Trends in Polymer Science,* 4, 408-415 (1996).

3) Soares, J.B.P.;Kim, J.D.;Rempel, G.L.; *Ind & Eng. Chem. Res.*, 36, 1144-1150 (1997).

4) Heiland, K.;Kaminsky, W.; *Makromol. Chem.*, 193, 601-610 (1992).

5) Foster, G.N.;Wasserman, S.H.; *Worldwide Metallocene Conf., MetCon*, Houston, TX (1997).

6) Chu, K.J. ; Soares, J.B.P. ;Penlidis,A.*; J. Polym. Sci., Part A, Polym. Chem*, 38, 462-468 (2000).

7) Chu, K.J.;Li Pi Shan, C.;Soares, J.B.P.; Penlidis, A.; *Macromol. Chem. Phys.*, 200, 2372-2376 (1999).

8) Resconi, L. ;Bossi, S. ; Abis, L. ; *Macromolecules*, 23, 4489-4491 (1990).

9) Soga, K.; Kaminaka, M.; *Macromol. Chem. Phys.* 195, 1369-1379 (1994).

10) Michiels, W. ; Munoz-Escalona, A.; *Macromol. Symp.*, 97, 171-183 (1995).

11) Soga, K. ;Kaminaka,M.; *Macromol. Chem., Rapid Commun.*, 13, 221-224 (1992).

12) Forlini,F. ; Fan,Z.Q. ;Tritto,I. ;Locatelli,P. ;Sacchi, M.C. ;*Macromol. Chem. Phys.*, 198, 2397-2408 (1997).

13) Maciejewski-Petoff, J.L.; Myers, C.L.;Waymouth, R.M.; *Macromolecules*, 32, 7984-7989 1999).

14) Naga, N. ;Mizunuma, K. ; *Polymer*, 21, 5059-5067 (1998).

15) Monrabal, B.; *J. Appl. Polym. Sci*., 52, 491-505 (1994).

16) Monrabal, B.; *Macromol. Symp*., 110, 81-86 (1996).

17) Nowlin, T.E.; Kissin, Y.V.; Wagner, K.P.; *J. Polym. Sci., Part A, Polym. Chem*., 26, 755-764 (1988).

18) Harrison, D.;Coulter, I.M.;Wang,S.;Nistala, S.;Kuntz, B.A.;Pigeon, M.;Tian, J.;Collins, S.; *J. Mol. Catal.*,128, 65-77 (1998).

Chapter 5

Mechanical Properties of Ethylene/1-Hexene Copolymers with Tailored Short Chain Branching Distributions

5.1 Introduction

Recently, there has been an emphasis on developing relations between microstructure and end-use physical/mechanical properties of polyolefins. With the advent of metallocene catalysts for olefin polymerization, there have been many claims on the ability to produce polymer with tailored microstructural distributions. Correspondingly, these distributions also result in resins with tailored physical/mechanical properties.

In a previous publication, we have reported a catalytic method that demonstrated the use of a heterogeneous metallocene catalyst to control the short chain branching distribution (SCBD) of ethylene/α-olefin copolymers (1). By exploiting the multi-site behaviour of these catalysts, it was possible to produce resins with broad and bimodal short chain branching distributions but with similar and narrow molecular weight distributions. Ziegler-Natta LLDPE can also have a characteristically broad SCBD but the molecular weight distribution tends to be broader when compared to a metallocene-synthesized LLDPE (2). Typically, for Ziegler-Natta resins, the comonomer content of the copolymer decreases as the molecular weight of the polymer chains increases.

Industrial methods to tailor the molecular weight distribution and short chain branching distribution of a polyolefin typically involve tandem or cascade reactors which produce the desired polymer depending on the polymerization conditions of each reactor (3). Another method is to use combined catalyst systems, with each catalyst producing the desired polymer microstructural distribution (4). Conventionally, tailored physical properties can also be achieved by the compounding and blending of polymers with the desired characteristics. Unfortunately, the blending of polymers is very energy intensive and it is inherently difficult to achieve uniform mixing.

It is well known that the underlying microstructure of polymers plays a critical role in determining their physical and mechanical properties. For linear polyolefins such as poly(ethylene/α-olefin) copolymers, both the molecular weight distribution and comonomer distribution of the polymer chains influence the crystallinity and density of the samples (5-9). Above a critical molecular weight, it is sometimes found that the crystallinity will decrease with increasing molecular weight, due to the inability of the longer chains to be incorporated in the crystalline structure (10-12). More significantly, by increasing the number of short chain branches via incorporation of α-olefin comonomers such as 1-butene, 1-hexene, 1-octene, etc., the polymer's crystallinity and density can be reduced, since these side chains do not crystallize and are rejected into the amorphous or interfacial regions of the polymer (5,7). The interplay between molecular weight and comonomer distribution influences the proportions of crystalline and amorphous polymer that determine its crystalline microstructure. The crystallinity and crystal structure are not only influenced by the microstructure of the polymer but also by the processing conditions that dictate the polymer's thermal history (8,11). In terms of mechanical properties a polymer's crystallinity influences its stiffness and toughness. In general, as the polymer crystallinity decreases, its flexibility increases. By lowering the density with the incorporation of comonomer to promote short chain branching, the polymer's ability to absorb and dissipate energy also increases (5,6).

In this study, we have produced a series of ethylene/1-hexene copolymers with tailored crystalline distributions while maintaining similar MWDs. By eliminating the effect of molecular weight, it is possible to investigate the net effect of crystalline distributions on the properties of these resins. This series of resins with controlled SCBDs was produced for comparison of their tensile and dynamic mechanical properties.

5.2 Experimental

5.2.1 Sample Production

Ethylene-1-hexene copolymer samples were produced with an in-situ supported metallocene catalyst system (13). This in-situ system eliminates the need for a catalyst supporting stage by combining the catalyst preparation and polymerization in one-step. The resulting polymer has good particle morphology and high bulk density. These studies utilized rac-(ethylenebis(indenyl))zirconium dichloride (Strem Chemicals), a silica support with a high weight percent of methylaluminoxane (provided by Witco), and mixtures of trialkylaluminums such as trimethyl and triethyl aluminums. Slurry polymerizations with n-hexane as a solvent were carried out in a 1 L semi-batch autoclave reactor (Pressure Product Industries, LC Series) operating at 60°C and ethylene pressure of 150 psig. The initial concentration of 1-hexene in the reactor was 30 mol%. The polymerization runs were carried out under similar conditions and limited in such a way to minimize the drift in comonomer composition.

5.2.2 Microstructural Characterization

The polymer samples were characterized for their molecular weight distributions using a Waters 150CV high temperature gel permeation chromatograph (GPC) and a Viscotek 150R viscometer. The mobile phase used was 1,2,4 trichlorobenzene operating at 140°C.

Short chain branching distributions were determined by crystallization analysis fractionation (CRYSTAF) in 1,2,4 trichlorobenzene using a CRYSTAF 200 unit (Polymer Char, Spain). The samples were dissolved at 160°C for one hour and then cooled to 95°C to begin the analysis. The sampling temperatures ranged between 95°C to 30°C at a cooling rate of 0.2 °C/min. 1-Hexene comonomer compositions were determined by integrating the resulting

CRYSTAF profiles while applying a calibration curve to relate the crystallization temperature and 1-hexene composition (14). This calibration curve was previously determined by ^{13}C NMR.

Melting endotherms were determined using a TA 2100 differential scanning calorimeter (DSC). The samples were heated from 35 to 200°C at 10°C/min. To take into account the thermal history of the samples used for mechanical testing, the melting point and crystallinity were estimated from the first pass. The crystallinity was estimated by comparison of the DSC melting enthalpy to that of a perfect polyethylene crystal ($\Delta H \approx 289$ J/g) (9).

5.2.3 Mechanical Testing

5.2.3.1 Tensile Testing

Tensile properties were determined according to ASTM D638 using an Instron 4465 materials tester. Dog-bone shaped samples (type V) were melt-pressed at 200°C into a 3.175 cm mold plate and then air-cooled to room temperature. The samples were tested at a displacement rate of 25 mm/min and the grip-to-grip length was 3 cm. The sample yield and ultimate break strengths were determined from the force versus displacement curves during deformation of the sample. After testing, the increase in the gage length as compared to the original was used to determine the overall % elongation.

5.2.3.2 Dynamic Mechanical Analysis

Dynamic mechanical properties were measured by a Rheometrics DMTA V mechanical spectrometer. These samples were also melt pressed into rectangular bars (20mm x 10mm x 3mm) under the same conditions as reported above. Storage and loss moduli were measured in single cantilever mode over a temperature range of -150°C to 100°C at a scanning rate of

2°C/min, a frequency of 1Hz and a strain of 0.05%. Frequency sweeps were performed over the range of 0.1 to 100 Hz at room temperature and 0.05 % strain.

5.3 Results and Discussion

As discussed previously, it was found that with certain in-situ supported metallocene catalyst systems it is possible to control the short chain branching distribution of ethylene copolymers by simply varying the amount and type of alkylaluminum activator present in the polymerization recipe (1). Based on the nature of the individual activators under copolymerization conditions, trimethylaluminum (TMA) produces a copolymer with unimodal short chain branching distributions, whereas triethyl (TEA) or triisobutyl aluminium (TIBA) activators produce copolymers with broad and bimodal SCBDs; upon mixing any two types of activators, a blended distribution results.

For this study, the samples were prepared under similar polymerization conditions and only differed by the amount and type of each activator used. The four resins were prepared by varying the mixing ratio of TMA and TEA. Sample A was prepared with 100% TMA, sample B with 50 % TMA and 50% TEA, sample C with 25% TMA and 75% TEA and sample D with 100% TEA.

The CRYSTAF profiles of the polymers made with these mixed activator systems are shown in Figure 5.1. A CRYSTAF profile can be correlated with the short chain branching distribution of a polymer. With the use of a temperature-composition calibration curve as shown in Figure 5.2, it is possible to relate the polymer's crystallization temperature with its % incorporated comonomer or branching frequency (as determined from ^{13}C NMR). It is clearly shown that samples A through D have very distinct and bimodal crystallinity distributions. Two

distinct regions are present, a homopolymer-like region (less than 1 branch per 100 carbon atoms) present at higher crystallization temperatures between 70-80°C, and a copolymer-like region (greater than 1 branch per 100 carbon atoms), present at lower temperatures between 50-70°C. It should be noted that the proportion of homopolymer increases from sample A to D. A comparison of the corresponding molecular weight distributions is shown in Figure 5.3. The MWDs of the four resins are quite similar. The number average molecular weights of these samples, listed in Table 5.1, are in the range of 40,000 g/mol. However their polydispersity indices do vary due to tailing in the high molecular weight region. This tailing is probably due to drift in comonomer concentration during the polymerization. As the polymerization proceeds to high yields, the comonomer concentration decreases and higher molecular weight material is formed. Nonetheless, the presence of this tail cannot account for the large differences in the short chain branching distributions observed for these samples. In a previous study, we have demonstrated that ethylene copolymers similar to the ones studied here, have SCBDs with uniform and narrow molecular weight distributions (1). Overall, these molecular weight distributions are similar in shape for the comparison of the short chain branching distributions shown in Figure 5.1. Also shown in Table 5.1 are the estimates of the overall 1-hexene comonomer content as determined from the temperature-composition calibration curve. As shown, the comonomer content decreases from samples A to D. Sample A contains an estimated average of 4.0 mol% of 1-hexene, while sample D contains 2.8 mol %, which also translates, in terms of backbone atoms, to a range from 2.0 to 1.4 branches per 100 carbons. It is assumed that with this level of branching, the copolymer/homopolymer phases are miscible. Rana et al. have reported that LLDPEs with up to 4 branches per 100 carbons were miscible with polyethylene

Table 5.1 - Microstructural properties of ethylene/1-hexene resins

Sample[a]	$\overline{M}_n$[b] (g/mol)	$\overline{M}_w/\overline{M}_n$[b]	1-Hexene Content[c] (mol %)	Average Branching Frequency[c] (branches per 100 C's)	Melting Peak[d] (°C)	Crystallinity[e] (≈ Density)[f] (%) (g/cm^3)
A	39,700	6.7	4.0	2	114.6	43.3 (0.925)
B	41,400	2.5	3.6	1.8	117.8	45.2 (0.9278)
C	43,800	4.9	3.4	1.7	119.8	45.6 (0.9283)
D	43,800	6.3	2.8	1.4	122.3	53.2 (0.939)

[a] Polymerization conditions: [$Et(Ind)_2ZrCl_2$] = 13.3 μmol/L, Al/Zr = 500, ethylene pressure = 150 psig, [1-hexene] = 30 mol % feed (41 mL), polymerization temperature = 60°C, stirring rate = 400 rpm.
[b] As determined from GPC analysis based on a universal calibration curve derived from narrow polystyrene standards.
[c] As determined from an integrated CRYSTAF profile and 1-hexene temperature-composition calibration curve.
[d] As determined by DSC. Note that these samples exhibited very broad melting distributions.
[e] Crystallinity estimates based on DSC melting enthalpy as compared to a perfect crystalline polyethylene ($\Delta H \approx 289$ J/g) (9)
[f] Approximate density range estimated from a % crystallinity versus density calibration curve from Kim et al (24).

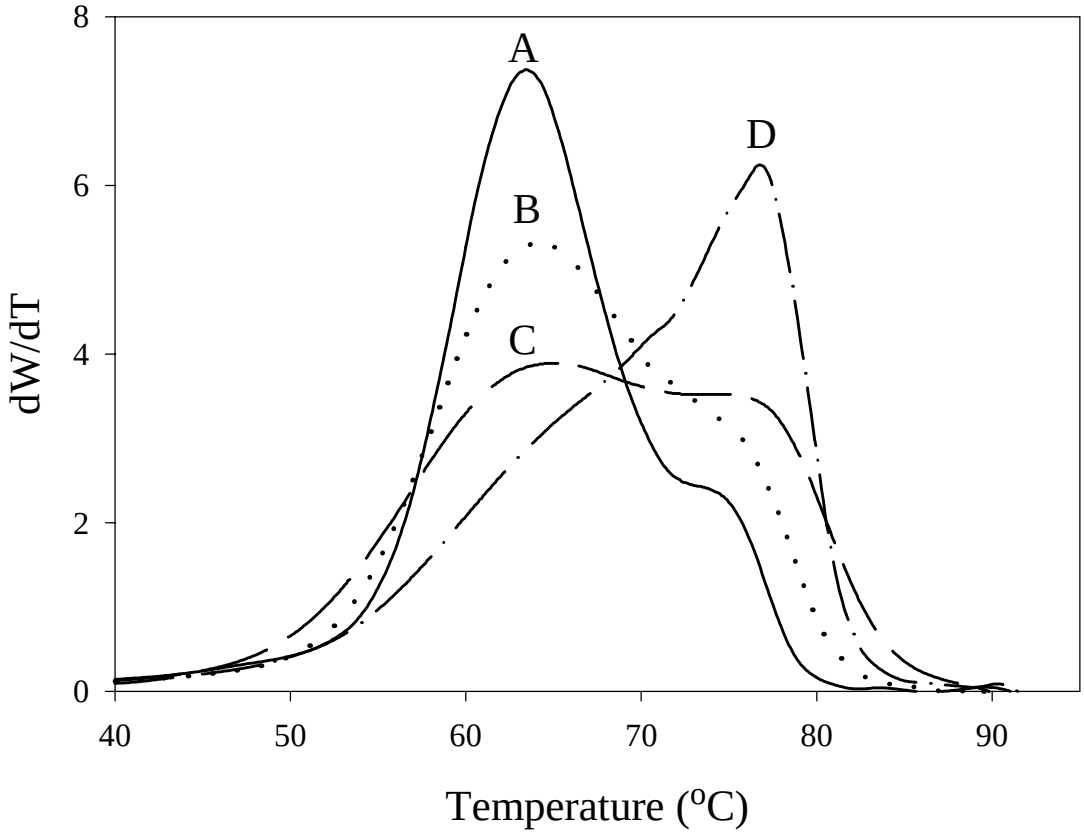

Figure 5.1 - Comparison of CRYSTAF profiles of tailored ethylene/1-hexene copolymers

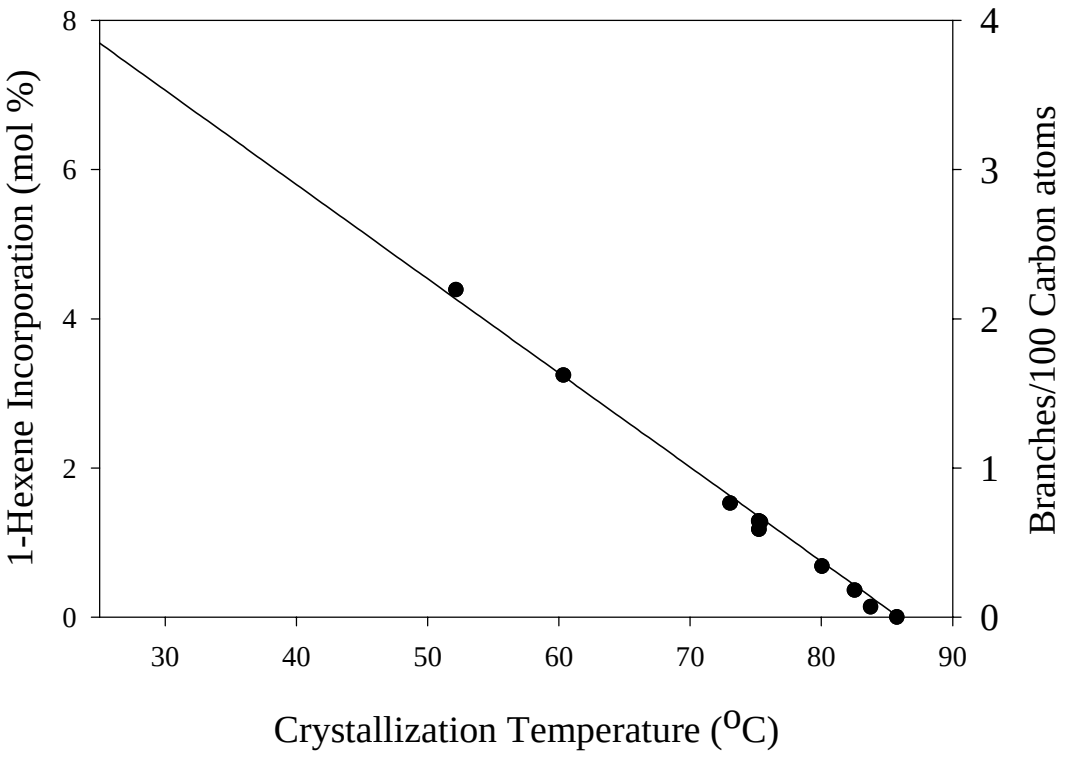

Figure 5.2 - Calibration curve relating the CRYSTAF crystallization temperature and 1-hexene incorporation in the copolymer

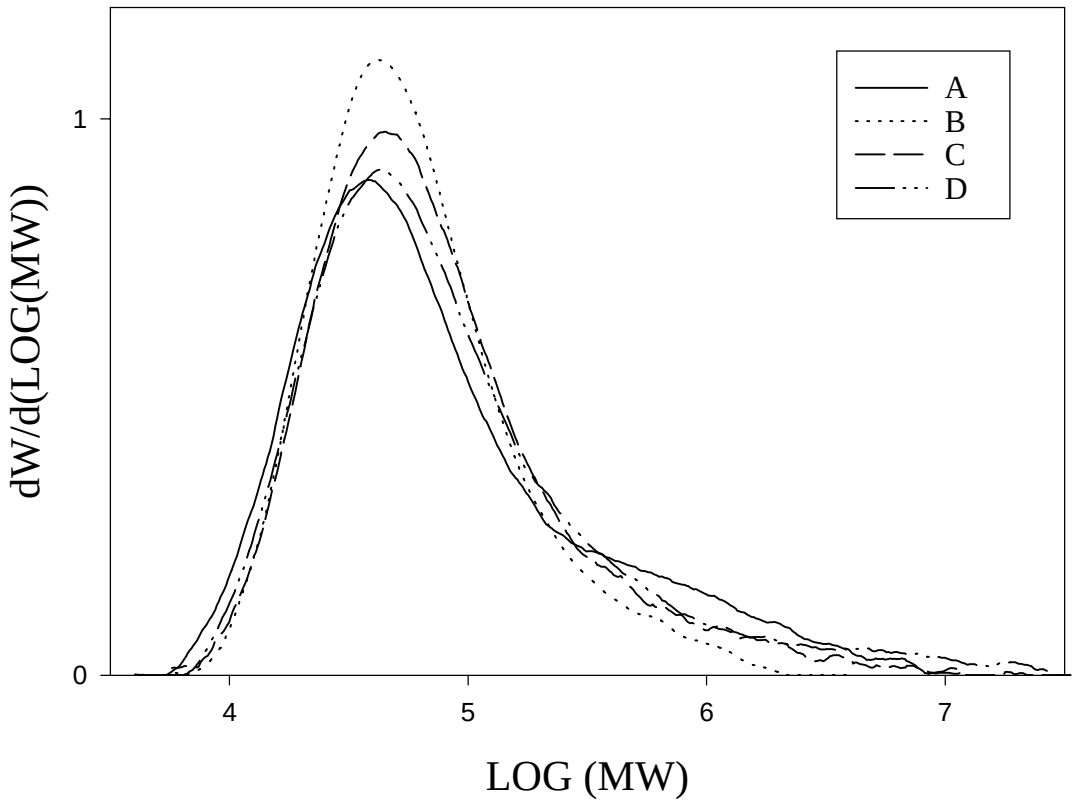

Figure 5.3 - Comparison of MWDs of tailored ethylene/1-hexene resins

homopolymer (15). Consequently, one can assume that copolymers with blended crystalline distributions are also miscible. Also shown in Table 5.1 are the estimates of the % crystallinity from DSC of the samples air-cooled from melt to room temperature. The corresponding melting profiles are shown in Figure 5.4. As seen, these melting profiles correspond well to the SCBDs measured by CRYSTAF. For samples B and C, the DSC melting profiles indicate the presence of two distinct populations of crystalline species.

A representative comparison of the force versus displacement curves during the deformation of the four resins is shown in Figure 5.5. In general, it was observed that all of the samples exhibited localized yielding and cold drawing that is characteristic to semi-crystalline polymers. Qualitatively examining the yielding region, it was observed that a narrowing of the yield zone occurred from sample A to D. For samples A and B, a broad yielding region was observed, which could be classified as a double yield point. This double yield behaviour has also been observed by others for polyethylene copolymers (6-8,16). This phenomenon may be caused by a partial melt-recrystallization process. At the first yield point, temporary plastic deformation occurs, followed by a recoverable recrystallization of the lamellae. The second point is the onset of permanent plastic deformation in which the lamellae are destroyed (16). Grahm et al. have reported that this type of behaviour may be related to the degree of crystallinity and thermal history of the polymer which both can influence the structure and morphology of the crystallites (8). Bensason et al. reported that with a decrease in density, the yield maximum broadens up to a point where it then becomes indistinguishable and no yield maximum is observed (6). Similarly for these samples, it appears that the yielding region broadens with a decrease in crystallinity or increase in comonomer content. Given the bimodal nature of the short chain branching distributions in these samples, it seems that increasing the proportion of higher crystalline

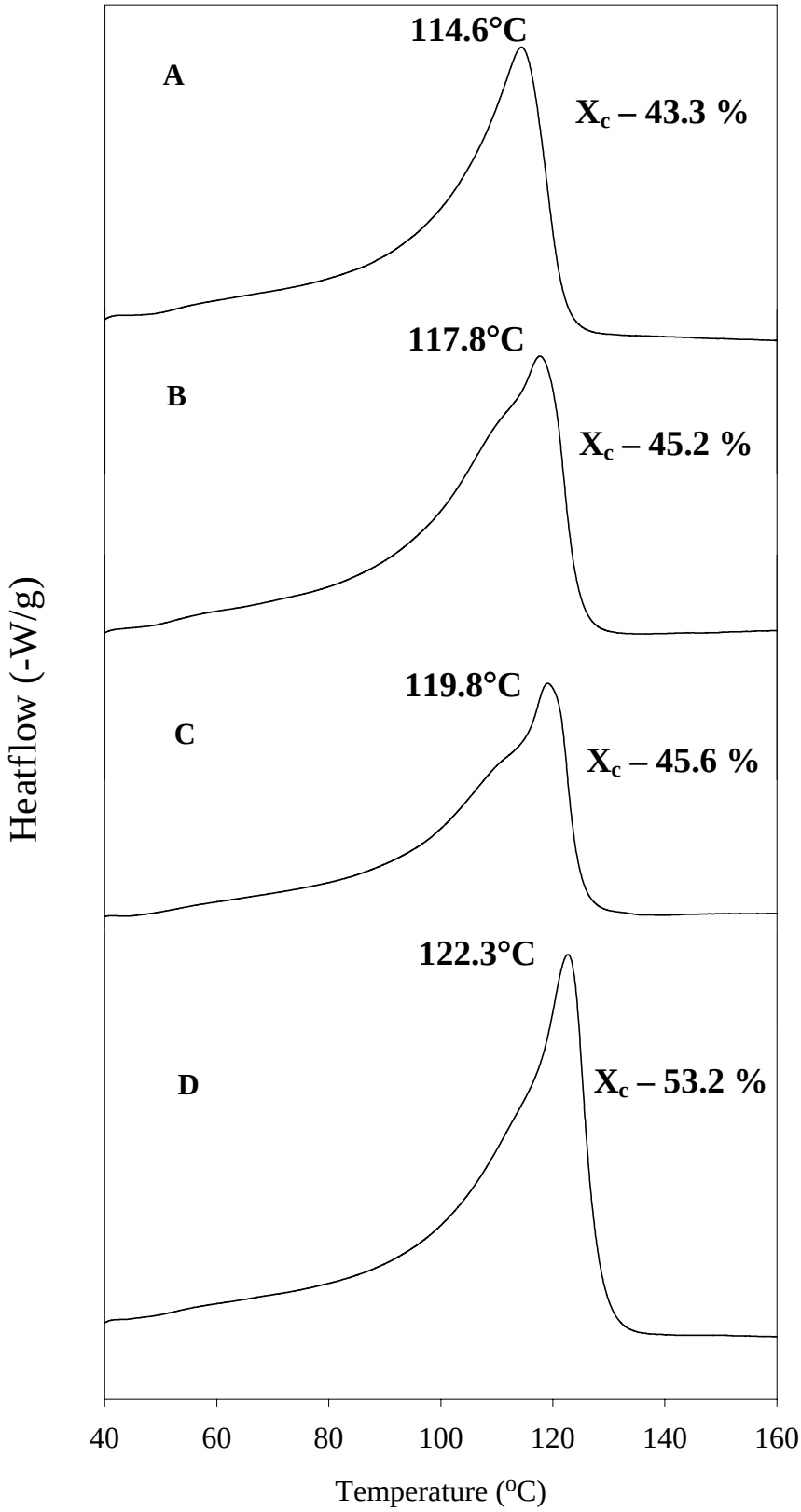

Figure 5.4 - DSC melting profiles of tailored ethylene/1-hexene

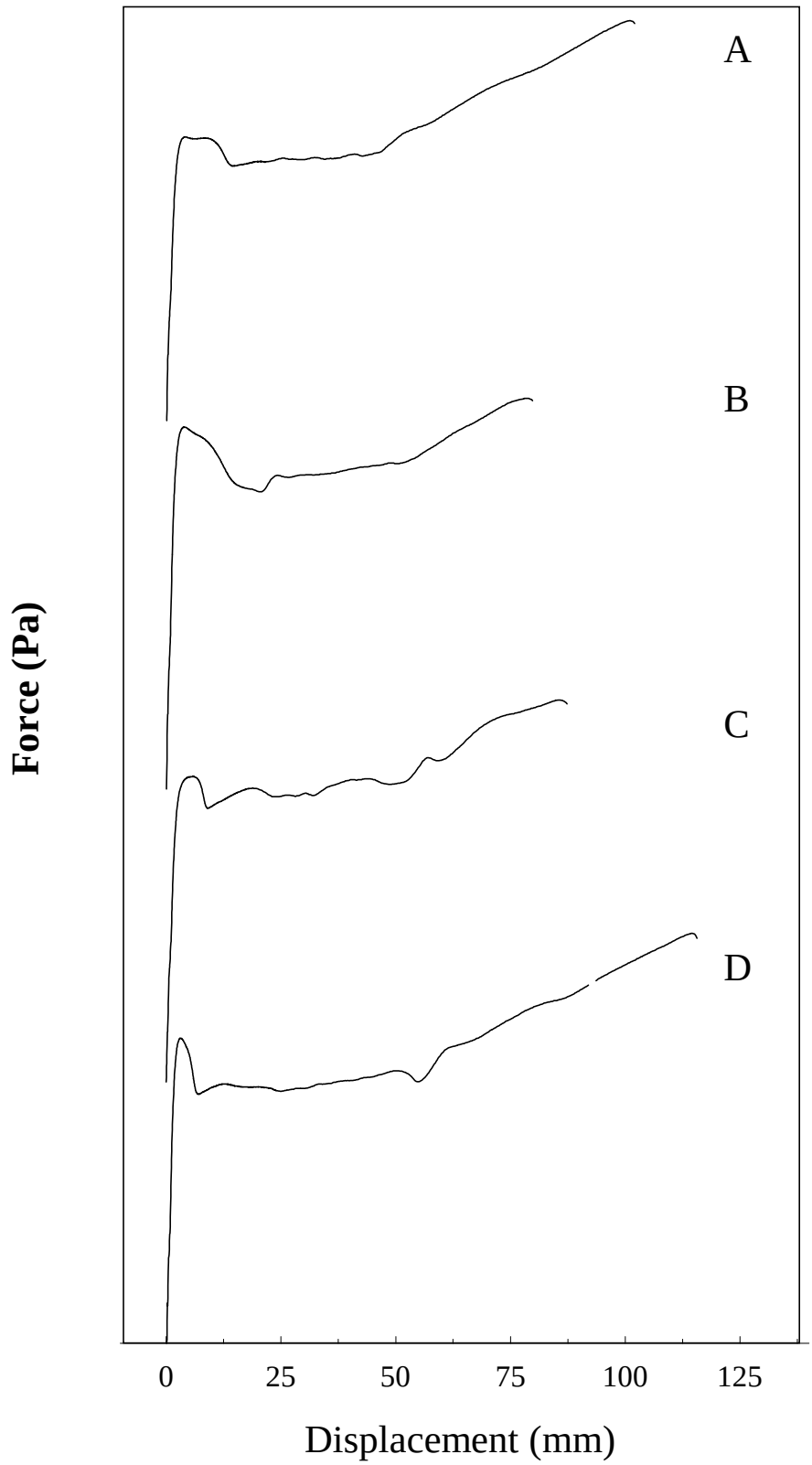

Figure 5.5 - Tensile deformation comparison of tailored ethylene/1-hexene resins

material results in a narrower yield maximum. A summary of the measured tensile properties is shown in Table 5.2. The tensile strength at yield increases while increasing the proportion of higher crystalline material. This increase in tensile strength is closely related to the stiffness of the samples. Estimates of the sample's overall crystallinity from DSC show that crystallinity increases from samples A to D (see Table 5.1), which confirms the increase in stiffness. The tensile strengths at yield of samples B and C predictably fall within the ranges of A and D. After the material exceeds the yield point and deforms, the ultimate tensile strengths (at break) also show that sample D has the highest value and sample A the lowest. In regards to the % elongation, which can be a measure of the material's ability to deform and dissipate energy, it was found that sample D had the highest value at 440%. It was expected that the sample with the highest comonomer content, such as sample A, would exhibit the highest % elongation at break. A sample with low crystallinity possesses a large fraction of amorphous polymer. It is the slippage and disentanglement of amorphous polymer that allows it to deform. In the literature, Jordens et al. noticed that with decreasing crystalline density, a higher % elongation was observed (11). Bensason et al. also observed for low crystalline poly(ethylene-*co*-1-octene) copolymers that, with increasing comonomer content, an increase in strain % was observed (6,17). Sample A's % elongation was quite high at 373 % but sample D's was even higher. Although the crystallinity of sample D was the greatest of the four samples studied, it exhibited the highest stiffness and ductility. Both sample B and C demonstrated intermediate values of tensile strengths and showed lower % elongations. Generally, for copolymers with unimodal SCBDs, the crystallinity of the polymer relates well to the stiffness and % elongation (5-7,17). At low strain, the sample's crystallinity is the dominant factor during a deformation process but at high strains the role of entanglements prevails (17-18). From the examination of the SCBDs

Table 5.2 - Tensile property data of ethylene/1-hexene copolymers[a]

Sample	Tensile Strength at yield (kPa) [± 666][b]	Tensile Strength at break (kPa) [± 1178][c]	Elongation at break (%) [± 43][d]
A	11490	15600	373
B	12110	14780	315
C	13800	14880	330
D	14150	19500	440

[a] Testing conditions: ASTM D638 (type V), 3.175 mm thickness, displacement rate 25 mm/min, grip to grip length 3 cm
[b,c,d] Calculated standard deviations based on replicate testing.

for these resins (Figure 5.1), it can be seen that sample D has a tail in the lower crystalline region. It is believed that this balance of low and high crystalline material resulted in a blending of the tensile properties. This balance of properties may be explained by the presence of this comonomer tail. This less crystallizable polymer would increase the number of entanglements and increase the amount of tie material. Generally, tie molecules are considered to be chains that bridge the amorphous and crystalline regions. The presence and amount of tie molecules have been known to influence the mechanism of failure (19). A transition from a ductile to brittle failure mechanism sometimes occurs if too few tie molecules or entanglements are present. These tie molecules can also affect the strain hardening behaviour (11). As a sample's crystallinity decreases (via branching or thermal treatment) or with an increase in molecular weight, the number of tie molecules present in the amorphous regions increases (5,19-20). The most effective tie molecules have been shown to be high in molecular weight and high in comonomer content up to a limiting value. From the results above, sample D was the toughest by displaying the highest percent elongation and tensile stress at break. Sample D was followed by sample A. It is believed that sample A performed well due to its lower crystallinity. To account for the toughness of the polymers observed in this study, two hypotheses will be given. For these samples, the molecular weight distributions as shown in Figure 3 showed slight tailing in the high end of the distribution. This is also reflected in both samples possessing the largest PDI's at 6.3 for sample D and 6.7 for sample A. As mentioned previously, it is believed that these tails are lower in comonomer content due to the slight drift in comonomer concentration during the polymerization. It is possible that this small amount of high molecular weight material increased the number of entanglements and resulted in the increase in toughness that was observed. Under this assumption, it would be reasonable to assume that sample A would

show the largest % elongation since it has the broadest MWD and highest comonomer content. However, sample D exhibited the highest % elongation. It is believed that the presence of the low crystalline tail shown in the SCBD increased the number of entanglements and increased the amount of tie material. The superior toughness of sample D is probably due to a combination of sample D's high crystallinity and large comonomer tail.

As a comparison to the tensile properties measured above, the solid-state dynamic mechanical responses of these resins were measured. Within the temperature range studied, it can be seen that the samples exhibited the characteristic γ, β and α transitions, as indicated by the changes in tan delta shown in Figure 5.6. Although there is much debate on the existence and nature of these transitions, it is believed that they are linked to the motions of the amorphous and crystalline portions of the polyethylene chains (6,21-23). Examining the tan delta behaviour (Figure 5.6), the γ transition is often associated with the rotation of four carbon chain segments (Schatzki-Crankshaft mechanism) and was observed around -120°C (25). The β-transition, that is often associated with the glass transition temperature of the amorphous polymer is due to the motion of the branched segments of the chains and occurred between -25°C and room temperature (6,22). As shown, sample A exhibited the largest tan delta during this transition followed by samples B,C and D, in the order of decreasing comonomer content. The α transition was observed above 50°C and this may be linked to the gradual motion of main chain units within the crystallites before the onset of melting.

The sample's ability to dampen energy at room temperature is reflected by the tan delta that decreases with the increase in crystallinity of the copolymers (as in Figure 5.6). Comparing the elastic response of all the samples, it is shown in Figure 5.7 that the storage moduli decreased with an increase in temperature. For these polymer samples, their elasticity decreased as the

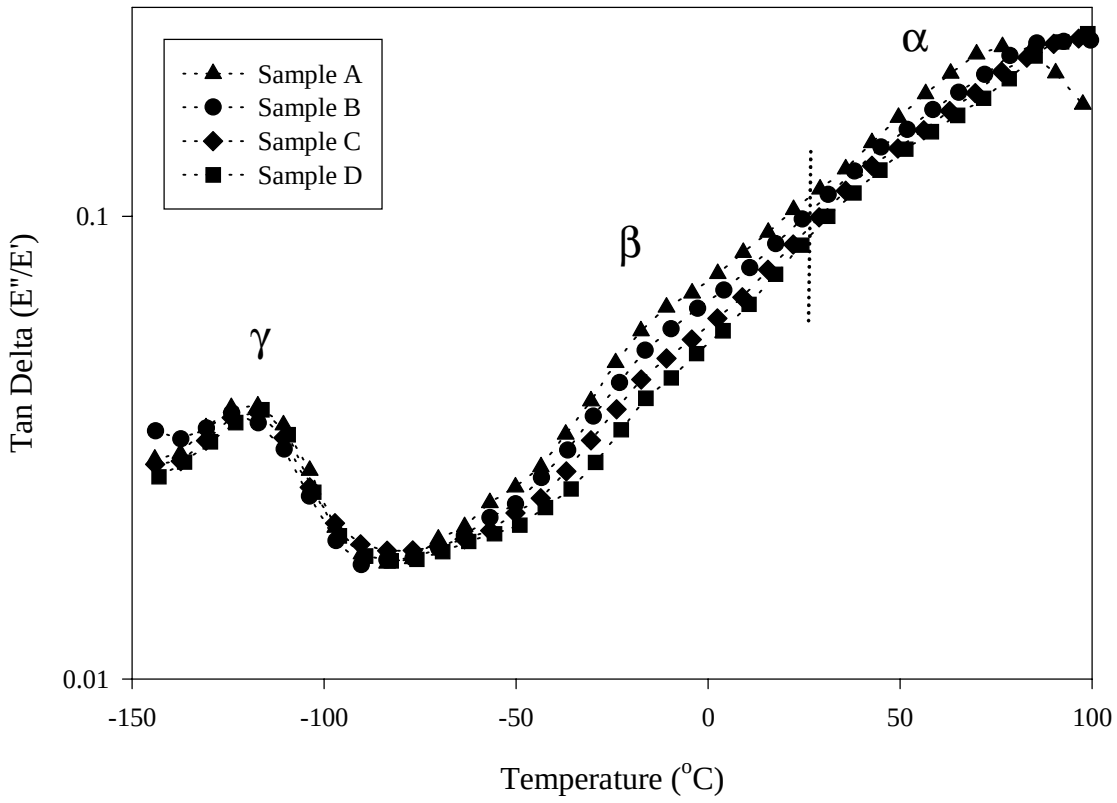

Figure 5.6 - Tan delta comparison of tailored ethylene/1-hexene copolymers carried out at 1 Hz

samples softened with the increase in temperature. At room temperature, the storage moduli of resins A through D increased. The increase in stiffness of the samples is a reflection of the increase in the sample's crystallinity that was also observed in the comparison of the tensile strengths (Table 5.2). Comparing the loss responses of the samples in Figure 5.8, it can be seen that at different temperatures the samples passed through γ,β and α transitions. The loss modulus can be associated with the energy lost due to friction and internal chain motion (23). It is believed that this energy loss is related to the relaxation of the entanglements present in the microstructure. The relaxation of these entanglements at a given frequency may give an indication to the high strain deformation behaviour in the tensile study. At room temperature it is shown that the loss modulus decreases from sample D to Sample A (Figure 5.8). This trend is different from the one observed in the tensile study in which sample A and sample D exhibited the greatest % elongation at break. Although the trend reported from the loss modulus is different, it is noted that the loss moduli sequence of the samples changed with temperature. At around 0°C a crossover of the E'' modulus occurs, changing the order to sample D, A, C and B. At this temperature, the order of the E'' moduli for these samples is closer to the one observed in the tensile study for the % elongation at break. It is well known that these dynamic responses from oscillatory measurements are frequency and temperature dependent (23). As the frequency of the test increases, the polymer chains have less time to relax and can appear to be stiffer. At lower temperatures, the relaxation of the polymer chains is slowed which also results in an increase in stiffness. For these oscillatory measurements, the analysis was carried out at 1 Hz. The tensile test was carried out at a higher strain rate than 1 Hz. Thus the process of a tensile test would presumably be better represented at a higher frequency since the strain rate used in these experiments was fairly high. Figure 5.9 shows the frequency dependence of the samples at room

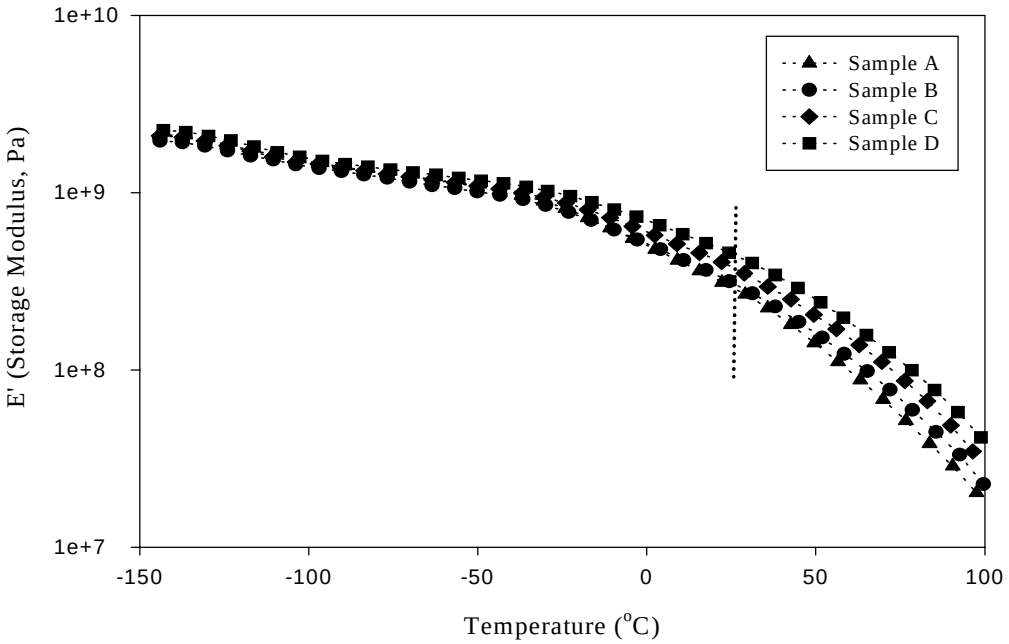

Figure 5.7 - Elastic response comparison of tailored ethylene/1-hexene copolymers carried out at 1 Hz

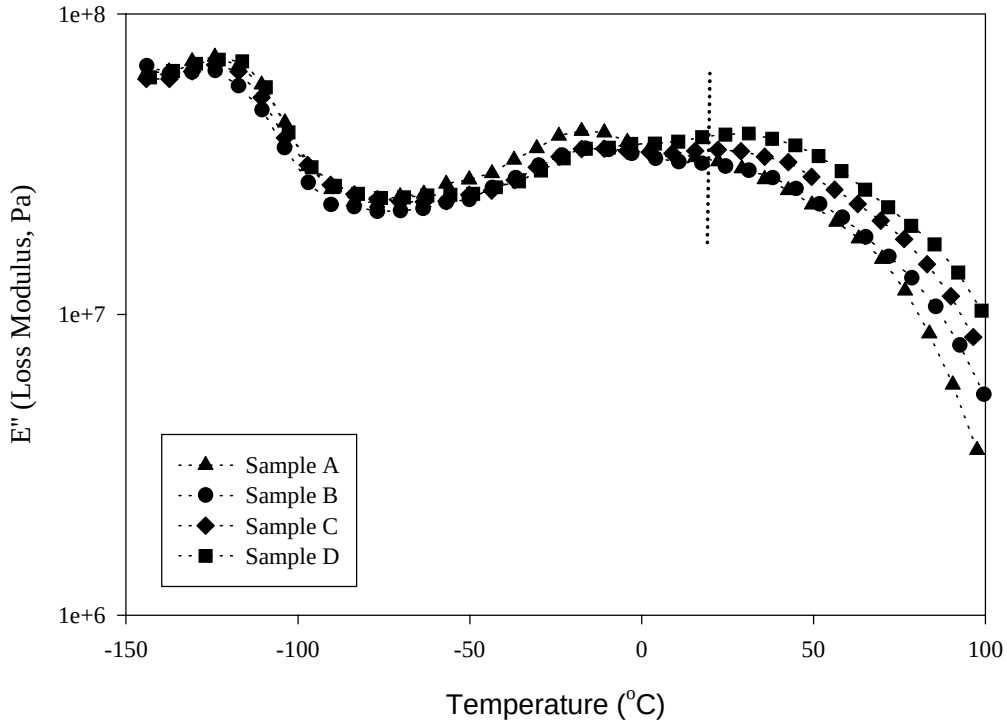

Figure 5.8 - Loss response comparison of tailored ethylene/1-hexene copolymers carried out at 1 Hz

temperature. As shown, the loss response of the samples changed with frequency. Sample A exhibited an increase in its loss response with an increase in frequency. At approximately 10 Hz, a crossover of the E'' ofsample A and sample D occurred. At this frequency the samples loss response compares well to the % elongation at break of the tensile test data (Table 5.2). Despite the consistency of the results, it is not clear on the relation between the high strain deformation behaviour as in the tensile test and low strain behaviour by DMTA. It is possible that the loss moduli obtained from the linear viscoelastic region is sensitive to a portion of the microstructure such as the relaxation of the entanglements that contributes to the high strain properties.

Overall, both tensile and dynamic mechanical properties have shown that sample D exhibited the greatest toughness. This sample had a bimodal short chain branching distribution with a large portion of high crystalline and a smaller fraction of lower crystalline material. As a result, this sample displayed a balance of stiffness and toughness. For this study, the balance of properties is attributed to the distribution of crystalline material as measured by CRYSTAF (Figure 5.1), however, the small fraction of high molecular weight material present in some of the samples may have influenced the observed properties.

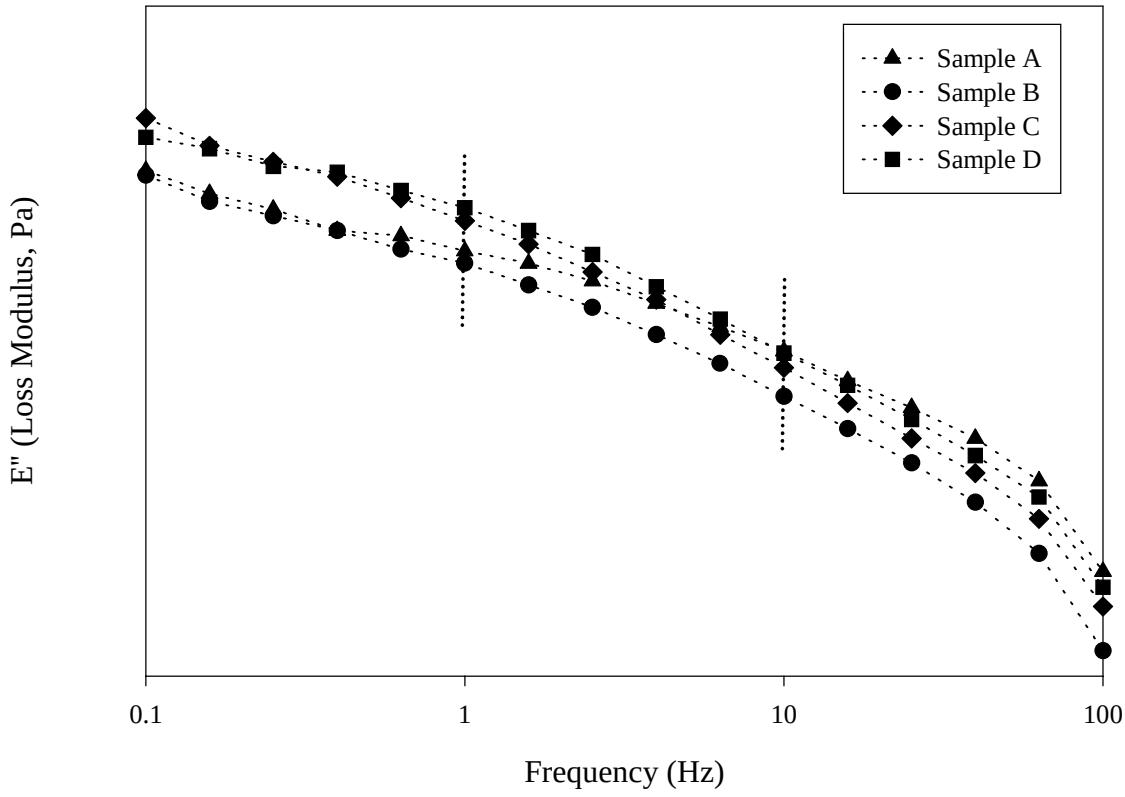

Figure 5.9 - Frequency dependence of E'' (Loss Modulus) of tailored ethylene/1-hexene copolymers at room temperature

5.4 Conclusions

It has been demonstrated how the microstructure and properties of metallocene-synthesized polymers can affect their mechanical properties. Using a heterogeneous metallocene catalyst system with mixtures of alkylaluminum activators, it was possible to control the crystalline distribution of polyethylene copolymers. Using this method, a series of poly(ethylene-*co*-1-hexene) resins with very distinct crystalline distributions but with similar molecular weight distributions was produced.

Given the unique characteristics of these resins, i.e., resins with broad/bimodal crystalline distributions but having uniform molecular weight distributions, structure-property studies have shown that the mechanical properties of these resins can be modified. Tensile testing and dynamic mechanical analysis demonstrated how an ethylene copolymer with portions of highly crystalline and low crystalline material exhibits a balance of stiffness and toughness, thus demonstrating how the structure and properties of an ethylene copolymer can be tailor-made with a metallocene catalyst system.

5.5 References

1. Li Pi Shan, C.; Chu, K.J.;Soares, J.B.P.; Penlidis, A.; *Macromol. Chem. Phys*., 201, 2195-2202 (2000).
2. Garbassi, F. ; Gila, L. ;Proto, A. ; *Polym. News*, 19, 367-371 (1994).
3. Scheirs, J.; Bohm, L.; Bout, L.; Leevers, P.S.; *Trends in Polymer Science*, 4, 408-415 (1996).
4. Soares, J.B.P.; Kim, J.D.; Rempel, G.L.; *Ind & Eng Chem. Res*., 36,1144-1150 (1997).
5. Kale, L.; Plumley, T.; Patel, R.; Redwine, O.; Jain, P.; *J. Plast. Film and Sheeting*, 12. 27-40 (1995).
6. Bensason, S.; Minick, J.; Moet, A.; Chum, S.; Hiltner, A.; Baer, E.; *J. Polym. Sci. Part B: Polym. Phys.*, 34, 1301-1315 (1996).
7. Simanke, A.G.; Galland, G.B.; Neto, R.B.; Quijada, R.; Mauler, R.S.; *J. Appl. Polym. Sci*., 74, 1194-1200 (1999).
8. Grahm, J.T. ; Alamo, R.G. ; Mandelkern, L.; *J. Polym. Sci. Part B: Polym. Phys.*, 35, 213-223 (1997).
9. Xu, X. ; Xu, J.; Feng, K. ; Chen, W.; *J. Appl. Polym. Sci.*, 77, 1709-1715 (2000).
10. Hosoda, S. ;Uemura, A. ; *Polym. Journal*, 24, 939-949 (1992).
11. Jordens, K.; Wilkes, G.L.; Janzen, J.; Rohlfing, D.C.; Welch, M.B.; *Polymer*, 41, 7175-7192 (2000).
12. Nunes, R.W.; Martin, J.R.; Johnson, J.F.; *Polym. Eng. Sci.*, 22, 205-228 (1982).
13. Chu, K.J.; Soares, J.B.P.; Penlidis, A. ; *J. Polym. Sci. Part A: Polym. Chem.*, 38, 462-468 (2000).
14. Monrabal, B.; *J. Appl. Polym. Sci.*, 52, 491-505 (1994).

15. Rana, D.; Lee, C.H.; Cho, K.; Lee, B.H.; Choe, S.; J. *Appl. Polym. Sci.*, 69, 2441-2450 (1998).

16. Brooks, N.W.J.; Duckett, R.A.; Ward, I.M.; *Polymer*, 40, 7367-7372 (1999).

17. Bensason, S.; Stepanov, E.V.; Chum,S.; Hiltner, A.; Baer, E.*; Macromolecules*, 30, 2436-2444 (1997).

18. Doyle, M.J.; *Polym. Eng. Sci.*, 40, 330-335 (2000).

19. Lustiger, A. ; Markham, R.L. ; *Polymer*, 24, 1647-1654 (1983).

20. Channel, A.D.; Clutton, E.Q.; *Polymer*, 33, 4108-4112 (1992).

21. Nitta, K.H.; Tanaka, A.; *Polymer*, 42, 1219-1226 (2001).

22. Simanke, A.G.; Galland, G.B.; Freitas, L.; da Jornada, J.A.H.; Quijada, R.; Mauler, R.S.; *Polymer*, 40, 5489-5495 (1999).

23. Menard, K.P. ; Dynamic Mechanical Analysis – A Practical Introduction, New York, CRC Press, 1999, pp. 151-162.

24. Kim, Y.S.;Chung, C.I.; Lai, S.Y.; Hyun, K.S.;*J. Appl. Polym. Sci.*, 59, 125-137 (1996).

25. Sperling, L.H.; Introduction to Physical Polymer Science, John Wiley & Sons., Inc., p. 328 (1992).

Chapter 6

Ethylene/1-Octene Copolymerization Studies with In-Situ Supported Metallocene Catalysts: Effect of Reaction Parameters on Catalyst Activity and Polymer Microstructure

6.1 Introduction

We have recently illustrated the use of a single metallocene catalyst to produce ethylene/α-olefin copolymers with broad and bimodal short chain branching distributions (SCBD) in a single reactor. Copolymers produced by an in-situ supported metallocene catalyst (a system that eliminates the need for a metallocene-supporting stage) can be affected by the type of alkyaluminum activator, the amount of activator, and the presence of chain transfer agents such as hydrogen (1). Ethylene copolymers with bimodal SCBDs were produced with different alkylaluminum activators and rac-(ethylenebis(indenyl)) zirconium dichloride supported on silica containing a high weight percent of impregnated MAO. Uniquely, these copolymers still maintained the narrow molecular weight distributions (MWD) expected from a single-site metallocene catalyst. Further studies demonstrated that these copolymers exhibited a blend of physical properties representative of bimodal crystallinity distributions (2).

The study reported herein investigates the effect of reaction parameters such as polymerization temperature and ethylene pressure, the presence of hydrogen and alkylaluminum activator, and the level of comonomer in the feed, on the resulting copolymer microstructure. Ethylene/1-octene copolymerizations were carried out with in-situ supported rac-(dimethylsilylbis(methylbenzoindenyl)) zirconium dichloride [$Me_2Si(2\text{-}Me\text{-}4,5\ BenzInd)_2ZrCl_2$]. Supported on the same silica used in our previous study (1). The catalyst was activated by triethyaluminum. This catalyst system was chosen in an attempt to tailor the microstructure of the copolymer by quantitatively predicting *a priori* the structure of the copolymer produced.

In preliminary studies with this in-situ supported system, we have observed some unique effects of polymerization conditions on the microstructures of the polymers formed. By varying the factors in accordance to an experimental design approach, we have attempted to quantify the

catalyst productivity and the changes in the copolymer microstructure in terms of the SCBD and MWD. Generally, olefin copolymerizations with homogeneous and some supported metallocene catalysts produce copolymers with narrow MWD and narrow SCBD (3). By manipulating some of the polymerization conditions mentioned above, it is usually possible to control the microstructure of the resulting polymer. Table 6.1 summarizes some of these effects. It must be noted that the observed trends are sometimes sensitive to the parameter range studied and are usually dependent on the monomer and catalyst type, as well as polymerization process. Attempts to explain the observed effects are usually linked to the polymerization kinetics and mechanism. Figure 6.1 shows a general polymerization mechanism for metallocene catalysts. Other side reactions may also exist but the focus will be on the mechanisms displayed. As shown, a number of reactions can occur: catalyst activation, monomer initiation, monomer propagation, chain transfer, and deactivation reactions (4). Catalytic sites that have interacted with other species such as the support material, comonomer and hydrogen, further complicate the number of possible reactions. The rate of propagation depends on the propagation rate constant, number of active sites and monomer concentration, as shown in Eq. (1).

$$\text{Rate of propagation} = k_p[Cat^*][M] \quad (1)$$

where k_p is the propagation rate constant, $[Cat^*]$ is the concentration of active sites and [M] is the monomer concentration.

A single parameter, τ, defines the whole MWD of polymer made with single-site metallocene catalysts. The parameter τ is defined as the ratio of all transfer rates to the propagation rate, as shown in Eq. (2):

Table 6.1 – Effect of Polymerization Conditions on Catalyst Activity and Polymer Microstructure

Polymerization Condition (Increase)	Activity	α-olefin Comonomer Incorporation	Molecular Weight and	References
Temperature	Increases (5,7-11,14-17) and Sometimes Bell shaped Maximum Reached Between 40-80°C (6,12,13)	Decreases (5,14)	Decreases (10,11,13,14,17)	5-17
Pressure of Ethylene	Increase (13,17-19) No Change (16)	No Change (14) Decreases (19)	Increases (13,17-19)	13,14,16-19
Hydrogen Chain Transfer Agent	Both increases (8,10,15,22,24) and Decreases are reported (15,18,21,23,24)	Increases (8,10,15,22,24)	Decreases MW/broadens PDI (10,11,18,20,23,24)	8,10,11,15,18,20-24
Comonomer/Ethylene Feed Ratio	Increases due to "Comonomer Effect" (18,19,25,26,28)	Increases	Decreases (18,19,27,28) Increases (7,9)	7,9,14,18,19,25-29
Al/Metal Ratio	Increases (16) until Maximum is reached (12,13) Decreases (17)	-	No Change (13,32) or Decreases (12,16,17,30,31)	12,13,16,17,30-32

$$\tau = \frac{\text{rate of transfer}}{\text{rate of propagation}} = \frac{k_\beta}{k_p[M]} + \frac{k_M}{k_p} + \frac{k_{CTA}[CTA]}{k_p[M]} + \frac{k_{Cm}[Cm]}{k_p[M]} + \frac{k_{Al}[Al]}{k_p[M]} + \ldots \quad (2)$$

where the rate constants are: k_p – propagation, k_β - beta hydride elimination
k_M – transfer to monomer, k_{CTA} – transfer to chain transfer agent, k_{Cm} – transfer to comonomer
k_{AL} – transfer to aluminium

The number average molecular weight is inversely proportional to the τ as shown in Eq.(3).

$$Mn = MW \times Rn = MW/\tau \quad (3)$$

where Mn is the number average molecular weight, MW is the molecular weight of the monomeric unit, Rn is the number average chain length.

Some of the most common responses of metallocene catalysts to polymerization conditions will be reviewed below. The activation energies of the reaction steps shown in Figure 6.1 are all unique and changes in temperature can affect their relative rates. This is generally observed as an increase in catalyst activity and a decrease in molecular weight, as the temperature increases (5-17). However, most metallocene catalysts deactivate at higher temperatures. This deactivation reduces the number of active sites and catalytic activity. As shown in Eq. 1, the propagation rate is first order with respect to monomer concentration. Therefore increasing the monomer pressure results in higher polymerization rates and molecular weights (13,17-19). The molecular weights of polymer made with many metallocene catalysts are highly sensitive to hydrogen as described by Eq. (2). However, when hydrogen is added as a chain transfer agent, the polymerization rate may increase (8,10,15,22,24) or decrease (15,18,21,23,24) depending on the catalyst system. The reasons for this behaviour are still under

Figure 6.1 – Polymerization Mechanisms

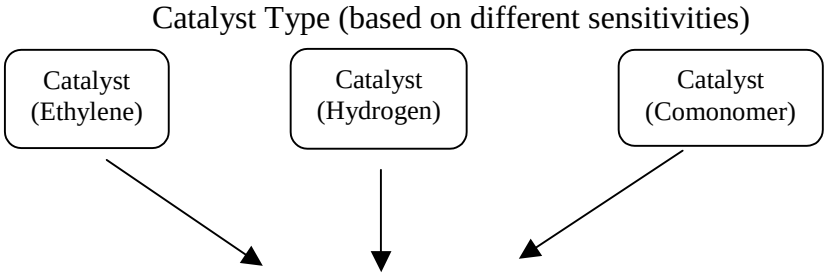

Activation (k_{act})

$$Cat + [Al] \xrightarrow{k_{act}} P_0^*$$

Alkylation of Catalyst by MAO or Alkylaluminum

Initiation (k_i)

$$P_{X,0}^* + [M_1] \xrightarrow{k_{i1}} P_{1,1}^*$$
$$P_{X,0}^* + [M_2] \xrightarrow{k_{i2}} P_{1,2}^*$$

Initiation of Active Site Type X by Ethylene (M1)

Initiation by Active Site Type X by Comonomer (M2)

Propagation (k_p)

$$P_{r,i}^* + [M_1] \xrightarrow{k_{pi1}} P_{r+1,1}^*$$
$$P_{r,i}^* + [M_2] \xrightarrow{k_{pi2}} P_{r+1,2}^*$$

Propagation by Ethylene (M1)

Propagation by Comonomer (M2) (1,2 or 2,1 insertion)

Chain Transfer (k_f)

$$P_{r,i}^* \xrightarrow{k_{f\beta}} P_0^* + Q_{r,i}$$
$$P_{r,i}^* + [H_2] \xrightarrow{k_{fH2}} P_{H,0}^* + Q_{r,i}$$
$$P_{r,i}^* + [Al] \xrightarrow{k_{fAl}} P_{Al,0}^* + Q_{r,i}$$
$$P_{r,i}^* + [M_1] \xrightarrow{k_{fM1}} P_{1,0}^* + Q_{r,i}$$
$$P_{r,i}^* + [M_2] \xrightarrow{k_{fM2}} P_{2,0}^* + Q_{r,i}$$

β-elimination

Transfer to Hydrogen

Transfer to Alkylaluminum

Transfer to Ethylene

Transfer to Comonomer

Deactivation (k_d)

$$P_{r,i}^* \xrightarrow{k_{d,spn}} C_d + Q_{r,i}$$
$$P_{r,i}^* + [Z] \xrightarrow{k_{d,Z}} C_{d,Z} + Q_{r,i}$$

Spontaneous Deactivation

Deactivation by Impurities or Poison (Z)

study. It is generally thought that hydrogen can reactivate dormant sites, thus increasing the total number of active sites. However, depending on catalyst type, the metal-hydrogen sites formed after transfer to hydrogen might have a slower initiation rate, thus decreasing the polymerization rate.

Ethylene is copolymerized with α-olefins to produce polymers with lower density. It is commonly observed that the addition of comonomer generally increases the polymerization rate significantly. This 'comonomer effect' is sometimes linked to the reduction of diffusion limitations by producing lower crystallinity polymer, or to the activation of catalytic sites by comonomer (7,9,14,18,19,25-29). Polymer molecular weight often decreases with comonomer addition, possibly due to transfer to monomer reactions. Lastly, the polymerization rate passes through a maximum as the ratio of aluminium to transition metal increases (12,13,16). The exact location of this maximum value depends on catalyst type and whether the polymerization is homogeneous or heterogeneous. Heterogeneous polymerizations tend to be less sensitive to changes in the aluminium/metal ratio. Chain transfer to aluminium is also favoured at high aluminium concentrations. This increase in chain transfer would presumably produce lower molecular weight polymer. However, some researchers have observed decreases (12,16,17,30,31) and some others have observed no changes in the molecular weight (13,32), with increasing aluminium concentration.

For the in-situ supported metallocene polymerization studied herein, many of these trends apply. However it is noted that the in-situ heterogenization process can complicate the interpretation of observed effects. We used the above explanations as a guideline to understand the responses to the variation of several polymerization parameters, such as temperature, ethylene pressure, hydrogen pressure, comonomer concentration and alkylaluminum

concentration according to the experimental design layout. The overall goal of the present investigation is to analyse the responses and possibly predict the effects of these polymerization conditions on catalyst productivity and copolymer microstructure.

6.2 Experimental

Rac-(dimethylsilylbis(methylbenzoindenyl)) zirconium dichloride [Me_2Si(2-Me-4,5 BenzInd)$_2ZrCl_2$] was purchased from Boulder Scientific Co. (BSC-366, Boulder, Colorado). Silica supported methylaluminoxane (SMAO, 24.4 wt% Al, purchased from Witco) was used as a catalyst support. CP grade ethylene and ultra high purity nitrogen (purchased from Linde) were purified by passing them through molecular sieves and de-oxygenating beds. Ultra high purity hydrogen (Praxair) was used without further purification. 1-Octene (Aldrich) was dried over 3A/4A molecular sieves and used without further purification.

Toluene was purified by refluxing over n-butyl lithium/styrene oligomers and by distillation. n-Hexane was dried over a mixture of 3A/4A molecular sieves (purchased from BDH) and degassed by bubbling with prepurified nitrogen.

Triethylaluminum (TEA) was purchased from Aldrich Chemicals and used without further purification.

6.2.1 Polymerization

Polymerizations were performed in a 300 mL Parr semi-batch autoclave reactor equipped with a temperature control unit comprising of a cooling coil and an electric heater. 150 mL of hexane was pre-treated with TEA to scavenge impurities and activate the catalyst. After evacuation of the reactor and backfilling with nitrogen, approximately 50 mL of hexane was

added. This was followed by the addition of 0.007–0.042 g SMAO and 0.125–1.0 μmol [Me_2Si(2-Me-4,5 BenzInd)$_2ZrCl_2$] (solution in toluene). The ratio of aluminium present in the SMAO to zirconium was fixed at 500. 1-octene was added in the range of 0 – 22 mol % feed in hexane to the reactor via a transfer syringe. 0 – 100 mL of hydrogen from a hydrogen bottle at atmospheric pressure was also injected into the reactor via a transfer syringe. The reactor was then heated to the polymerization temperature in the range of 25-85°C. Once the reaction temperature was reached, a stirring rate of 350 rpm was set and the reactor was pressurized with ethylene to begin the polymerization. After 30 min the polymerization was quenched with an excess of ethanol. The resulting polymer was then filtered, washed and dried in an oven at 60°C.

6.2.2 Characterization

Molecular weight distributions were determined by high temperature gel permeation chromatography (GPC). A Waters GPC 150CV instrument with a Viscotek 150R viscometer was used with 1,2,4-trichlorobenzene as a mobile phase operating at 140°C. Short chain branching distributions were determined by crystallization analysis fractionation (CRYSTAF) using a CRYSTAF 200 instrument (Polymer Char, Valencia, Spain). CRYSTAF is a technique similar to temperature rising elution fractionation (TREF), but with significantly shorter analysis time (35)**.** 1-Octene copolymer compositions were estimated by integration of the CRYSTAF profiles using a calibration curve relating the crystallization temperature (T_c) and the 1-octene content that had been previously determined by C^{13} NMR. The calibration curve used to determine the 1-octene content is shown in Figure 6.2.

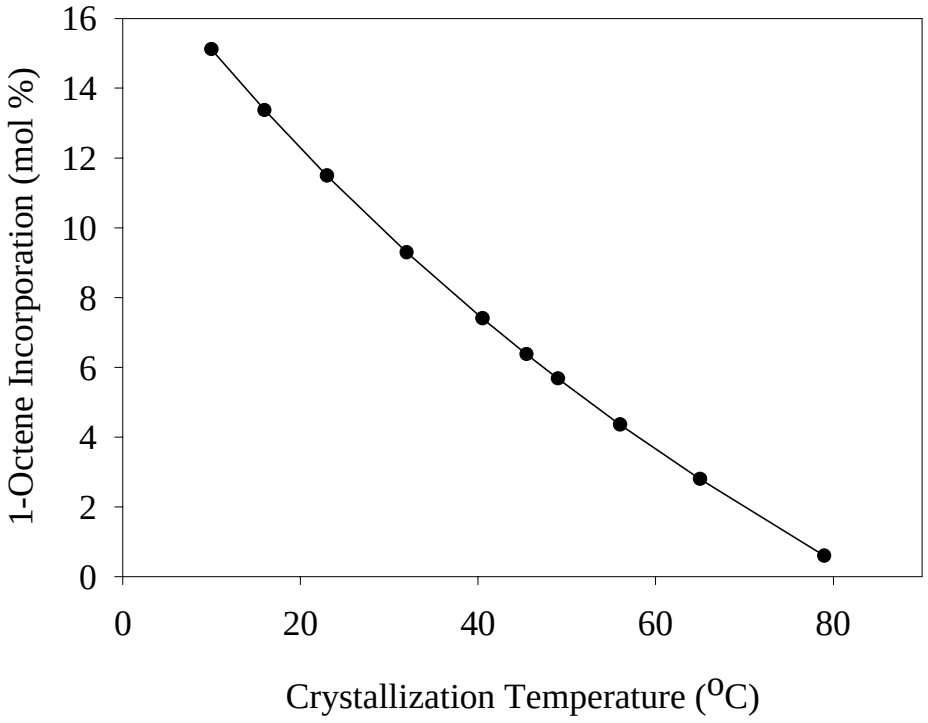

Figure 6.2 – CRYSTAF Calibration Curve - 1-Octene Comonomer Incorporation

6.2.3 Experimental Design Procedure

To study the effect of polymerization conditions on the copolymerization of ethylene and 1-octene with in-situ $Me_2Si(2\text{-}Me\text{-}4,5\ BenzInd)_2ZrCl_2$, a two level, five factor fractional factorial design was carried out with a resolution of V (2_V^{5-1}), indicating that no two factor interactions or main effects are correlated (34).

The experimental conditions chosen for the design levels are shown in Table 6.2, including the levels for the 2_V^{5-1} fractional design and the upgraded levels to a central composite design with the use of star points. The star points are included as additional levels to be used in the model predictions. The chosen alpha level was set at 2 to balance the prediction errors of the design (rotatable) (34). Due to the unfeasibility of reaching the star points for the ethylene pressure and hydrogen level, they were adjusted as face-centered points. The experimental runs were carried out in a randomized order. Polymerizations were carried out at constant ethylene pressure with a fixed comonomer/ethylene ratio, as required by the design. To estimate the amount of 1-octene required for the desired ratio at the various temperatures and pressures, bubble point calculations based on the Chao-Seader method were made using a Fortran 77 program (35). The activator to support ratio reflects the amount of aluminum present on the support and added as soluble MAO. For this study, the supported aluminum to catalyst metal ratio was fixed at 500.

Table 6.3 shows the estimated 1-octene and ethylene concentrations in hexane for the temperatures and pressures investigated in this study.

Table 6.2 – Experimental Conditions for the Experimental Design Levels

Factor	Design Levels				
	High (1)	Low (2)	Center (0)	Highstar(2)*	Lowstar(-2)*
Temp (°C)	70	40	55	85	25
Pressure (psig)	200	100	150	200 (1)	50
Hydrogen (mL)	50	0	25	75	0 (-1)
Comonomer/ Ethylene	0.21	0.07	0.14	0.28	0
Activator/Support	15	5.335	10.1675	19.8325	0.5025

* The central composite design star points were set at an alpha level = 2. Note that the high star for pressure and low starpoint for hydrogen were adjusted to be face centered due to experimental constraints.

Table 6.3 - Estimates of the 1-Octene and Ethylene Concentrations in Hexane at the Experimental Design Levels

Temperature	Pressure	Comonomer/Ethylene Ratio							
		0.07		**0.14**		**0.21**		**0.28**	
		Liquid Phase Compositions[a]							
(°C)	(psig)	[1-Octene] (mol/L)	[ethylene] (mol/L)	[1-Octene] (mol/L)	[ethylene] (mol/L)	[1-Octene] (mol/L)	[ethylene] (mol/L)	[1-Octene] (mol/L)	[ethylene] (mol/L)
25	150	-	-	0.2587	1.8475	-	-	-	-
40	100	0.06376	0.9109	-	-	0.1907	0.9079	-	-
40	200	0.1392	1.9882	-	-	0.4134	1.9688	-	-
55	50	-	-	0.04331	0.3094	-	-	-	-
55	150	-	-	0.1573	1.1234	-	-	0.3133	1.1188
55	200	-	-	0.2182	1.5624	-	-	-	-
70	100	0.0381	0.5443	-	-	0.1141	0.5432	-	-
70	200	0.0871	1.2449	-	-	0.2602	1.2393	-	-
85	150	-	-	0.0966	0.6900	-	-	-	-

[a] Calculated using a vapour liquid equilbirium program based on bubble point calculations (35)

6.2.4 Response Analysis

The responses for the design were measured in terms of polymerization activity, 1-octene incorporation, SCBD broadness, weight average molecular weight, and polydispersity index. Polymerization activity was determined as the ratio (mass of polymer produced)/(catalyst moles x polymerization time). Note that this does not include the contribution of monomer pressure. The 1-octene content was determined from the integration of the SCBD. The SCBD broadness was quantified as the difference between the number average temperatures (T_n) for the homopolymer and copolymer peaks as described below.

$$T_n = \frac{1}{\sum \frac{wi}{Ti}} \tag{4}$$

where w_i is the weight fraction of polymer and T_i is the temperature of the fraction.

The average molecular weights and polydispersity indices were calculated from the GPC analysis using standard GPC techniques.

Analysis of the experimental design data was carried out using StatSoft Inc. STATISTICA, Version 5.1 ’97 Edition. Factor significance was determined using the analysis of variance method with a pure error estimate calculated from 6 replicate runs of the center point. Marginal mean plots and prediction profiles were generated to include error bars at a 95% confidence level. The prediction profiles generated represent each response and its parameter dependence as a 2nd order polynomial. The form of the empirical model is shown in Eq. (5).

$$\begin{aligned} Y = {} & \beta_0 + \beta_1 T + \beta_2 P + \beta_3 C + \beta_4 H + \beta_5 A + \text{ 2 parameter interactions} \\ & + \beta_{16} T^2 + \beta_{17} P^2 + \beta_{18} C^2 + \beta_{19} H^2 + \beta_{20} A^2 + \text{error} \end{aligned} \tag{5}$$

where the β’s are the parameter estimates for the factors of (T)emperature, (P)ressure, (C) comonomer to ethylene ratio, (H)ydrogen concentration and (A)luminum concentration.

6.3 Results and Discussion

The run layouts of the fractional factorial and central composite design along with the measured results from the polymerizations are shown in Tables 6.4 to 6.9. The analysis of the data will be described in the next three sections based on the values obtained for polymerization activity, short chain branching distribution, and molecular weight distribution of the synthesized copolymers.

Twenty-six unique polymerizations and 6 replicated center points were carried out for the estimation of inherent variation. These runs were carried out under the prescribed polymerization conditions and limited to low polymer yields to minimize the drift in comonomer concentration.

6.3.1 Activity

From the analysis of the design data, it was found that the polymerization activity was sensitive to all of the reaction parameters studied. The predicted response profiles of the polymerization activity with respect to each parameter are shown in Figures 6.3 (a-e). These plots indicate how catalyst activity depends on each parameter. However, these are model predictions and some lack of fit was present, especially towards the parameter extremes. Figure 6.3a shows how activity varies with temperature. The temperature of the polymerization medium affects the kinetics of the reaction. For the temperature range studied, with increasing temperature, the catalyst activity increased (5-17). This is not always the case, since the rate of catalyst deactivation also increases with temperature. It has been reported that catalyst activity can reach a maximum between 40 and 80°C (6,12,13) and depends on the polymerization time and polymerization conditions. With an increase in ethylene pressure, the activity also increased

Table 6.4 – ½ Fractional Design Responses: Activity

Factor Design Levels[a]						Responses
Run[b]	Temperature	Pressure	Hydrogen	Comonomer/ Ethylene Ratio	Activator/ Support Ratio	Activity[c]
#	(°C)	(psig)	(mL)			(kg PE/mol cat hr)
1	40	100	0	0.07	15	2107
2	70	100	0	0.07	5.335	8448
3	40	200	0	0.07	5.335	6713
4	70	200	0	0.07	15	10880
5	40	100	50	0.07	5.335	392
6	70	100	50	0.07	15	1589
7	40	200	50	0.07	15	2381
8	70	200	50	0.07	5.335	5040
9	40	100	0	0.21	5.335	15387
10	70	100	0	0.21	15	5440
11	40	200	0	0.21	15	10880
12	70	200	0	0.21	5.335	26560
13	40	100	50	0.21	15	1387
14	70	100	50	0.21	5.335	3000
15	40	200	50	0.21	5.335	6320
16	70	200	50	0.21	15	5520
17 (C)	55	150	25	0.14	10.1675	5216
18 (C)	55	150	25	0.14	10.1675	5824
19 (C)	55	150	25	0.14	10.1675	3740

[a] As determined by 2_v^{V-1} factorial design

[b] Experiments were carried out with $Me_2Si(2\text{-}Me\text{-}4,5\ BenzInd)_2ZrCl_2$ catalyst, silica supported MAO, triethylaluminum activator, ethylene monomer and 1-octene comonomer. Runs shown here were carried out in a randomized fashion. (C) indicates a center point replicate.

[c] Based on the amount of polymer recovered.

Table 6.5 – ½ Fractional Design Responses: CRYSTAF Analysis

Factor Design Levels[a]						Responses				
Run[b]	Temperature	Pressure	Hydrogen	Comonomer/ Ethylene Ratio	Activator/ Support Ratio	% Homo-polymer[c]	% Copolymer[d]	Overall 1-Octene Content in Copolymer[e]	Num. Average Temperature Homopolymer[f]	Num. Average Temperature Copolymer[g]
#	(°C)	(psig)	(mL)			(%)	(%)	(%)	(°C)	(°C)
1	40	100	0	0.07	15	100.0	0.0	0.41	80.03	-
2	70	100	0	0.07	5.335	100.0	0.0	1.00	76.11	-
3	40	200	0	0.07	5.335	100.0	0.0	0.29	80.94	-
4	70	200	0	0.07	15	100.0	0.0	0.87	77.06	-
5	40	100	50	0.07	5.335	67.8	32.2	2.21	76.27	51.26
6	70	100	50	0.07	15	87.2	12.8	2.11	72.26	47.36
7	40	200	50	0.07	15	75.8	24.2	1.58	79.25	50.46
8	70	200	50	0.07	5.335	100.0	0.0	0.93	75.80	-
9	40	100	0	0.21	5.335	19.5	80.5	5.71	75.56	75.74
10	70	100	0	0.21	15	10.5	89.5	3.98	74.67	55.02
11	40	200	0	0.21	15	52.0	48.0	3.02	78.15	48.78
12	70	200	0	0.21	5.335	16.1	83.9	3.50	70.97	58.73
13	40	100	50	0.21	15	7.5	92.5	7.06	74.47	37.95
14	70	100	50	0.21	5.335	4.9	95.1	5.89	72.43	44.20
15	40	200	50	0.21	5.335	55.9	44.1	2.78	78.91	46.57
16	70	200	50	0.21	15	14.2	85.8	3.93	75.37	54.71
17 (C)	55	150	25	0.14	10.1675	62.3	37.7	1.91	77.18	58.88
18 (C)	55	150	25	0.14	10.1675	72.2	27.8	1.59	77.30	59.56
19 (C)	55	150	25	0.14	10.1675	66.8	33.2	1.79	77.05	59.01

[a] As determined by 2_v^{V-1} factorial design

[b] Experiments were carried out with $Me_2Si(2\text{-}Me\text{-}4,5\ BenzInd)_2ZrCl_2$ catalyst, silica supported MAO, triethylaluminum activator, ethylene monomer and 1-octene comonomer. Runs shown here were carried out in a randomized fashion. (C) indicates a center point replicate.

[c,d] Estimated from the areas in the CRYSTAF profiles determined as homopolymer and copolymer

[e] Estimated from the CRYSTAF profile using a calibration curve relating 1-octene content and crystallization temperature

[f,g] Number average crystallization temperatures from the homopolymer and copolymer regions in the CRYSTAF profiles

Table 6.6 – ½ Fractional Design Responses: Molecular Weight Analysis

Factor Design Levels[a]						Responses	
Run[b] #	Temperature (°C)	Pressure (psig)	Hydrogen (mL)	Comonomer/ Ethylene	Activator/ Support	Wt. Average Molecular Weight[c] (g/mol)	Poly-dispersity Index[d]
1	40	100	0	0.07	15	354,900	2.95
2	70	100	0	0.07	5.335	114,000	2.66
3	40	200	0	0.07	5.335	373,200	3.77
4	70	200	0	0.07	15	213,800	2.17
5	40	100	50	0.07	5.335	26,000	2.32
6	70	100	50	0.07	15	33,600	1.79
7	40	200	50	0.07	15	41,800	4.73
8	70	200	50	0.07	5.335	49,300	2.55
9	40	100	0	0.21	5.335	153,200	2.48
10	70	100	0	0.21	15	57,500	2.00
11	40	200	0	0.21	15	427,600	2.25
12	70	200	0	0.21	5.335	463,800	2.53
13	40	100	50	0.21	15	32,400	2.15
14	70	100	50	0.21	5.335	47,000	1.94
15	40	200	50	0.21	5.335	46,600	3.53
16	70	200	50	0.21	15	64,100	2.02
17 (C)	55	150	25	0.14	10.1675	67,100	2.78
18 (C)	55	150	25	0.14	10.1675	64,300	2.77
19 (C)	55	150	25	0.14	10.1675	76,500	2.69

[a] As determined by 2_v^{V-1} factorial design

[b] Experiments were carried out with $Me_2Si(2\text{-}Me\text{-}4,5\ BenzInd)_2ZrCl_2$ catalyst, silica supported MAO, triethylaluminum activator, ethylene monomer and 1-octene comonomer. Runs shown here were carried out in a randomized fashion. (C) indicates a center point replicate.

[c,d] As determined by GPC using narrow polystyrene standards and the universal cali bration curve

Table 6.7 – Central Composite Design Responses: Activity

Factor Design Levels[a]						Responses
Run[b] #	Temperature (°C)	Pressure (psig)	Hydrogen (mL)	Comonomer/ Ethylene Ratio	Activator/ Support Ratio	Activity[c] (kg PE/mol cat hr)
20	25	150	25	0.14	10.1675	1296
21	85	150	25	0.14	10.1675	26560
22	55	50	25	0.14	10.1675	427
23	55	200	25	0.14	10.1675	6640
24	55	150	0	0.14	10.1675	15160
25	55	150	75	0.14	10.1675	1156
26	55	150	25	0	10.1675	4267
27	55	150	25	0.28	10.1675	13200
28	55	150	25	0.14	0.5025	42480
29	55	150	25	0.14	19.8325	1680
30 (C)	55	150	25	0.14	10.1675	4640
31 (C)	55	150	25	0.14	10.1675	5200
32 (C)	55	150	25	0.14	10.1675	-

[a] Additional runs to follow a central composite design with starpoints at alpha level = 2.
[b] Experiments were carried out with $Me_2Si(2\text{-}Me\text{-}4,5\ BenzInd)_2ZrCl_2$ catalyst, silica supported MAO, triethylaluminum activator, ethylene monomer and 1-octene comonomer. Runs shown here were carried out in a randomized fashion. (C) indicates a center point replicate.
[c] Based on the amount of polymer recovered.

Table 6.8 – Central Composite Design Responses: CRYSTAF Analysis

Factor Design Levels[a]						Responses				
Run[b]	Temperature	Pressure	Hydrogen	Comonomer/ Ethylene Ratio	Activator/ Support Ratio	% Homo-polymer[c]	% Copolymer[d]	Overall 1-Octene Content in Copolymer[e]	Num. Average Temperature Homopolymer[f]	Num. Average Temperature Copolymer[g]
#	(°C)	(psig)	(mL)			(%)	(%)	(%)	(°C)	(°C)
20	25	150	25	0.14	10.1675	74.1	26.0	1.29	81.01	55.12
21	85	150	25	0.14	10.1675	100.0	0.0	2.30	67.29	-
22	55	50	25	0.14	10.1675	11.1	88.9	3.88	75.80	55.43
23	55	200	25	0.14	10.1675	66.8	33.3	1.86	77.52	57.07
24	55	150	0	0.14	10.1675	62.2	37.8	1.74	75.95	63.82
25	55	150	75	0.14	10.1675	42.3	57.7	2.80	74.31	57.41
26	55	150	25	0	10.1675	100.0	0.0	0.36	79.90	-
27	55	150	25	0.28	10.1675	7.0	93.0	6.64	76.27	40.72
28	55	150	25	0.14	0.5025	34.7	65.3	2.35	78.36	61.73
29	55	150	25	0.14	19.8325	78.8	21.2	1.15	79.24	60.54
30 (C)	55	150	25	0.14	10.1675	56.2	43.8	1.77	78.63	61.39
31 (C)	55	150	25	0.14	10.1675	78.4	21.6	1.23	78.75	60.27
32 (C)	55	150	25	0.14	10.1675	83.3	16.7	1.38	77.60	54.71

[a] Additional runs to follow a central composite design with starpoints at alpha level = 2.
[b] Experiments were carried out with $Me_2Si(2\text{-}Me\text{-}4,5\ BenzInd)_2ZrCl_2$ catalyst, silica supported MAO, triethylaluminum activator, ethylene monomer and 1-octene comonomer. Runs shown here were c arried out in a randomized fashion. (C) indicates a center point replicate.
[c,d] Estimated from the areas in the CRYSTAF profiles determined as homopolymer and copolymer
[e] Estimated from the CRYSTAF profile using a calibration curve relating 1-octene content and crystallization temperature
[f,g] Number average crystallization temperatures from the homopolymer and copolymer regions in the CRYSTAF profiles

Table 6.9 – Central Composite Design Responses: Molecular Weight Analysis

Factor Design Levels[a]						Responses	
Run [b]	Temperature	Pressure	Hydrogen	Comonomer/ Ethylene	Activator/ Support	Wt. Average Molecular Weight[c]	Poly-dispersity Index[d]
#	(°C)	(psig)	(mL)			g/mol	
20	25	150	25	0.14	10.1675	13,800	3.04
21	85	150	25	0.14	10.1675	104,500	2.69
22	55	50	25	0.14	10.1675	32,700	2.10
23	55	200	25	0.14	10.1675	88,000	2.60
24	55	150	0	0.14	10.1675	280,900	2.99
25	55	150	75	0.14	10.1675	105,100	3.85
26	55	150	25	0	10.1675	63,500	6.11
27	55	150	25	0.28	10.1675	95,000	2.05
28	55	150	25	0.14	0.5025	204,300	6.93
29	55	150	25	0.14	19.8325	63,100	2.48
30 (C)	55	150	25	0.14	10.1675	95,800	2.72
31 (C)	55	150	25	0.14	10.1675	71,800	3.08
32 (C)	55	150	25	0.14	10.1675	55,800	2.61

[a] Additional runs to follow a central composite design with starpoints at alpha level = 2

[b] Experiments were carried out with $Me_2Si(2\text{-}Me\text{-}4,5\ BenzInd)_2ZrCl_2$ catalyst, silica supported MAO, triethylaluminum activator, ethylene monomer and 1-octene comonomer. Runs shown here were carried out in a randomized fashion. (C) indicates a center point replicate.

[c,d] As determined by GPC using narrow polystyrene standards and the universal calibration curve

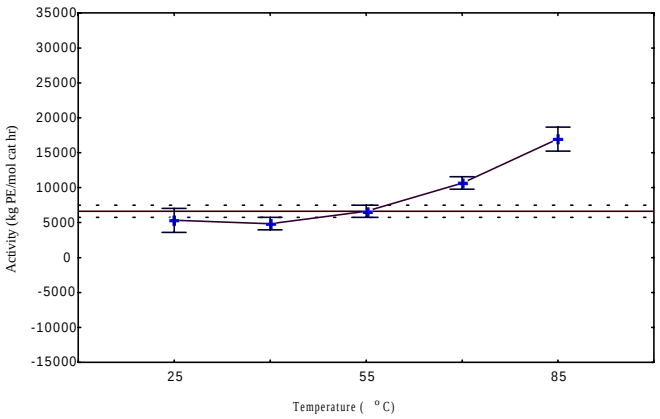

(a)

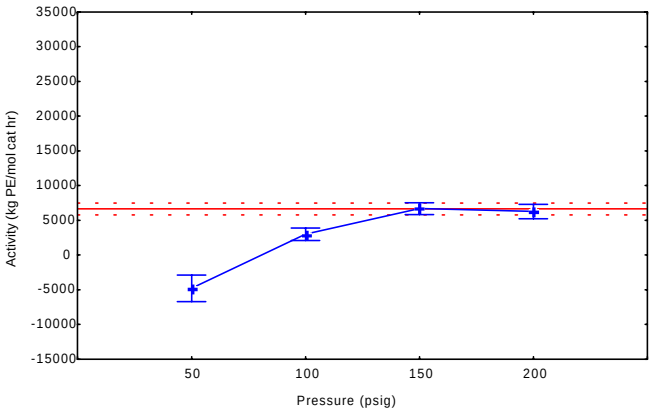

(b)

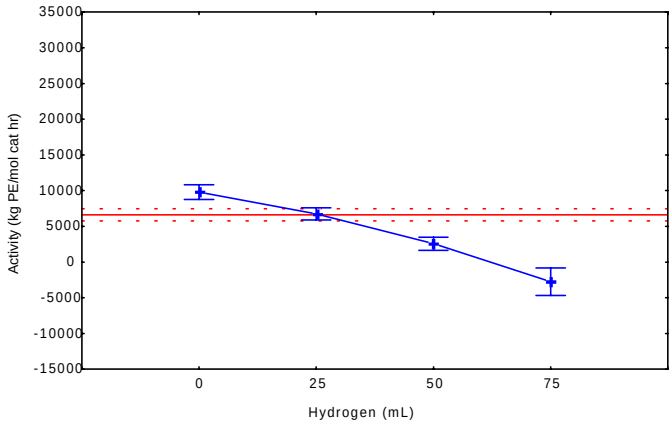

(c)

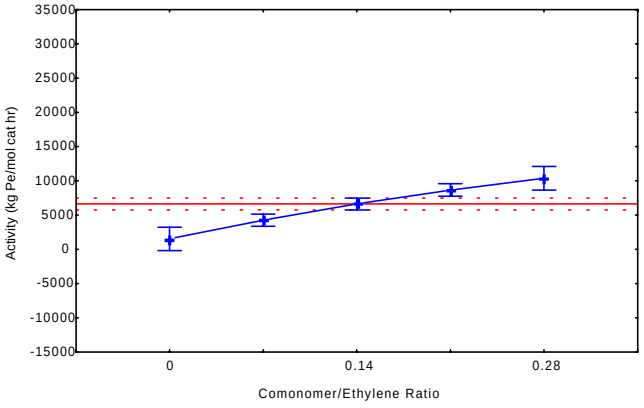

(d)

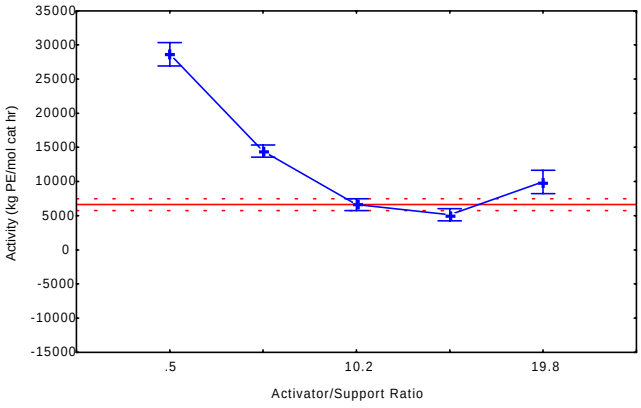

(e)

Figure 6.3 – Effect of Polymerization Conditions on Catalyst Activity

(Figure 6.3b). This increase in activity with pressure is fairly typical, since the propagation rate is assumed to be first order in monomer concentration (13). There is, however, some levelling off for ethylene pressures greater than 150 psig. Catalyst activity decreases significantly with the addition of hydrogen. Both increases (8,10,15,22,24) and decreases (15,18,21,23,24) in activity have been reported in the literature upon the addition of hydrogen, as a function of catalyst type, monomer type and polymerization conditions. This reduction in activity has been tentatively linked to a slower addition of monomer to the catalyst-hydrogen bond that is formed after chain transfer to hydrogen. An increase in activity was observed with increased addition of comonomer as shown in Figure 6.3d (7,9,14,18,19,25-29). This increase is presumably due to the comonomer effect that is often associated with polymerization rate enhancement. The origin and nature of this effect is still in debate (18,19,25,26,28). It is believed that this effect might be both physical and chemical in nature. Physically, the presence of comonomer enhances the diffusion of monomer to the active sites since polymer with low crystallinity is formed. The presence of the comonomer activates and increases the number of catalytic sites that were not formerly present in the absence of comonomer. Recently, Ystenes has proposed an insertion mechanism that involves a monomer unit triggering the insertion of an already complexed monomer (36). This mechanism accounts for the formation of different catalytic sites and different propagation rates in the presence of comonomer. Catalyst activity decreases with the addition of activator (Figure 6.3e). Although activators are required to activate the catalyst (37), it is possible that a large excess of activator may block the catalytic sites. For a similar system, it was observed that increasing the trimethylaluminum to silica MAO support ratio, a decrease in activity occurred at ratios up to 3.33 (16). This decrease was attributed to the bimolecular deactivation caused by the complexation of homogeneous metallocene and trimethylaluminum.

Further analysis of the two-factor interaction parameters reveals more insight into the interplay that the reaction conditions may have on each other, as illustrated by the activity interaction plots (Figures 6.4(a-e)). It is reasonable to assume that factors at different levels may lead to different polymerization mechanisms and catalyst sensitivities. It can be seen from the temperature-pressure activity interaction plot (Figure 6.4a), that the catalyst exhibits different sensitivities to temperature depending on ethylene pressure. At the low pressure level (100 psig ethylene), the catalyst seems to be temperature-insensitive from 40 and 70°C. However catalyst activity depends strongly on temperature at the high pressure level (200 psig ethylene). This behaviour is difficult to explain and might be related to reactor non-idealities.

The interactions of hydrogen/comonomer and hydrogen/activator are shown in Figures 6.4b and 6.4c. Catalyst activity is greatly lowered in the presence of hydrogen, despite the levels of comonomer and activator present in the reactor. The activity interaction plots for activator/temperature (Figure 6.4d) and activator/comonomer (Figure 6.4e) indicate that catalyst activity always decreases with increasing activator concentration, irrespectively of the polymerization temperature and comonomer concentration used in this investigation.

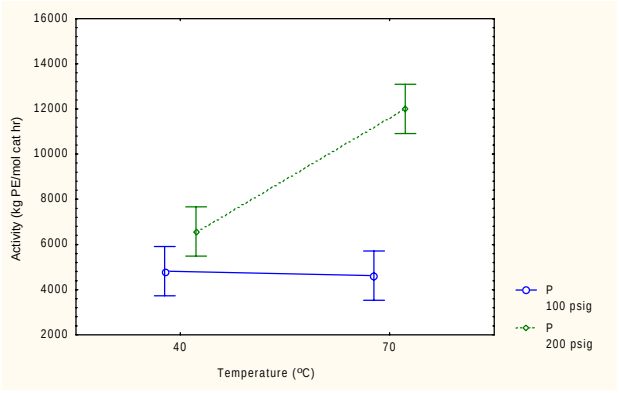

(a)

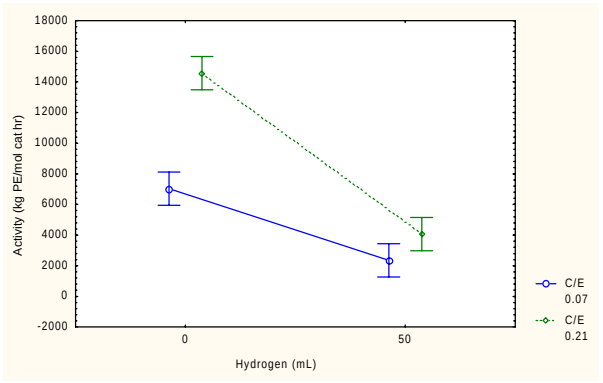

(b)

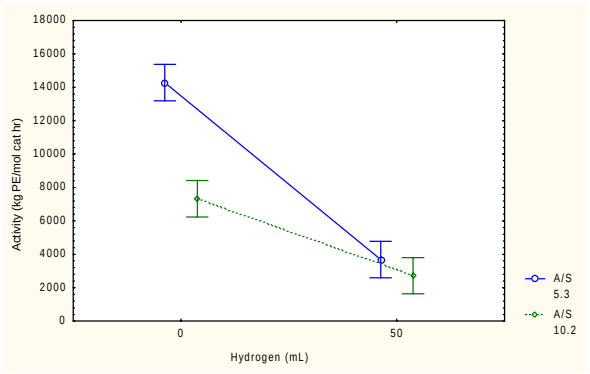

(c)

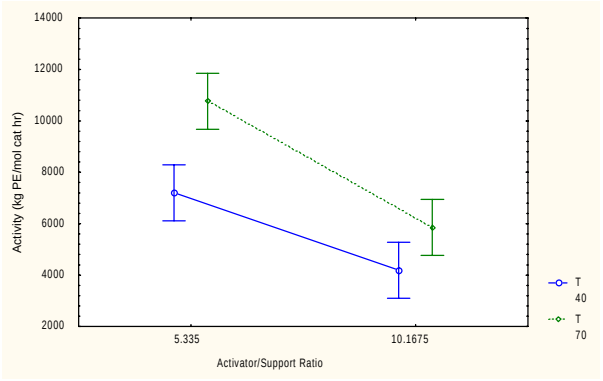

(d)

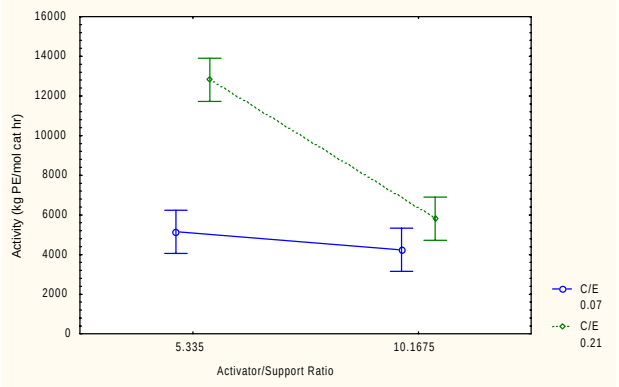

(e)

Figure 6.4 – Interaction of Polymerization Conditions on Catalyst Activity

6.3.2 Short Chain Branching Distributions

Ethylene/α-olefin copolymers produced with in-situ supported catalysts can sometimes have very broad and bimodal SCBDs (1). It was shown in our previous study that different alkylaluminum activators could generate active sites with quite different reactivity ratios. One of the motivations for the present study was to examine the effect of polymerization conditions on the broadening of the SCBDs made with in-situ supported catalysts.

Firstly, to establish a basis for the type of SCBD of these ethylene/1-octene copolymers, the SCBDs of the 6 center point runs (Run #'s 17-19, 30-32) are shown in Figure 6.5. The center point polymerizations were carried out at the conditions set out in the design of experiments and produced copolymers with broad SCBDs. The distributions possess a homopolymer-like portion (indicated by a high crystallization temperature around 78°C) and a copolymer-tail with an average crystallization temperature around 59°C, thus verifying that indeed two distinct site types are present at these polymerization conditions. To characterize these copolymers with such broad SCBDs, two response measures were used in the analysis. To estimate the 1-octene content in the copolymer, the area of the CRYSTAF profile was integrated and then applied to a 1-octene calibration curve which relates the crystallization temperature to the incorporated mol % of 1-octene (Figure 6.2). The relation is shown below:

$$\int m\ f(m)\, dm \tag{6}$$

where m is the mol % of 1-octene obtained from the calibration curve and f(m) is the weight fraction of polymer.

To characterize the broadness of the distribution, the number average temperature was determined (Eq 4) for the region deemed as homopolymer (above 70°C) and copolymer (below 70°C). The difference of these number average temperatures was used as a response for the

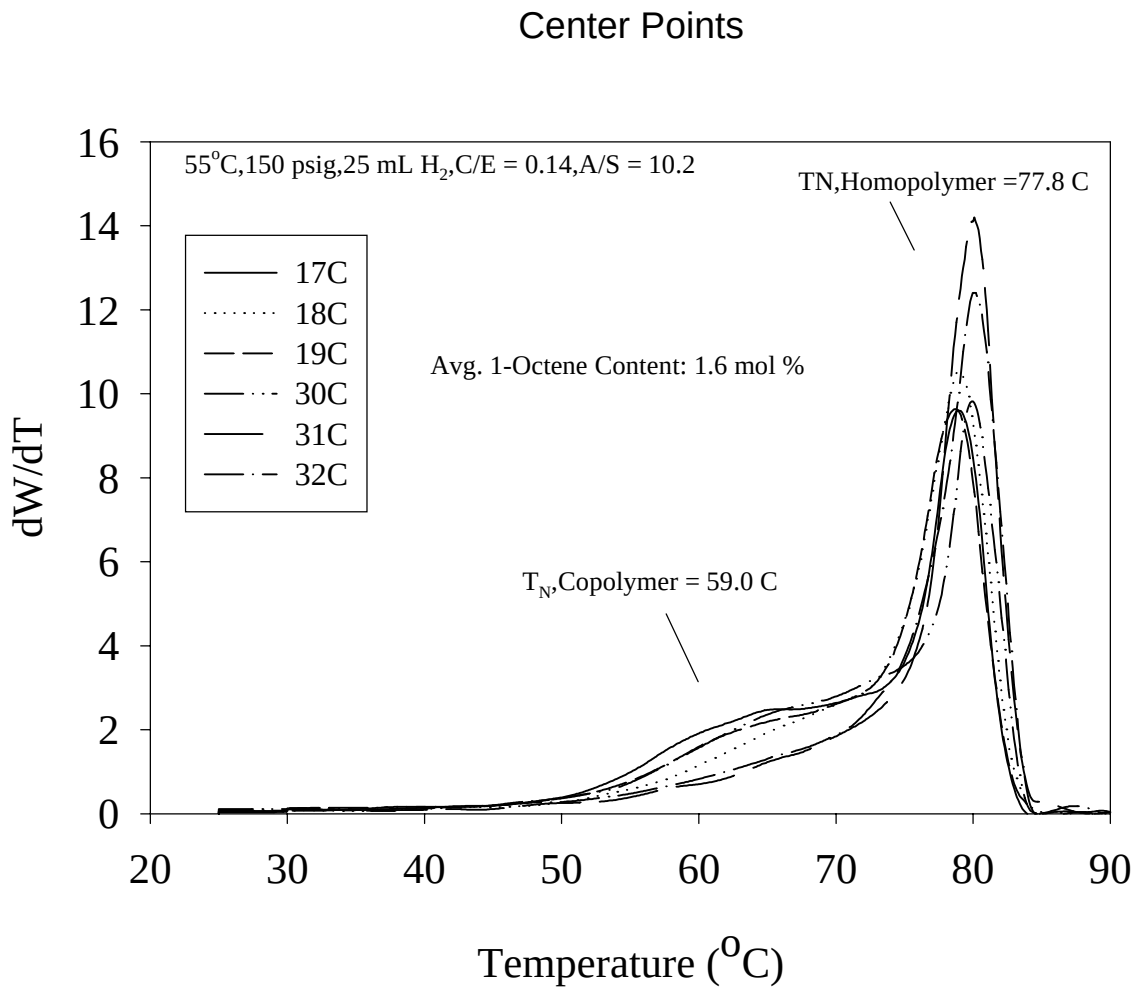

Figure 6.5 – SCBD Comparison of Replicate Center points

design. An increasing temperature difference indicates further peak separation. Summaries of the responses observed from the designed data are shown in Tables 6.5 and 6.8. One of the most remarkable observations with these distributions was the effect of temperature on the SCBD. Figure 6.6 contrasts the differences between polymerizations carried out at 40°C and 70°C at the high comonomer level in the absence of hydrogen. At the low temperature, a very distinct separation of the homopolymer and copolymer peaks was observed. Interestingly, this temperature effect depends highly on other polymerization factors, such as hydrogen presence and comonomer concentration, as indicated in Figures 6.7 and 6.8.

Figures 6.9 (a-e) and Figures 6.10 (a-e) summarize the response profiles for both 1-octene content and homopolymer and copolymer number average temperature difference. Figures 6.9a shows that temperature had a minimal effect on the overall 1-octene content. However decreasing temperature accentuates the separation between the homo and copolymer peaks (Figure 6.10a). In fact the broadening of the SCBD with decreasing polymerization temperature was one of the most notable observations of this investigation. It might be speculated that the active site type that favours ethylene incorporation (i.e., with the lowest reactivity ratio towards 1-octene) is more active at lower polymerization temperatures. Pryzbala et al. observed that SiO_2/MAO/rac-Me_2Si[2-Me-4-Ph-Ind]$_2ZrCl_2$ produced poly(ethylene-co-1-hexene) with polyethylene and amorphous copolymer fractions (7). This behaviour was attributed to mass transfer limitations within the growing polymer particle that limits the access of 1-hexene but not of ethylene to the active sites. For the current system, similar mass transfer limitations cannot be discarded *a priori* since it is observed that the SCBD broadens at lower polymerization temperatures. However, our previous work with poly(ethylene-*co*-1-hexene)

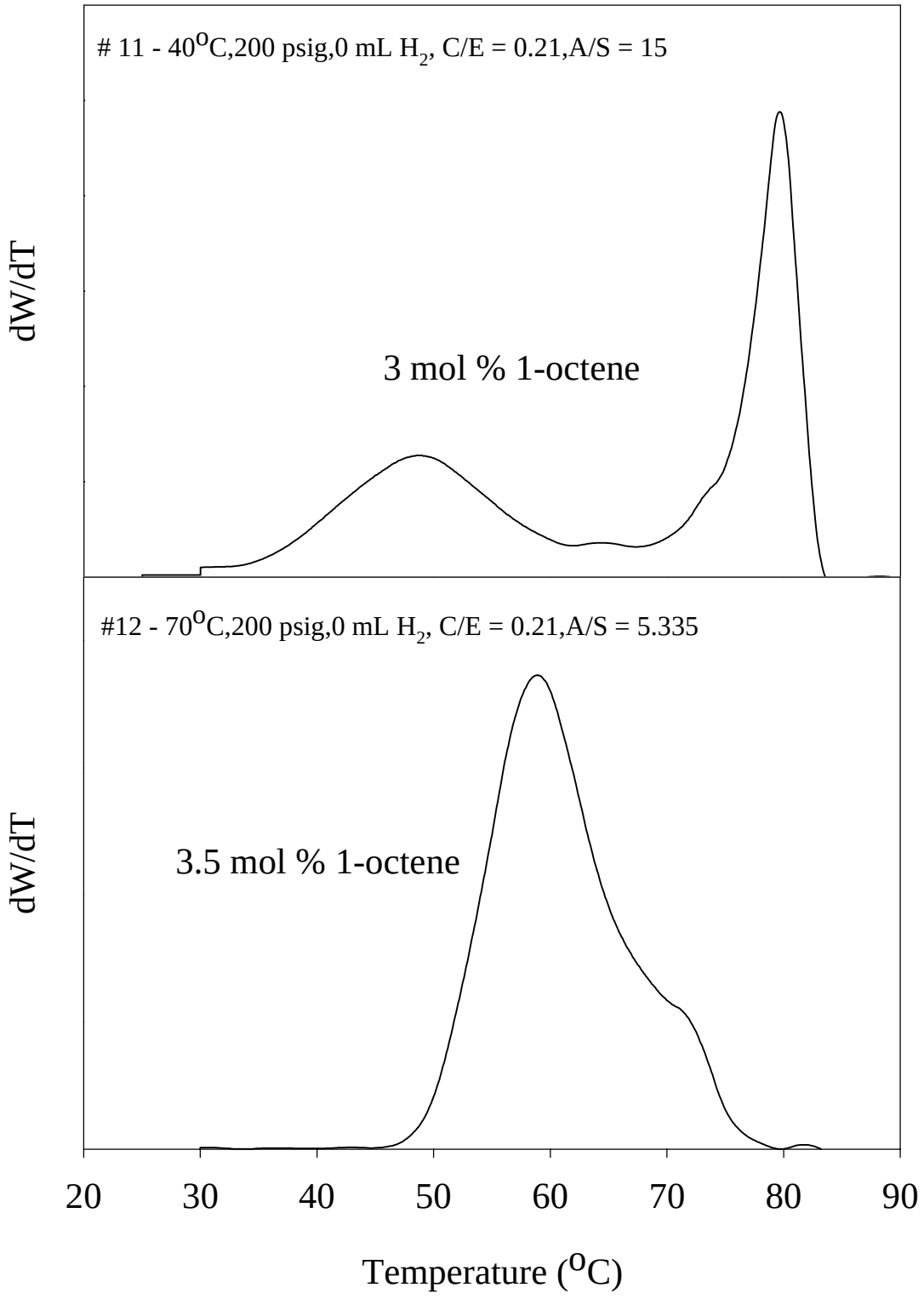

Figure 6.6 – Effect of Temperature Without Hydrogen on the SCBD

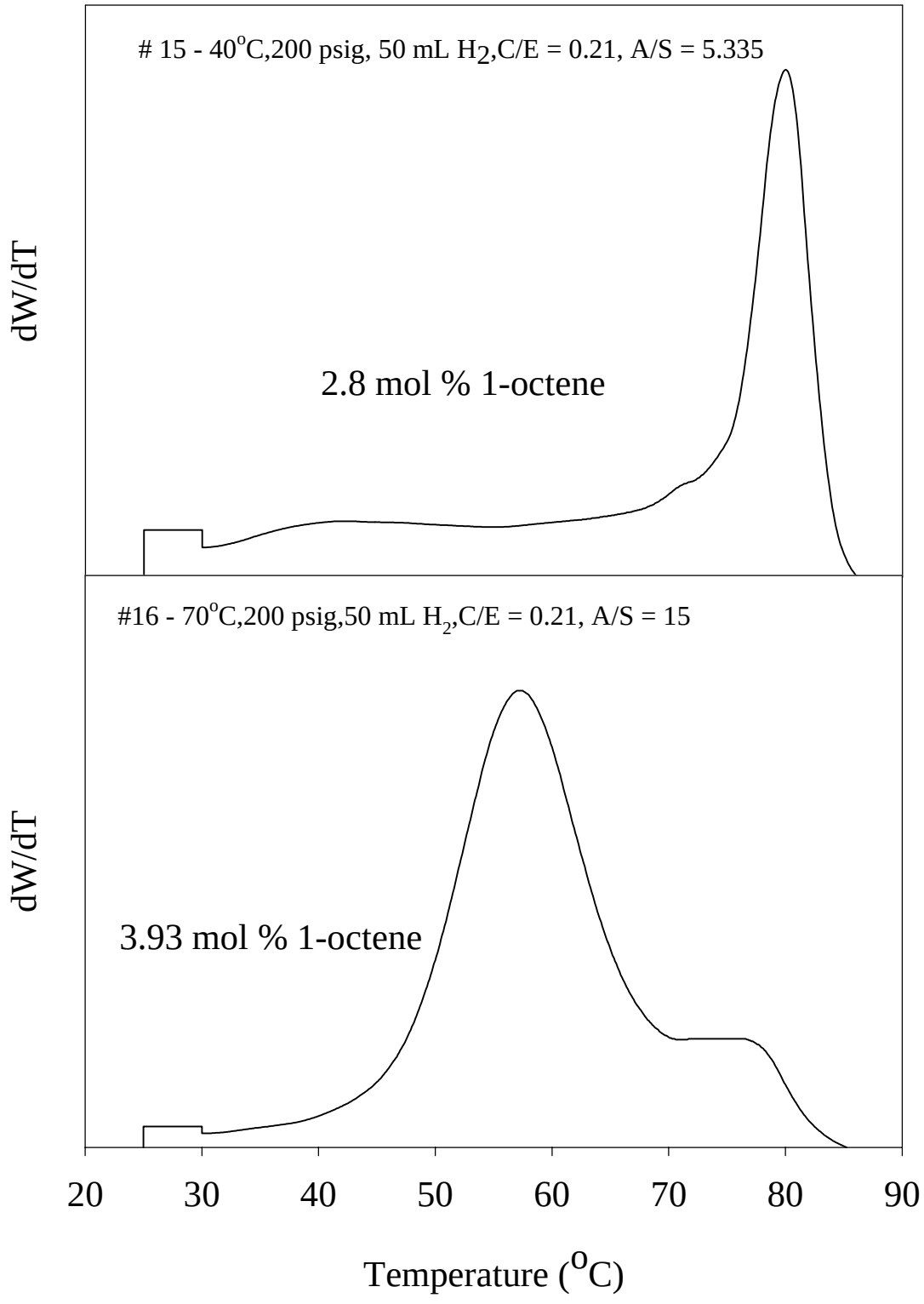

Figure 6.7 – Effect of Temperature With Hydrogen on the SCBD

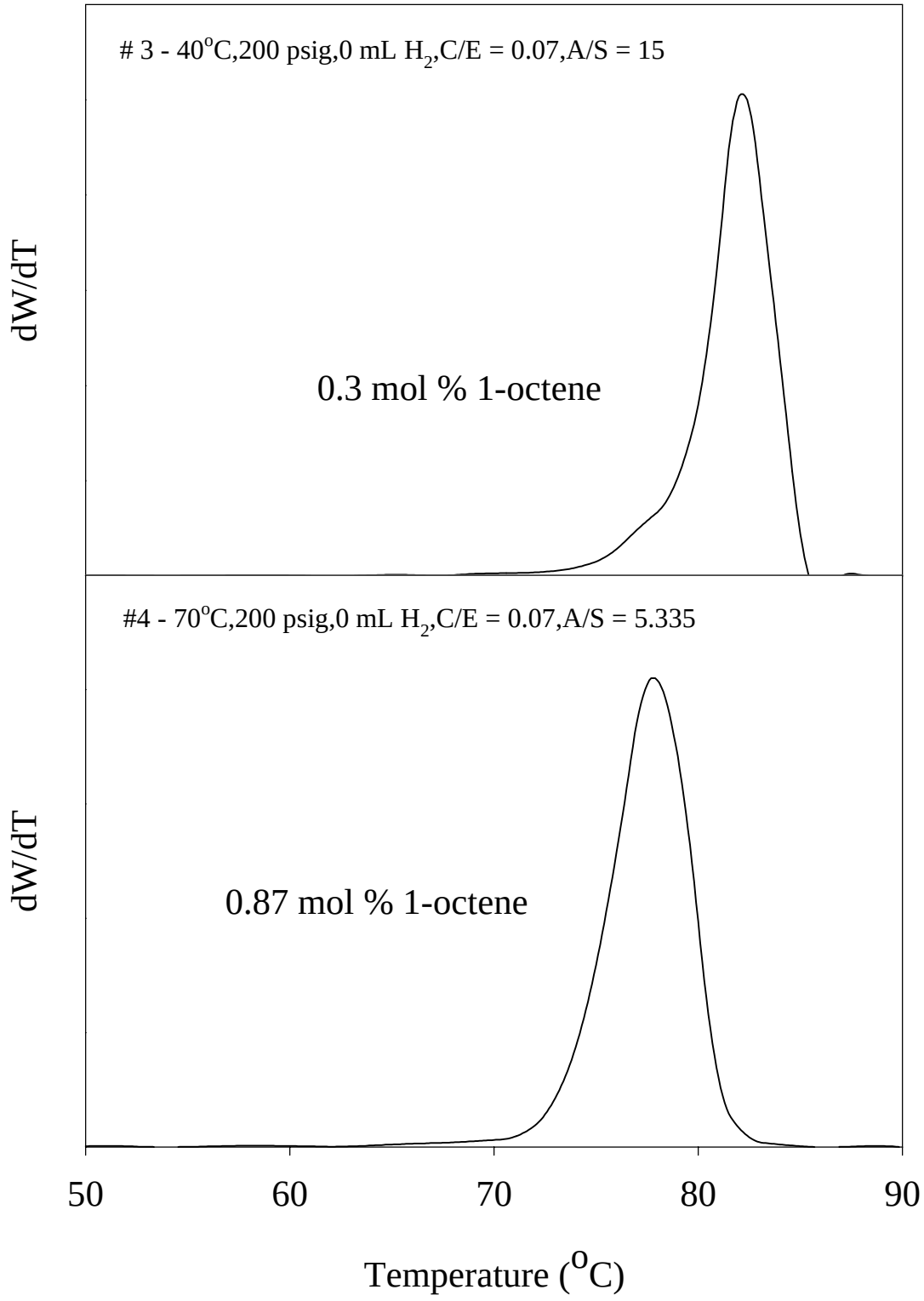

Figure 6.8 – Effect of Temperature at the Low Comonomer Level Without Hydrogen on the SCBD

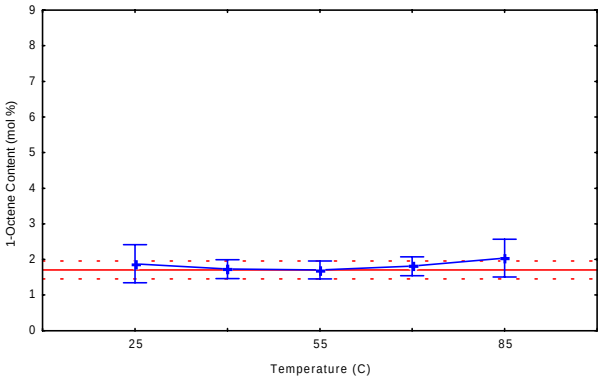

(a)

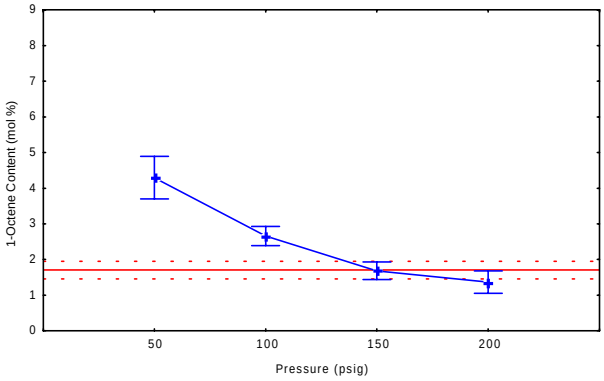

(b)

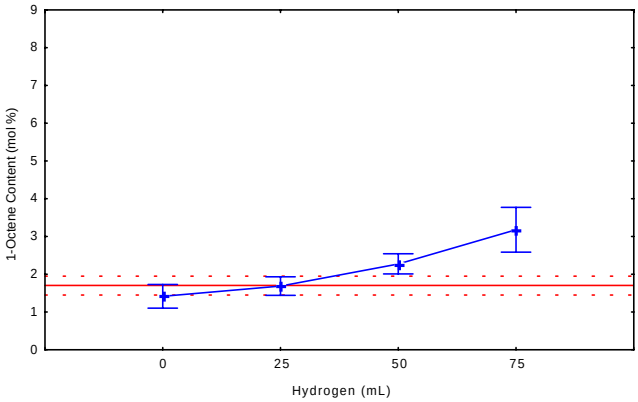

(c)

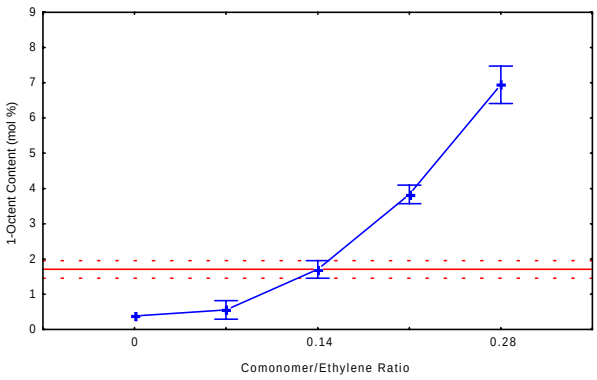

(d)

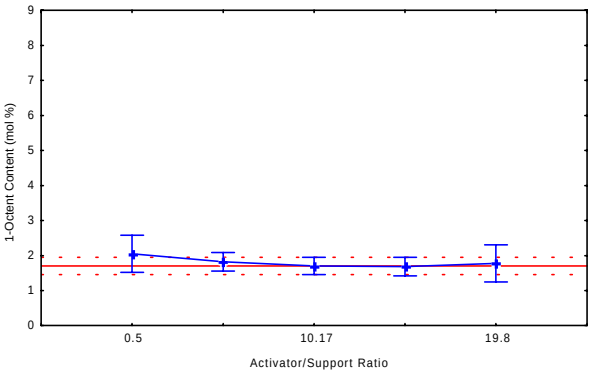

(e)

Figure 6.9 – Effect of Polymerization Conditions on Comonomer Incorporation

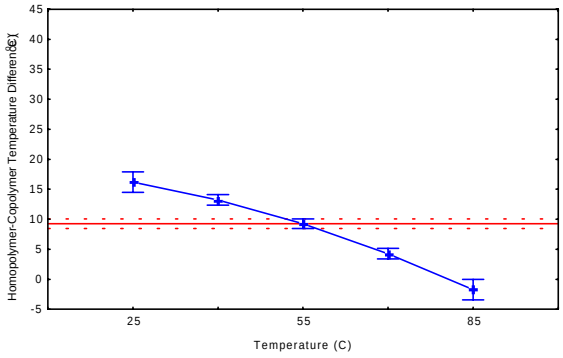

(a)

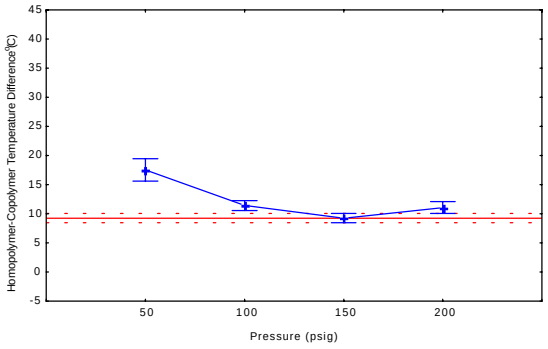

(b)

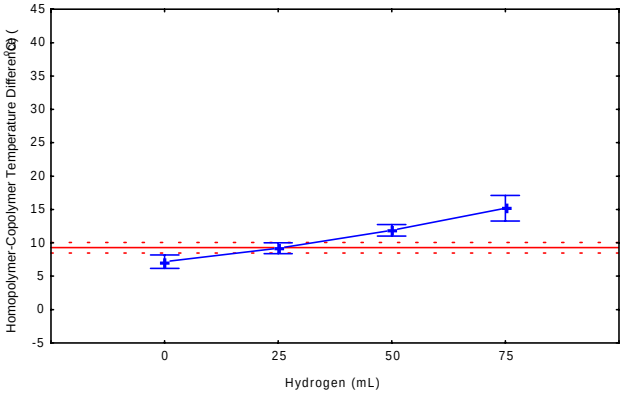

(c)

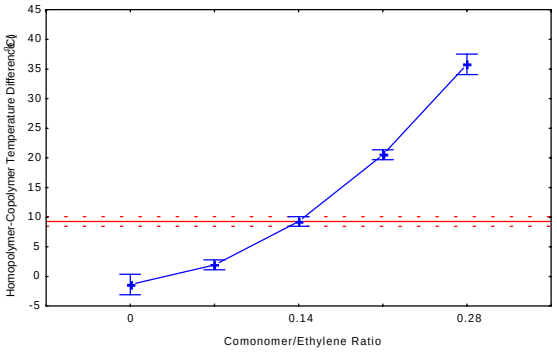

(d)

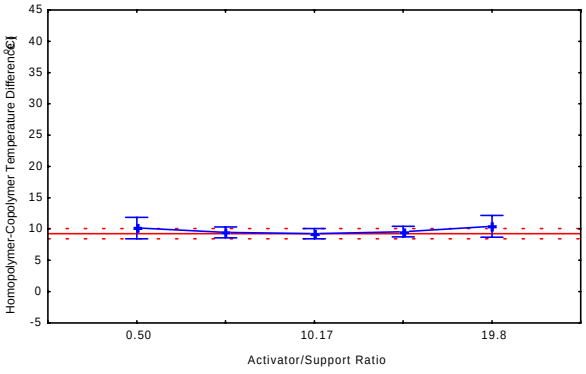

(e)

Figure 6.10 – Effect of Polymerization Conditions on Homopolymer/Copolymer Temperature Difference (Peak Separation)

made with in-situ supported Et[Ind]$ZrCl_2$ indicates that this effect has a chemical nature (1). In that investigation, it was noticed that changing the type of activator (trimethylaluminum, trimethylaluminum, triisobutylaluminum) led to polymers with unimodal or bimodal SCBD. Since it is unlikely that the type of activator will have a marked influence on mass transfer resistances, one is led to conclude that the observed bimodal SCBD are at least in part, due to the presence of different site types on the in-situ supported catalyst.

1-Octene content decreased significantly with increasing ethylene pressure (Figure 6.9b) while the crystallization peak temperature separation was only marginally affected (Figure 6.10b), even though the comonomer to ethylene feed ratio was kept constant at different ethylene pressures. Therefore, this might be related to other factor such as mass transfer resistances during polymerization.

A steady increase in comonomer content was also observed with increasing hydrogen pressure (Figure 6.9c). This increase in comonomer content appeared as broadening of the SCBDs and consequently increased peak separation (Figure 6.10c). Hydrogen decreases the molecular weight of the polymer and might reduce mass transfer limitations, thus favouring comonomer incorporation. The increase in peak separation at higher hydrogen levels may also be attributed to the generation of different active sites that have higher reactivity ratios towards 1-octene (15,18).

As expected, for an increase in the comonomer/ethylene ratio (increasing the comonomer feed), comonomer incorporation in the copolymer increased (Figure 6.9d). Additionally, an increase in the peak separation also occurred resulting in broadening of the SCBD (Figure 6.10d). The effect of the activator to catalyst support ratio is negligible on both 1-octene content and SCBD peak separation Figures 6.9e and 6.10e. Figures 6.11 and 6.12 illustrate the most

important 2-factor interactions. The effect of temperature, although not prominently shown in the response profiles, indicated that at the low pressure level, the comonomer incorporation decreased with increasing polymerization temperature (Figure 6.11a). However, the opposite behaviour was seen at the higher pressure level. At low monomer pressure, the observation of decreasing comonomer content with increasing temperature is similar to others (5,14). It has been suggested that different activation energies exist for the transfer mechanisms (5). For the peak separation difference, broadening of the distribution was also sensitive to the polymerization temperature (Figure 6.12a). At the high comonomer level, an increase in SCBD broadening occurred at lower temperatures. Little broadening was observed at the low comonomer level, possibly due to superposition of the lower and higher crystalline peaks in the SCBD. As the polymerization temperature decreases, it is possible that the catalytic site that has higher 1-octene reactivity ratio becomes more active. Towards higher temperatures, the SCBD becomes unimodal as shown in Figure 6.6. This might be related to changes in the reactivity ratios of both site types, but it might also be possible that at high temperatures extraction of the metallocene or MAO from the catalyst support occurs, leading to homogeneous polymerization. It was observed that the morphology of the resulting polymer became poorer as the polymerization temperature increased, which supports the hypothesis of metallocene or MAO leaching from the silica particles.

It seems that ethylene pressure can also change the incorporation characteristics of the catalyst system (Figure 6.11b). At a high comonomer level, it can be suggested that with an increase in ethylene pressure, a decrease in comonomer incorporation occurs. At a low level of

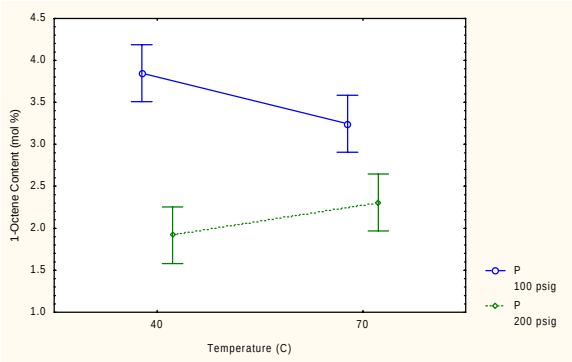

(a)

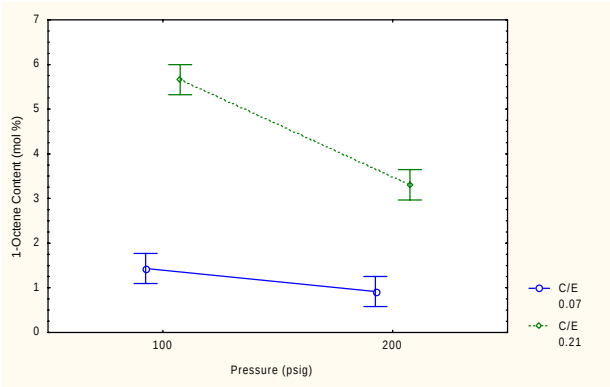

(b)

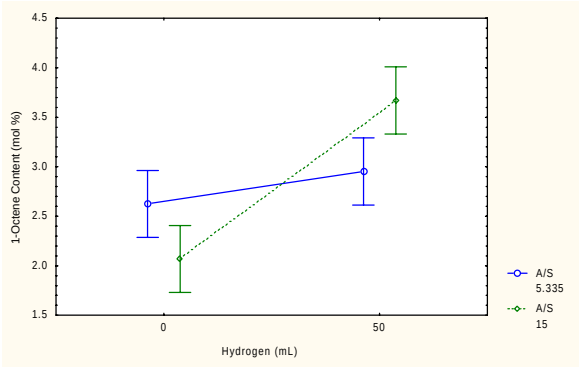

(c)

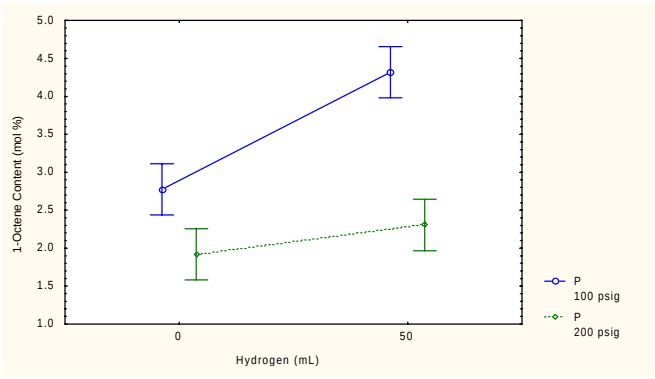

(d)

Figure 6.11 – Interaction of Polymerization Conditions on Comonomer Incorporation

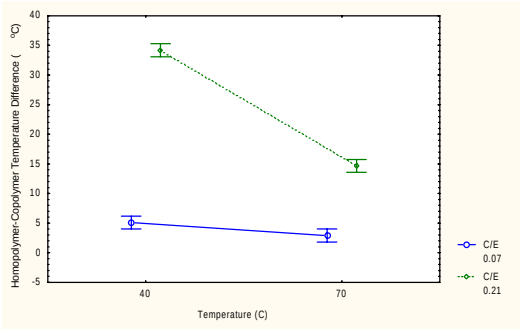

(a)

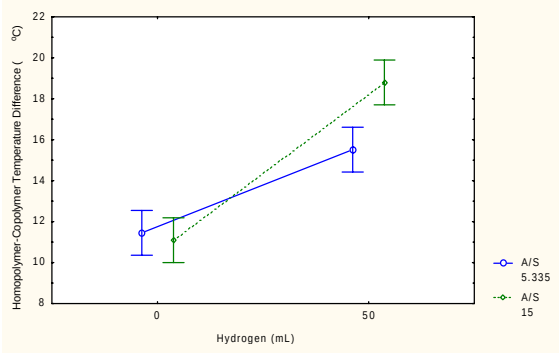

(b)

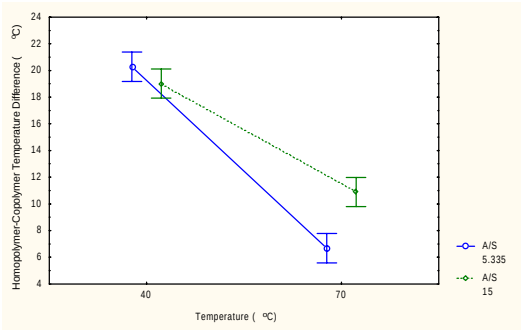

(c)

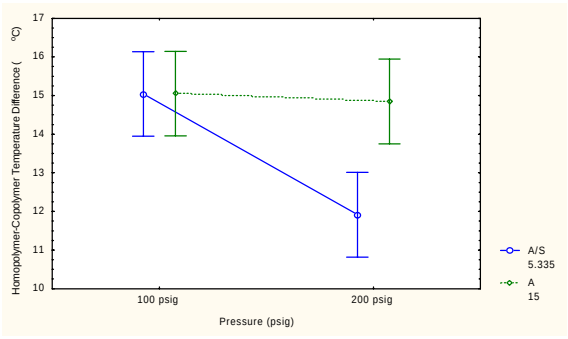

(d)

Figure 6.12 – Interaction of Polymerization Conditions on Homopolymer/Copolymer Temperature Difference (Peak Separation)

comonomer, ethylene pressure does not play as prominent an effect in decreasing the comonomer content. Remember that the comonomer/ethylene ratio in the reactor was kept constant for all ethylene pressures. Therefore, if the catalyst did not exhibit different sensitivities to ethylene pressure, no change in the 1-octene content in the copolymer should be observed.

The effect of hydrogen was also significant and is confounded with the effects of the activator/support ratio and ethylene pressure. As mentioned above, hydrogen increased comonomer incorporation (Figure 6.9c). At the low activator level, very little difference in comonomer incorporation is observed with changes in the hydrogen level (Figure 6.11c). However at the high activator level, comonomer incorporation increased greatly with the addition of hydrogen. The interaction between hydrogen and activator cannot be readily explained, but it may be linked to new active sites that can possibly be created with the addition of hydrogen. The interaction between hydrogen and polymerization pressure is also interesting. At the low ethylene pressure, comonomer incorporation increases with the addition of hydrogen, but at the high pressure level, comonomer incorporation does not change significantly with the addition of hydrogen. This again can be explained by the different sensitivities of the catalyst towards ethylene pressure and hydrogen. Examining the relation of the hydrogen and activator level on the peak separation difference, regardless of the activator level, it can be seen that with the addition of hydrogen the peak separation increases greatly, indicating that the SCBD broadens (Figure 6.12b). Again this may be linked to the catalytic sites generated by hydrogen which may better incorporate the comonomer.

Figures 6.12c and 6.12 shows the effects of temperature and ethylene pressure on the SCBD broadening depends on the activator level. This unusual behaviour demonstrates how

sensitive the catalytic sites are to changes in the electronic environment that surrounds them (i.e. presence of alkylaluminums).

6.3.4 Molecular Weight

Generally, the molecular weight of polymers is quite sensitive to polymerization conditions. Changing these conditions can affect the rates of propagation and transfer, and consequently the molecular weight of polymer. For truly single-site catalyst, changes in the polydispersity index (PDI) cannot occur, since PDI is always equal to 2, by definition. Therefore, any change in PDI can be associated to the presence of multiple site types, mass transfer resistances or reactor non-uniformities.

The response profiles illustrating the various effects on molecular weight and polydispersity are shown in Figures 6.13(a-e) and Figures 6.14(a-e) respectively. Figure 6.13a shows that as the polymerization temperature increases, the molecular weight decreases. At higher temperatures, chain transfer reactions such as β-elimination occur more readily and it was expected that the molecular weight would be lower (10,11,13,14,17). Figure 6.14a shows that PDI decreases from an average of 3 to a value lower than 2 with increasing temperature. A PDI of 3 is reasonable for a polymer produced with a supported metallocene catalyst, since broadening of the MWD generally occurs due to heterogeneity of the catalyst sites on the silica support (13). This observation reinforces that the catalyst becomes “more single-site” at higher polymerization temperatures. This behaviour was also observed for the SCBDs as indicated in Figure 6.10a. Molecular weight increases with increasing ethylene pressure (Figure 6.13b), as expected. As ethylene concentration increases, the rate of propagation increases, as well as the molecular weight, which indicates that chain transfer is not regulated by transfer to monomer. It

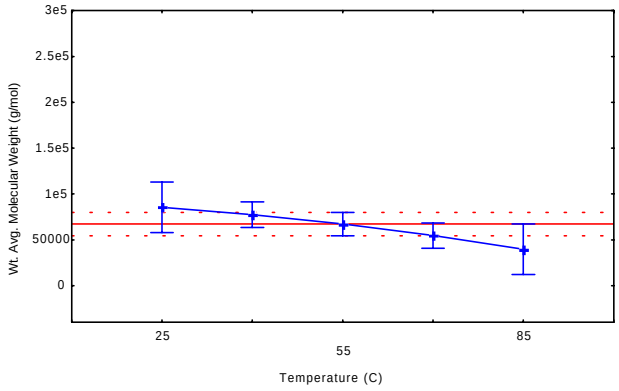

(a)

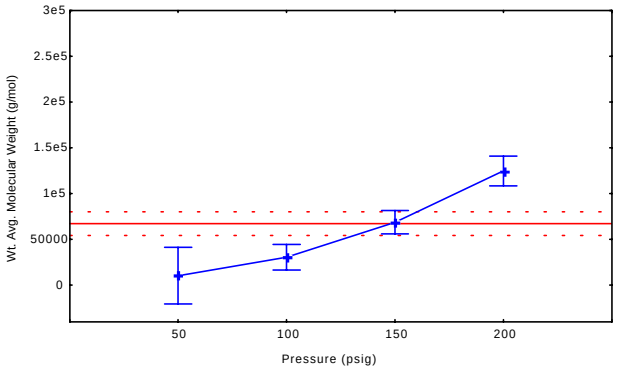

(b)

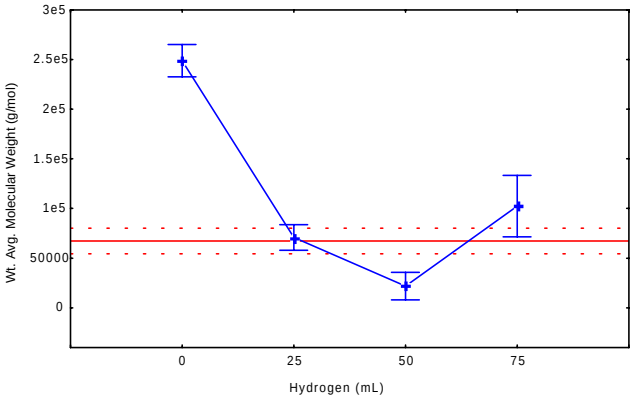

(c)

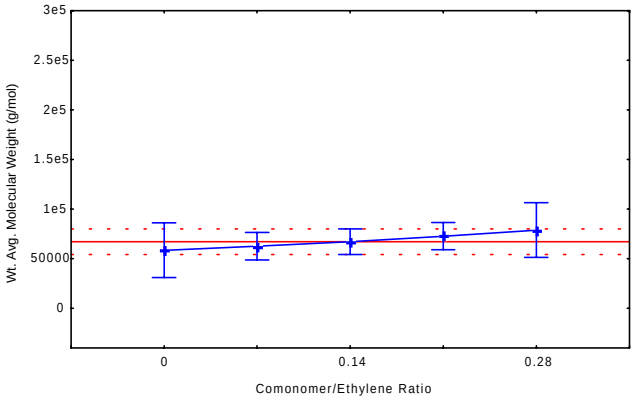

(d)

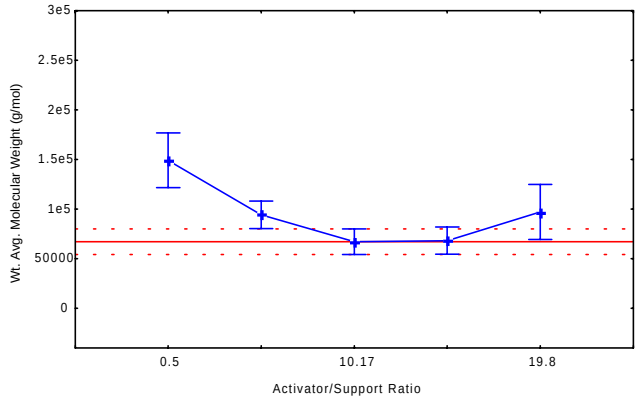

(e)

Figure 6.13 – Effect of Polymerization Conditions on Molecular Weight

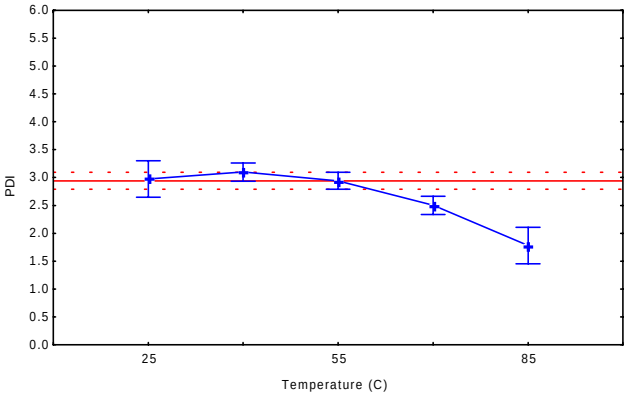

(a)

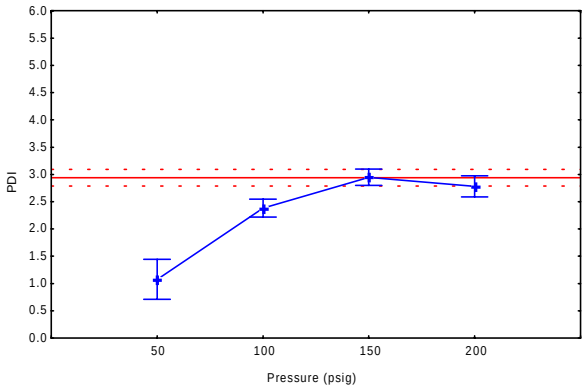

(b)

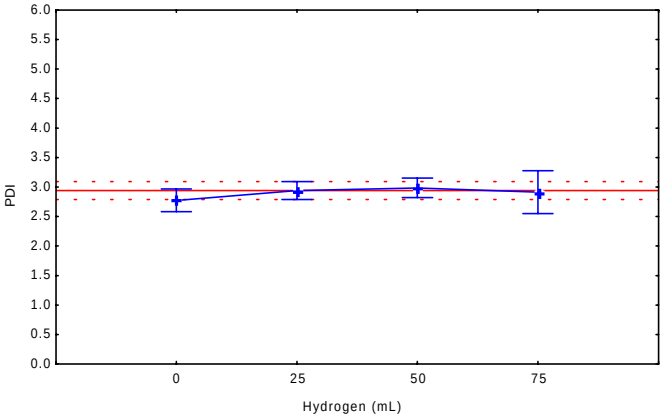

(c)

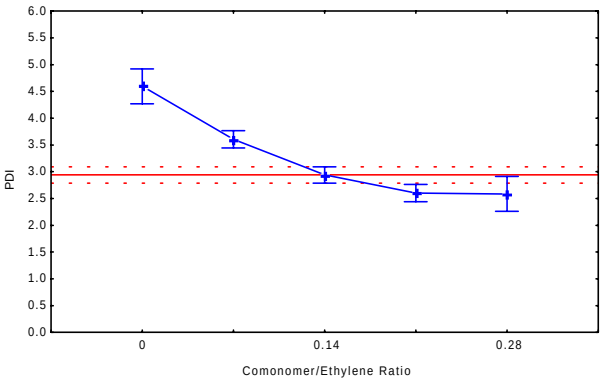

(d)

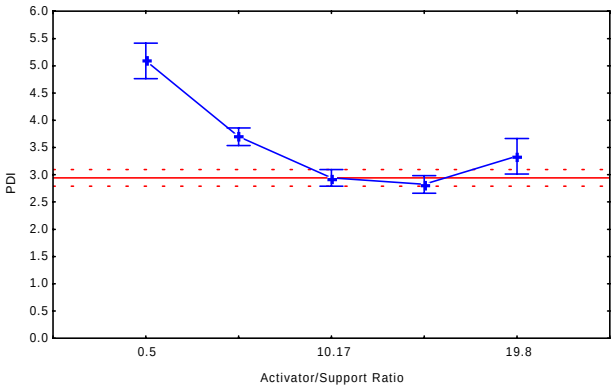

(e)

Figure 6.14 – Effect of Polymerization Conditions on MWD

was observed that the MWD broadened as the pressure increased above 100 psig and eventually reached a plateau (Figure 6.14b). The values predicted for PDI at 50 psig are unreasonably low and indicate that some lack of fit exists for these predictions. However, the trend shows that as ethylene pressure increases, PDI tends to a value around 3.

A significant decrease in the weight average molecular weight occurred even with the addition of a small amount of hydrogen (Figure 6.13c). However, at the highest amount of hydrogen investigated (75 mL), some anomalous behaviour was detected. The model predicts that, with the highest amount of hydrogen, the molecular weight increases. This is unusual but it may indicate that certain interactions are significant or that this data point is an outlier. The response of the MWD with hydrogen showed that the PDI remained unchanged at the different levels of hydrogen (Figure 6.14c) which is reassuring that the other observed effects may be significant. Weight average molecular weight increases slightly with the level of comonomer (Figure 6.13d). Other researchers have reported that molecular weight increases (7,9) and sometimes decreases (18,19,27,28) with addition of comonomer, but generally, the molecular weight decreases due to increased transfer to comonomer.

PDI decreases as the comonomer amount increases (Figure 6.14d). It is interesting to notice that the SCBD can vary greatly and the MWD can still remain narrow, as illustrated by Figures 6.6 to 6.8.

Figure 6.13c indicates that molecular weight decreases with increasing amount of activator, up to an activator/support ratio of about 10, which is consistent with the activator acting as a chain transfer agent (12,16,17,30,31). A similar effect was observed for PDI (Figure 6.14c).

The molecular weight and PDI responses to some parameter interactions are shown in Figures 6.15(a-e) and 6.16(a-c). The molecular weight decreases with an increasing temperature in the absence of hydrogen (Figure 6.15a). In the presence of hydrogen, chain transfer to hydrogen dominates and the molecular weight is not influenced by temperature. Figure 6.15a shows that as the temperature increased the PDI decreased, regardless of the level of pressure. The narrowing of the MWD due to a more single-site like behaviour has already been discussed above. At the high pressure level possibly due to the higher rate of polymerization, a wider range of chains are formed.

The effect on molecular weight with the interaction of temperature and activator level is shown in Figure 6.15b. The molecular weight was independent of the temperature, at the low level of activator, but the molecular weight decreased with the increasing temperature at the high level. For the influence on PDI, it is again shown that, despite the activator level, the PDI decreases with the increase in temperature (Figure 6.16b).

For the interaction of pressure with hydrogen, Figure 6.15c shows that the molecular weight of the copolymer increases with increasing ethylene pressure in the absence of hydrogen. However in the presence of hydrogen, ethylene pressure does not influence the molecular weight indicating that chain transfer to hydrogen dominates.

Different behaviour with temperature was also observed at different comonomer levels (Figure 6.15d). At the low comonomer level, it was seen that the molecular weight decreased with increasing temperature, as expected. However, at the high comonomer level, molecular weight is unaffected by the changes in temperature, possibly because transfer to comonomer dominates over changes in temperature. Figure 6.16c shows that the PDI decreases with increasing temperature.

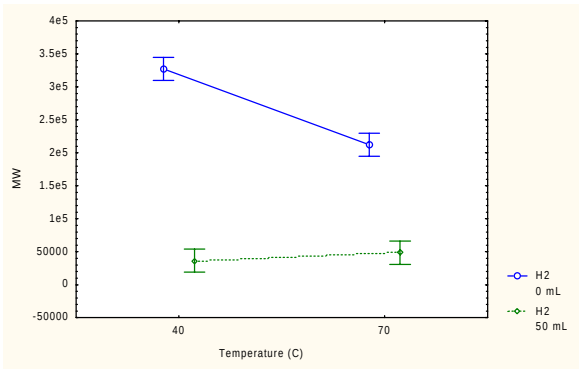

(a)

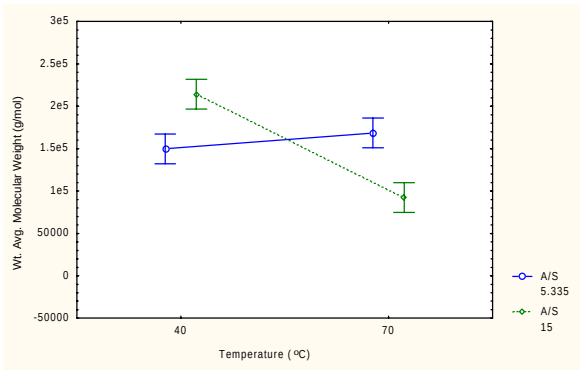

(b)

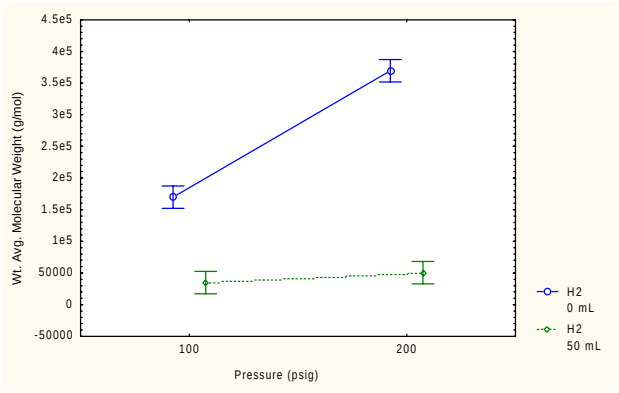

(c)

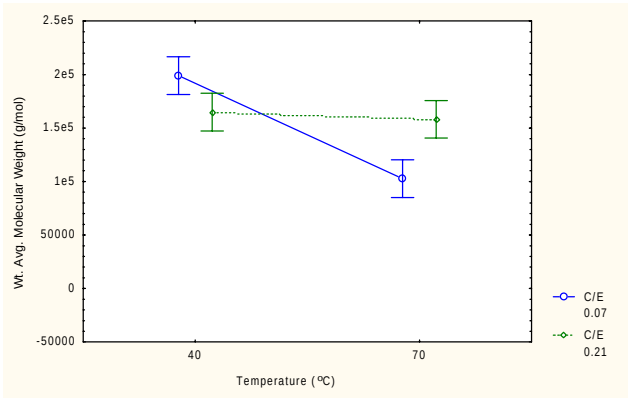

(d)

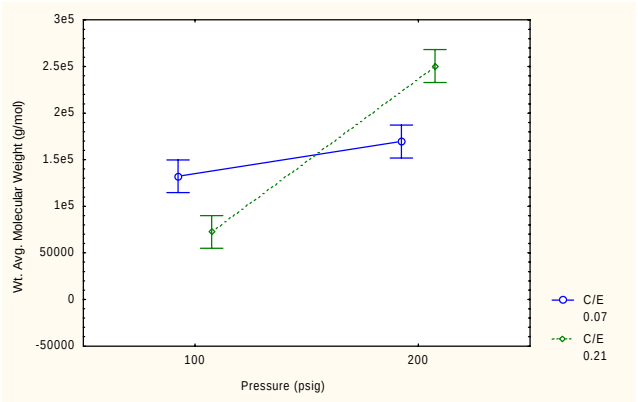

(e)

Figure 6.15 – Interaction of Polymerization Conditions on Molecular Weight

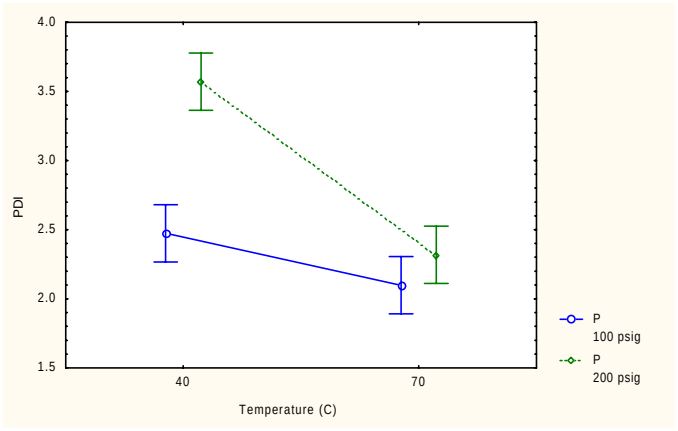

(a)

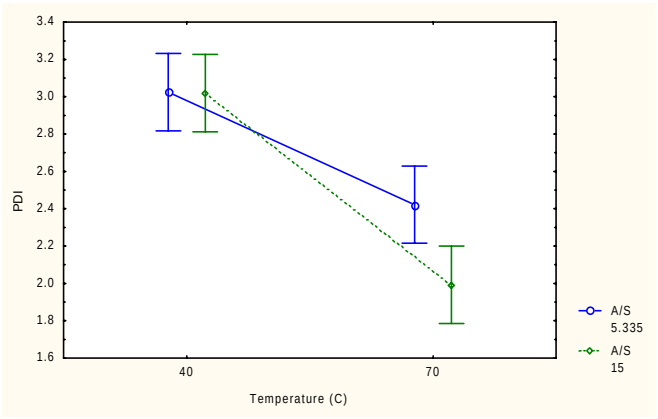

(b)

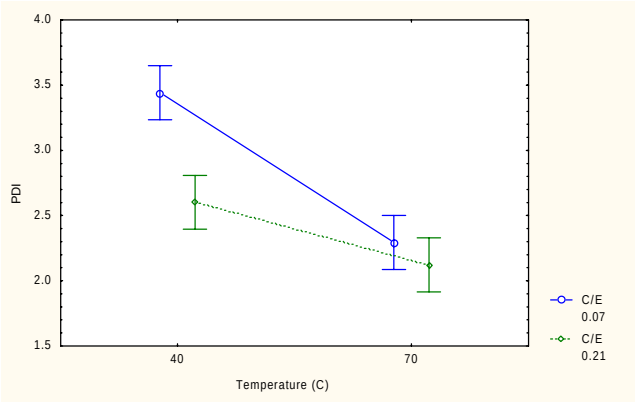

(c)

Figure 6.16 – Interaction of Polymerization Conditions on MWD

Figure 6.15e shows at the high comonomer level, the molecular weight increases with increasing ethylene pressure. At the low comonomer level, the molecular weight increased at a slower rate. At this comonomer level, it seems that transfer to comonomer dominates since increasing monomer pressure does not influence the molecular weight as greatly.

6.3.5 Single Factor Experiments

From the experimental design layout, a number of single factor experiments were carried out to examine the effect of each reaction parameter at the star point levels. For these experiments, only the factor of interest was varied and the other parameters were held at the levels used for the center points. Although it was found above that interactions between several polymerization parameters are important, the analysis of the single factor runs will help better understand some of the observed effects.

As mentioned above, large changes in the SCBD were observed upon changing the polymerization conditions. These changes in the SCBD are very important, since they influence the crystalline properties. Figure 6.17 shows the effect of polymerization temperature on the polymer SCBD, along with the average molecular weight and catalyst activity. The SCBD narrows considerably when the polymerization temperature is increased from 25°C to 85°C. With the increase in temperature, the rate of polymerization and the weight average molecular weight also increase. Samples synthesized at 25°C also show intriguing behaviour. The SCBDs broadened (Figure 6.18), by decreasing the ethylene pressure. Even though the comonomer/ethylene feed ratios were kept constant for each polymerization condition. These observations are consistent with the predictions made above from the response profiles: as ethylene pressure is increased the comonomer incorporation decreases, as well as the peak separation. Surprisingly, the SCBD also changes with varying hydrogen levels (Figure 6.19).

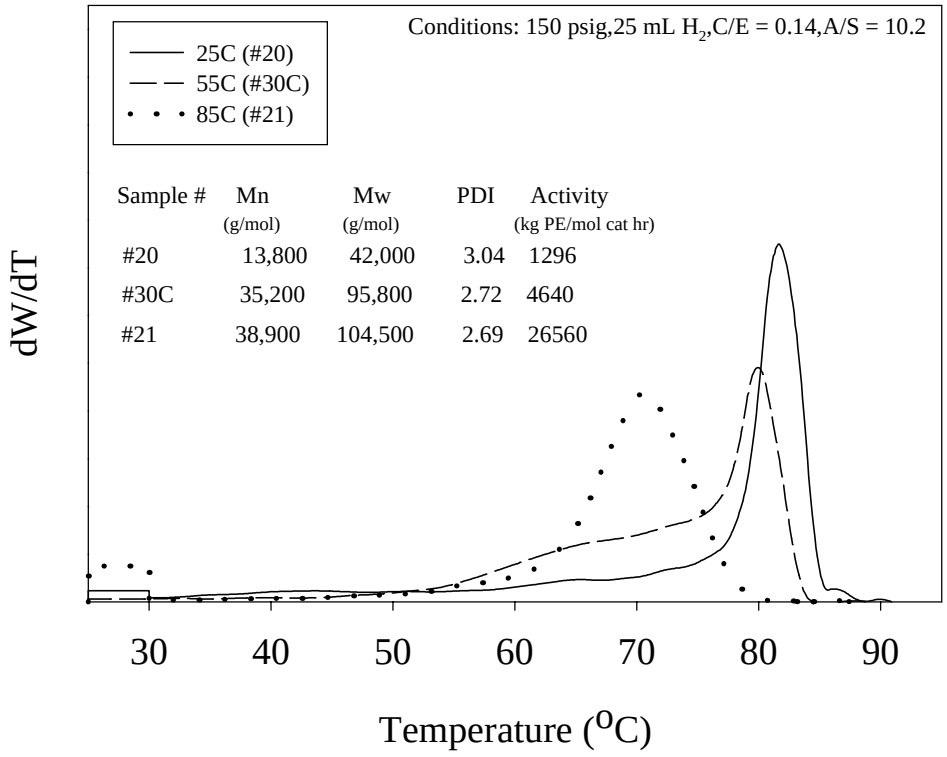

Figure 6.17 – Single Factor: Effect of Temperature on SCBDs

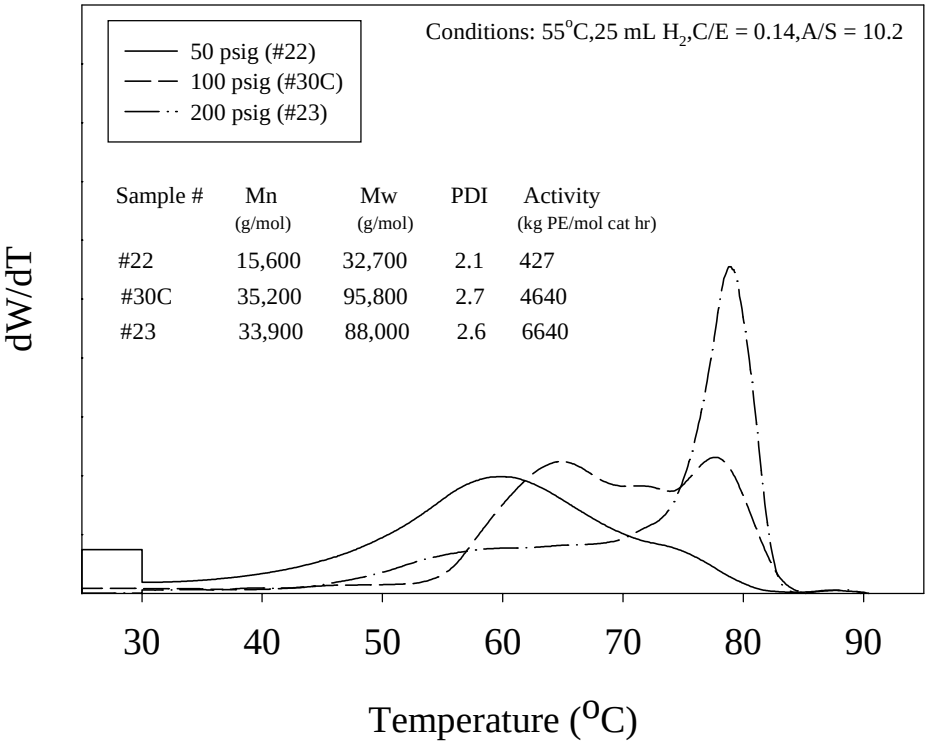

Figure 6.18 – Single Factor: Effect of Pressure on SCBDs

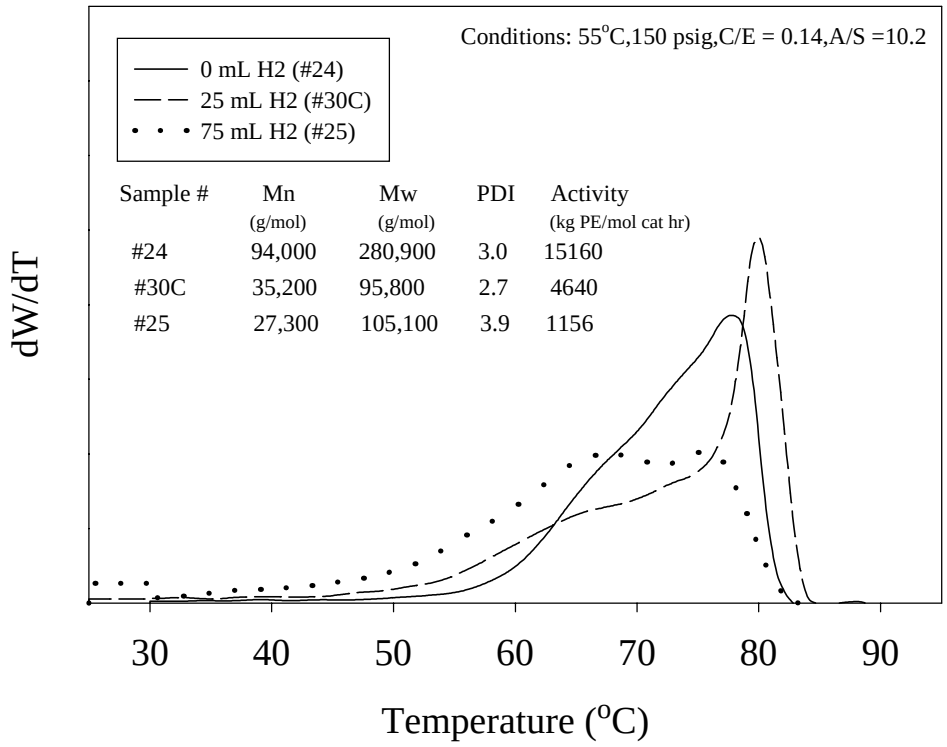

Figure 6.19 – Single Factor: Effect of Hydrogen on SCBDs

Without hydrogen a broad SCBD resulted that did not overlap with the other two samples. As noted, it is believed that changes in the catalyst comonomer reactivity ratios occur with the addition of hydrogen. By increasing the amount of hydrogen the SCBD also broadens, as indicated for samples #30C and #25. From the design predictions this corresponds to the increase in comonomer content with the addition of hydrogen and also results in broadening of the SCBD.

Figure 6.20 shows that when ethylene is polymerized alone, a narrow high crystallinity homopolymer peak is obtained. Addition of 1-octene leads to bimodal SCBD peaks, where a portion of homopolymer can still be detected, a main characteristic of multiple site type catalysts.

Figure 6.21 shows that as the activator amount increases, the SCBD broadens and the formation of a copolymer peak takes place. This was not well predicted from the design data since the copolymer and homopolymer peak temperatures do not change, and consequently the peak separation is not affected. In the design data, no indication of an increase in comonomer content was observed which contradicts the observations made here, since it can be clearly seen that sample #28 has higher comonomer incorporation. It was shown in the design analysis that the activator can interact with many factors such as hydrogen, temperature and pressure. It is possible that the changes observed here are the results of conflicting effects.

Overall, the analysis of the experimental design results has revealed some insight into the nature of the polymerization with in-situ supported catalysts. It was demonstrated that the effect of several polymerization parameters on this heterogeneous system is not straightforward. Given the multiple site nature of the catalyst and possible mass transfer limitations, it was shown that predicting the polymerization activity and resulting microstructure of the polymer is a challenging task.

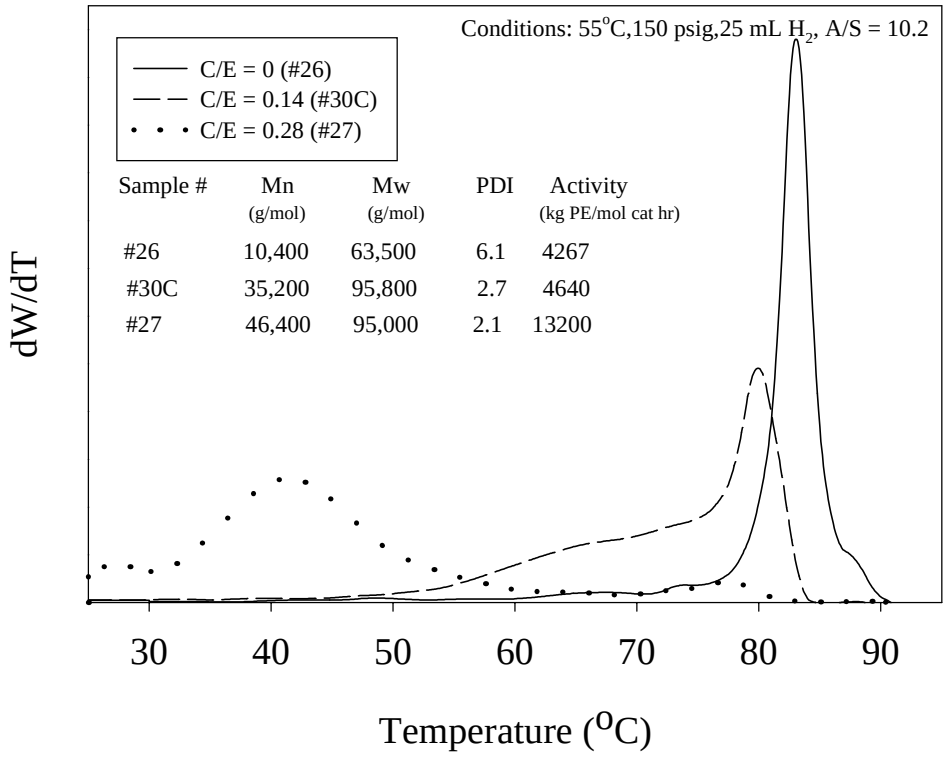

Figure 6.20 – Single Factor: Effect of Comonomer/Ethylene (C/E) Ratio on SCBDs

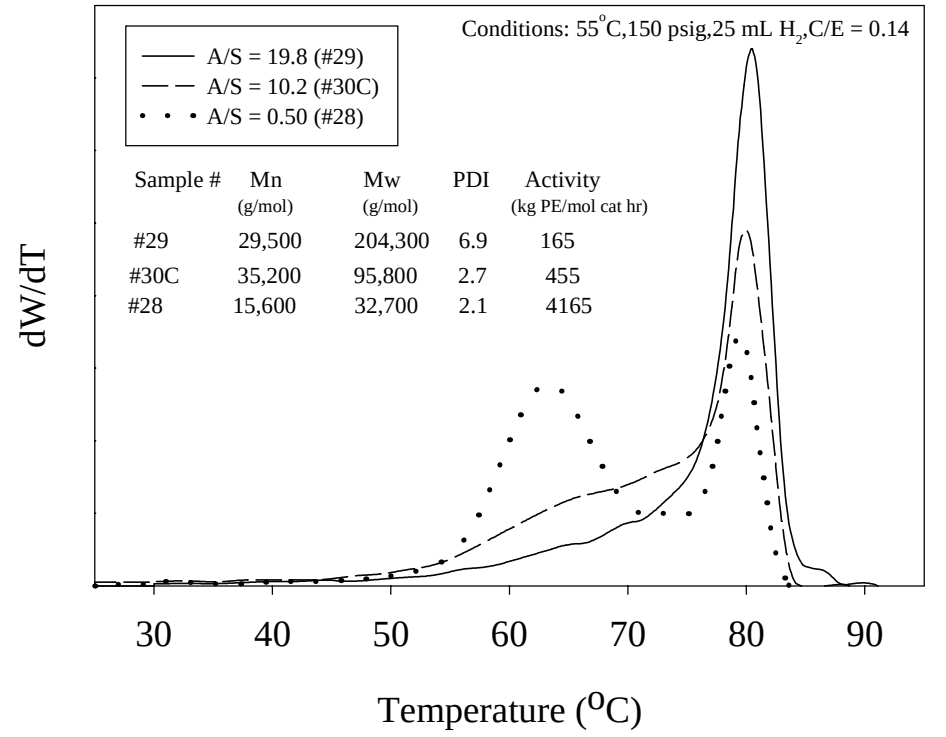

Figure 6.21 – Single Factor: Effect of Aluminium/Support (A/S) Ratio on SCBDs

6.4 Conclusion

The results of this experimental design clearly show that in-situ supported Me_2Si(2-Me-4,5 BenzInd)$_2ZrCl_2$ is not a typical single site catalyst. Some responses to important polymerization conditions are not easily predicted from typical polymerization mechanism steps, and several two-factor interactions play important roles in determining polymer MWD and SCBD, as well as catalyst activity. Additionally, the presence of more than one site type and mass transfer limitations, further difficult model predictions.

Nonetheless, the experimental approach used herein is very important to detect and quantify the complex nature of this particular system and can be readily extended to other supported metallocene systems. The ability to produce polyolefins with multimodal microstructural distributions in a single metallocene/single reactor set-up is very attractive and could in principle be used to produce polyolefin resins with advanced molecular architecture.

6.5 References

1. Li Pi Shan, C.; Chu, K.J.;Soares, J.B.P.; Penlidis, A.;*Macromol. Chem. Phys.*, 201, 2195-2202 (2000).
2. Li Pi Shan, C.; Soares, J.B.P.; Penlidis, A.; *Polymer*, 43, 767-773 (2002).
3. Brintzinger, H.; Fischer, D.; Mulhaupt, R.; Rieger, B.; Waymouth, R.M.; *Angew. Chem. Int. Ed. Engl.*, 34, 1143-1170 (1995)
4. Xie, T.;McAuley, K.B.;Hsu, J.C.C.;Bacon,D.W.;*Ind. Eng. Chem. Res.*; 33, 449-479 (1994).
5. Chien, J. C. W. ; He, D. ; *J. Polym. Sci., A, Polym. Chem.*, 29, 1595-1601 (1991).
6. Thorshaug, K.;Strovneng, J.A.;Rylter, E.;Ystenes; *Macromolecules*, 31, 7149-7165 (1998).
7. Przybyla, C.; Tesche, B.; Fink, G. ; *Macromol. Rapid. Commun.*, 20, 328-332 (1999).
8. Fink, G.; Steinmetz, B.; Zechlin, J.; Przybyla, C.; Tesche, B.; *Chem. Rev.*, 100, 1377-1390 (2000).
9. Jungling, S.; Koltzenburg, S.; Mulhaupt, R.; *J. Polym. Sci., A: Polym. Chem.*; 35, 1-8 (1997).
10. Soares, J.B.P.; Hamielec, A.E.; *Polymer*, 37, 4607-4614 (1996).
11. Zucchini, U.; Cecchin, G.; *Adv. Polym. Sci.*, 51, 101-154 (1983).
12. Huang, J.; Rempel, G.L.; *Prog. Polym. Sci.*, 20, 459-526 (1995).
13. dos Santos, J.H.Z.; da Rosa, M.B. ; Krug, C. ; Stedile, F.C. ; Haag, M.C. ; Dupont, J. ; Forte, M.D.C.; *J. Polym. Sci., A: Polym. Chem.*, 37, 1987-1996 (1999).
14. Suhm, J.; Schneider, M.J.; Mulhaupt, R.; *J. Polym. Sci., Part A: Polym. Chem.*, 35, 735-740 (1997)
15. Han-Adebekunn, G.C.; Hamba, M.; Ray, W.H.; *J. Polym. Sci. A: Polym. Chem.*, 35, 2063-2074 (1997).

16. Chu, K.J.; Soares, J.B.P.; Penlidis, A.; *J. Polym. Sci, Part A: Polym. Chem.*, 38, 1803-1810 (2000)

17. Liu, J.;Stoveng, J.A.;Rytter, E.; *J. Polym. Sci; Part: Polym. Chem.*; 39, 3566-3577 (2001).

18. Kissin, Y.V.; Mink, R.I.; Nowlin, T.E.; *J. Polym. Sci., A: Polym. Chem.*, 37, 4255-4272 (1999).

19. Quijada, R.; Rojas, R.; Mauler, R.S. ; Galland, G.B. ; Scipioni, R.B. ; *J. Appl. Polym. Sci.*, 64, 2567-2574 (1997).

20. Kim, J.D.; Soares, J.B.P.; Rempel, G.L.; *Macromol. Rapid Commun.*, 18, 197-299 (1998).

21. Han, T.K.; Choi, H.K.; Jeung, D.W.; Ko, Y.S.; Woo, S.I.; *Macromol. Chem. Phys.*, 196, 2637-2647 (1995).

22. Sacchi, M.C.; Forlini, F; Tritto, I.; Locatelli, P.; *Metalorganic catalysts for synthesis and polymerization : recent results by Ziegler-Natta and metallocene investigations;* Springer, New York, 1999, pp. 294-303.

23. Blom, R.; Dahl, I.M.; *Macromol. Chem. Phys.*, 200, 442-449 (1999)

24. Chu, K.J.; Soares, J.B.P.; Penlidis, A.; *Macromol. Chem. Phys.*, 201, 552-557 (2000).

25. Chien, J.C.W.; Nozaki, T.; *J. Polym. Sci., Part A: Polym. Chem.*, 31, 227 (1993).

26. Herfert, N.; Montag, P.; Fink, G.; *Makromol. Chem.*, 194, 3167 (1993).

27. Bergemann, C.; Cropp, R.; Luft, G.; *J. Mol. Cat., A: Chemical*, 105, 87-91 (1996).

28. Miri, N.; Hetzer, D.; Miles, A.; Pecak, M.; Riscili, B.; *Metalorganic catalysts for synthesis and polymerization : recent results by Ziegler-Natta and metallocene investigations;* Springer, New York, 1999, pp. 509-515.

29. Chien, J.C.W.; Xu, B.; *Makromol. Chem. Rapid Commun.*,14, 109-115 (1993).

30. D'Agnillo, K.; Soares, J.B.P.; Penlidis, A.; *Macromol. Chem. Phys.*, 955-962 (1998).

31. Rieger, B.; Janiak, C.; *Angew. Makromol. Chem.*, 215, 35-46 (1994).

32. Vela Estrada, J.M.; Hamielec, A.E. ; *Polymer*, 35, 808-818 (1994).

33. Monrabal, B.; *J. Appl. Polym. Sci*., 52, 491-505 (1994).

34. Box, G.E.P.; Hunter, W.G.; Hunter, J.S.; Statistics for Experimenters – An Introduction to Design, Data Analysis and Model Building; John Wiley & Sons., Toronto, 1978 pp. 306-535.

35. Smith, J.M.; Van Ness, H.C.; Introduction to Chemical Engineering Thermodynamics, 3rd Ed.; McGraw-Hill Inc., Toronto, 1975 pp. 314-331.

36. Ystenes, M.; *J. Catal.*,129, 383-401 (1991).

37. Chu, K.J.; Soares, J.B.P.; Penlidis, A.; *J. Polym. Sci.: Part A, Polym. Chem.*,38, 462-468 (2000).

Chapter 7

Mechanical and Rheological Properties of HDPE/LLDPE Reactor Blends with Bimodal Microstructures

7.1 Introduction

Commercially, there are numerous polymer resins available that have been tailored specifically for certain product applications and polymer processing operations. The applications range from piping, packaging, household and industrial containers, to automotive, and are processed by extrusion, blown film, blow moulding and injection moulding processes, just to name a few. Many grades of resins are manufactured around the world and are commonly classified by their chemical composition, crystalline density, and melt index to identify their end-use application and processing operation (1).

For polyolefins, it is well known that both the molecular weight and comonomer distribution of a polymer plays a vital role in determining its physical and processing properties. The microstructural features of a polymer include: the monomer and comonomer type, long chain branch length and distribution, comonomer content and comonomer distribution, molecular weight, and molecular weight distribution (MWD) of the polymer chains. All of these structural features can be traced back to the original production of the polymer (2).

The structural features of polyethylene are controlled during the polymerization and depend on the catalyst type and polymerization process. High-pressure processes using free radical initiators can produce high density polyethylene (HDPE) and low density polyethylene (LDPE) that are relatively linear and randomly branched. Better microstructural control has evolved with heterogeneous Ziegler-Natta or Phillips type processes to produce linear polyethylene and copolymers such as linear low density polyethylene (LLDPE). Currently, the polyolefin industry is developing and producing polymers with single-site catalyst technology to further control the microstructure to produce resins with narrow MWDs and uniform comonomer distributions (3).

However, with a single catalyst and single reactor process, polymers with unimodal structural distributions are usually obtained. It is difficult to tailor the properties of resins with unimodal structural distributions. If the molecular weight distribution needs to be tuned, the entire distribution is shifted, resulting in a trade-off; one property is improved and another property is compromised (4). Physical properties of the polymer such as stiffness and toughness are influenced by its molecular weight and degree of crystallinity. Increasing the molecular weight of a polymer decreases its degree of crystallinity (5-6). Greater control over the crystalline density is often achieved by copolymerizing ethylene with α-olefin comonomers to increase the degree of short chain branching. Short chain branching reduces the crystalline density and lowers the polymer stiffness, but increases its toughness and optical clarity (7,8).

Even though high molecular weight (HMW) materials exhibit good toughness, they are inherently difficult to process because of their high melt viscosities. Processing polymers with high melt viscosities can be overcome with the use of processing aids but this solution is costly.

To overcome the shortcoming of this property-processing relationship, a balance of properties can be achieved by the blending of polymers. One option is to melt blend the polymers using an extruder or melt mixer. However, difficulties arise in obtaining well-dispersed morphologies at an attractive cost if the structural units differ greatly (9). To tailor the polymer microstructure during polymerization, tandem or cascade type processes are often used to control the molecular weight and comonomer distribution of the polymer. A multiple staged process allows for the production of a reactor blend containing the desired molecular components. Tailoring the microstructure of polyolefin resins through the use of bimodal structures, allows the control of the properties of each resin to fit the desired end-use properties and applications (4,10-12).

A comparison of the structural distributions produced from a single reactor and a series process is shown in Figure 7.1.

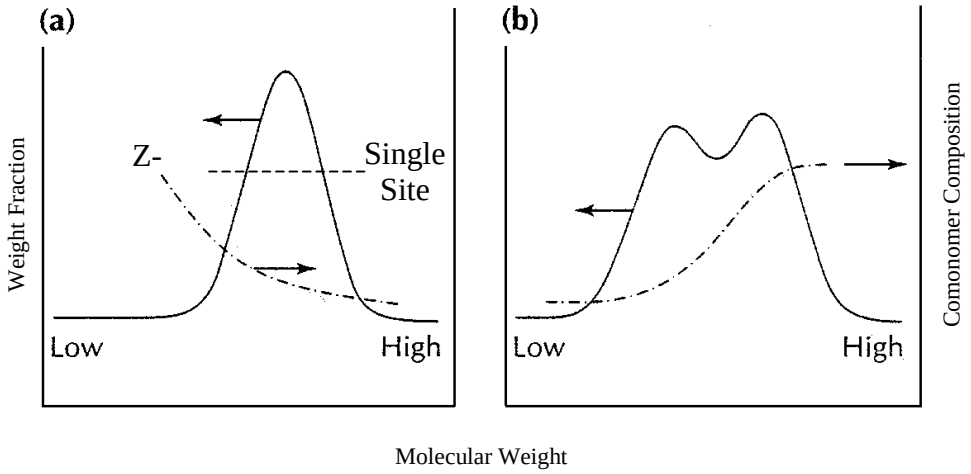

Figure 7.1 – Typical Molecular Weight and Comonomer Distributions of Polyethylene (11)
(c) Conventional Ziegler-Natta and Single-site PE made in a single reactor
(d) Bimodal PE made in a series of reactors

For the conventional Ziegler-Natta resin shown in Figure 7.1a, the MWDs are unimodal and generally broad. Given the multiple site nature of a Ziegler-Natta catalyst, the incorporated comonomer tends to be unevenly distributed. Ethylene/α-olefin copolymers such as ethylene/1-butene, ethylene/1-hexene, ethylene/1-octene, produced by heterogeneous catalysts, have a greater concentration of comonomer in the low molecular weight polymer chains. The HMW chains tend to have less comonomer and are similar to HDPE. On the other hand, it is generally recognized that single-site catalysts produce polymer with narrow molecular weight and uniform comonomer distributions (13,14). The interest in single-site catalyzed polymers arises from the improved physical properties that result from the uniform structural distributions. Unfortunately,

the difficulties in processing such resins are compounded without the low molecular weight molecules present in polymers with broad MWDs.

Commercially, pipe resins are often produced with 'reverse' comonomer distributions. Figure 7.1b shows that these resins are reactor blends of HMW copolymer and low molecular weight (LMW) homopolymer (4,10-12, 15). Resins with tailored distributions are often prepared in multiple step polymerization processes; the desired polymer fractions are produced in individual stages under the appropriate reaction conditions. The advantage is that the polymer fractions can be independently tailored to balance the end-use properties. Resins with reversed comonomer distributions exhibit good toughness and environmental stress crack resistance. The presence of the HMW copolymer increases the concentration of tie molecules between the polyethylene crystallites to prevent their disentanglement under creep conditions (4,10-12). The fraction of LMW homopolymer is included to maintain the polymer density and to decrease the melt viscosity at high shear rates.

Industrially, these processes often include a combination of reactors such as Borealis's slurry-loop-gas phase process or Hoechst cascade CSTR slurry process. These processes are used to produce reactor blends of HMW copolymer followed by LMW homopolymer (11,16). Tailoring of the microstructure can easily be achieved by controlling the reactor conditions and polymerization rates.

Given the recent interest in resins with bimodal structural distributions, our study was initiated to investigate and further develop the understanding of structure-property relationships of these resins. Of interest was the influence of the molecular weight and comonomer content of the individual polymer components and their contribution to the physical properties. Using a heterogeneous metallocene catalyst system, under the appropriate polymerization conditions,

resins with controlled molecular weight and chemical composition distributions were synthesized. As an alternative to a tandem or cascade type process, a two-step polymerization method was carried out in a single reactor on a laboratory scale. Utilizing this two-step polymerization process, reactor blends of LMW homopolymer and HMW copolymer were produced, similar to industrial resins with reverse comonomer distributions. For comparison, resins with conventional comonomer distributions were also synthesized, thus mimicking Ziegler-Natta LLDPE. These reactor blends consist of high molecular weight homopolymer and low molecular weight copolymer. For example, to synthesize a reactor blend of LMW homopolymer and HMW copolymer the method used is shown in Scheme 1. In the first stage, ethylene was polymerized in the presence of a chain transfer agent such as hydrogen to produce LMW copolymer. After venting the reactor to remove hydrogen, the second stage of the polymerization was carried out in the presence of 1-octene. Depending on the polymerization time and rate for each stage, reactor blends of polyethylene/poly(ethylene-*co*-1-octene) resulted. The homopolymer/copolymer ratios were manipulated by varying the polymerization time for each stage.

Scheme 2 shows the method to produce blends with conventional comonomer distributions. A blend of HMW homopolymer and LMW copolymer was produced by the addition of hydrogen and comonomer to the second copolymerization stage. Note that due to the difficulty of removing the unreacted comonomer from the reactor, only copolymer could be produced in the second stage.

Scheme 1: Reactor Blend of LMW Homopolymer/HMW Copolymer

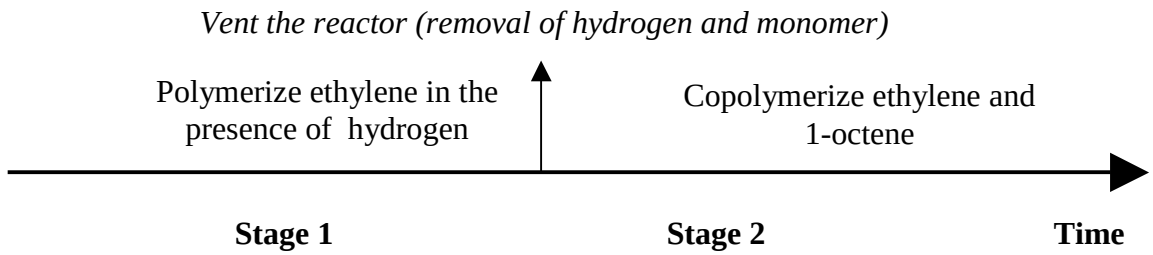

Scheme 2: Reactor Blend of HMW Homopolymer/LMW Copolymer

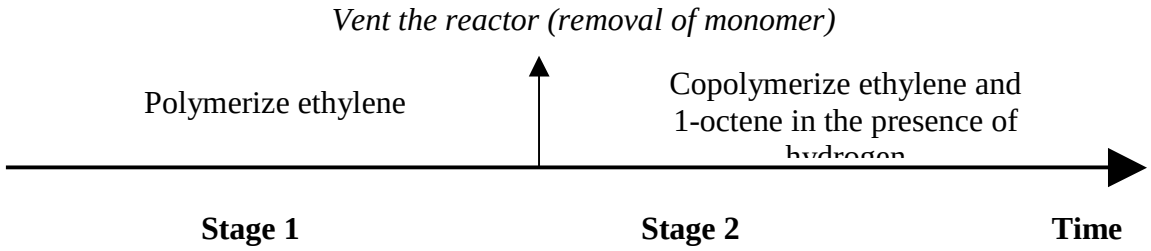

In this study, three sets of polyethylene/poly(ethylene-*co*-1-octene) resins were produced. The compositions of these blends range from LMW homopolymer to HMW copolymer and, vice versa, HMW copolymer to LMW homopolymer. The microstructure of each polymer was characterized for its molecular weight and short chain branching distribution. Physical property testing included: uniaxial tensile testing under short-term loading conditions, the viscoelastic properties from dynamic mechanical analysis, and melt rheological properties from oscillatory shear measurements.

7.2 Experimental

As mentioned above, reactor blends covering a wide product range were synthesized. Using the two-step polymerization process, reactor blends of LMW homopolymer and HMW copolymer and blends of HMW homopolymer and LMW copolymer were prepared. The blends varied in composition from 100% homopolymer to 100% copolymer with mixtures ranging from 20 to 70%.

7.2.1 Sample Production

Reactor blends of polyethylene homopolymer and poly(ethylene-*co*-1-octene) copolymer samples were produced with an in-situ supported metallocene catalyst system (17-18). This in-situ system eliminates the need for a catalyst supporting stage by combining the catalyst preparation and polymerization in one-step. The resulting polymer has good particle morphology and high bulk density. These studies utilized rac-(dimethylsilylbis(methylbenzoindenyl)) zirconium dichloride [Me_2Si(2-Me-4,5 BenzInd)$_2ZrCl_2$] (Boulder Scientific, BSC 366), a silica support with a high weight percent of methylaluminoxane (provided by Witco), and triethylaluminum as an activator. Slurry polymerizations with n-hexane as a solvent were carried out in a 1 L semi-batch autoclave reactor (Pressure Product Industries, LC Series) operating between 60 and 70 °C and ethylene pressure of 250 psig.

The reaction conditions for each polymerization and stage are listed in Table 7.1. Both the comonomer and solvent were dried over molecular sieves and sparged with prepurified nitrogen. When required, hydrogen was added via a transfer syringe from a hydrogen bottle. Depending on the reactor blend required, the chain transfer agent was added prior to stage 1 or stage 2 polymerization. After stage 1, the reactor was depressurized and vented to the atmosphere. Prior to the second stage, 1-octene was added into the reactor via a transfer syringe.

Table 7.1 – Reaction Conditions for the Two-Step Polymerizations

Sample[a]	Stage	Temp-erature (° C)	Ethylene Pressure (psig)	Hydrogen (mL)	1- Octene/ Ethylene Ratio	Theoretical Fraction[b] (%)	Estimated Fraction[c] (%)
1-A	1st	70	250	150	-	100	100
1-B	1st	70	250	150	-	61.8	80.3
	2nd	70	250	-	0.265	38.2	19.7
1-C	1st	70	250	150	-	40.2	66.5
	2nd	70	250	-	0.265	59.8	43.5
1-D	1st	70	250	150	-	20.9	41.5
	2nd	70	250	-	0.265	79.1	58.5
1-E	1st	70	250	150	-	15.2	32.2
	2nd	70	250	-	0.265	84.8	67.8
1-F	1st	70	250	-	0.265	100	100
2-A	1st	70	250	75	0.035	100	100
2-B	1st	70	250	75	0.035	72	79
	2nd	70	250	-	0.265	28	21
2-C	1st	70	250	75	0.035	25.1	30
	2nd	70	250	-	0.265	74.9	70
2-D	1st	70	250	0	0.265	100	100
3-A	1st	60	250	0	0	100	100
3-B	1st	60	250	0	0	33.8	68.3
	2nd	70	250	250	0.265	66.2	31.7
3-C	1st	60	250	0	0	9.5	51.1
	2nd	70	250	250	0.265	90.5	48.9
3-D	1st	70	250	250	0.265	100	100

[a] Polymerization conditions: [Me_2Si(2-Me-4,5 BenzInd)$_2ZrCl_2$] = 1.25 μmol/L, Support Al/Zr = 500, Activator Al/Support Al = 5.335

[b] Theoretical fraction of polymer based on the consumption of ethylene

[c] Estimated fraction of polymer as determined from an integrated CRYSTAF profile with regions deemed as polyethylene homopolymer and poly(ethylene-*co*-1- octene)

The initial concentration of 1-octene in the reactor was 0.425 mol/l or 21 mol % of 1-octene in the feed. The polymerization runs were carried out under similar conditions and limited in such a way to minimize the drift in comonomer composition. After the completion of each polymerization, acidified ethanol was injected into the reactor before depressurization. The polymer and solvent were washed with copious amounts of ethanol and then filtered and dried in an oven at 80°C.

7.2.2 Microstructural Characterization

The polymer samples were characterized for their molecular weight distributions using a Waters 150CV high temperature gel permeation chromatograph (GPC) and a Viscotek 150R viscometer. The mobile phase used was 1,2,4 trichlorobenzene operating at 140°C. The average molecular weights were determined using a universal calibration curve derived from narrow polystyrene standards.

Short chain branching distributions were determined by crystallization analysis fractionation (CRYSTAF) in 1,2,4 trichlorobenzene using a CRYSTAF 200 unit (Polymer Char, Spain). The samples were dissolved at 160°C for one hour and then cooled to 95°C to begin the analysis. The sampling temperatures ranged from 95°C to 30°C at a cooling rate of 0.2 °C/min. 1-Octene comonomer compositions were determined by integrating the resulting CRYSTAF profiles while applying a calibration curve to relate the crystallization temperature and 1-octene composition (19). This calibration curve was previously determined by ^{13}C NMR.

Melting endotherms were determined using a TA 2100 differential scanning calorimeter (DSC). The samples were heated from 35 to 200°C at 10°C/min, air cooled to 35°C and then reheated from 35 to 200°C at 10°C/min. The melting point and degree of crystallinity of the

polymer were estimated from the second pass. The degree of crystallinity was estimated by comparing the DSC melting enthalpy to that of a perfect polyethylene crystal ($\Delta H \approx 289$ J/g) (20).

7.2.3 Mechanical Testing

7.2.3.1 Tensile Testing

Tensile properties were determined according to ASTM D638 using an Instron 4465 materials tester. Dog-bone shaped samples (type V) were micro-injection moulded at 250°C using an in-house melt mixing and moulding device. The samples were melted for 5 minutes and then injected under hand pressure into a heated mould. The mould and samples were then water-cooled. The samples were tested at a displacement rate of 25 mm/min and the grip-to-grip length was 3 cm. The sample yield and ultimate break strengths were determined from the force versus displacement curve during deformation of the sample. After testing, the increase in the gage length as compared to the original was used to determine the overall percent elongation.

7.2.3.2 Dynamic Mechanical Analysis

The dynamic mechanical properties of the polymer samples were measured by a Rheometrics DMTA V mechanical spectrometer. The samples were melt pressed at 200°C into thin films and quenched in a water bath. The films were then cut into rectangular specimens (25 mm x 10mm x 0.1 to 0.2 mm). Storage (E') and loss (E'') moduli were measured in the tensile mode. Dynamic strains sweeps were carried out between 0.005 to 1.2 % strain at 10 Hz and room temperature. Dynamic frequency sweeps were performed over the range of 0.01 to 100 Hz at room temperature and 0.05% strain. Dynamic temperature sweeps were carried out over a

temperature range of -150°C to 100°C at a scanning rate of 3°C/min, a frequency of 10Hz and a strain of 0.05%.

7.2.3.3 Small Amplitude Oscillatory Shear Experiments

The linear viscoelastic properties of the polymer in the melt state were measured using a TA instruments AR2000 rotational rheometer. Measurement of the storage (G') and loss (G'') moduli as well as the complex viscosity were made using parallel plate mode. The samples were melt-pressed at 200°C into 25 mm x 2.5 mm circular disks and quenched in a water bath. To determine the linear viscoelastic region of the polymer, dynamic strain sweeps were carried out between 0.1 to 10 % strain at 10 Hz and 230°C. Dynamic frequency sweeps were performed over the range of 0.01 to 100 Hz at 230°C and 2.5% strain.

7.3 Results and Discussion

In this study, three sets of resins were produced. Each set contains a pure homopolymer, a pure copolymer and blends that increase in copolymer content. Set 1 and set 2 are reactor blends of LMW homopolymer and HMW copolymer, similar to industrial resins with reverse comonomer distributions. The difference between these two sets of polymer is that the homopolymer produced in set 2 was higher in molecular weight than in set 1, resulting in blends with narrower molecular weight distributions. The blends in set 3 are the opposite in composition of sets 1 and 2 and are composed of HMW homopolymer and LMW copolymer. Table 7.1 shows the experimental details for the production of these resins. The homopolymer/copolymer ratio in the blend was achieved by monitoring the polymerization rate and the polymerization time for each stage. Figures 7.2(a-c) compare the flow consumption of ethylene during the production of the three sets of resins. In general, the homopolymerization rates in stage 1 were lower than the copolymerization rates in stage 2 for the production of LMW homopolymer/HMW copolymer blends shown in Figures 7.2a and 7.2b. This 'comonomer effect' is common to olefin polymerizations and has been attributed to a reduction in the diffusion limitation within the particles or to the activation of new catalytic sites sensitive to comonomer (21-22). Due to the high copolymerization rates experienced during stage 2, short polymerization times were used. Diffusion limitation may be significant during the production of the HMW homopolymer/LMW copolymer resins in set 3. Figure 7.2c shows that the copolymerization rates in stage 2 were much lower than that of homopolymerization rates in stage 1. Note that the rate of polymerization for the pure LMW copolymer (sample 3-D) produced with hydrogen was higher than the homopolymerization (3-A) as expected. Therefore

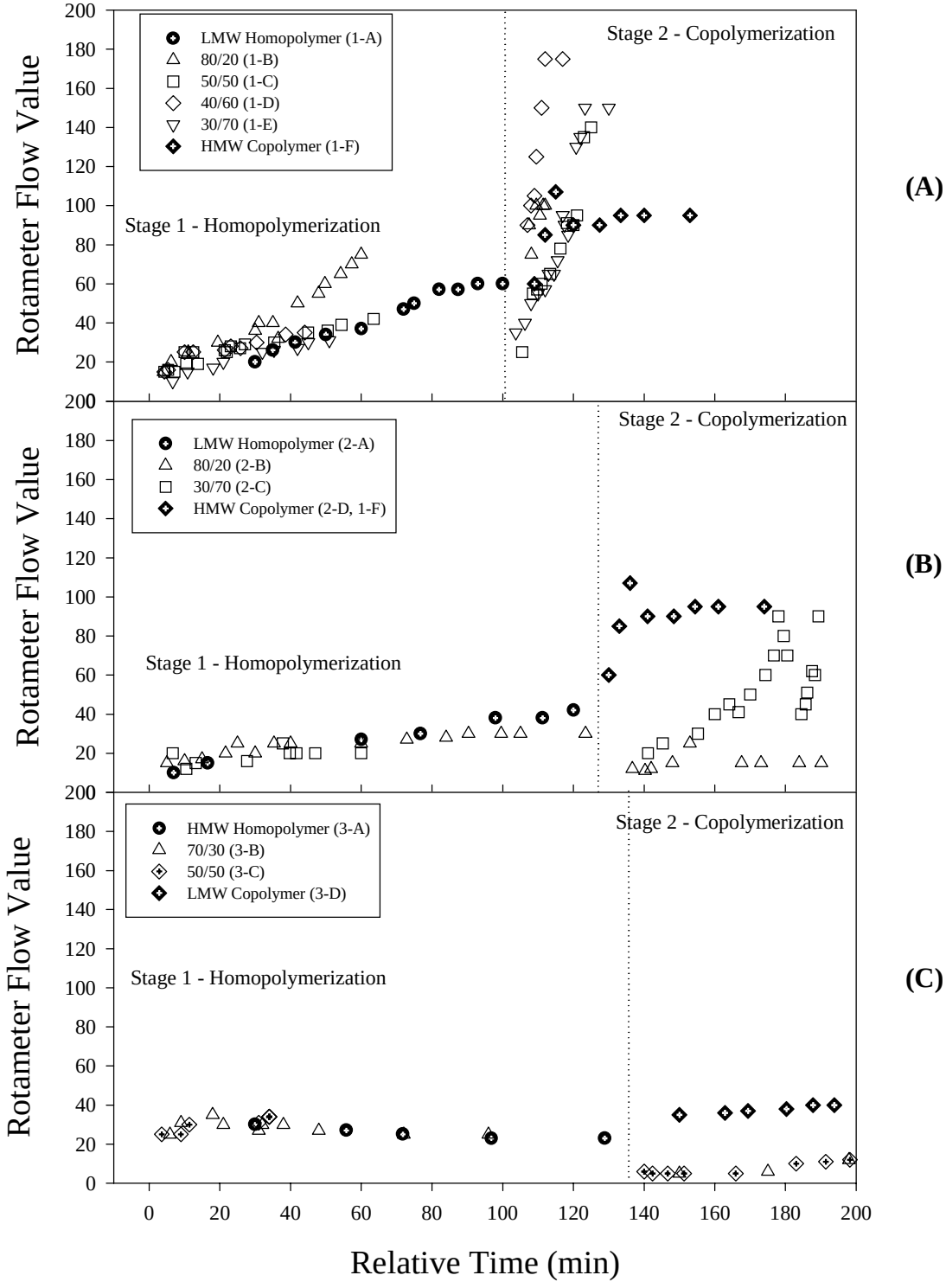

Figure 7.2 – Ethylene Flow Profiles from Two-step polymerizations

in the second stage, it is believed that the 1-octene comonomer and ethylene had difficulties penetrating the HMW homopolymer produced in stage 1. It is possible that diffusion of ethylene and 1-octene was limited by the HMW and highly crystalline polymer shell that formed around the active sites. Jungling et al. and Pryzybyla et al., discuss the influence of mass and heat transfer limitations in high bulk density polymers that may limit comonomer access (23-24). This limited access would result in a lower polymerization rate until sufficient penetration of the copolymer occurs. Given the low polymerization rates, the highest copolymer content that could be achieved in a reasonable polymerization time was 50 % (sample 3-C).

Overall, the two-step polymerization method was successful in producing reactor blends in high yields, for characterization and physical property testing. The discussion of the experimental results will be organized as follows:

Microstructural characterization

- Chemical composition distribution analysis by CRYSTAF – profile of the distribution of crystalline species, fractional estimation of homopolymer/copolymer amounts and comonomer content estimation
- Molecular weight distribution analysis by GPC – number and weight average molecular weights, polydispersity index

Physical Property Testing

- Melting characteristics as determined by DSC – melting point and degree of crystallinity estimates
- Tensile properties (short term loading), yield stress, break stress and percent elongation

- Dynamic Mechanical Properties – viscoelastic properties measured as elastic (E') and loss (E'') and tan delta (E''/E') responses with the effect of strain %, temperature and frequency
- Melt viscosity characteristics – as measured by small amplitude oscillatory shear measurements for estimates of the elastic (G'), loss (G'') and tan delta (G''/G'). Comparison of shear viscosity behaviour with estimates of the zero-shear viscosity and rate indices from rheological models.

7.3.1 Microstructural Characterization

Two of the most important structural features of these resins are their short chain branching and molecular weight distribution. The short chain branching distributions (SCBD) of the resins were determined by crystallization analysis fractionation (CRYSTAF). From the CRYSTAF analysis, a weighted profile of the crystallinity distribution of the copolymer was measured. The SCBD verified the presence and location of the copolymer fraction within the blended polymer. By comparing the SCBD of a pure homopolymer and pure copolymer, the location and amount of copolymer in the blend can be inferred. The molecular weight distributions (MWD) were determined from gel permeation chromatography (GPC).

Figures 7.3-7.5 compare the SCBDs of the three sets of resins. Set 1 includes two pure resins, a LMW Homopolymer (1-A) and HMW Copolymer (1-F) along with 4 reactor blends that increase in copolymer content (Samples 1C-1E). The pure homopolymer (1-A) exhibits a narrow crystallization peak at high temperature around 82.5 °C. A high crystallization temperature is typical of polyethylene homopolymer that have very long ethylene sequences and crystallize readily upon cooling. Polymer crystallizing in this high temperature region will be considered to

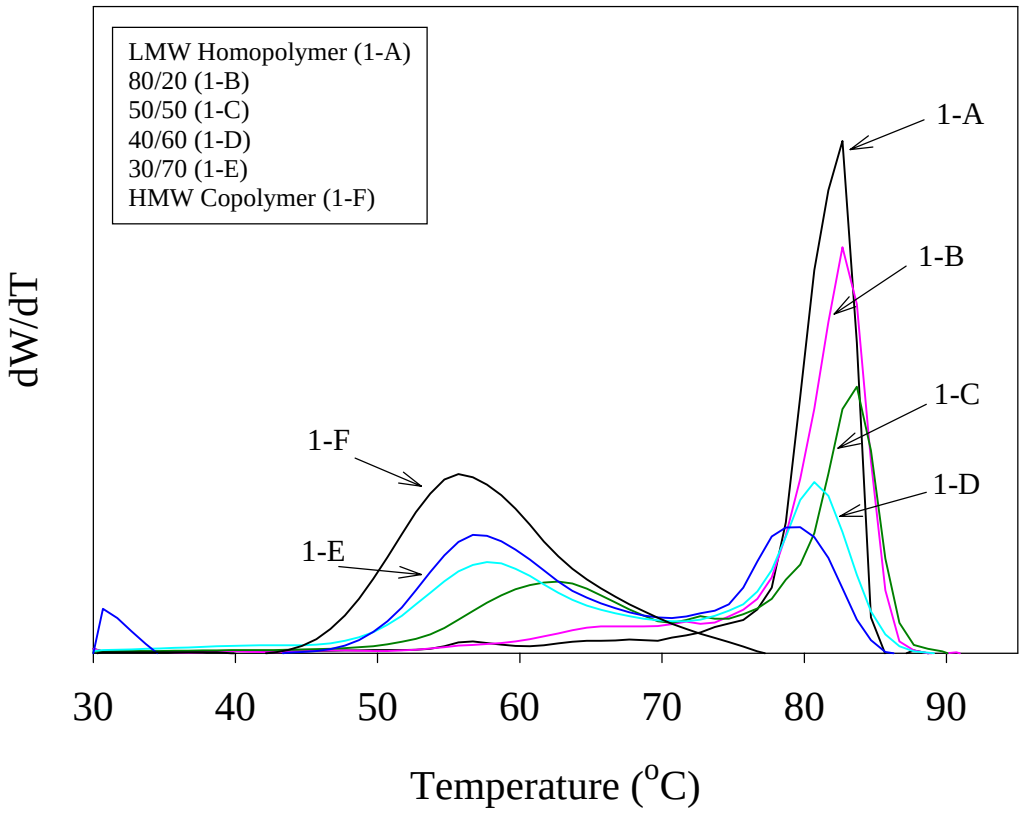

Figure 7.3 – Set #1: Comonomer Distribution Comparison of Reactor Blends

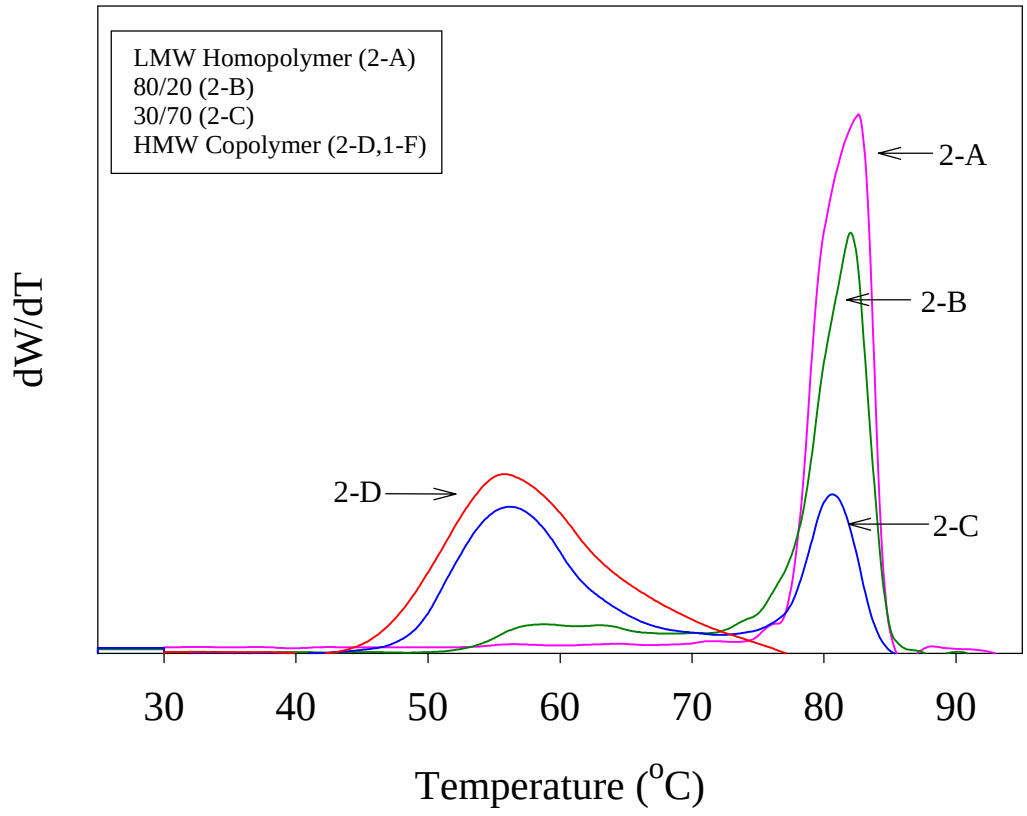

Figure 7.4 – Set #2: Comonomer Distribution Comparison of Reactor Blends

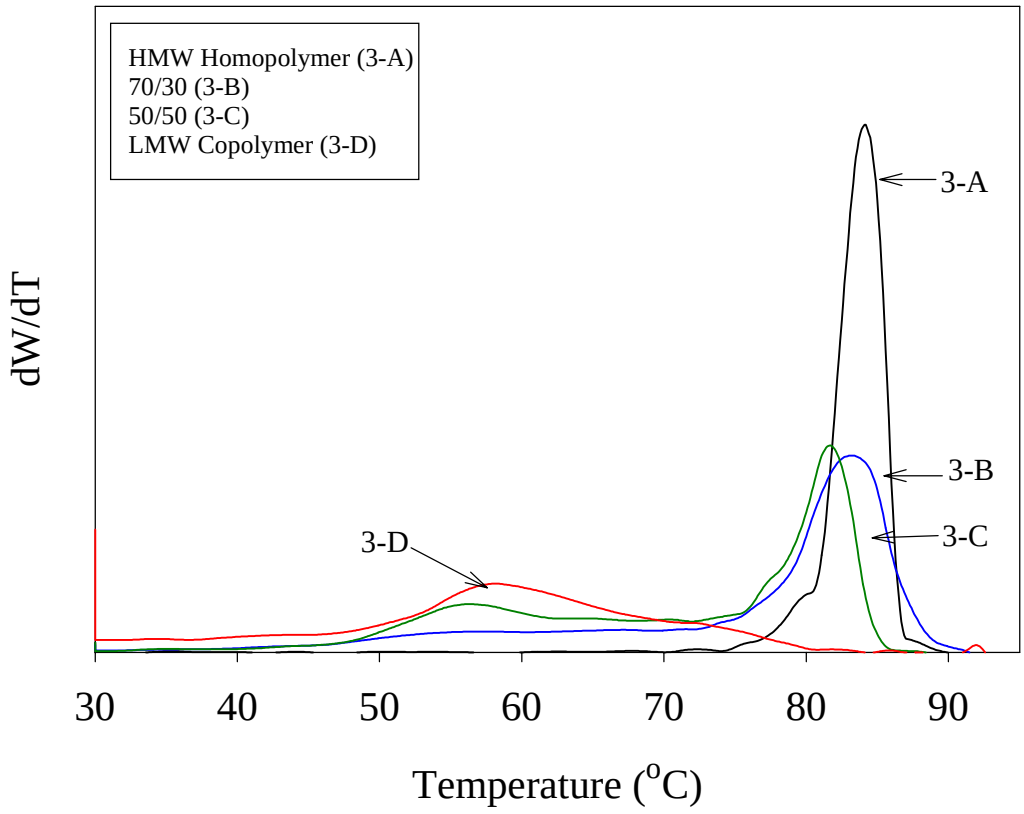

Figure 7.5 – Set #3: Comonomer Distribution Comparison of Reactor Blends

be homopolymer with very little or no comonomer in the polymer. The pure copolymer (1-F) displays a very broad SCBD with a much lower crystallization temperature around 55°C. Polymers that crystallize in this low temperature range have fairly high comonomer content around 4.0 mol %. The SCBD for this sample was quite broad between 50 and 70°C. For a single-site catalyst, a sharp and narrow distribution was expected, but copolymers produced with in-situ supported catalysts sometimes exhibit broad SCBDs (18). This broadening may be due to the heterogeneity in the catalyst support sites or the solubility of the copolymer formed. For these reactor blends, it is fairly easy to distinguish the LMW homopolymer and HMW copolymer, since the peaks and tails of each polymer are fairly well separated. As shown, the copolymer peak increases for reactor blends 1B through 1-E with the increasing fraction of copolymer. Also observed is the decrease in the height of the homopolymer peaks with the increasing fraction of copolymer. The height and area of these peaks are related to the weight fraction of the polymer present. Using a calibration curve to relate the crystallization temperature with the 1-octene content of the copolymer (which was previously estimated by ^{13}C NMR) the comonomer content in mol % was estimated by integration of the SCBD. Table 7.2 shows for sets 1 and 2 that the comonomer content reaches a maximum of 4 mol % of 1-octene for the HMW copolymer (1-F,2-D) and the 1-octene content increases with the fraction of copolymer present in the blend. The measured weight fractions of the homopolymer and copolymer present in the blends are listed in Table 7.2. These fractions were estimated by integration of the CRYSTAF profiles for the regions deemed as homopolymer and copolymer.

Set 2 also consists of blends of LMW Homopolymer and HMW copolymer. This set has four samples: a pure LMW homopolymer (2-A) and pure HMW copolymer (2-D same as 1-F), and two reactor blends of 80/20 (2-B) and 30/70 (2-C) homopolymer/copolymer. The

Table 7.2 - Microstructural properties of LMW Homopolymer/HMW Copolymer Blends

Sample[a]	$\overline{M}_N$[b] (g/mol)	$\overline{M}_w$[b] (g/mol)	$\overline{M}_w/\overline{M}_n$[b]	1-Octene Content[c] (mol %)	Estimated Homopolymer /Copolymer Fraction[d]	Melting Peak[e] (°C)	Crystallinity[f] (≈ Density)[g] (%) (g/cm^3)
100 % LMW Homopolymer (1-A)	17,150	157,500	9.2	0	100/0	133.8	78.8 (0.967)
80/20 (1-B)	19,000	268,350	14.1	0.8	80/20	-	-
50/50 (1-C)	23,300	318,400	13.7	1.5	57/43	126.0	60.0 (0.948)
40/60 (1-D)	25,400	411,500	16.2	2.4	42/58	-	-
30/70 (1-E)	44,250	458,150	10.5	2.9	32/68	124.0[e]	48.1 (0.932)
100 % HMW Copolymer (1-F)	133,100	423,000	3.2	4.0	0/100	100.8	21.3 (0.881)
100% LMW Homopolymer (2-A)	30,300	180,850	6.0	0.0	100/0	-	-
80/20 (2-B)	49,400	282,450	5.7	1.0	79/21	-	-
30/70 (2-C)	82,950	494,150	6.0	3.0	30/70	-	-
100 % HMW Copolymer (2-D,1-F)	133,100	423,000	3.2	4.0	0/100	100.8	21.3 (0.881)
100% HMW Homopolymer (3-A)	238,450	542,750	2.3	0.0	100/0	130.7	65.5 (0.954)
70/30 (3-B)	16,766	334,567	20.0	1.3	68/32	126.5	60.5 (0.948)
50/50 (3-C)	17,350	272,800	15.7	2.1	51/49	125.0	58.2 (0.946)
100 % LMW Copolymer (3-D)	21,950	84,250	3.8	5.9	0/100	107.1	41.9 (0.923)

[a] Polymerization conditions: $[Me_2Si(2\text{-Me-}4,5\ BenzInd)_2ZrCl_2]$ = 1.25 μmol/L, Support Al/Zr = 500, Activator Al/Support Al = 5.335,
Stage 1: polymerization temperature = 70°C, ethylene pressure = 250 psig, 150 mL hydrogen
Stage 2: polymerization temperature = 70°C, ethylene pressure = 250 psig, [1-octene] = 0.425 mol/L (52 mL)

[b] As determined from GPC analysis based on a universal calibration curve derived from narrow polystyrene standards. The molecular weight averages reported are based on replicate runs.

[c] As determined from an integrated CRYSTAF profile and 1-octene temperature-composition calibration curve.

[d] As determined from an integrated CRYSTAF profile with regions deemed as polyethylene homopolymer and poly(ethylene-co-1-octene) copolymer

[e] As determined by DSC. Note that these samples exhibited very broad but unimodal melting distributions with the exception of sample 1-E (25/75) which displayed a bimodal melting profile.

[f] Crystallinity estimates based on DSC melting enthalpy as compared to a perfect crystalline polyethylene ($\Delta H \approx 289$ J/g)[20]

[g] Approximate density range estimated from a % crystallinity versus density calibration curve from Kim et al.[45]

difference between set 1 and these resins is that the LMW homopolymer portion of the blend was produced with a low amount of comonomer and less hydrogen. These samples were part of pre-trial work that investigated the addition of comonomer in an attempt to enhance the polymerization rate of the homopolymer fraction. These samples were included in this study to examine the effect of the molecular weight of the homopolymer fraction on the physical properties of the polymer blend. Figure 7.4 shows that the crystallization temperature of the homopolymer region is approximately the same as for set 1. This indicates that very little incorporation of the comonomer occurred during stage 1 to produce the LMW homopolymer. Table 7.2 lists the estimated comonomer contents and homopolymer/copolymer ratios for these resins.

Set 3 consists of reactor blends of HMW homopolymer and LMW copolymer. Set 3 has four resins: a pure HMW Homopolymer (3-A), a pure LMW copolymer (3-D), and reactor blends of 70/30 (3-B) and 50/50 HMW homopolymer/LMW copolymer (3-C). Figure 7.5 shows the CRYSTAF profiles of the resins produced. A large homopolymer fraction is present for reactor blends 3-B and 3-C. The profile of the LMW copolymer (3-D) is also quite broad with the copolymer region extending from 50-80 °C. For these reactor blends, it can be seen that the profiles are not as well distinguished as sets 1 and 2. The difficulty in producing these resins is probably linked to the diffusion limitation discussed above. Table 7.2 shows that the 1-octene content increases with the fraction of copolymer present in the blend. For the pure copolymer (3-D), the comonomer incorporation was 6.0 mol % which is higher than the content of the HMW copolymer (1-F,2-D) from sets 1 and 2. The polymerization conditions used to produce this copolymer fraction was similar to the second stage for sets 1 and 2, except for the fact that no hydrogen was added. The addition of hydrogen lowered the molecular weight of the polymer but

also increased the incorporation of the comonomer. The CRYSTAF profile exemplifies this by showing very broad distributions for the copolymer blends. The broadening of the SCBD might be related to a change in the nature of the active sites or the increased solubility of the LMW copolymer in the reactor solvent.

From the CRYSTAF profiles, the measured crystallization temperatures, comonomer contents, and weight fractions verified that the reactor blends contain fractions of homopolymer and copolymer corresponding to the recipes of the two-step polymerizations used.

Figures 7.6-7.8 show the MWDs of the resins that were obtained from GPC analysis. The MWDs for set 1 are shown in Figure 7.6 and confirm that the copolymer (1-F) has higher molecular weight than the homopolymer (1-A). The separation between the number average molecular weights of these resins is approximately 8 fold, with the homopolymer having an average of ≈ 17,000 and the copolymer ≈ 133,000. In previous attempts, difficulties arose in obtaining polymers with bimodal-looking MWDs. Very often the resins produced would display broad MWDs but remain unimodal. It has been reported by other researchers that the difference in the molecular weights must be around 10 times to achieve good separation (11,25). After fine-tuning the polymerization conditions, reactor blends with bimodal MWDs were successfully produced for this study. The bimodal characteristics of the MWDs increase with increasing the fraction of HMW copolymer, thus demonstrating that the MWDs follow the recipe of the two-step polymerization method used. The polydispersity indices of these reactor blends were quite broad, ranging from 10 to 16. It is noted that the polydispersity index of the pure LMW homopolymer was around 9 and is much broader than expected from a single-site catalyst. It is possible that the hydrogen concentration in the reactor drifted during the polymerization and

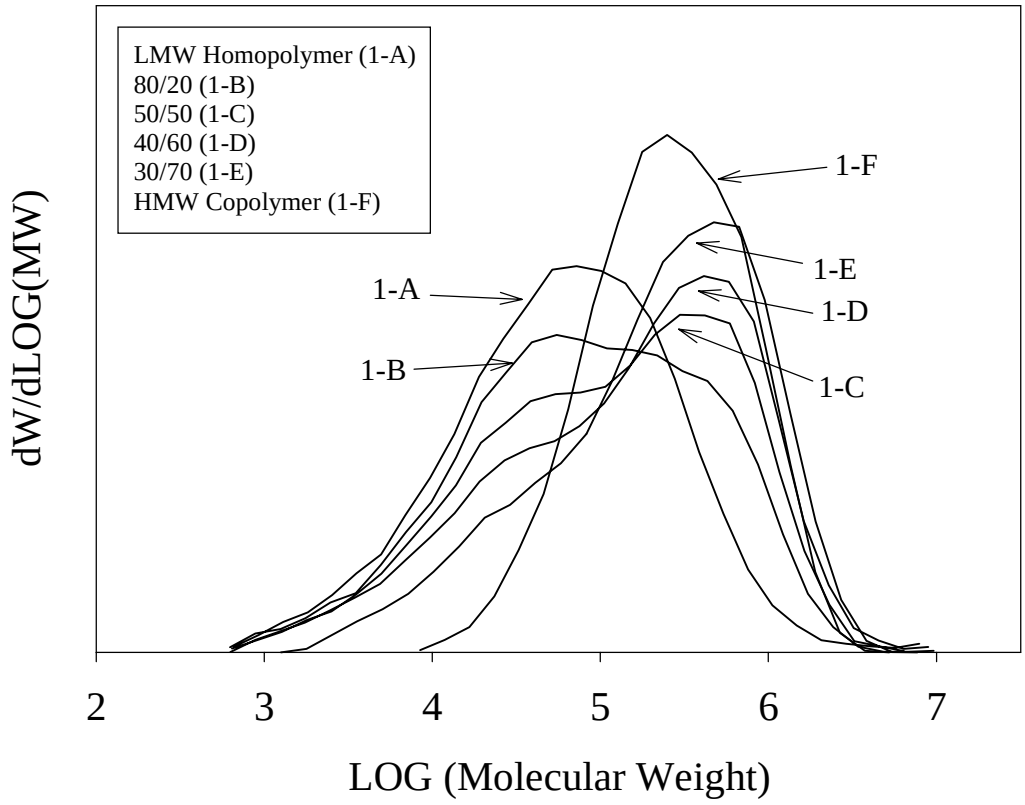

Figure 7.6 – Set #1: Molecular Weight Distribution Comparison of Reactor Blends

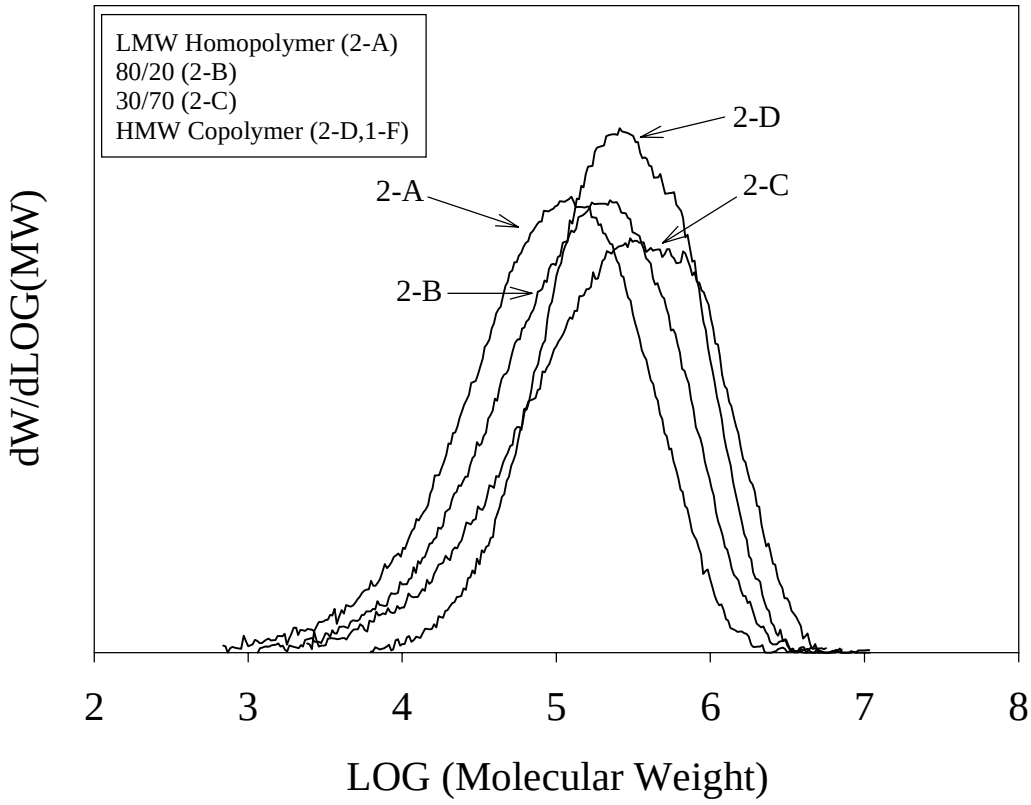

Figure 7.7 – Set #2: Molecular Weight Distribution Comparison of Reactor Blends

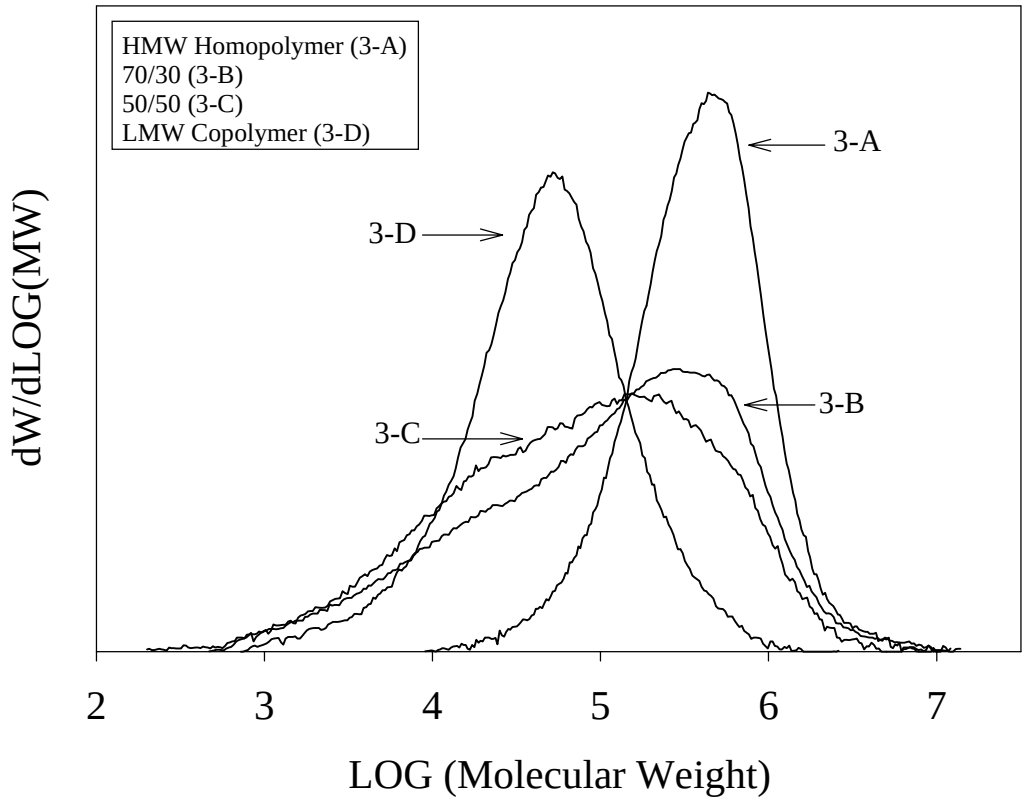

Figure 7.8 – Set #3: Molecular Weight Distribution Comparison of Reactor Blends

consumed by a β-hydrogen elimination process. As a result, the hydrogen concentration will decrease and higher molecular weight polymer will be produced as the polymerization proceeds (26). Overall for the resins in set 1, the two-step polymerization method was successful in producing reactor blends of LMW homopolymer and HMW copolymer.

Figure 7.7 shows that the MWDs for the resins in set 2 are unimodal. With the lower amount of hydrogen added in the production of the homopolymer, the separation of the molecular weights of the homopolymer and copolymer decreased and the individual peaks overlap. Table 7.2 also shows that the molecular weights of the homopolymer (2-A) are higher than the homopolymer (1-A) from set 1. The ratio of the number average molecular weights between the pure homopolymer (2-A) and pure copolymer (2-D,1-F) was only 4 times. The closeness of the molecular weights resulted in blends with polydispersity indices that range from 3 to 6. Overall, the MWDs of the samples produced for set 2 are also consistent with the method of polymerization.

Figure 7.8 shows the MWDs of the HMW homopolymer/LMW copolymer blends in set 3. Good separation was achieved between the pure HMW homopolymer (3-A) and pure LMW copolymer (3-D). This separation resulted in reactor blends with very broad MWDs. Table 7.2 indicates that the molecular weight difference between the pure LMW copolymer and pure HMW copolymer is about 10 times, with number average molecular weights of 22,000 g/mol and 240,000 g/mol respectively. Both the homopolymer and copolymer exhibited fairly narrow MWDs with polydispersity indices of 2.3 and 3.8 respectively. The LMW copolymer (3-D) exhibited less broadening of the MWD than that of LMW homopolymer (1-F,2-D) in sets 1 and 2. It is possible that the combination of the comonomer and hydrogen together, created active

sites that were more uniform and exhibited more single-site behaviour. As a result of this large separation in the molecular weights, the reactor blends show very distinct and bimodal MWDs.

Overall, the GPC and CRYSTAF analyses have shown that the two-step polymerization method was successful in producing polyethylene/poly(ethylene-*co*-1-octene) resins with bimodal MWDs and bimodal SCBDs. Both the MWDs and SCBDs of these blends reflect the individual reactor conditions in which the polymer was produced.

7.3.2 Mechanical Properties

The characterization of the resins produced by the two-step polymerizations has shown that their structures are well defined. Given these three sets of resins with bimodal structural distributions, structure-property relationships have been developed to better understand the influence of molecular weight, molecular weight distribution, copolymer content and the molecular weight of the copolymer for these reactor blends. The contribution of each individual component, LMW and HMW homopolymer, LMW and HMW copolymer to the properties of the blends was observed. Commercially there are numerous applications of these polymers and it is difficult to outline an 'optimum' formulation unless a specific target grade was desired. The results from this study illustrate the general properties of these bimodal microstructures and could be used as a guideline for product development

In this study, the influence of these bimodal resins on the solid-state and melt properties was examined. In the solid-state, both the tensile and dynamic mechanical properties of these bimodal resins were compared. The melt rheological characteristics were also measured to examine the influence on the material's processability.

7.3.2.1 Tensile Testing

The tensile properties of the resins were measured under short-term loading conditions. The samples were stretched at a constant speed while the force and displacement were measured. From these deformation experiments, the yield and failure behaviour up to high strain were used to estimate the tensile stresses at yield and at break. From the change in gage length of the sample, the percentage elongation at break was also calculated. The measured values for the 3 sets of resins are listed in Table 7.3 and compared in Figures 7.9-7.11. In general, most of the samples exhibited localized yielding and cold drawing that is characteristic to semi-crystalline polymers. Figures 7.12-7.14 compare the initial yielding behaviour of the resins. It was found that the yield stress measurements were the most reliable. The error in the measurement of the yield stress was quite low when compared to the error associated with the tensile stress at break and percentage elongation at break. These errors may be linked to the difficulties encountered in the preparation of 'clean' sample bars that were free from defects.

Figure 7.9 compares the tensile stresses at yield for the blends of LMW homopolymer and HMW copolymer in set 1. The tensile stress at yield was much higher for the LMW homopolymer (1-A) than the HMW copolymer (1-F). For the reactor blends, it can be clearly seen that yield stress decreases with increasing percentage of HMW copolymer. The results are quite consistent since the yield stresses decrease in an almost linear fashion. The trend observed should reflect the decrease in crystallinity of the polymer with the addition of the lower density material. The DSC measurements of the melting points and degree of crystallinity for these resins are listed in Table 7.2. As expected, the peak melting point of the pure homopolymer was the highest with a value of approximately 134°C. Corresponding with the high melting point of the homopolymer, a high degree of crystallinity of 79% was estimated. On the other hand,

Table 7.3 - Tensile property data of ethylene/1-hexene copolymers[a]

Sample	Tensile Strength at yield (kPa) (± 777)[b]	Tensile Strength at break (kPa) (± 3650)[c]	Elongation at break (%) (± 79.6)[d]
100 % LMW Homopolymer (1-A)	29,200 (319)	20,800 (2963)	505 (112)
80/20 (1-B)	22,700 (178)	23,800 (1966)	505 (74.0)
50/50 (1-C)	16,000 (226)	18,900	440
40/60 (1-D)	12,300 (331)	16,900 (3279)	376 (76.5)
30/70 (1-E)	11,100 (554)	14,000 (2738)	362 (75.2)
100 % HMW Copolymer (1-F)	7,440 (283)	16,300 (4,343)	468 (75.8)
100% LMW Homopolymer (2-A)	23,400 (68)	20,500	558
80/20 (2-B)	15,400 (662)	15,700 (4593)	444 (64.9)
30/70 (2-C)	10,700 (77)	17,500 (599)	565 (9.3)
100 % HMW Copolymer (2-D,1-F)	7,440 (283)	16,300 (4,343)	468 (75.8)
100% HMW Homopolymer (3-A)	19,400 (367)	16,100 (1741)	195 (119)
70/30 (3-B)	15,700 (1904)	15,300 (4550)	333 (239)
50/50 (3-C)	16,600 (319)	27,900 (292)	705 (22.3)
100 % LMW Copolymer (3-D)	9,480 (163)	17,200 (4506)	696 (140)

[a] Testing conditions: ASTM D638 (type V), 3.175 mm thickness, displacement rate 25 mm/min, grip to grip length 3 cm
[b,c,d] Calculated standard deviations based on replicate testing.

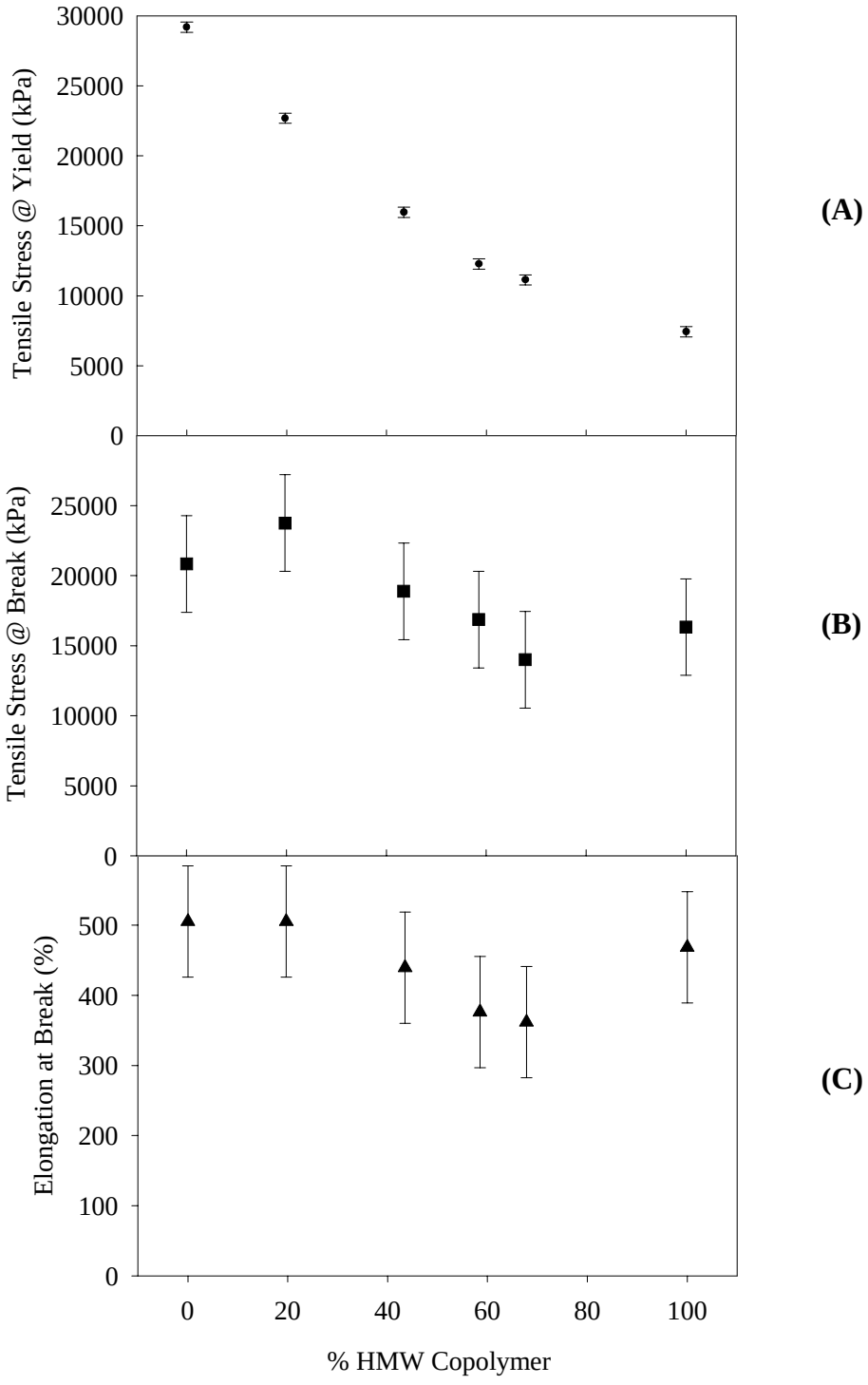

Figure 7.9 – Set #1: Comparison of Tensile Properties of Reactor Blends

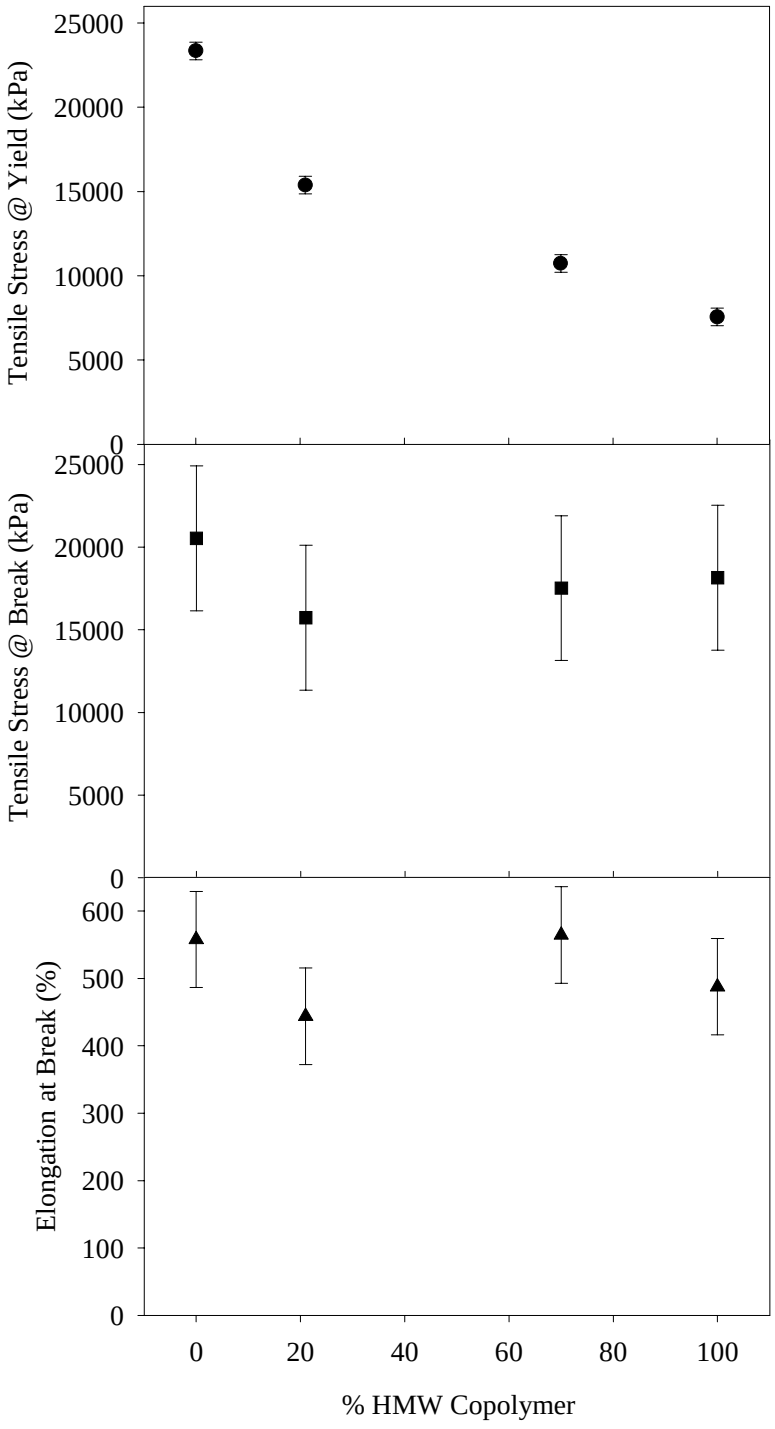

Figure 7.10 – Set #2: Comparison of Tensile Properties of Reactor Blends

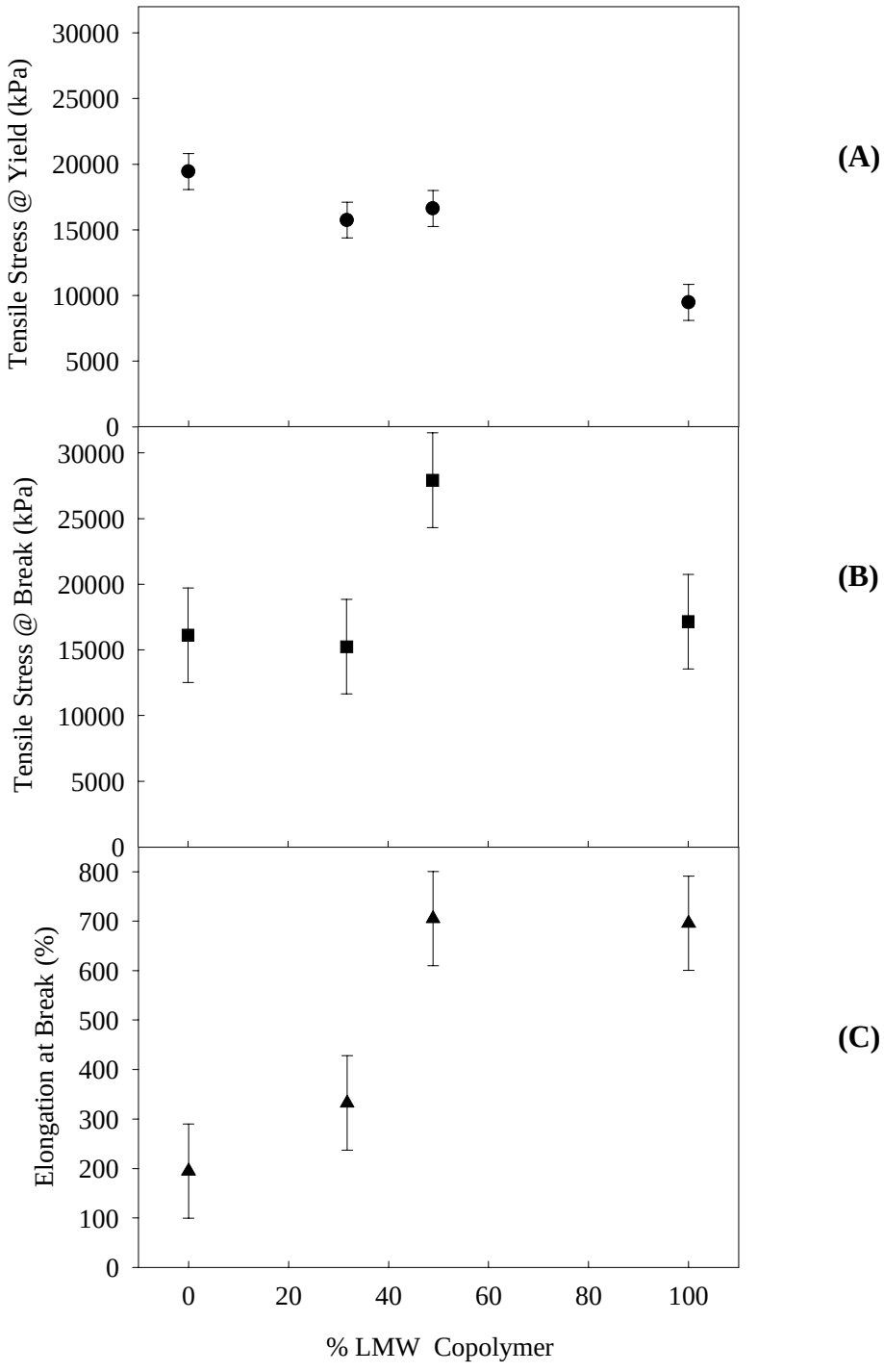

Figure 7.11 – Set #3: Comparison of Tensile Properties of Reactor Blends

the pure copolymer had the lowest melting point at 101°C with a low degree of crystallinity of 21%. Both the melting point and degree of crystallinity decreases with increasing fraction of copolymer. The blends have values that are between that of the pure homopolymer and pure copolymer. Following the rule of additivity, it would be predicted that the yield stress would decrease linearly with increasing fraction of copolymer. However, a slight negative deviation was observed, since the yield stresses of the blends are slightly lower than predicted. Figures 7.9b and 7.9c show the polymer deformation behaviour at high strains. Increases in the fraction of HMW copolymer in the blends results in decreasing break strength and elongation at break. This may indicate that the LMW homopolymer and HMW copolymer do not cocrystallize efficiently resulting in a dispersed morphology. For these blends, it is not unreasonable that the crystallization behaviour would be altered by the presence of different structural units. Cho et al. have reported that blends of HDPE/LLDPE with similar molecular weights can cocrystallize with each other to result in blended properties closely following the rule of additivity (27). For the resins in set 1, the molecular weights and comonomer contents of the individual components of these blends are quite distinct and the resulting crystal structure may not be as regular or intermixed as one would expect.

Figure 7.10a shows a similar trend in the tensile stresses for set 2. As the percentage of HMW copolymer increases in the blends, the tensile stresses at yield decrease. Once again, a slight negative deviation was observed from the linear behaviour. However, the tensile properties at high strains for these blends (Figures 7.10b and 7.10c) were very similar. It is possible that more uniform crystal structures are formed since the individual molecular weights of the components are more closely matched for resins in set 2.

For set 3, the composition of the blends (HMW homopolymer/LMW copolymer) is reverse to that of sets 1 and 2 (LMW homopolymer/HMW copolymer). Despite the differences in composition, Figure 7.11a shows that the tensile stress at yield decreases with increasing LMW copolymer. However, it is noted that the tensile stresses at yield for sample 3-B (70/30) and sample 3-C (50/50) were very similar. Their degrees of crystallinity are also very similar (Table 7.2). Note that the degree of crystallinity for the HMW homopolymer (3-A) is lower than that of the LMW homopolymer (1-A) due to its high molecular weight and narrower MWD which slows the crystallization process. The low degree of crystallinity also resulted in an unusually low estimate of the crystalline density for this high density sample. However, despite the large fraction of copolymer, the HMW homopolymer seems to dominate the crystallization process, resulting in a degree of crystallinity that is similar for these blends. Figures 7.11b and 7.11c compare the high strain tensile properties of these resins. As shown, the HMW homopolymer had very poor elongational properties. This poor performance may be attributed to testing errors, but, it might also be possible that the high molecular weight chains cannot disentangle within the crystallites and brittle fracture occurs.

Figures 7.12-7.14 compare the initial deformation behaviour for the three sets of resins. It was observed that broadening of the yielding zone occurs with increasing percentage of copolymer in the blend. For blends with greater than 50% copolymer, a broad yielding region was observed that could be classified as a double yield point. This double yield behaviour has also been observed by others for polyethylene copolymers (8,28-30). Bensason et al. reported that, with a decrease in density, the yield maximum broadens up to a point where it becomes indistinguishable and no yield maximum is observed (8). Similarly for these samples, it appears that the yielding region broadens with decreasing degree of crystallinity or increasing

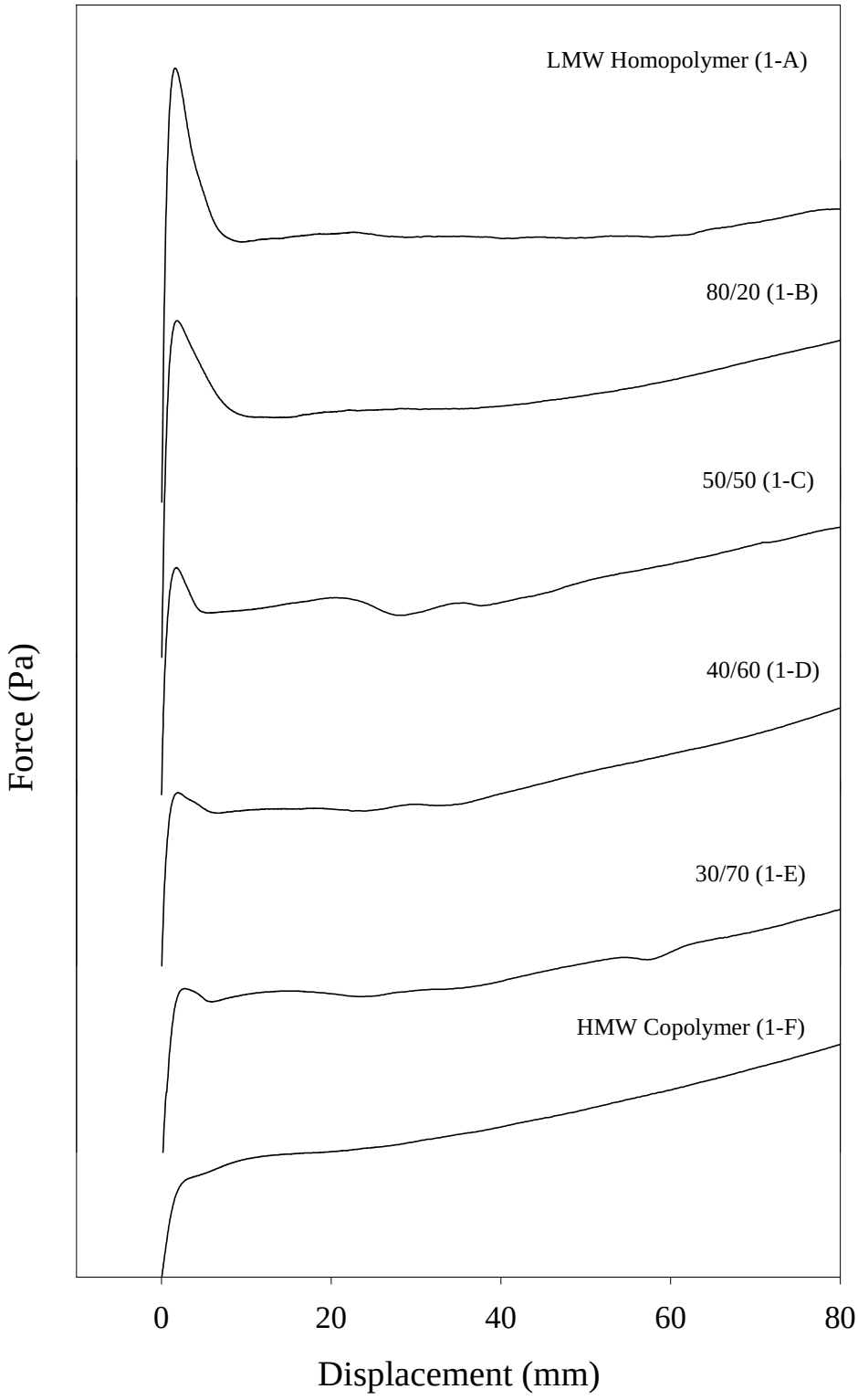

Figure 7.12 – Set #1: Comparison of Initial Tensile Yielding Behaviour

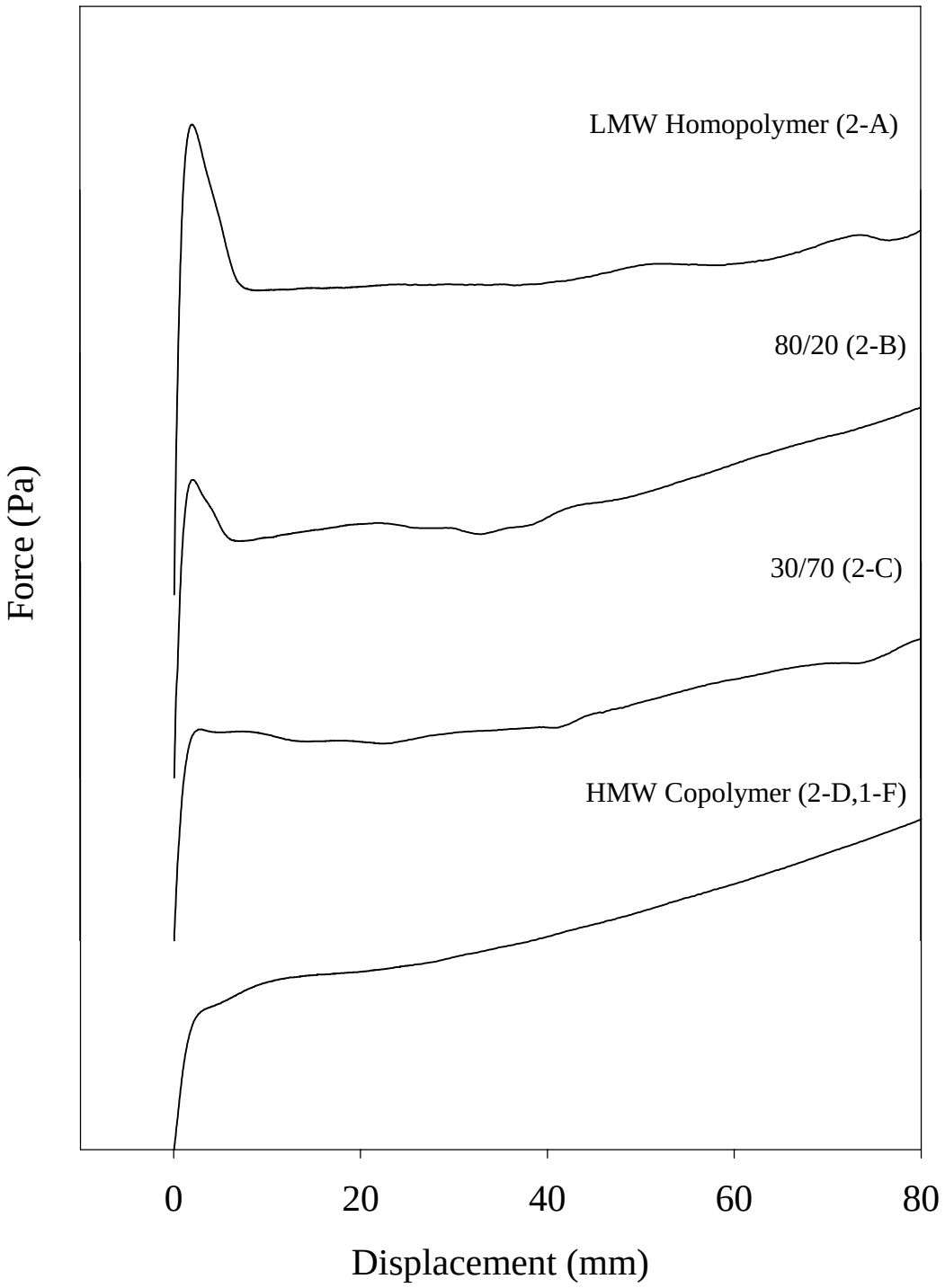

Figure 7.13 – Set #2: Comparison of Initial Tensile Yielding Behaviour

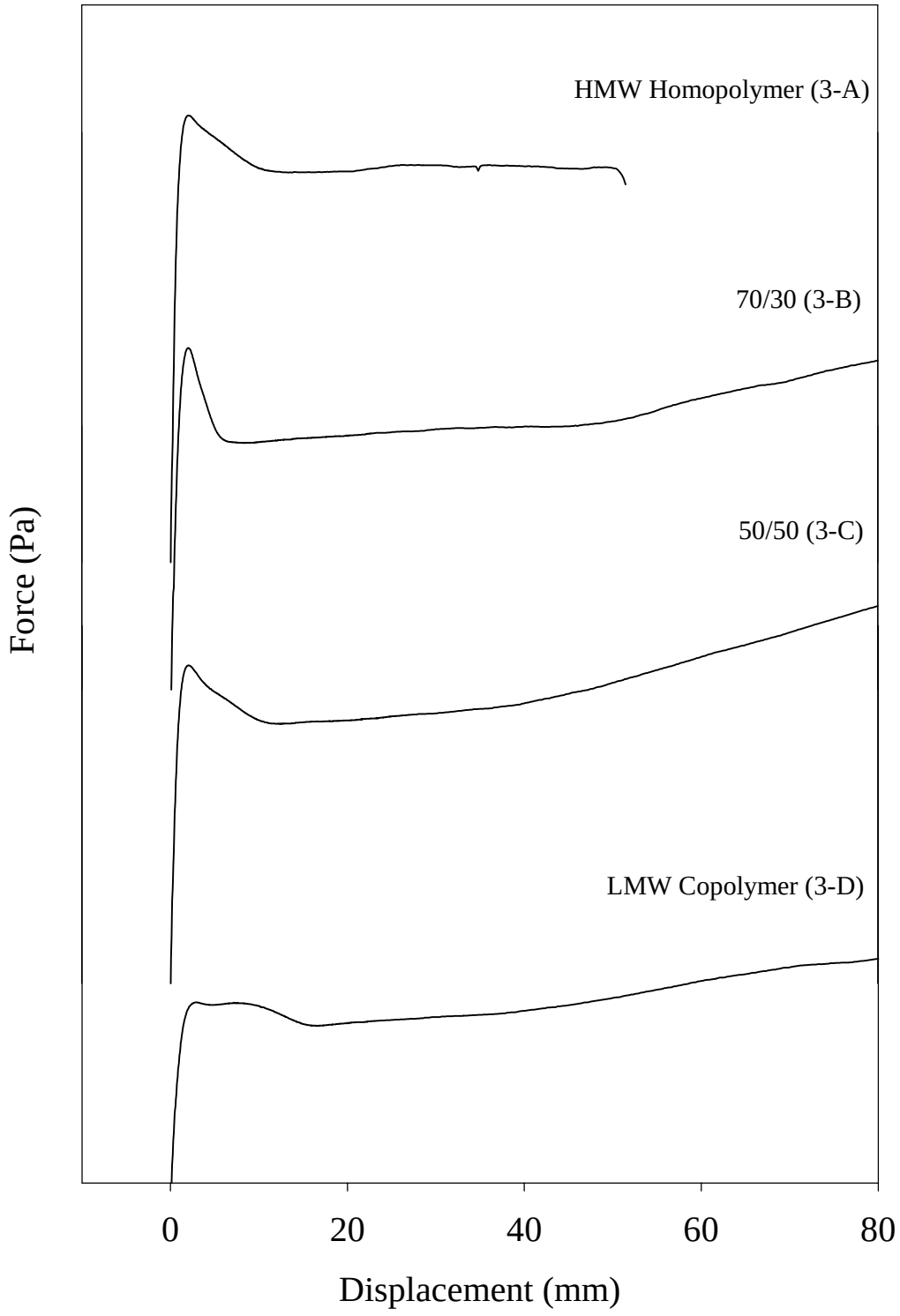

Figure 7.14 – Set #3: Comparison of Initial Tensile Yielding Behaviour

comonomer content. Given the bimodal nature of these short chain branching distributions, increasing the proportion of higher crystalline homopolymer results in a narrower yield maximum except for the pure HMW homopolymer (3-A) in set 3. This sample should exhibit a narrower yield zone when compared to the reactor blends (3-B,3-C). However, this was not the case. This sample is very high in molecular weight. Comparing this HMW homopolymer to the LMW homopolymer (sample 1-A), the overall crystallinity for this sample is lower (66 %) than that of the LMW homopolymer (1-A) (79%). The HMW homopolymer may produce a wider distribution of crystallites.

Contrasting sets 1 and 3, it is possible to compare the effects of molecular weight and degree of crystallinity on the tensile properties of these polymers. Figure 7.15 displays an overlay of the tensile stresses at yield and the degrees of crystallinity for sets 1 and 3. Despite the fact that sets 1 and 3 have very different microstructures with varying compositions, it is shown that the data points overlap. Regardless of the microstructure, the degree of crystallinity seems to be the governing factor influencing the initial yield stress. Thus, it is inferred that the stiffness of a polymer mostly depends on the achievable degree of crystallinity by its microstructure. This finding has also been evidenced by Simanke et al. for polyethylene copolymers with varying branch lengths (28) and by Grahm et al. for polyethylene with different molecular weights (29).

Overall, it can be inferred from these results that the tensile stress at yield decreases with decreasing degree of crystallinity of the polymer. The degree of crystallinity of the polymer can be lowered by the incorporation of comonomer or reactor blending of copolymers. Depending

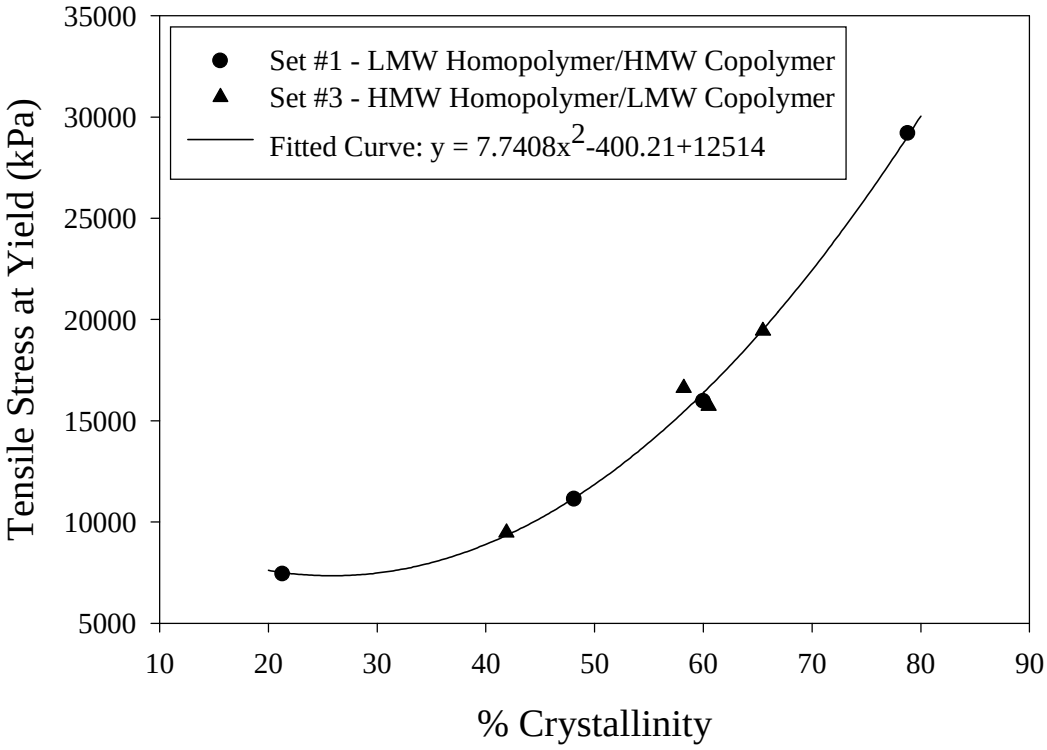

Figure 7.15 – Effects of Blend Composition and Degree of Crystallinity on Tensile Yield

on the blend composition, different structural units may not form uniform crystal structures as evidenced by the negative deviations from linearity of the tensile properties.

7.3.2.2 Dynamic Mechanical Properties

In the following discussion, the dynamic mechanical properties of the resins will be compared to the tensile properties measured above. A dynamic stress-strain sweep is generally used to determine the strain range required for the test to remain within the viscoelastic region of the polymer. For these polymers, a strain level of 0.05 % was found to be adequate. Figure 7.16 compares the dynamic stress-strain behaviour of the 3 polymer sets. Strains greater than 1% were not achievable due to the limitations of the analysis equipment. The deformation behaviour of these resins was quite clear. The LMW homopolymer (1-A,2-A) requires much higher dynamic stresses to achieve the desired % strain than the HMW copolymer (1-F,2-D). The slope of the dynamic stress-strain curve decreases with increasing the fraction of copolymer in the blend (samples 1-B to 1-E and samples 2-B to 2-C). As shown, the stiffness of the HMW copolymer can be enhanced with the addition of a small fraction of LMW homopolymer (compare samples 1-F and 1-E).

Slightly different stress-strain behaviour was observed for the blends of HMW homopolymer and LMW copolymer (set 3). Figure 7.16c shows little difference between the HMW homopolymer and the blends with 30% and 50% copolymer (3-B, 3-C). Contrasting these with the LMW copolymer (3-D), the copolymer is much softer since it requires less stress to achieve the desired strain. These results compare well with those from the tensile testing, confirming that the HMW homopolymer tends to dominate the initial yielding behaviour. The

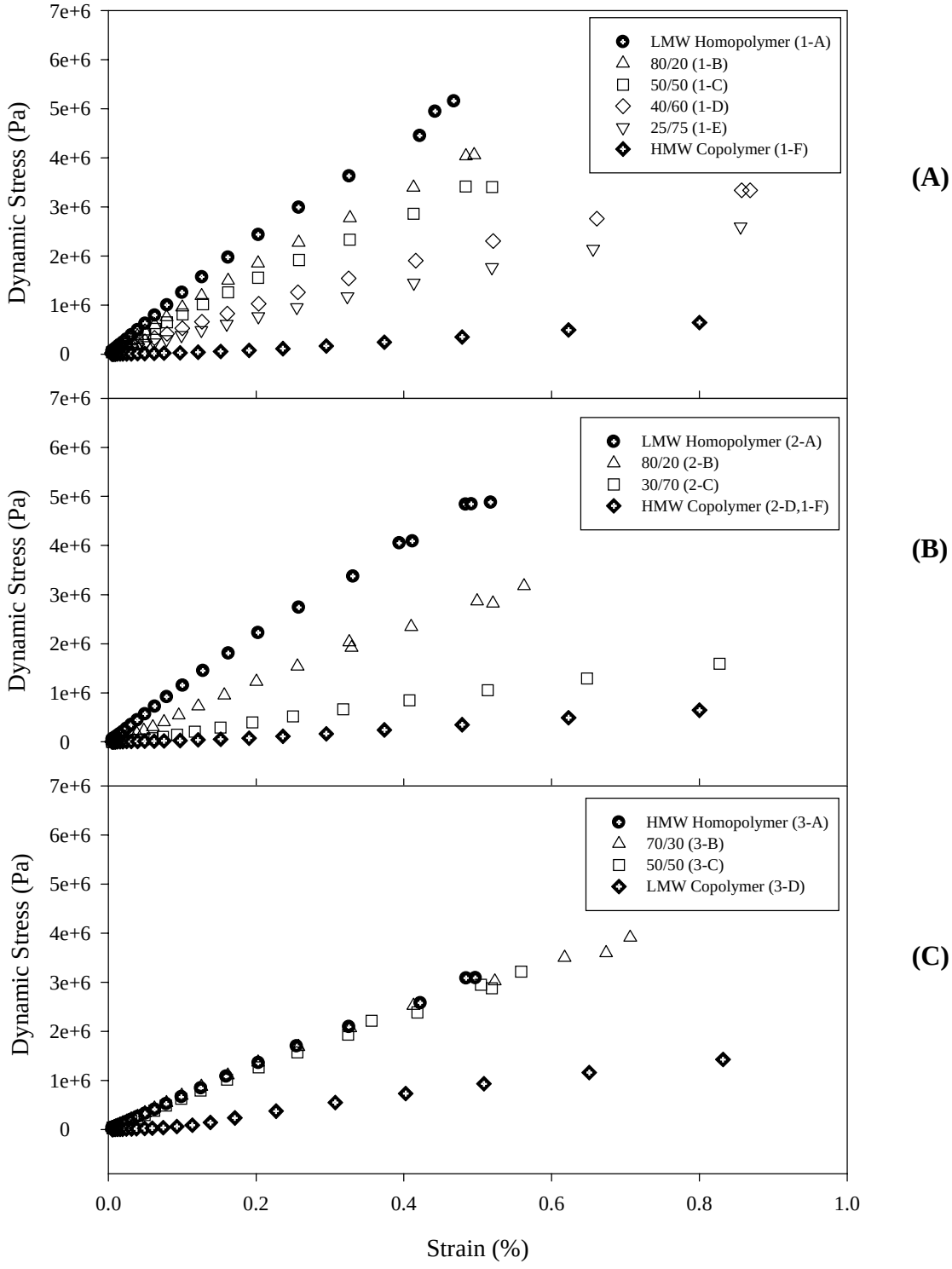

Figure 7.16 – Dynamic Stress-Strain Comparison of Reactor Blends

stiffness of these polymers seems to be dominated by the presence of very long molecules that are unable to relax and disentangle.

Figure 7.17a and 7.17b show that the energy dampening can be influenced by the fraction of LMW homopolymer for sets 1 and 2. At low percent strains (up to 0.05 % in the linear viscoelastic region), the tan delta of the HMW copolymer (1-F, 2-D) is the highest. The tan delta decreases with decreasing percentage of copolymer, with the LMW homopolymer reaching the lowest value. It is consistent that the tan delta would decrease as the degree of crystallinity of the polymer increases because of the dissipation of energy into the amorphous regions. Increasing the strain beyond the linear viscoelastic region, the homopolymer's ability to dampen energy also increases. With increasing strain, the tan delta of the reactor blends eventually surpasses the tan delta of the HMW copolymer. The data for the LMW homopolymers (1-A, 2-A) and samples (1-B, 1-C) end abruptly at ≈ 0.5% strain due to the stress limitation of the testing instrument. In general, the energy dampening behaviour of the blends benefits from the presence of LMW homopolymer at high strains. The enhancement of the tan delta is probably related to the strain hardening behaviour of the sample once irreversible deformation occurs. Figure 7.17c compares the tan delta versus % strain for set 3. Similar to the behaviour found for sets 1 and 2, at low strains, the LMW copolymer shows the highest energy dampening and decreases with increasing the fraction of HMW homopolymer. However, at high strains, the LMW copolymer (3-D) maintained a higher tan delta than the HMW homopolymer (3-A) and the blends (3-B, 3-C). In the discussion above, it was speculated that the elastic properties were dominated by the HMW homopolymer. From results shown in Figure 7.17, it can be inferred that the loss properties are highly influenced by the LMW copolymer.

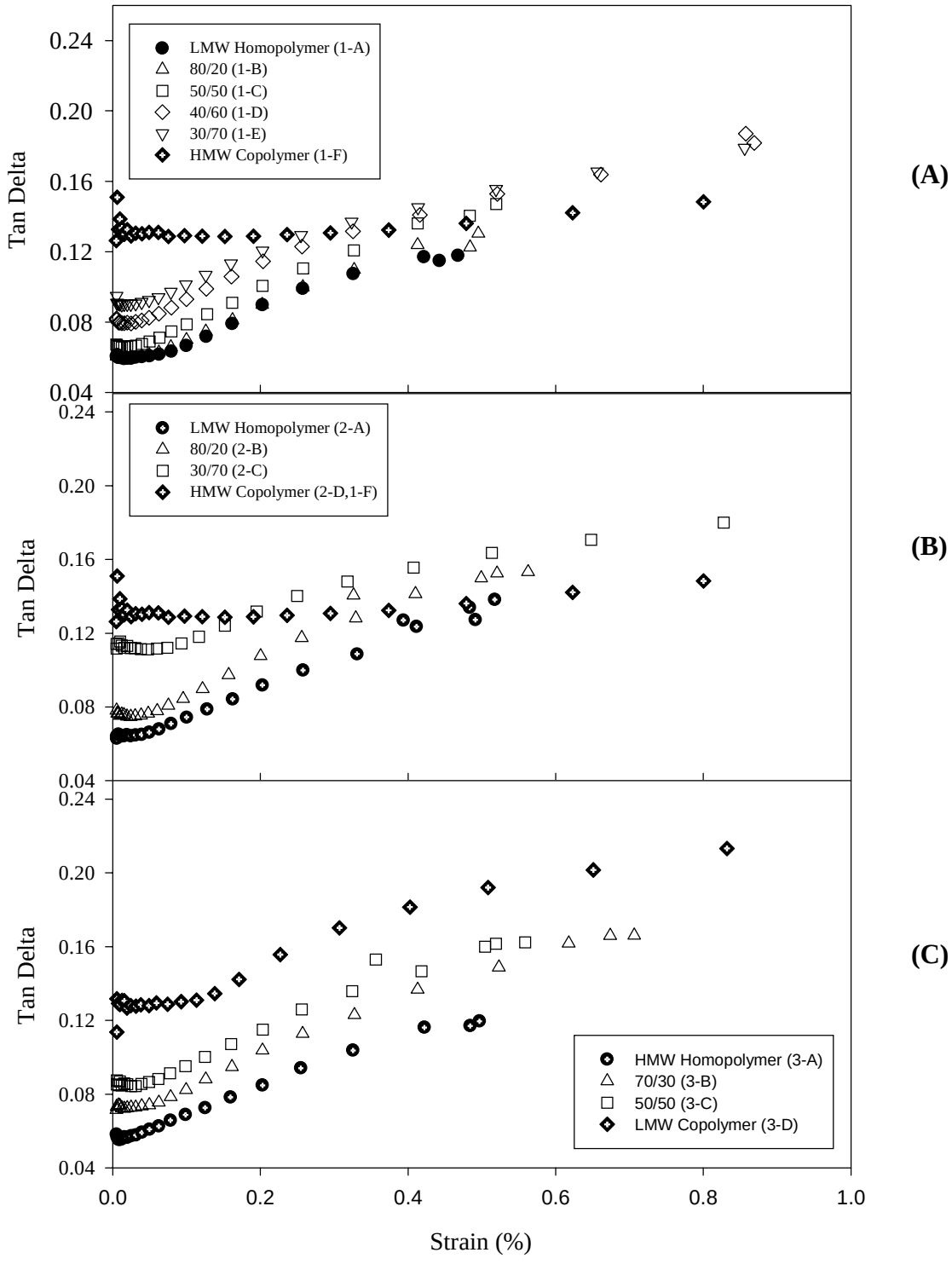

Figure 7.17 – Energy Dampening Comparison of Reactor Blends under Dynamic Strain

Figures 7.18-7.20 compare the effect of temperature on the dynamic mechanical properties for sets 1 and 3. Figure 7.18a shows that the storage modulus (E') decreases with increasing temperature for the resins in set 1. This behaviour is typical of polymeric materials since the chain movement and relaxation times of the polymer are reduced at lower temperatures (31). Above room temperature, the storage modulus decreases with increasing fraction of copolymer as expected. Below room temperature, the storage moduli were in the order of: LMW homopolymer (1-A) and 50/50 (1-C), HMW copolymer (1-F) and then 30/70 (1-E). The deformation behaviour of these resins change as the temperature approaches the glass transition of amorphous polyethylene (≈ -120°C). It is believed that there are two competing factors that determine the order in this region: the degree of crystallinity of the polymer and the molecular weight of the chains. In this set, since the storage modulus of the HMW copolymer (1-F) has a value between that of the 30/70 and 50/50 blend, it can be speculated that the HMW chains of the copolymer may restrict the chain movement at these low temperatures.

For set 3, Figure 7.18b shows that the behaviour of the storage modulus with temperature is even less clear. The storage moduli of the reactor blends of 70/30 (3-B) and 50/50 (3-C) are sometimes lower and sometimes higher than the HMW homopolymer (3-D) below room temperature. The HMW homopolymer has a degree of crystallinity of 65% and that of both the blends is approximately 60%. The number and weight average molecular weights of the homopolymer are higher, but the polydispersity index is much lower than those of the blends. At and above room temperature, the storage moduli of these resins are consistent with the stress-strain results. Figures 7.19 and 7.20 show the effect of temperature on the loss and tan delta responses. For the temperature range studied, the samples exhibited the characteristic γ, β and α

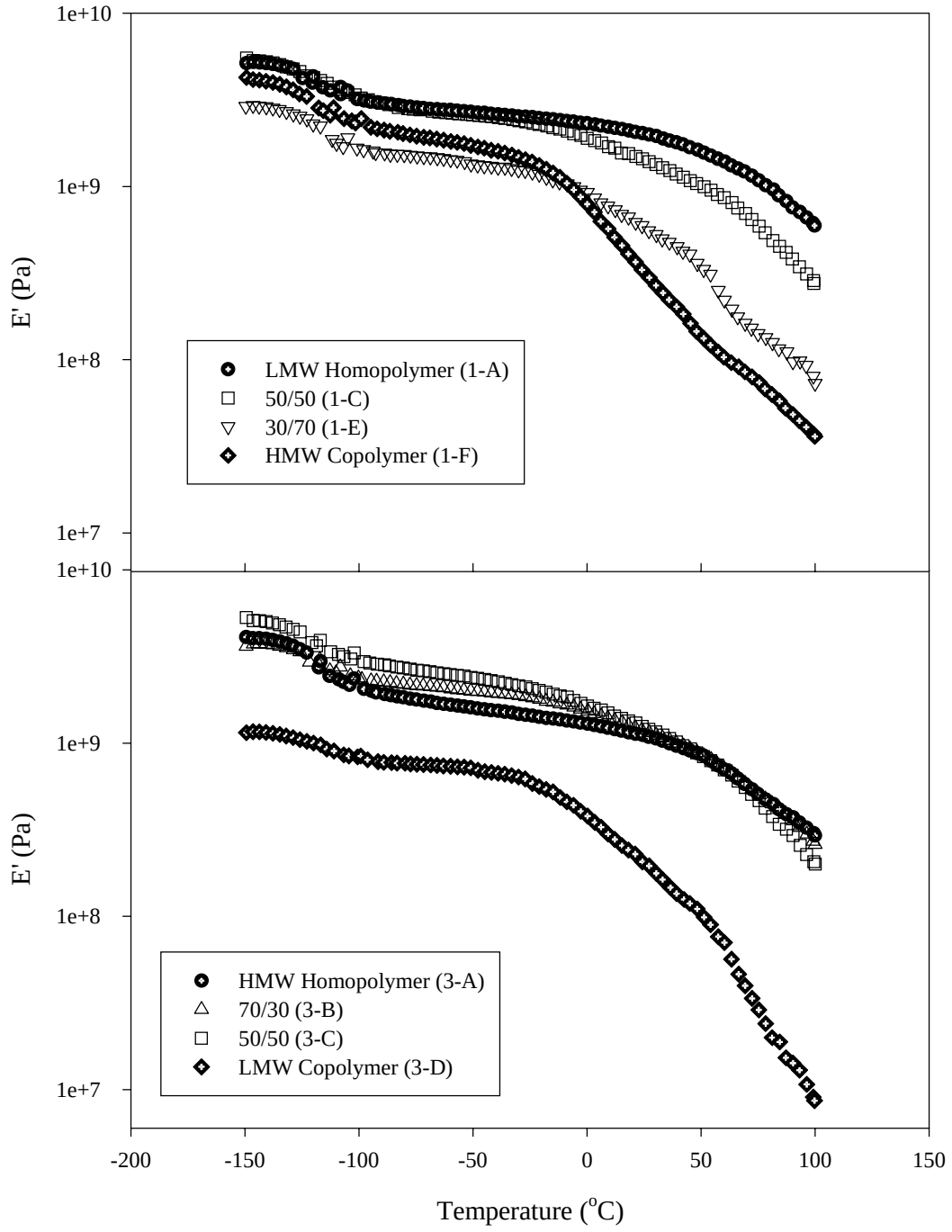

Figure 7.18 – Effect of Temperature on Storage Modulus of Reactor Blends

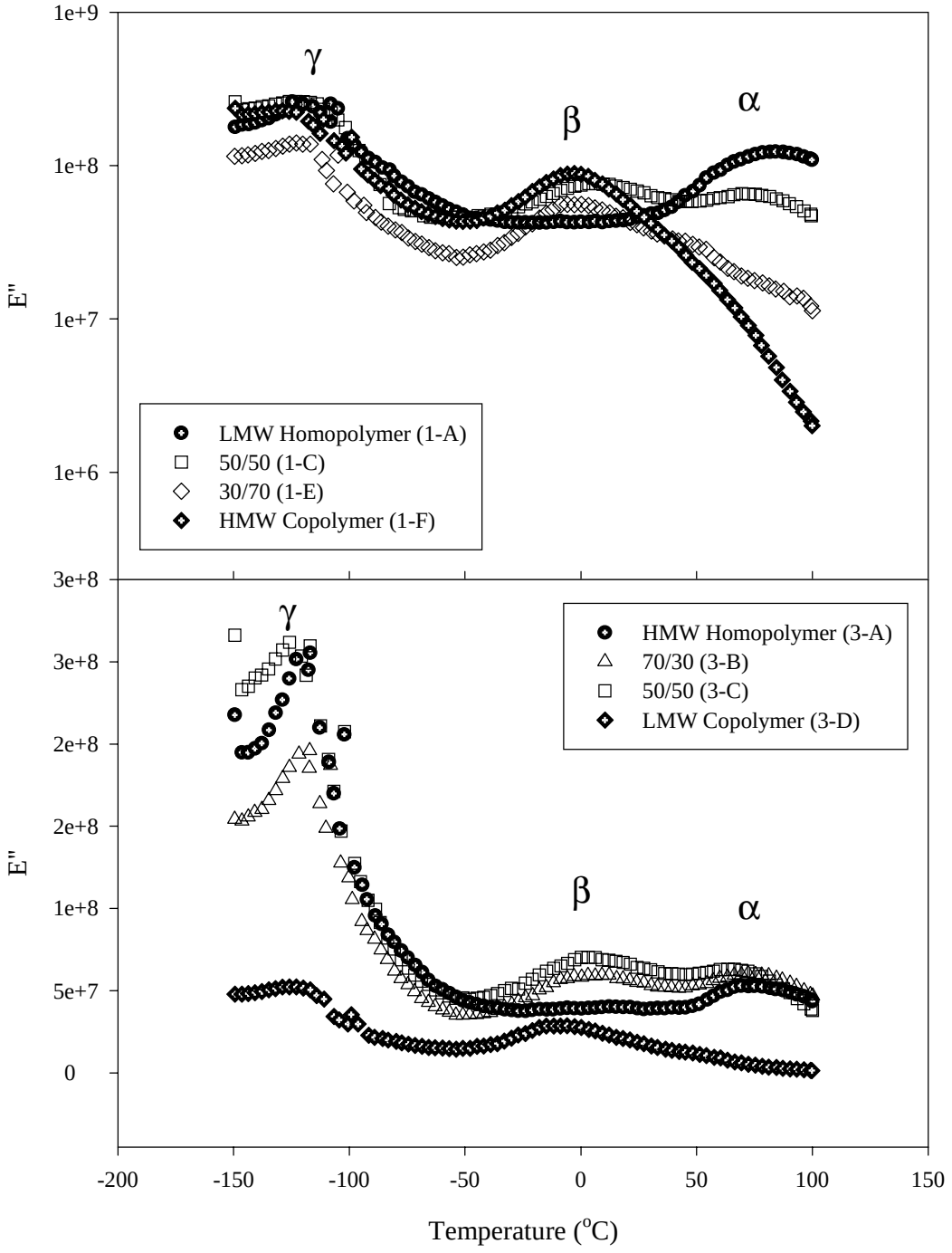

Figure 7.19 – Effect of Temperature on Loss Modulus of Reactor Blends

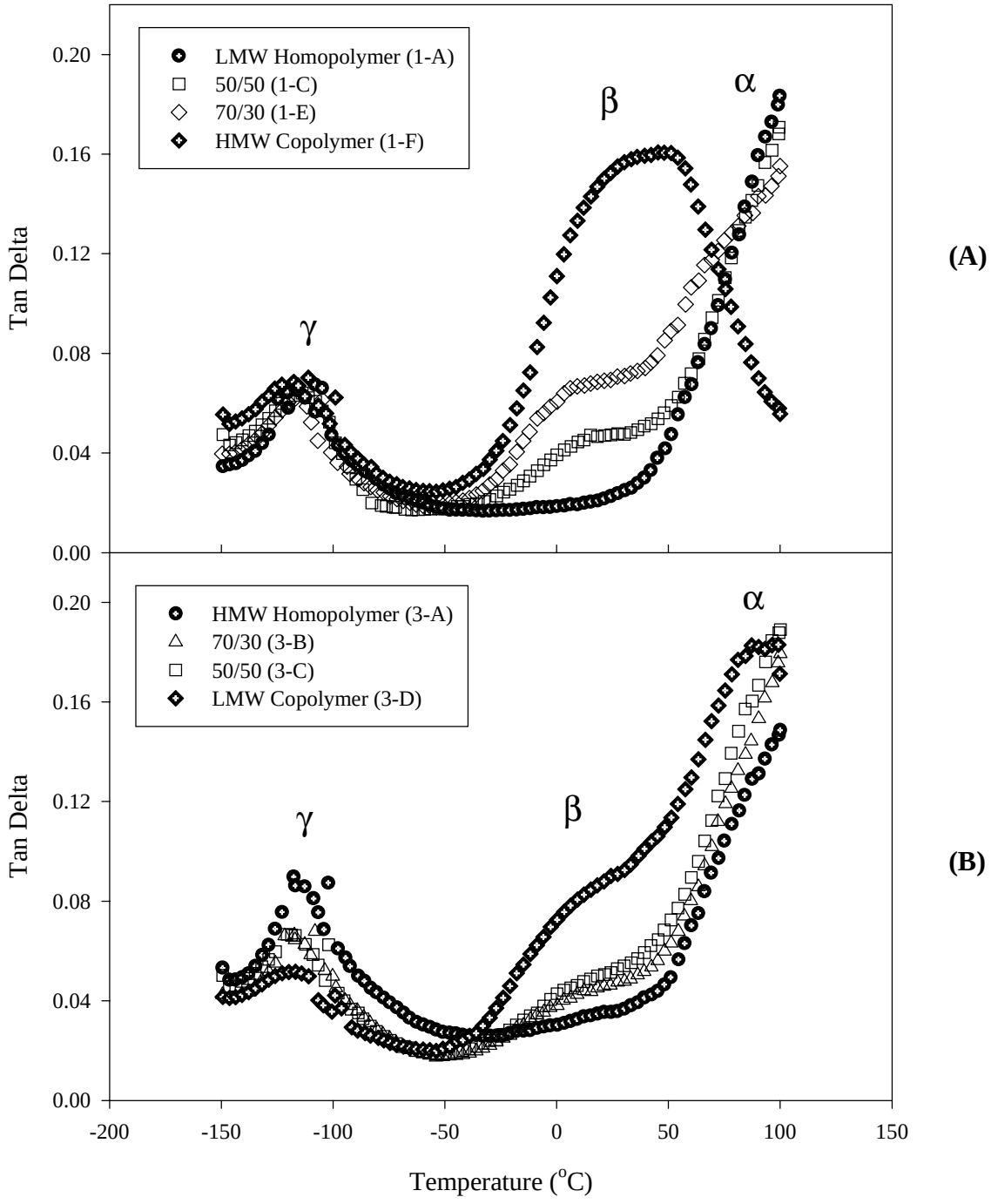

Figure 7.20 – Effect of Temperature on the Tan Delta of Reactor Blends

transitions for the loss modulus and tan delta. Although there is much debate on the existence and nature of these transitions, it is believed that they are linked to the motions of the amorphous and crystalline portions of the polyethylene chains (8,31-33). Examining the tan delta behaviour (Figure 7.20a and 7.20b), the γ transition is often associated with the rotation of four carbon chain segments (Schatzki-crankshaft mechanism) and was observed around -120°C (46). The β-transition, that is often associated with the glass transition temperature of the amorphous polymer is due to the motion of the branched segments of the chains and occurred between -25°C and room temperature (8,33). Lastly, the α transition was also observed above 50°C and this is generally attributed to the gradual motion of main chain units within the crystallites before the onset of melting. Comparing the tan delta response during γ-transition for both sets 1 and 3, the tan delta values reached a maximum value at approximately -125°C. For set 3, it appears that the magnitude of this transition depends on the fraction of the HMW homopolymer: the pure HMW homopolymer exhibits the largest transition and the pure LMW copolymer the smallest. However, for set 1, no discernible differences between the transition of the LMW homopolymer and HMW copolymer were observed. Therefore, it is difficult to pinpoint the influence of the microstructure on the nature of this transition. In the region of the β-transition, the effect of the fraction of copolymer is quite prominent. In both sets, the tan delta response increases with increasing copolymer fraction. Both homopolymers (samples 1-A and 3-A) show similar tan delta in this region. After the β-transition, the α-transition occurs as main chain motion between the crystallites begins. This α- transition occurs above room temperature and depends on the polymer composition. The earliest transition was displayed by the pure copolymers (samples 1-F and 3-D) and the latest by the pure homopolymers (samples 1-A and 3-A), as expected.

Frequency sweeps were performed at room temperature to verify the frequency dependence of the dynamic mechanical behaviour. For sets 1 and 2, the LMW homopolymer/HMW homopolymer blends, the stiffness (elastic modulus) of the polymer increases with increasing frequency (Figures 7.21a and 7.21b). This behaviour is typical since the polymer chains appear stiffer due to the reduced relaxation time. For these blends, the storage moduli decrease with increasing fraction of copolymer, thus reconfirming the observations from the tensile testing and other dynamic mechanical measurements.

Figure 7.21c shows the dependence of the storage modulus with frequency for the HMW homopolymer/LMW copolymer blends (set 3). As shown, the HMW homopolymer and the blends exhibit similar high moduli. These results are consistent in that the HMW homopolymer dominates the stiffness of the blends, as was also observed from other measurements discussed above.

Figures 7.22 and 7.23 examine the frequency dependency of the loss (E'') and tan delta (E''/E') responses for the resins. Both the loss and tan delta responses of the samples decrease with decreasing frequency of the test. The change in tan delta with frequency corresponds to a larger decrease in the viscous response (E'') as compared to the increase in elastic response (E'). As the frequency of the test increases, the relaxation of the chains become faster lessening the viscous response. The reduction in tan delta varied depending on the blend composition. At high frequencies around 1 Hz, the tan delta decreases with increasing fraction of HMW copolymer. The dampening behaviour becomes more separated at higher frequencies, showing that HMW copolymer dampens energy more efficiently then the LMW homopolymer. However, the dampening behaviour of the HMW copolymer depends on the frequency of the test. Above 2 Hz, the tan delta of the HMW copolymer reaches a level greater than the other samples. Given

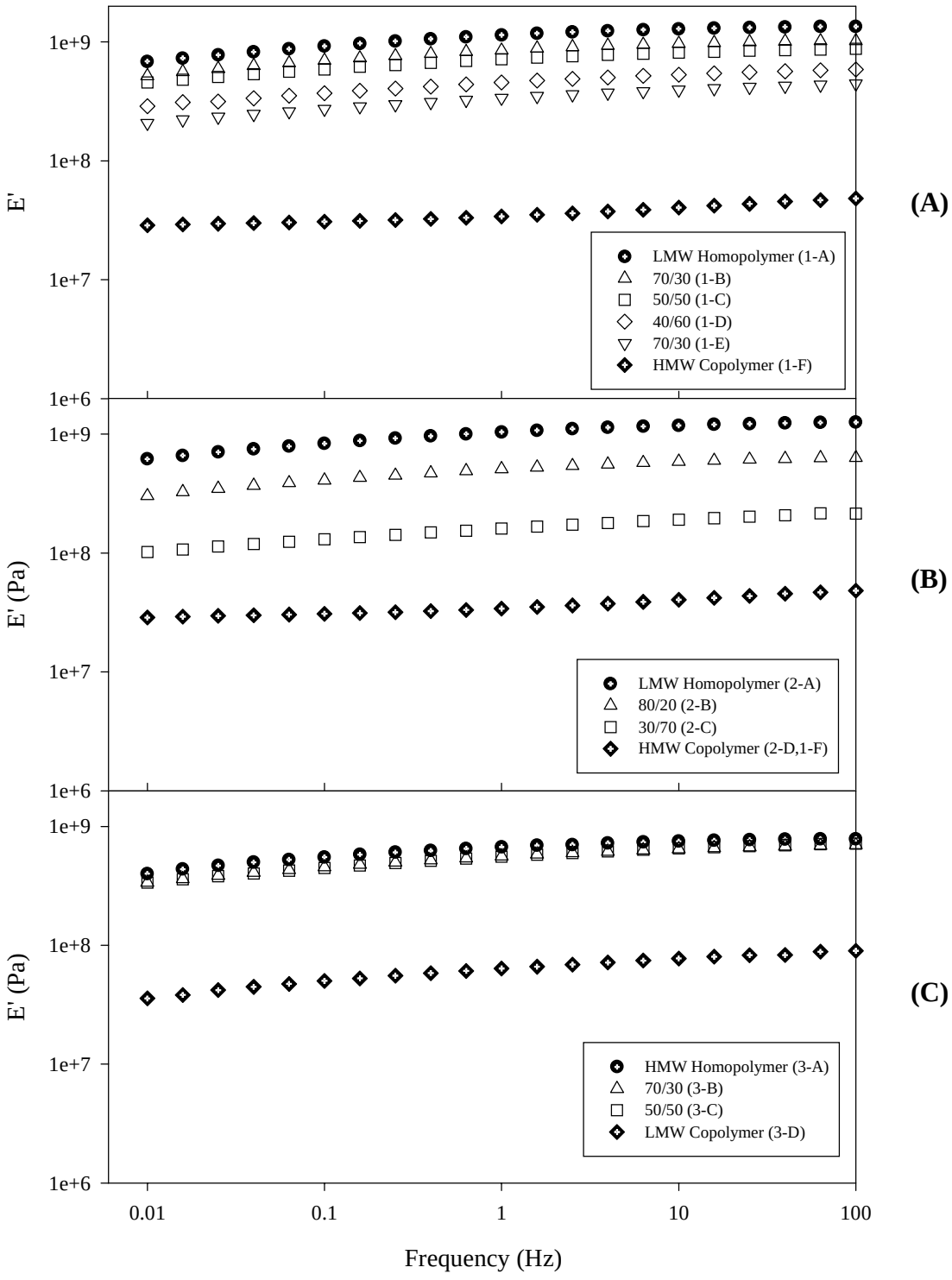

Figure 7.21 – Effect of Frequency on the Storage Modulus of Reactor Blends

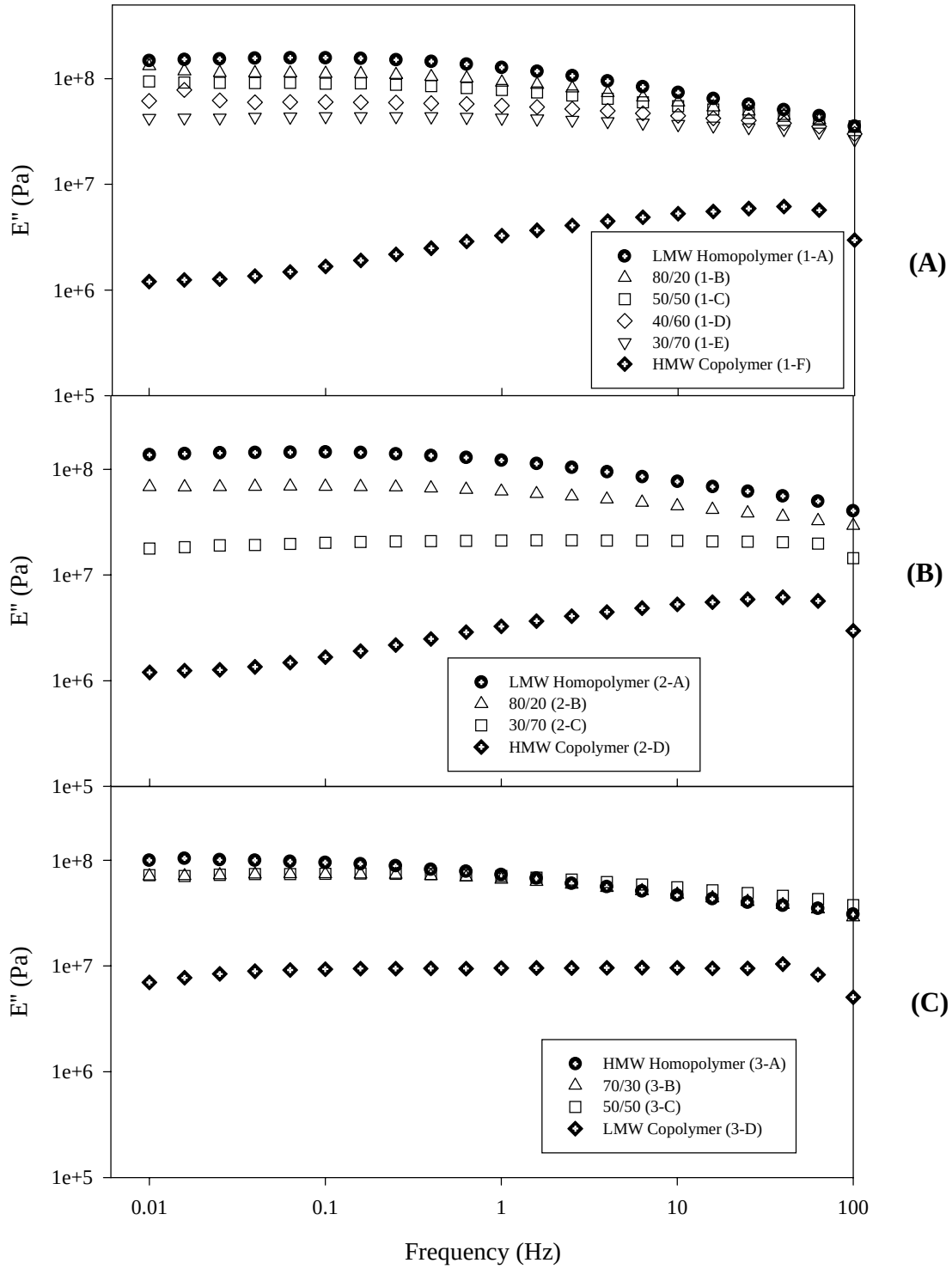

Figure 7.22 – Effect of Frequency on the Loss Modulus of Reactor Blends

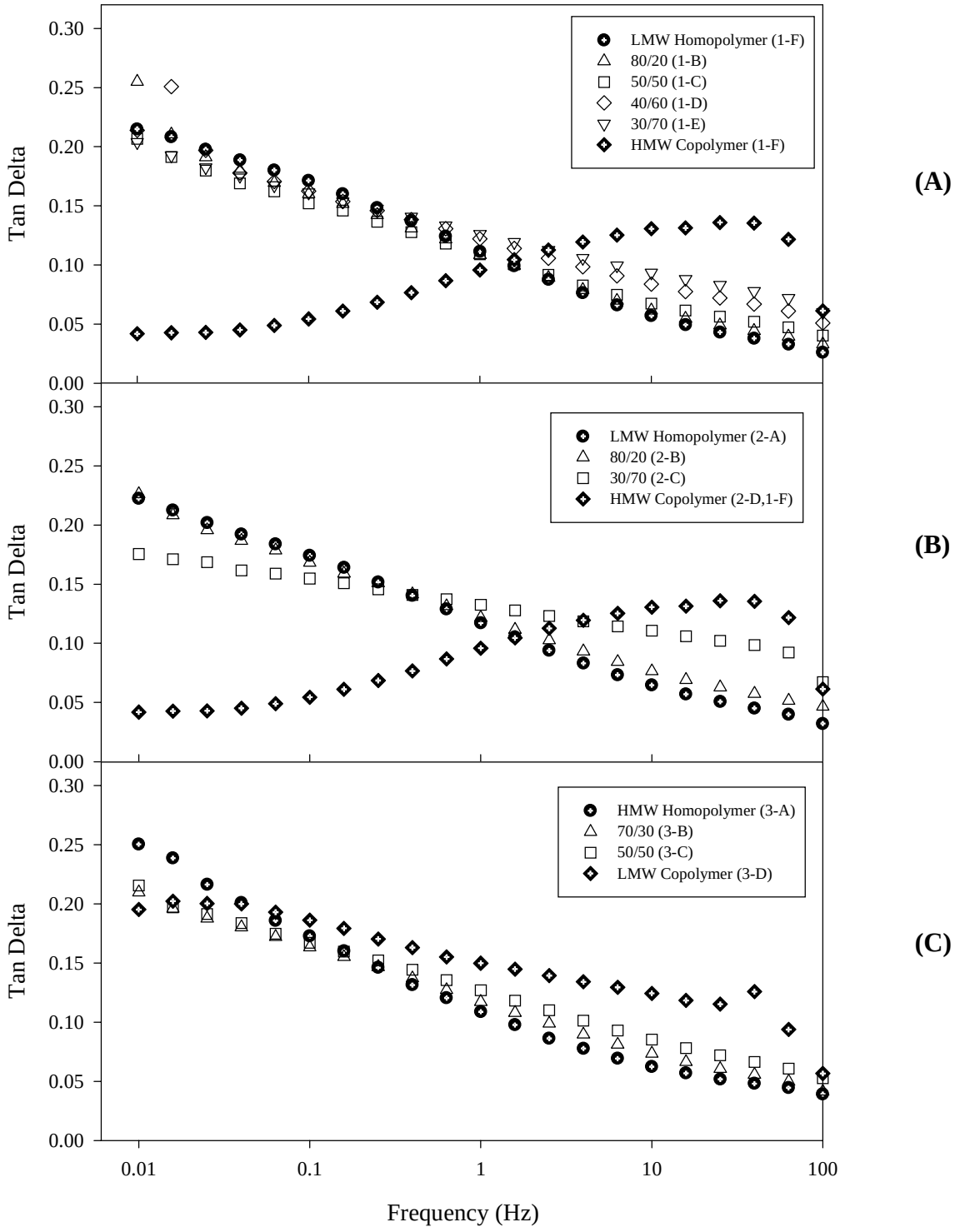

Figure 7.23 – Effect of Frequency on the Energy Dampening of Reactor Blends

the high amorphous content of this copolymer, the movement of the branched chains are hindered as they slowly recoil to absorb energy. The low frequency behaviour for this copolymer was unexpected. The tan delta response of this copolymer increases instead of decreasing with increasing frequency of the test. It is possible that the chain mobility is limited at low frequencies. The presence of these long molecules may hinder disentanglement and rearrangement of the polymer chains. In essence, the molecular weight dominates the chain movement in the low frequency range until a high enough frequency is reached to have the chains slip and dissipate energy. An alternative explanation for this behaviour relates to the α-transition of this copolymer. Figure 7.20a shows that the HMW copolymer (1-F) passes through the α-transition at around 50°C. This α-transition depicts the onset of main chain motion before the onset of melting. A frequency sweep can also exhibit transitions depending on the frequency range and temperature of the test. The dynamic responses from oscillatory measurements depend on the frequency and temperature of the test (31). As the frequency of the test increases, the polymer chains appear stiffer since they have less time to relax. Similarly, at low temperatures, the relaxation of the polymer chains is slowed, which also increases their stiffness. For these oscillatory measurements, the temperature sweep was carried out at 10 Hz. At room temperature, the frequency sweep was carried out between 0.01 to 100 Hz. At 0.01 Hz, the polymer chains have more time to relax than at 10 Hz. The value of tan delta at 0.01 Hz at room temperature is approximately 0.04. The corresponding value of 0.04 on the temperature sweep for the HMW copolymer occurs around 100°C. Between 100°C and 50°C, the tan delta increases and is similar to the increase observed in the frequency sweep. Due to this time-temperature equivalence, it is believed the copolymer material passes through the α-transition in

the frequency range tested. A comparison of the other resins shows the tan delta decreases with a decreasing temperature which is similar to that observed in the frequency sweep.

Figure 7.23c shows frequency dependence of the tan delta response for set 3. As expected, the tan delta decreases with increasing frequency of the test, due to the apparent increase in stiffness of the material. Again in the low frequency range, there is little difference in the energy dampening until 0.1 Hz where the tan delta responses of the samples diverge. Thus demonstrating the ability of the copolymer to absorb energy. However, it is noted that the stiffness of these materials was quite high. The dominance of the HMW material maintains the stiffness but the copolymer improves the energy dampening behaviour.

Given the complete characterization of the properties of the homopolymer/copolymer blends, it is possible to compare the viscoelastic properties according to the contribution of each component.

Figure 7.24 shows a summary of the elastic properties of the resins characterized in this study. Comparing the elastic response of the pure homopolymers (samples 1-A,2-A,3-A), it can be concluded that the stiffness of these polymers decreases with increasing molecular weight. This trend also holds for pure copolymers (samples 1-F, 3-D). Additionally, the stiffness of the reactor blends decreases with decreasing homopolymer/copolymer ratios. However, the degree of change in the stiffness depends on the molecular weight of the homopolymer matrix. For the HMW homopolymer/LMW copolymer blends, the elastic properties of these blends up to 50 % did not differ greatly and were dominated by the homopolymer. All of the changes in stiffness correspond well to the degree of crystallinity of the polymer. As shown in Figure 7.15, the tensile stresses at yield of these polymer blends depend mostly on their degree of crystallinity, regardless of the composition of the blend (LMW homopolymer/HMW copolymer or HMW

homopolymer/LMW copolymer). However, the achievable degree of crystallinity depends on the molecular weight and comonomer content of the polymer. The degree of crystallinity decreases with increasing molecular weight of the polymer due to the inability of the longer chains to fold and form crystal lamellae.

Figure 7.25 shows a summary of the energy dampening properties of the resins characterized in this study. Comparing the tan delta response for the pure homopolymers (1-A,2-A,3-A) and pure copolymers (1-F,3-D), the energy dampening does not strongly depend on the molecular weight of the polymer. The energy dampening did not change greatly, despite the large differences in molecular weight and degrees of crystallinity for these pure samples. Instead, the dampening behaviour depends on the comonomer content of the polymer. The tan delta increases with increasing fraction of copolymer in the blend. The presence of branched chains affects the loss behaviour to slow the relaxation of the polymer chains. Increasing the comonomer content of the polymer increases the number of entanglements, presumably within the amorphous regions. However, the dampening behaviour of the copolymer depends on the frequency of the test. Figure 7.23 had already illustrated how the dampening behaviour of a homopolymer/copolymer blend can benefit from the presence of the copolymer.

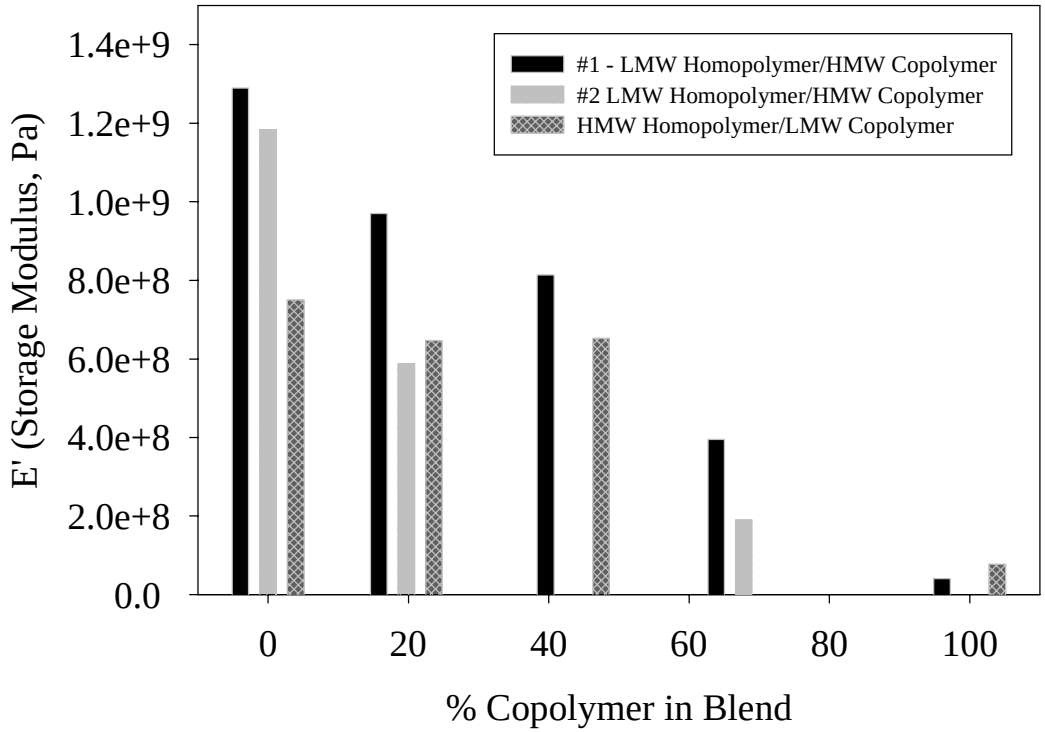

Figure 7.24 – Elastic Property Comparison of Reactor Blends at Room Temperature and a Testing Frequency of 10 Hz

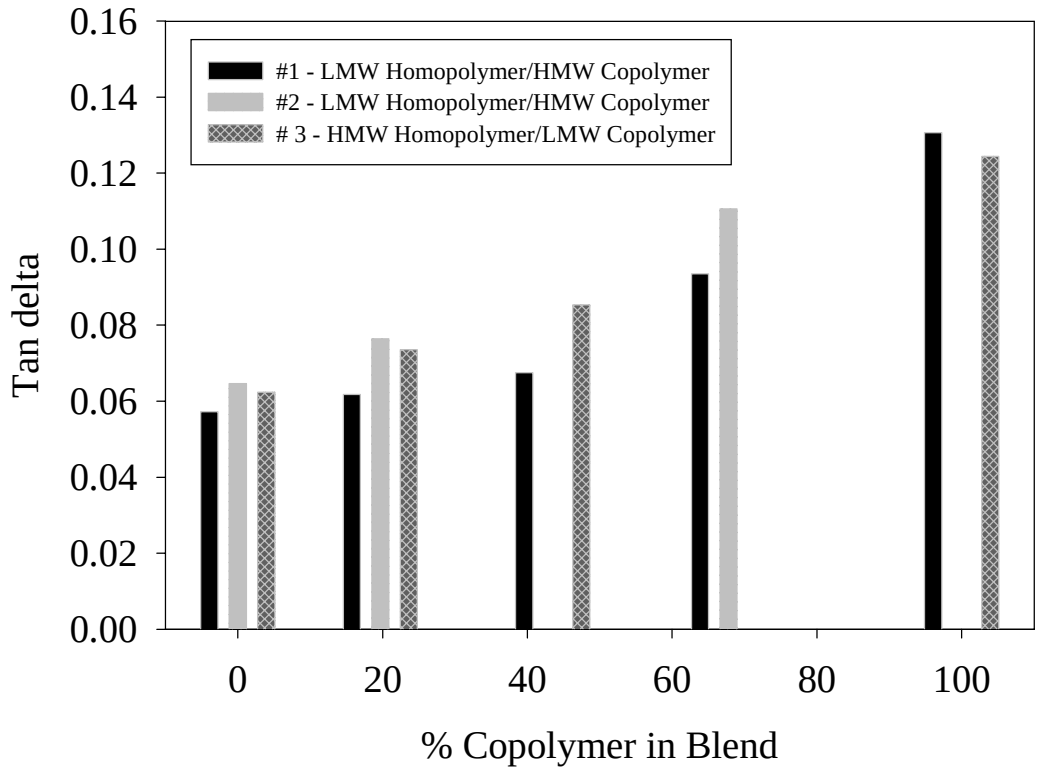

Figure 7.25 – Energy Dampening Comparison of Reactor Blends at a Room Temperature and a Testing Frequency of 10 Hz

7.3.2.3 Melt Rheology

Small amplitude oscillatory shear experiments were carried out to determine the rheological characteristics of the blends of LMW homopolymer/HMW copolymer and HMW homopolymer/LMW copolymer. From these experiments, insights were gained into the processing characteristics of these resins. Of interest was the frequency dependence of the storage and loss moduli as related to the shear viscosity and shear rate dependence. From this dependence, the shear thinning behaviour of the resins was compared. Other melt characteristics include zero-shear viscosity, melt elasticity and melt miscibility.

Using the relation developed by Cox-Merz, complex viscosity versus frequency can often be interchanged with the shear viscosity and shear rate (34). This relation complements shear viscosity data collected from other instruments such as a capillary rheometer or continuous flow experiments. Figure 7.26a compares the flow behaviour of the resins for set 1. Pure HMW copolymer exhibits greater viscosity (shear or complex) than LMW homopolymer. It is well known that both the molecular weight and molecular weight distribution govern the melt behaviour of linear polymers (34-37). The influence of the short chain branches on the rheological behaviour has been found to be minimal by several authors (36,45). For these blends, the viscosity of the polymer decreases with increasing fraction of LMW copolymer. Assuming that the HMW copolymer and LMW homopolymer fractions are melt-miscible, the viscosity should reflect the mixture of polymer chains. Shear thinning behaviour was observed for all the resins (decrease in viscosity with increasing frequency of the test). Shear thinning of the polymer occurs when the chains begin to disentangle and slip past each other. This slippage allows for orientation of the polymer in the flow direction, leading to a lowering of the viscosity. The rate at which shear thinning occurs for a polymer melt is of great importance during polymer

processing. To compare the shear thinning behaviour of these resins, a Power-law model was fitted to the data in the high shear rate region. The Power-law is one of the simplest rheological models that can be used to describe the dependence of the melt viscosity (η) at high shear rates ($\dot{\gamma}$) (34):

$$\eta = K\dot{\gamma}^{n-1} \quad (1)$$

where K is consistency index, η is the viscosity at a frequency of 1 s^{-1} and n is the rate index

This model generally predicts the viscosity behaviour well for many polymers in the high shear rate region, but lacks a parameter to estimate the zero shear viscosity. Even though the application to this blended homopolymer/copolymer system may not be entirely valid since they are based on observations from linear polymers, the estimates of the rate indices were used to compare the shear thinning behaviour. Table 7.4 lists the estimates for the viscosities at frequency of 1 s^{-1} and rate indices for the polymers, as well the standard errors of the predicted viscosities. The estimates for the viscosity at a frequency of 1 s^{-1} are from the consistency index of the Power-law. The rate index relates to the slope (n-1) of the viscosity versus shear rate curve. The uncertainty for the model was found to be acceptable for shear rates greater than 1 s^{-1}. As shown, the viscosities increase with increasing fraction of HMW copolymer, as expected. With the addition of the HMW copolymer, the slope increases indicating greater shear thinning**.** Estimates for the zero-shear viscosity of the polymers were obtained from the Cross model. The Cross model is a modification of the Power-law to include parameters to account for the Newtonian behaviour of the polymer in the low shear rate region. The form of the Cross model is shown below (35):

$$\eta = \eta_0[(1+\left|\lambda\dot{\gamma}\right|^m)]^{-1} \quad (2)$$

where η_0 is the zero shear viscosity, λ is the characteristic time and m is the rate index

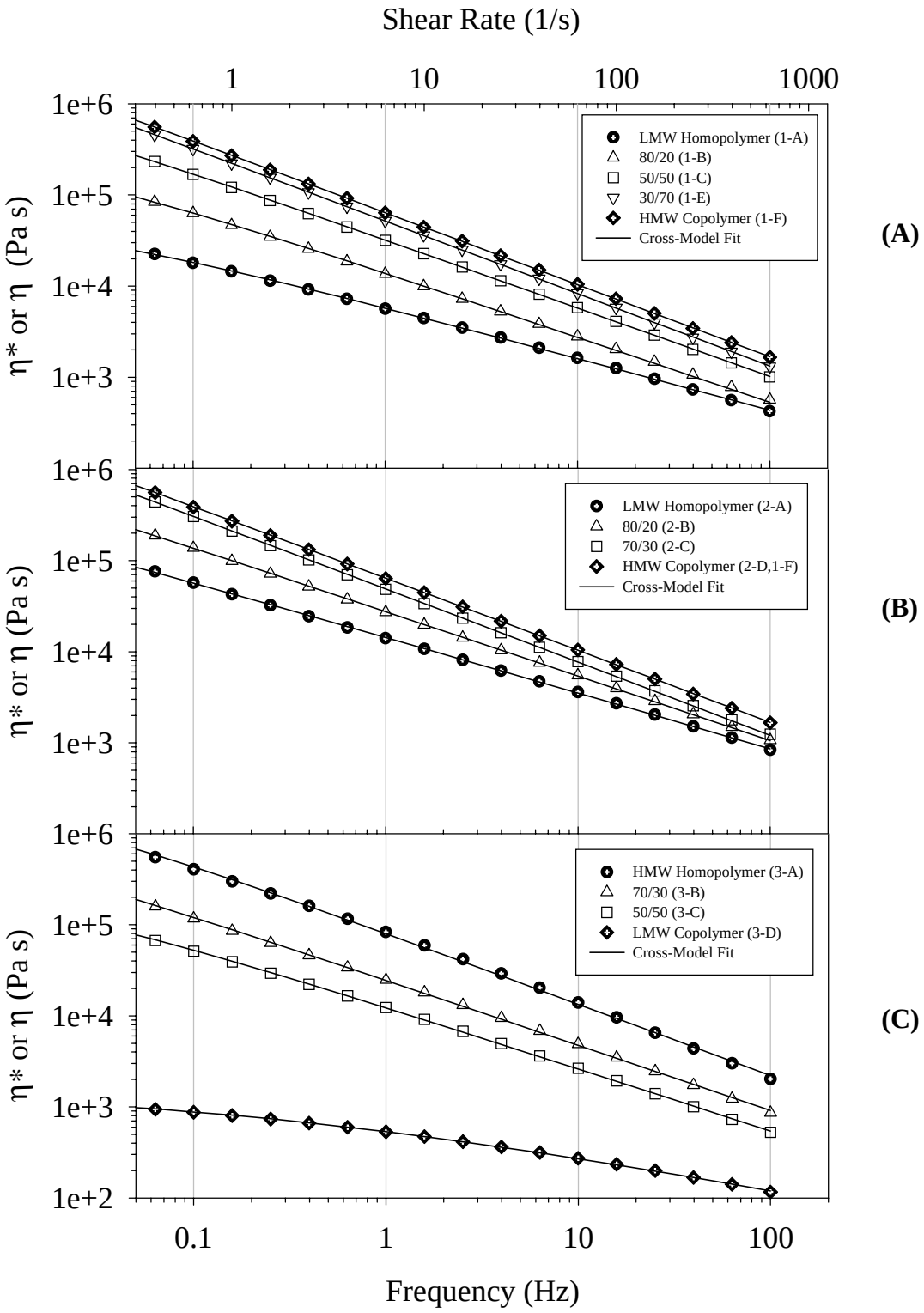

Figure 7.26 – Melt Viscosity (Complex) Comparison of Reactor Blends

Table 7.4 – Rheological Property Comparison of Reactor Blends

	Sample	K – viscosity[a] (Pa s)	Rate index[b] (n-1)	η_0[c] (Pa s)	Std. Error[d] Power-Law Model	Std. Error[d] Cross Model
Set #1	LMW Homopolymer (1-A)	17200	-0.573	87000	8.22	4.16
	80/20 (1-B)	48700	-0.691	4.62×10^5	2.39	3.44
	50/50 (1-C)	1.28×10^5	-0.750	2.38×10^6	6.54	1.51
	30/70 (1-E)	2.27×10^5	-0.799	2.24×10^7	5.06	1.03
	HMW Copolymer (1-F)	2.76×10^5	-0.793	2.17×10^7	4.89	0.817
Set #2	LMW Homopolymer (2-A)	45900	-0.619	1.37×10^6	9.13	3.88
	80/20 (2-B)	1.00×10^5	-0.704	3.80×10^6	4.82	2.40
	30/70 (2-C)	2.10×10^5	-0.797	1.30×10^7	2.87	1.11
	HMW Copolymer (2-D, 1-F)	2.76×10^5	-0.793	2.17×10^7	4.89	0.817
Set #3	HMW Homopolymer (3-A)	3.72×10^5	-0.804	3.36×10^6	27.4	4.89
	70/30 (3-B)	98000	-0.731	1.84×10^6	14.2	4.17
	50/50 (3-C)	45000	-0.689	3.83×10^5	10.3	3.38
	LMW Copolymer (3-D)	1240	-0.365	1540	8.59	7.95

[a] Viscosity estimate from Power-Law model (Eqn. 1) (Shear Rate Range: $1s^{-1}$ to $1000s^{-1}$)

[b] Rate index estimated from n from Power-Law model (Eqn. 2)

[c] Zero Shear viscosity estimated from Cross model

[d] $Std.Error = \frac{\left[\sum \frac{(y-\hat{y})^2}{n-2}\right]^{1/2}}{Range} x1000$ where y is measured viscosity, $\hat{y}$ is calculated viscosity, n is number of values and range is the difference between the maximum and minimum of measured values.

The parameter of interest for this study is the zero-shear viscosity. The characteristic time of the material is the reciprocal of the shear rate at which the zero-shear viscosity occurs. In the low shear rate region, the viscosity of a polymer generally approaches a constant value where the viscosity is independent of the shear rate. This behaviour was not readily apparent with the materials studied here. This is generally observed for industrial resins with broad molecular weight distributions or polymers with very high contents of long chain branching (LCB) (34). The molecular weight distributions of the resins studied were quite broad and no long chain branching was detected using GPC/viscometer. However, this does not confirm the absence of long chain branches, since others have reported that both ^{13}C NMR and GPC are not sensitive enough to detect very low amounts of LCBs (38-39). Since single-site catalysts have the ability to produce LCBs during polymerization, it is possible that low amounts of LCB are present to influence the rheological behaviour of these samples. From the viscosity plots, the viscosity increases with increasing fraction of HMW material. Qualitatively, it can be inferred that the zero-shear viscosities (η_0) of these polymers would follow a similar trend. At low shear rates, the entanglements of the polymer chains prevail and the value of the zero-shear viscosity reflects the microstructure of the material. It should be noted that many of these samples did not exhibit distinguishable plateaus; this leads to extrapolation errors in the estimates of the zero shear viscosities. Table 7.4 lists the estimates of the zero-shear viscosities and the standard error of the fitted model. Figures 7.26(a-c) show that the Cross-model fitting of the data points is quite good. As shown, the η_0 increase with increasing fraction of HMW copolymer. The LMW homopolymer (1-A) has the lowest η_0 and the sample 1-E and the HMW copolymer (1-F) have the highest values. Actually, sample 1-E exhibited the highest η_0 despite the presence of 30% LMW homopolymer. Comparing the molecular weight values, sample 1-E has a much broader

MWD and slightly higher weight average MW than the pure HMW homopolymer. It has been confirmed by Kazatchkov et al. that polyethylene with broad MWDs exhibit higher zero shear viscosities than narrow ones (40). The comparison of these values from the rheological data to the GPC data reinforce each other and demonstrate the sensitivity of the rheometer to the weight average molecular weight.

Figure 7.26b shows that the shear viscosity curves of set 2 have similar behaviour to the resins in set 1 (Figure 7.24a). The difference between set 1 and 2 is that the LMW homopolymer portion of set 2 was higher in molecular weight. For these rheological measurements, the influence of the molecular weight should be readily apparent. The viscosity of the blends decreases with increasing fraction of HMW copolymer. Examining the viscosity values estimated from the Power-law in Table 7.4, for roughly the same blend composition, the viscosity was approximately double of that of resins in set 1. Comparing the rate indices, the resins in set 2 shear-thin slightly faster than the resins in set 1. These observations are consistent with the trend in molecular weights measured by GPC. It appears that the degree of shear-thinning depends mostly on the weight average molecular weight. This seems reasonable since the weight average molecular weight reflects the presence of the longer chains that would contribute to the entanglements of the polymer. Comparing the η_0 values for the LMW homopolymer (2-A) and 80/20 (2-B), they are higher than those of set 1. However, the η_0 of the 30/70 (2-C) in set 2 was lower than that of the 30/70 (1-E) in set 1. The difference is readily explained by the competition of the narrower MWD and the high molecular weight; sample 2-C's MWD is narrower than 1-E's but is slightly higher in molecular weight.

Figure 7.26c compares the flow behaviour of set 3 that are composed of HMW homopolymer and LMW copolymer. The HMW homopolymer exhibited the highest viscosity.

The viscosities of the blend decrease with increasing fraction of HMW homopolymer. For the pure LMW copolymer, the viscosity values were much lower than the blends and pure HMW homopolymer. Table 7.4 lists the viscosity trend from the Power-Law estimates. As shown, the viscosity of the HMW homopolymer is almost 4 times that of the 50/50 blend (3-B). It seems that the addition of LMW copolymer has a detrimental effect in reducing the overall viscosity. The large separation in viscosities is reinforced by the separation in molecular weights measured from GPC. Examining the rate indices from the Power-Law estimates, a wide range of shear thinning behaviour also exists. The HMW homopolymer exhibited the highest rate of shear thinning followed by the blends (3-B and 3-C) and then finally the LMW copolymer with a much lower rate than the others. The zero-shear viscosity, η_0, decreases with increasing the fraction of LMW copolymer. Comparing the values of the η_0 for set 3 to those of sets 1 and 2 for similar compositions, it appears that the values are lower for set 3. Although a direct comparison cannot be made for the blends since the molecular weight distributions and compositions vary, it seems that the η_0 of the HMW copolymer (1-F) is higher than that of the HMW homopolymer (3-A). This seems a bit unusual since the molecular weight of the homopolymer is higher than that of the copolymer by 50 to 25 % for both the number and weight average molecular weights. The molecular weight distribution of these samples are both narrow. It appears that the presence of the short chain branches in the copolymer increases the η_0. Wood-Adams et al. have reported that the presence of ethyl branches does not influence the zero shear viscosity (36). It is possible that the zero shear viscosities of these copolymers are influenced by small amounts of LCB that may be present (although none was detected by GPC/viscometer). However, if LCBs are present, the level of long branching was not sufficient to increase the shear thinning behaviour as shown by the similar rate indices.

Figure 7.27 summarizes the molecular weight dependencies of the zero shear viscosity for the resins. It has been found by Raju et al.(41) and verified by others (34,36) that for linear polyethylene, the zero shear viscosity depends on the weight average molecular weight by a power of 3.4-3.6. For the three sets of blends, the exponents vary 2.6 to 5.5, demonstrating a severe deviation from the above relation. Given that these samples possess very broad MWDs, this lack of fit is probably due to the poor use of the weight average molecular weight to represent the distribution of chain lengths. The presence of any LCBs would also invalidate the use of this model, as demonstrated by Carella (42).

Figure 7.28 shows the shear viscosity and shear rate dependence of the blends, to examine the blending nature of the polymers and their contribution to the viscosities. For these composition plots, the log additivity rule does not hold for polymer blends that are melt immiscible. Partially miscible or immisicble blends that possess different phase morphologies exhibit positive deviations from linearity (27,43). Figures 7.28a and 7.28b show for sets 1 and 2 that the viscosity and the fraction of HMW copolymer in the blend follow the additivity rule quite well for the three shear rates shown. The viscosity ratio between the LMW homopolymer and HMW copolymer is around 16 for the values estimated at a frequency of 1 s^{-1} in Table 7.4. Despite this large difference, the polymers produced as a reactor blend are melt miscible. It is reasonable to observe this, since the samples were synthesized in a two-step polymerization process. On a microscale, the LMW copolymer and HMW homopolymer form layered particles with inner cores of copolymer and shells of homopolymer. Immiscibility might be observed if the samples were obtained from melt blending. Utracki suggests that a viscosity ratio of 1:3 would allow for fine dispersion in a melt-blending process (9).

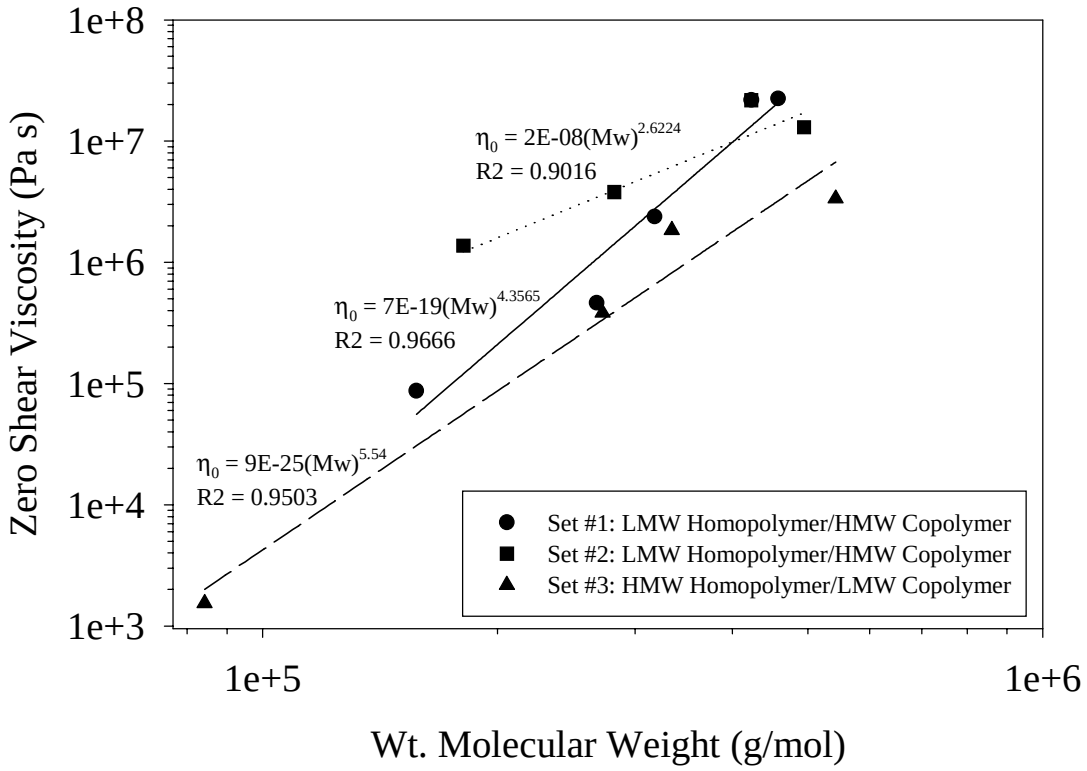

Figure 7.27 – Molecular Weight Dependence of Zero-Shear Viscosity of Reactor Blends

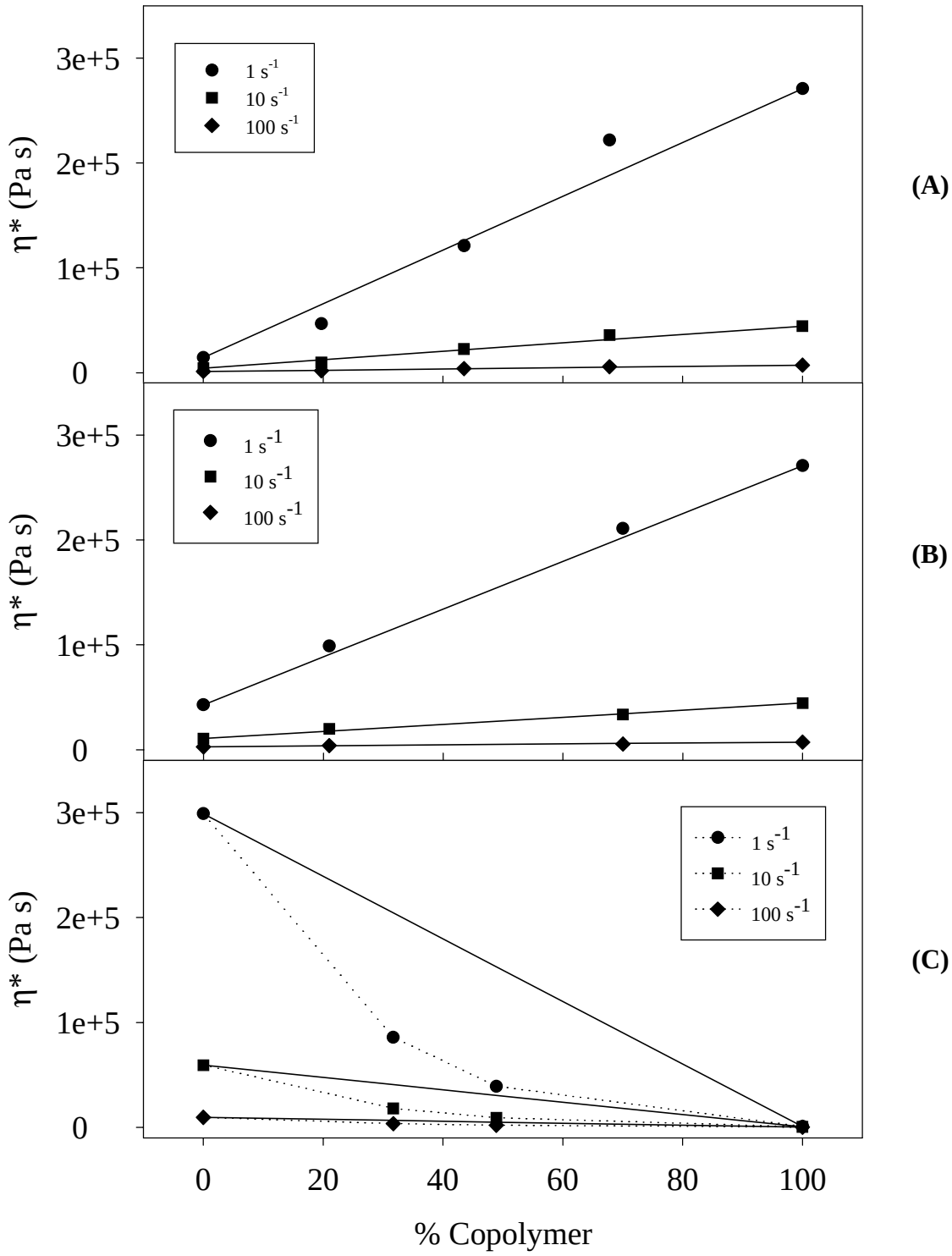

Figure 7.28 – Log Additivity of Viscosity and Blend Composition

Figure 7.28c shows a mixing trend for the resins in set 3. For these blends, large negative deviations occur for the viscosity and composition. The HMW homopolymer has much higher viscosity. The viscosity ratio between the HMW homopolymer and LMW copolymer for the viscosities shown at a frequency of 1 s^{-1} is 300. This extremely high viscosity ratio leads to miscibility problems despite being reactor blended. However, the viscosity trends for set 3 suggests that the addition of LMW copolymer can greatly reduce the viscosity of the HMW homopolymer. This reduction in viscosity was not as prominent for the addition of LMW homopolymer to HMW copolymer as in sets 1 and 2.

Comparison of the storage (elastic) modulus with frequency can also provide more insight in to the polymer microstructure. The behaviour of the elastic modulus with frequency is analogous to the relaxation modulus of the polymer. A relaxation spectrum that depicts the chains relaxation modulus with time can sometimes be used to distinguish polymers with different molecular weight and molecular weight distributions (34). Figures 7.29 (a-c) show that the elastic modulus increases with increasing frequency of the test. This behaviour is similar to that of polymer in the solid-state: at low frequencies the chains can rearrange amongst themselves but, as the frequency increases, they have less time to relax and become glassy. For these resins, the melt elasticity decreases with increasing proportion of HMW material. It seems that the molecular weight of the polymer dominates the melt properties and that the chemical composition has little or no influence. The separation of the curves allow for an approximate view of the range of molecular weights. However, it is difficult to distinguish the broadness of the molecular weight distribution since the molecular weights cover a wide range.

G'' versus G' plots were compared to determine the miscibility of the blends. Plots comparing the viscous (G'') and the elastic (G') behaviour are often used to detect phase

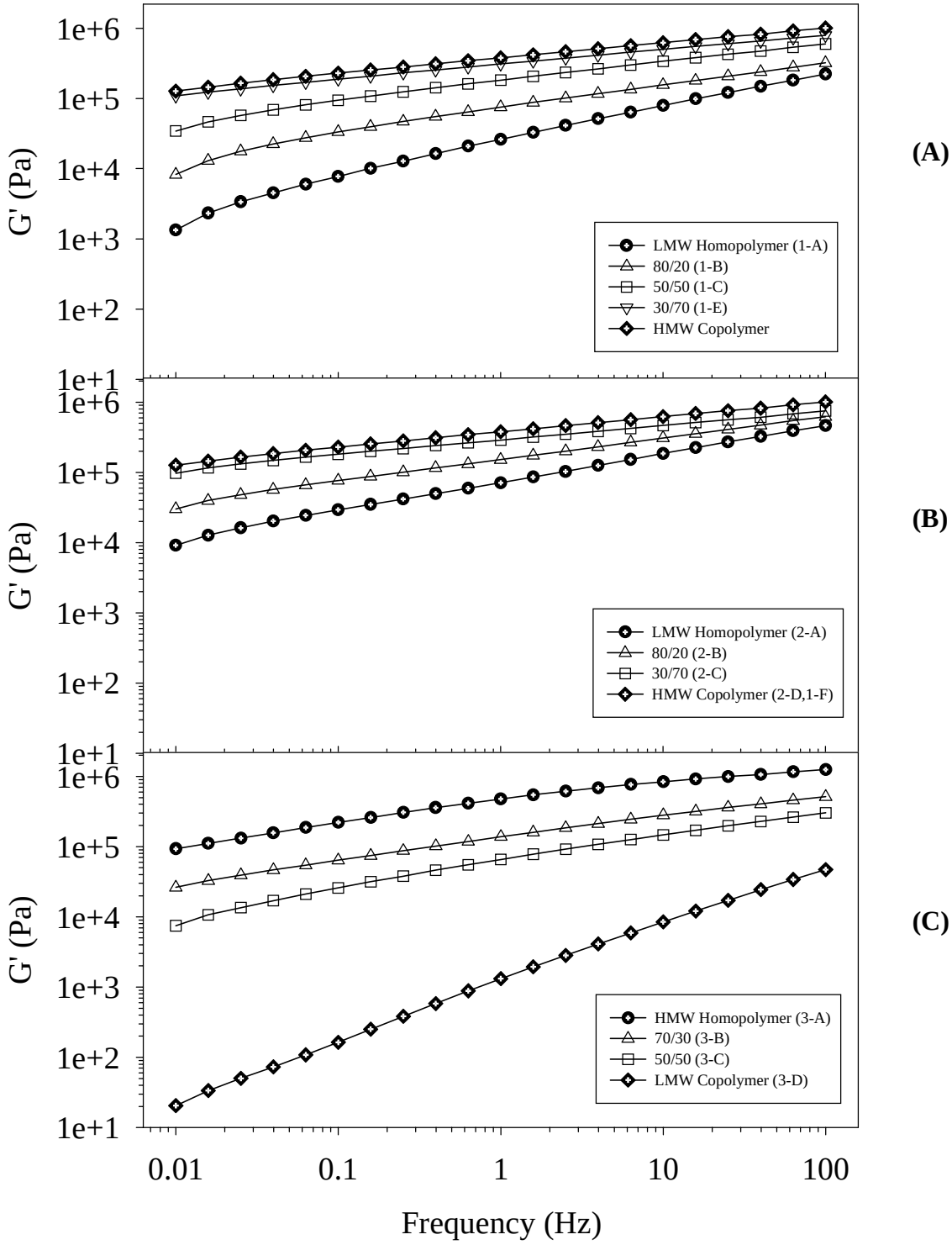

Figure 7.29 – Melt Elasticity Comparison of Reactor Blends

separation due to differences in structural units (39,44). Figures 7.30 (a-c) shows the G'' versus G' plots for sets 1, 2 and 3. As shown, the viscous and elastic response depends on the composition of the blends. For the LMW homopolymer/HMW copolymer blends of sets 1 and 2, the LMW homopolymer exhibits the lowest viscous and elastic modulus over the largest range. Both the elastic and loss properties increase with increasing fraction of HMW copolymer. It also appears that the range of elasticity and loss narrows. For the most part, the G'' versus G' of these resins exhibits single-phase behaviour since the plots were generally linear, and the regions of the blends properties overlap that of the homopolymer and copolymer. Thus, the LMW copolymer and HMW homopolymer are melt miscible for these samples.

For set 3, Figure 7.30c shows similar behaviour for the HMW homopolymer and LMW copolymer. Again, the LMW material (copolymer) exhibits the lowest G' and G''. The elasticity and loss increases with increasing fraction of HMW homopolymer. However, for these blends, the HMW homopolymer tends to dominate the elastic and loss behaviour. A large separation exists between the properties of the LMW copolymer and that of the HMW homopolymer and the associated blends. Given the viscosity evidence that the blends of HMW homopolymer and LMW copolymer shown in Figure 7.28c in set 3 are slightly immiscible, it is possible that this large separation in G'' and G' reinforces this finding.

Figure 7.31 compares the tan delta behaviour of the resins in the melt. The tan delta (G''/ G') quantifies the balance of the loss and elastic properties. A high value of tan delta indicates that the polymer material has poor recovery characteristics since the chains relax slowly after being stressed. From a processing point of view, this value can indicate how well a material will recover after being deformed. A material that withholds stress histories may lead to melt flow instabilities such as melt fracture. Figure 7.31a and 7.31b compares the tan delta responses for

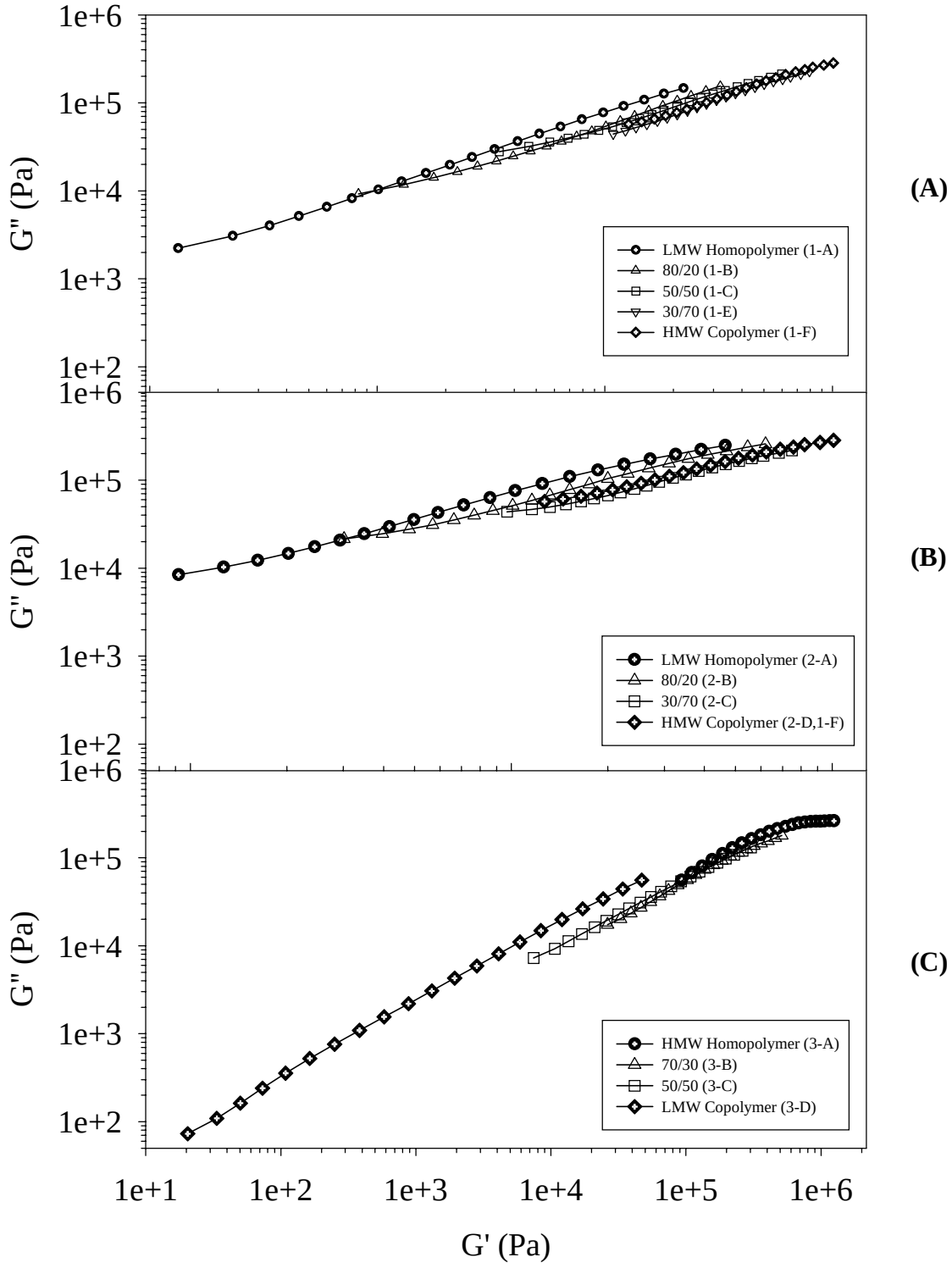

Figure 7.30 – G'' versus G' Plot Comparison

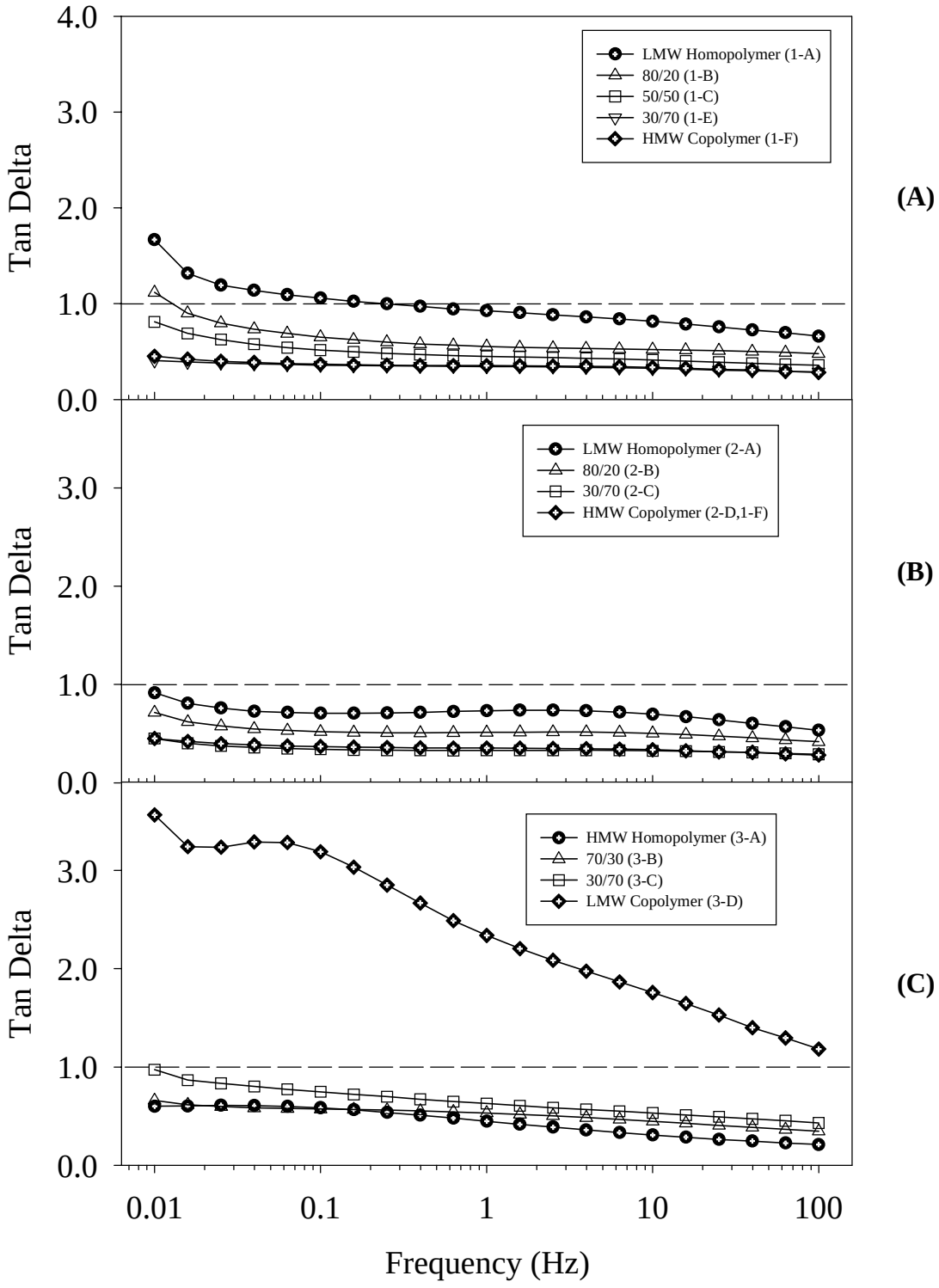

Figure 7.31 – Flow Recovery Comparison of Reactor Blends

sets 1 and 2. As the fraction of HMW copolymer increases, the tan delta decreases. The flow recovery of the blends increases with the addition of HMW material. The flow recovery also increases with increasing frequency. Comparing samples 30/70 (1-E), 30/70 (2-C) and the pure HMW copolymer (1-F), their tan delta values are quite similar to the HMW copolymer. For these samples, the MWDs are much broader than the narrow HMW copolymer. Despite the differences in the MWDs, the longer chains dominate the flow recovery as represented by the weight average molecular weight. Figure 31c shows the tan delta response for set 3. As shown, the tan delta range was quite separated between the LMW copolymer (3-D) and the others. The LMW copolymer showed the lowest flow recovery.

Overall, it has been demonstrated that the rheological properties of these reactor blends reflect the nature of the individual components. From the comparison of the shear viscosities and viscoelastic properties G' and G'', it was confirmed that both the molecular weight and MWD govern the melt behaviour. It was also confirmed that the reactor blends of LMW homopolymer and HMW copolymer were melt miscible. However, some immiscibility was detected with the large viscosity differences between HMW homopolymer and LMW copolymer.

7.4 Conclusions

Reactor blends of polyethylene and poly(ethylene-*co*-1-octene) with bimodal structural distributions were successfully produced via a two-step polymerization process. The microstructural characterization of these blends indicates that both the molecular weight and comonomer distributions are consistent with the method of polymerization. The physical properties of the blends containing LMW homopolymer/HMW copolymer and HMW homopolymer/LMW copolymer are consistent with the nature of the individual components. For the tensile properties, the stiffness decreases with increasing fraction of the copolymer, regardless of the molecular weight of the homopolymer fraction. It was confirmed that the degree of crystallinity governs the stiffness of a polymer. However, the energy dampening properties of the polymers do benefit from the presence of the copolymer. Depending on the desired application, a balance of stiffness and toughness can be obtained by altering the composition of the blends. For some blends, the presence of HMW homopolymer can dominate the tensile properties showing little variation in the stiffness with the increased addition of copolymer. For these blends, some evidence was found that indicate that some of the components do not cocrystallize efficiently. Nonuniform crystal structures sometimes leads to properties that deviate from linearity.

From the melt rheological studies, it was observed that the viscosity of HMW polymers was reduced with the addition of LMW material. The shear flow characteristics of these polymers in the typical processing range mostly depend on the molecular weight and MWD of the polymer and are independent of the short chain branch content. For the polymers produced with this two-step polymerization process, the LMW homopolymer and HMW copolymer blends were melt miscible. However, there was some evidence that the HMW homopolymer/LMW

copolymer blends may be melt immiscible, presumably due to the extreme viscosity differences of the components.

Overall it has been demonstrated that reactor blends of LMW homopolymer/HMW copolymer and HMW homopolymer/LMW copolymer can exhibit a wide range of physical properties. Depending on the desired application, the viscoelastic properties of the blends, both in the solid-state and melt state can be tailored by controlling the individual components that are present.

7.5 References

1. Elvers, B.; Hawkins, S.; Schulz, G.; Ullman's Encyclopedia of Industrial Chemistry 5th Ed.,VCH Publishers, New York, A21, pp 487-576. (1992)
2. Foster, G.N.; Wasserman, S.H.; Metallocene and Gas Phase Polymerization: Molecular Engineering Pathway for Advantaged Polyethylene Products, Metcon '97, Houston, Tx
3. Hamielec, A.E.; Soares, J.B.P.; *Prog. Polym. Sci.*, 21, 651-706 (1996).
4. Avela, A.; Karling, R.; Takarhu, J.; *Dcheme Monographs*, 134, 3-23 (1998).
5. Martin, J.R.; Johnson, J.F.; Cooper, A.R.; *J. Macromol. Sci.-Revs., Macromol. Chem.*, C8(1), 57-199 (1972).
6. Nunes, R.W.; Martin, J.R.; Johnson, J.F.; *Polym. Eng. Sci*., 222, 205-228 (1982).
7. Kale, L.; Plumley, T.; Patel, R. ; Redwine, O.; Jain, P.; *J. Plast. Film and Sheeting*, 12, 27-40 (1995).
8. Bensason, S.; Minick, J.; Moet, A.; Chum, S.; Hiltner, A.; Baer, E.; *J. Polym. Sci.: Part B: Polym. Phys*., 34, 1301-1315 (1996).
9. Utracki, L.A.; Polymer Alloys and Blends, Thermodynamics and Rheology, Hanser Publishers, New York, pp. 1-27 (1990)
10. Berthold, J.; Bohm, L.L; Enderle, H.-F.; Gobel, P.; Luker, H.; Lecht, R.;Schulte, U.; *Plastics, Rubber and Composites Processing and Applications*, 25, 368-372 (1996).
11. Scheirs, J.; Bohm, L.; Boot, J.; Leevers, P.S.; *Trends in Polymer Science*, 4, 408-415 (1996).
12. Bohm, L.L.; Berthold, J.; Enderle, H.-F., Fleissner, M.; Metalorganic Catalysts for Synthesis and Polymerization : Recent Results by Ziegler-Natta and Metallocene Investigations, Springer, New York, pp. 3-13 (1999).
13. Manders, P.W.; *Modern Plastics*, B:3-5, (1994).

14. H. Brintzinger, D. Fischer, R. Mulhaupt, B. Rieger, R.M. Waymouth, *Angew. Chem. Int. Ed. Engl.*, 34, 1143-1170 (1995)
15. Matsushita, F.; Kishimoto, Y.; Pierce, J.K.; New High Density Polyethylenes from Slurry Insite* Technology, Metallocenes Europe ’98, pp. 201-220.
16. Sinclair, K.B.; The New Generation Polyethylene Technologies: A Comparison, Polyolefins XI, Society of Plastics Engineers, Houston, Texas, Feb. 21-24, 1999.
17. K.J. Chu, J.B.P. Soares, A. Penlidis, *J. Polym. Sci., Part A, Polym. Chem*, 38, 462-468 (2000)
18. K.J. Chu, C. Li Pi Shan, J.B.P. Soares,A. Penlidis, *Macromol. Chem. Phys.*, 200, 2372-2376 (1999)
19. Soares, J.B.P.; Monrabal, B.; Nieto, J.; Blanco, J.; *Macromol. Chem. Phys*., 199, 1917-1927 (1998).
20. Xu, X., Xu, J, Feng, K., Chen, W.; *J. Appl. Polym. Sci.*, 77, 1709-1715 (2000).
21. Chien, J.C.W.; Nozaki, T.; *J. Polym. Sci., Part A: Polym. Chem*., 31, 227 (1993).
22. Herfert, N.; Montag, P.; Fink, G.; *Makromol. Chem*. 194, 3167 (1993).
23. Jungling, S.; Koltzenrug, S.; Mulhaupt, R.*; J. Polym. Sci., A: Polym. Chem.*; 35, 1-8 (1997).
24. Pryzybyla, C.; Tesche, B.; Fink, G. ; *Macromol. Rapid. Commun.*, 20, 328-332 (1999).
25. Soares, J.B.P.; Kim, J.D.; *J. Polym. Sci.; Part A: Polym. Chem.*, 38, 1408-1416 (2000).
26. Blom, R. ;Dahl, I.M. ; *Macromol. Chem. Phys.*, 200, 442-449 (1999).
27. Cho, K.; Lee, B.H.; Hwang, K.M.; Lee, H.; Choe, S.; *Polym. Eng. Sci.*, 38, 12, 1969-1975 (1998)
28. Simanke, A.G. , Galland, G.B. , Neto, R.B. , Quijada, R. , Mauler, R.S.; *J. Appl. Polym. Sci.*, 74, 1194-1200 (1999).

29. Grahm, J.T. , Alamo, R.G., Mandelkern, L.; *J. Polym. Sci. Part B: Polym. Phys.*, 35, 213-223 (1997).

30. Brooks, N.W.J., Duckett, R.A., Ward, I.M;. *Polymer* , 40, 7367-7372 (1999).

31. Menard, K.P. Dynamic Mechanical Analysis – A Practical Introduction New York, CRC Press, 1999, pp. 151-162.

32. Nitta, K.H., Tanaka, A., *Polymer*, 42, 1219-1226 (2000).

33. Simanke, A.G., Galland, G.B., Freitas, L., da Jornada, J.A.H., Quijada, R., Mauler, R.S. *Polymer*, 40, 5489-5495 (1999).

34. Dealy, M.; Wissbrun, K.F.; Melt Rheology and Its Role in Plastics Processing: Theory and Applications, Van Nostrand Reinhold, New York, 1990 Chapt. 4, 10.

35. Mavridis, H.; Shroff, R.*; J. Appl. Polym. Sci.*, 49, 299-318 (1993).

36. Wood-Adams, P.M.;Dealy, J.M.;deGroot, A.W.; Redwine, O.D.; *Macromolecules*, 33, 7489-7499 (2000).

37. Kzatchkov, I.B.; Bohnet, N.;Goyal, S.K.; Hazikiriakos, S.G.; *Polym. Eng. Sci.*, 39, 804-815 (1999).

38. Vega, J.F.; Santamaria, A.; Munoz-Escalona, A. ;Lafuente, P. ; *Macromolecules*, 31, 3639-3647 (1998).

39. Vega, J.F. ; Fernandez, M. ; Santamaria, A. ; Munoz-Escalona, A. ; Lafuente, P. ; *Macromol. Chem. Phys.*, 200, 2257-2268 (1999).

40. Kazatchkov, I.B. ; Bohnet, N. ; Goyal, S.K.; Hatzikiriakos, S.G.; *Polym. Eng. Sci.*, 39, 804-815 (1999).

41. Raju, V.R.; Smith, G.C.; Marin, G.; Knox, J.R.; Graessley, W.W.; *J. Polym. Sci, Polym. Phys. Ed*., 17, 1183-1195 (1979).

42. Carella, J.M.; *Macromolecules*, 29, 8280-8281 (1996).

43. Xanthos, M.; Tan, V.; Ponnusamy, A.; *Polym. Eng. Sci.*, 37, 1102-1112 (1997).

44. Kwag, H.; Rana, D.; Cho, W.; Rhee, J.; Woo, T.; Lee, B.H.; Choe, S.; *Polym. Eng. Sci.*, 40, 1672-1681 (2000).

45. Kim, Y.S.;Chung, C.I.; Lai, S.Y.; Hyun, K.S.;*J. Appl. Polym. Sci.*, 59, 125-137 (1996).

46. Sperling, L.H.; Introduction to Physical Polymer Science, John Wiley & Sons., Inc., p. 328 (1992).

Chapter 8

Contributions to Research

8.0 Contributions to Research

The concept of controlling the short chain branching distribution of ethylene/α-olefin copolymers with a heterogeneous metallocene catalyst and different alkyaluminums was introduced and systematically investigated for the first time. With the use of a single metallocene catalyst and a single reactor, it was possible to tailor the crystalline distribution of ethylene copolymers. This process is inherently simpler than the use of a combined metallocene catalyst or tandem reactor technology.

Given the unique ability of in-situ supported metallocenes to produce ethylene copolymers with bimodal short chain branching distributions, a structure-property study was initiated. By isolating the effect of molecular weight, samples were synthesized and tested to examine the tensile properties of resins with varying crystalline distributions. It was found that resins with a mixture of high crystalline and low crystalline material exhibited an overall balance of tensile properties, thus demonstrating how these catalysts can be used to tailor the physical properties of the copolymers.

The experimental design study to investigate the effect of polymerization conditions on the catalyst activity and microstructure showed that in-situ supported Me_2Si(2-Me-4,5 BenzInd)$_2$ZrCl2 is not a typical single-site catalyst. The responses to important polymerization conditions were not easily predicted from typical polymerization mechanism steps, and several two-factor interactions play important roles in determining polymer MWD and SCBD, as well as catalyst activity. Nonetheless, the experimental approach used was very important to detect and quantify the complex nature of this particular system and can be readily extended to other supported metallocene systems. The ability to produce polyolefins with multimodal

microstructural distributions in a single metallocene/single reactor set-up is very attractive and could in principle be used to produce polyolefin resins with advanced molecular architecture.

Lastly, a structure-property study was carried out demonstrating the effect of molecular weight and short chain branching distribution on the physical properties of polyolefins. Using a single reactor and a single metallocene catalyst, reactor blends of high and low molecular weight polymer with varying comonomer content were produced and tested. Overall, polyethylene copolymers with bimodal structural distributions exhibit a wide range of physical properties. Depending on the desired application, the microstructure of the polymer can be tailored to achieve a balance of physical properties, such as stiffness and toughness. For the resins in this study, it was observed that the stiffness of the polymers depended on the degree of crystallinity regardless of the underlying composition. The properties of polyethylene blends do benefit from the addition of the copolymer to increase its energy dampening properties. However, the energy dampening behaviour of the HMW copolymer studied showed that the testing conditions drastically influence the response. The melt flow properties of these blends are mostly influenced by the molecular weight of the polymers. Increasing the fraction of HMW polymer leads to higher viscosities and greater shear thinning. Depending on the end-use application and process, the property-processability relationship can be tailored for resins with bimodal structural distributions.

9.0 Bibliography

Avela, A.; Karling, R.; Takakarhu, J.*; Borstar™ - The Enhanced Bimodal Polyethylene Technology*, Dechema Monographs, 134, 3-23 (1998).

Bensason, S.; Minick, J.; Moet, A.; Chum, S.; Hiltner, A.; Baer, E.; *Classification of Homogeneous Ethylene-Octene Copolymers Based on Comonomer Content*, J. Polym. Sci.: Part B: Polym. Phys., 34, 1301-1315 (1996).

Bensason, S.; Stepanov, E.V.; Chum,S.; Hiltner, A.; Baer, E.; *Deformation of Elastomeric Ethylene-Octene Copolymers*, Macromolecules,30, 2436-2444 (1997).

Bergemann, C.; Cropp, R.; Luft, G.; *Copolymerization of Ethylene and Linear 1-Olefins with A Metallocene Catalyst System Under High Pressure. Part II. Comparison of Propene, 1-Butene, 1-Hexene and 1-Decene*, J. Mol. Cat., A: Chemical, 105, 87-91 (1996).

Berthold, J.; Bohm, L.L.; Enderle, H.F.; Gobel, P.; Luker, H.; Lecht, R.; Schulte, U.; *Advanced polymerization process for tailor made pipe resins*, Plastics, Rubber and Composites Processing and Applications, 25, 368-372 (1996).

Box, G.E.P.; Hunter, W.G.; Hunter, J.S.; *Statistics for Experimenters – An Introduction to Design, Data Analysis and Model Building*; John Wiley & Sons., Toronto, 1978 pp. 306-535.

Blom, R.; Dahl, I.M.; *On the Sensitivity of Metallocene Catalysts Toward Molecular Hydrogen During Ethylene Polymerization*, Macromol. Chem. Phys., 200, 442-449 (1999).

Bohm, L.L.; Berthold, J.; Enderle, H.-F.; Fleissner, M.; *Polyethylene: Polymer with Future*, Metalorganic Catalysts for Synthesis and Polymerization : Recent Results by Ziegler-Natta and Metallocene Investigations, Springer, New York, 1999, pp. 3-13.

Brintzinger, H.;Fischer, D.;Mulhaupt, R.;Rieger, B.;Waymouth, R.M.; *Stereospecific Olefin Polymerization with Chiral Metallocene Catalysts*, Angew. Chem. Int. Ed. Engl., 34, 1143-1170 (1995).

Brooks, N.W.J., Duckett, R.A., Ward, I.M., *Effects of Crystallinity and Stress State on the Yield Strain of Polyethylene*, Polymer,40, 7367-7372 (1999).

Browstow, W.; Corneliussen, R.D.; Failure of Plastics, Hanser Publishers, Toronto, 1986, pp. 304-329.

Carella, J.M.; *Comments on the Paper "Comparison of the Rheological Properties of Metallocene-Catalyzed and Conventional High Density Polyethylenes*",Macromolecules, 29, 8280-8281, (1996).

Channel, A.D.; Clutton, E.Q.; *The Effects of Short Chain Branching and Molecular Weight on the Impact Fracture Toughness of Polyethylene*, Polymer, 33, 4108-4112 (1992).

Chien, J.C.W.; He, D.*; Olefin Copolymerization with Metallocene Catalyst. I. Comparison of Catalysts*, J. Polym. Sci., Part A: Polym. Chem., 29, 1585-1593 (1991).

Chien, J.C.W.; Nozaki, T.; *Ethylene-Hexene Copolymerization by Heterogeneous and Homogeneous Ziegler-Natta Catalysts and the Comonomer Effect*, J. Polym. Sci., Part A: Polym. Chem., 31, 227(1993).

Chien, J.C.W.; Xu, B.; *Olefin Copolymerization and Olefin/Diene Terpolymerization with a Zirconocenium Catalyst System*, Makromol. Chem. Rapid Commun.,14, 109-115 (1993).

Cho, K.; Lee, B.H.; Hwang, K.M.; Lee, H.; Choe, S.; *Rheological and Mechanical Properties in Polyethylene Blends*, Polym. Eng. Sci., 38, 12, 1969-1975 (1998).

Chu, K.J.; Soares, J.B.P.; Penlidis, A.; *Polymerization Mechanism for In Situ Supported Metallocene Catalysts*, J. Polym. Sci. Part A: Polym. Chem., 38, 462-468 (2000).

Chu, K.J.;Li Pi Shan, C.;Soares, J.B.P.; Penlidis, A.; *Copolymerization of Ethylene and 1-Hexene with In-situ Supported Et[Ind]2ZrCl2*, Macromol. Chem. Phys., 200, 2372-2376 (1999).

Chu, K.J.; Soares, J.B.P.; Penlidis, A.; *Effect of Hydrogen on the Ethylene Polymerization Using In-Situ Supported Metallocene Catalysts*, Macromol. Chem. Phys., 201, 552-557 (2000).

Chu, K.J.; Soares, J.B.P.; Penlidis, A.; *Effect of Experimental Conditions on Ethylene Polymerization with In-Situ Supported Metallocene Catalyst*, J. Polym. Scil, Part A: Polym. Chem, 38, 1803-1810 (2000).

Chum, P.S. ; Kao, C.I. ; Knight, G.W. ; *Structure/Proeprty Relationships of Polyolefins Made by Constrained Geometry Catalyst Technology*, Plastics Eng., June, 21-23 (1995).

D'Agnillo, K.; Soares, J.B.P.; Penlidis, A.; *Effect of Operating Conditions on the Molecular Weight Distribution of Polyethylene Synthesized by Soluble Metallocene/Methylaluminoxane Catalysts*, Macromol. Chem. Phys., 955-962 (1998).

D'Agnillo, L.;Soares, J.B.P.; Penlidis, A.;*A Hiearchical Data Analysis of a Replicate Experiment in Polyethylene Synthesis with High Temperature Gel Permeation Chromatography*, Polym. Rxn. Eng., 7, 259-281 (1999).

Dealy, M.; Wissbrun, K.F.; Melt Rheology and Its Role in Plastics Processing: Theory and Applications, Van Nostrand Reinhold, New York, 1990 Chapt. 4, 10.

Dos Santos, J.H.Z.; da Rosa, M.B. ; Krug, C. ; Stedile, F.C. ; Haag, M.C. ; Dupont, J. ; Forte, M.D.C.; *Effects of Ethylene Polymerization Conditions on the Activity of SiO_2-Supported Zirconocane and on Polymer Properties*, J. Polym. Sci., A: Polym. Chem. 37, 1987-1996 (1999).

Doyle, M.J., *On the Effect of Crystallinity on the Elastic Properties of Semicrystalline Polyethylene*, Polym. Eng. Sci., 40, 330-335 (2000).

Elvers, B.; Hawkins, S.; Schulz, G.; Ullman's Encyclopedia of Industrial Chemistry 5th Ed., VCH Publishers, New York, A21, 1992, pp 486-496.

Fink, G.; Steinmetz, B.; Zechlin, Joachim, J.;Przybyla, C.; Tesche, B.; *Propene Polymerization with Silica-Supported Metallocene/MAO Catalysts*, Chem. Rev., 1000, 1377-1390 (2000).

Forlini,F.;Fan,Z.Q.;Tritto,I.;Locatelli,P.;Sacchi, M.C.; *Metallocene-Catalyzed Propene/1-Hexene Copolymerization: Influence of Amount and Bulkiness of Cocatalyst and of Solvent Polarity*, Macromol. Chem. Phys., 198, 2397-2408 (1997).

Foster, G.N.; Wasserman, S.H.; *Metallocene and Gas Phase Polymerization: Molecular Engineering Pathway For Advantaged Polyethylene Products*, Worldwide Metallocene Conf., MetCon, Houston, TX (1997).

Galli, P.; *Forty Years of Industrial Developments in the Field of Isotactic Polyolefins*, Macromol. Symp., 89, 13-26 (1995).

Galli, P.; *The Reactor Granule Techonology: The Ultimate Expansion of Polypropylene Properties?*, J.M.S. Pure. Appl. Chem., A36, 11561-1586 (1999).

Garbassi, F., Gila, L.,Proto, A., *Metallocenes: New Catalysts for New Polyolefins*, Polym. News, 19: 367-371 (1994).

Goyal, S.K.; *Influence of Polymer Structure on the Melt Strength Behavior of Polyethylene Resins*, SPE Antec '94, 1232-1238 (1994).

Grahm, J.T. , Alamo, R.G., Mandelkern, L., *The Effect of Molecular Weight and Crystallite Structure On Yielding in Ethylene Copolymers*, J. Polym. Sci. Part B: Polym. Phys.,35, 213-223 (1997).

Hamielec, A.E.; Soares, J.B.P.; *Polymerization Reaction Engineering – Metallocene Catalysts*, Prog. Polym. Sci., 21, 651-706 (1996).

Hamielec, A.E.; Soares, J.B.P.; *Polymerization Reaction Engineering – Metallocene Catalysts*, Prog. Polym. Sci., 21, 651-706 (1996).

Han, T.K.; Choi, H.K.; Jeung, D.W.; Ko, Y.S.; Woo, S.I.; *Control of Molecular Weight and Molecular Weight Distribution in Ethylene Polymerization with Metallocene Catalysts*, Macromol. Chem. Phys, 196, 2637-2647 (1995).

Han-Adebekunn, G.C.; Hamba, M.; Ray, W.H.; *Kinetic Study of Gas Phase Olefin Polymerization with a $TiCl_4/MgCl_2$ Catalyst I. Effect of Polymerization Conditions*, J. Polym. Sci. A: Polym. Chem., 35, 2063-2074 (1997).

Harrison, D.;Coulter,I.M.;Wang, S.;Nistala,S.;Kuntz,B.A.;Pigeon,M.;Tian, J.;Collins, S.; *Olefin Polymerization Using Supported Metallocene Catalysts: Development of High Activity Catalysts for Use In Slurry and Gas Phase Ethylene Polymerizations, J. Mol. Catal.*,128, 65-77 (1998).

Heiland, K.; Kaminsky, W.; *Comparison of Zirconocene and Hafnocene Catalysts for the Polymerization of Ethylene and 1-butene*, Markomol. Chem., 193, 601-610 (1992).

Herfert, N.; Montag, P.; Fink, G.; *Ethylene,α-Olefin and Norbornene Copolymerization with Stereorigid Catalyst Systems iPr[FluCp]ZrCl$_2$/MAO and Me$_2$Si[Ind]$_2$ZrCl$_2$/MAO*, Makromol. Chem. 194, 3167 (1993).

Hltaky, G.G.; *Heterogeneous Single-Site Catlaysts for Olefin Polymerization*, Chem. Rev., 100, 134701376 (2000).

Hosoda, S.,Uemura, *A. Effect of Structural Distribution on the Mechanical Properties of Linear Low-Density Polyethylenes*, Polym. Journal, 24, 939-949 (1992).

Huang, J.; Rempel, G.L.; *Ziegler-Natta Catalysts for Olefin Polymerization: Mechanistic Insights from Metallocene Systems*, Prog. Polym. Sci., 20, 259-526 (1995).

Jordens, K., Wilkes, G.L., Janzen, J., Rohlfing, D.C., Welch, M.B., *The Influence of Molecular Weight and Thermal History on the Thermal, Rheological, and Mechanical Properties of Metallocene-Catalyzed Linear Polyethylenes*, Polymer, 41, 7175-7192 (2000).

Jungling, S.; Koltzenburg, S.; Mulhaupt, R.; *Propene Homo- and Copolymerization Using Homogeneous and Supported Metallocene Catalysts Based on Me$_2$Si(2-Me-Benz[e]Ind)$_2$ZrCl$_2$*, J. Polym. Sci., A: Polym. Chem.; 35, 1-8 (1997).

Kale, L., Plumley, T., Patel, R., Redwine, O., Jain, P. J, *Structure-Property.Relationships of Ethylene/1-Octene And Ethylene/1-Butene Copolymers Made Using Insite* Technology*, Plast. Film and Sheetingm 12: 27-40 (1995).

Kazatchkov, I.B. ; Bohnet, N. ; Goyal, S.K.; Hatzikiriakos, S.G.; *Influence of Molecular Structure on the Rheological and Processing Behaviour of Polyethylene Resins*, Polym. Eng. Sci., 39, 804-815 (1999).

Kim, J.D.; Soares, J.B.P., Rempel, G.L., *Use of hydrogen for the tailoring of the molecular weight distribution of polyethylene in bimetallic supported metallocene catalyst system*, Macromol. Rapid Commun.,19,197-199 (1998).

Kim, Y.S.;Chung, C.I.; Lai, S.Y.; Hyun, K.S.; *Melt Rheological and Thermodynamic Properties of Polyethylene Homopolymers and Poly(ethylene/α-Olefin) Copolymers with Respect to Molecular Composition and Structure*, J. Appl. Polym. Sci., 59, 125-137 (1996).

Kissin, Y.V.; Mink, R.I.; Nowlin, T.E.; *Ethylene Polymerization Reactions with Ziegler-Natta Catalysts. I. Ethylene Polymerization Kinetics and Kinetic Mechanism*, J. Polym. Sci., A: Polym. Chem., 37, 4255-4272 (1999).

Kwag, H.; Rana, D.; Cho, W.; Rhee, J.; Woo, T.; Lee, B.H.; Choe, S.; *Binary Blends of Metallocene Polyethylene with Conventional Polyolefins: Rheological and Morphological Properties*, Polym. Eng. Sci., 40, 1672-1681 (2000)

Li Pi Shan, C.; Chu, K.J.; Soares, J.B.P.; Penlidis, A.; *Using Alkylaluminum Activators to Tailor the Short Chain Branching Distribution of Ethylene/1-Hexene Copolymers Using In-Situ Supported Metallocene Catalysts*, Macromol. Chem. Phys., 201, 2195-2202 (2000).

Li Pi Shan, C.;Soares, J.B.P.; Penlidis, A.; *Mechanical Properties of Ethylene/α-Olefin Copolymers with Tailored Short Chain Branching Distributions*, Polymer, 43, 767-773 (2002).

Li Pi Shan, C.; Soares, J.B.P.; Penlidis, A.; *Effect of Reaction Parameters on the Microstructure of Poly(Ethylene-co-1-octene) Copolymers Made with In-Situ Supported Metallocene Catalysts*, J. Polym. Sci. Part A: Polym. Chem., submitted (2002).

Li Pi Shan, C.; Soares, J.B.P.; Penlidis, A.; *Mechanical and Rheological Properties of HDPE/LLDPE Reactor Blends with Bimodal Structural Distributions*, Polym. Eng. Sci., submitted (2002).

Liu, J.;Stoveng, J.A.;Rytter, E.; *Possible Effects of Polyethylene Chain Structure of Trimethylaluminum Coordination to Zirconocene Catalysts*,J. Polym. Sci; Part A: Polym. Chem., 39, 3566-3577 (2001).

Lustiger, A.; Markham, R.L.; *Importance of Tie Molecules in Preventing Polyethylene Fracture Under Long-Term Loading Conditions*, Polymer, 24, 1647-1654 (1983).

Manders, P.W.; *Polyethylene: New Branches of the Polymer Family Extend into Specialized Applications*, Modern Plastics Encyclopedia ‘95, B3 (1995).

Maciejewski-Petoff, J.L.;Myers, C.L.;Waymouth, R.M.; *Influence of Trialkylaluminum Reagents on the Propylene Polymerization Behavior of Bridged and Unbridged 2-Arylindene Metallocene Polymerization Catalysts*, Macromolecules, 32, 7984-7989 (1999).

Martin, J.R.; Johnson, J.F.; Cooper, A.R.; *Mechanical Properties of Polymers: The Influence of Molecular Weight and Molecular Weight Distribution*, J. Macromol. Sci.-Revs., Macromol. Chem., C8(1), 57-199 (1972).

Matsushita, F.; Kishimoto, Y.; Pierce, J.K.; *New High Density Polyethylenes from Slurry Insite* Technology*, Metallocenes Europe ’98, pp. 201-220 (1998).
Mavridis, H.; Shroff, R.; *Appraisal of Molecular Weight Distribution-to-Rheology Convesion Scheme for Linear Polyethylenes*, J. Appl. Polym. Sci., 49, 299-318 (1993).

Menard, K.P. Dynamic Mechanical Analysis – A Practical Introduction, New York, CRC Press, 1999, pp. 151-162.
Michiels, W. ;Munoz-Escalona, A. ; *Mixed Cocatalyst Systems in Metallocene Ethylene Polymerization*, Macromol. Symp., 97, 171-183 (1995).

Miri, N.; Hetzer, D.; Miles, A.; Pecak, M.; Riscili, B.; *Ethylene/α-Olefin Copolymerization With Dimethylsilyl-bis(2-methyl-4-phenyl-indenyl) Zirconium Dichloride and Methylaluminoxane: Influences on Polymerization Activity and Molecular Weight*, Metalorganic catalysts for synthesis and polymerization : recent results by Ziegler-Natta and metallocene investigations; Springer, New York, 1999, pp. 509-515.

Monrabal, B.; *Crystallization Analysis Fractionation: A New Technique for the Analysis of Branching Distribution in Polyolefins, J. Appl. Polym. Sci*., 52, 491-505 (1994).

Monrabal, B.; *CRYSTAF: Crystallization Analysis Fractionation. A New Approach to the Composition Anlaysis of Semicrystalline Polymers*, Macromol. Symp.,110, 81-86 (1996).

Naga, N.;Mizunuma, K.; *Chain transfer reaction by trialkylaluminum (AlR_3) in the stereospecific polymerization of propylene with metallocene - $AlR_3/Ph_3CB(C_6F_5)_4$*, Polymer, 39, 5059-5067 (1998).

Nitta, K.H., Tanaka, A., *Dynamic Mechanical Properties of Metallocene Catalyzed Linera Polyethylenes*, Polymer, 42,1219-1226 (2001).

Nowlin, T.E.; Kissin, Y.V.; Wagner, K.P.; *High Activity Ziegler-Natta Catalysts for the Preparation of Ethylene Copolymers*, J. Polym. Sci., Part A, Polym. Chem., 26, 755-764 (1988).

Nunes, R.W.; Martin, J.R.; Johnson, J.F.; *Influence of Molecular Weight and Molecular Weight Distribution on Mechanical Proeprties of Polymers*, Polym. Eng. Sci., 22, 205-228 (1982).

Przybyla, C.; Tesche, B.; Fink, G. ; *Ethylene/Hexene Copolymerization with the Heterogeneous Catalyst System $SiO_2/MAO/rac\text{-}Me_2Si[2\text{-}Me\text{-}4\text{-}Ph\text{-}Ind]_2ZrCl_2$: The Filter Effect*, Macromol. Rapid. Commun., 20, 328-332 (1999).

Quijada, R.; Rojas, R.; Mauler, R.S. ; Galland, G.B. ; Scipioni, R.B.; *Study of the Effect of the Monomer Pressure on the Copolymerization of Ethylene with 1-Hexene*, J. Appl. Polym. Sci.; 64, 2567-2574 (1997).

Raju, V.R.; Smith, G.C.; Marin, G.; Knox, J.R.; Graessley, W.W.; *Properties of Amorphous and Crystallisable Hydrocarbons. I. Melt Rheology of Fractions of Linear Polyethylene*, J. Polym. Sci, Polym. Phys. Ed., 17, 1183-1195 (1979).

Rana, D., Lee, C.H., Cho, K., Lee, B.H., Choe, S., *Thermal and Mechanical Properties for Binary Blends of Metallocene Polyethylene with Conventional Polyolefins*, J. Appl. Polym. Sci., 69, 2441-2450 (1998).

Reddy, S.S.; Sivaram, S.; *Homogeneous Metallocene – Methylaluminoxane Catalyst for Ethylene Polymerization*, Prog. Polym. Sci., 20, 309-367 (1995).

Reid, R.C.;Prausnitz, J.M.; Sherwood, T.K.; The Properties of Liquids and Gases, 3rd Ed., McGaw-Hill Inc., New York, 1977, Appendix A.

Resconi, L.; Bossi, S.;Abis, L.; *Study of the Role of Methylalumoxane in Homogeneous Olefin Polymerization*, Macromolecules, 23, 4489-4491 (1990).

Ribeiro, M.R.; Deffieux, A.; Portela, M.F.; *Supported Metallocene Complexes for Ethylene and Propylene Polymerizations: Preparation and Activity*, Ind. Eng. Chem. Res., 36, 1224-1237 (1997).

Rieger, B.; Janiak, C.; *Concentration Effects of Methylaluminoxane, Zirconocane Dichloride and Trimethylaluminum in Ethylene Polymerization*, Angew. Makromol. Chem., 215, 35-46 (1994).

Rudin, A.; The Elements of Polymer Science and Engineering, Academic Press Inc., pg 41, 1982, pp 339-343.

Sacchi, M.C.; Forlini, F; Tritto, I.; Locatelli, P.; *In-depth Investigation of Unsaturated Chain-End Groups: A Tool for Understanding Hydrogen Activation Mechanism in Zirconocane Catalysed Propene Polymerization*, Metalorganic catalysts for synthesis and polymerization : recent results by Ziegler-Natta and metallocene investigations; Springer, New York, 1999, pp. 294-303.

Scheirs, J.; Bohm, L.L.; Boot, J.C.; Leevers, P.S.; *PE100 Resins for Pipe Applications*, Trends in Polymer Science, 4, 408-415 (1996).

Simanke, A.G., Galland, G.B., Freitas, L., da Jornada, J.A.H., Quijada, R., Mauler, R.S., *Influence of Comonomer Content on the Thermal and Dynamic Mechanical Properties of Metallocene Ethylene/1-Octene Copolymers*, Polymer, 40, 5489-5495 (1999).

Simanke, A.G. , Galland, G.B. , Neto, R.B. , Quijada, R. , Mauler, R.S., *Influence of the Type of Comonomer Contents on the Mechanical Behaviour of Ethylene/α-Olefin Copolymers*, J. Appl. Polym. Sci., 74, 1194-1200 (1999).

Soares, J.B.P.; Hamielec, A.E.; *Kinetics of Propylene Polymerization With a Non-Supported Heterogeneous Ziegler-Natta Catalyst – Effect of Hydrogen on Rate of polymerization, stereoregularity, and Molecular Weight Distribution*, Polymer, 37, 4607-4614 (1996).

Soares, J.B.P., Kim, J.D.; Rempel; *Analysis and Control of the Molecular Weight and Chemical Composition Distributions of Polyolefins Made with Metallocene and Ziegler-Natta Catalysts*, Ind. Eng. Chem. Res., 36, 1144-1150 (1997).

Soares, J.B.P.; Monrabal, B.; Nieto, J.; Blanco, J.;*Crystallization Analysis Fractionation (CRYSTAF) of Poly(Ethylene-co-1-Octene) Made with Single-Site-Type Catalysts: A Mathematical Model for the Dependence of Composition Distribution on Molecular Weight*, Macromol. Chem. Phys., 199, 1917-1927 (1998).

Soares, J.B.P.; Kim, J.D.; *Copolymerization of Ethylene and α-Olefins with Combined Metallocene Catalysts. I. A Formal Criterion for Molecular Weight Bimodality*, J. Polym. Sci., Part A: Polym. Chem., 38, 1408-1416 (2000).

Smith, J.M.;Van Ness, H.C.; Introduction to Chemical Engineering Thermodynamics, 3rd Ed.; McGraw-Hill Inc., Toronto, 1975, Chapt. 8, pp. 314-331.

Soga, K.;Kaminaka, M.; *Polymerizatin of Propene with the Heterogeneous Catalyst System Et[IndH$_4$]ZrCl$_2$/MAO/SiO$_2$ Combined with Trialkylaluminum*, Macromol. Chem., Rapid Commun.,13, 221-224 (1992).

Soga, K.;Kaminaka, M.; *Copolymerization of Olefins with SiO$_2$-,AL$_2$O$_3$-, and MgCl$_2$-supported Metallocene Catalysts Activated by Trialkylaluminums*, Macromol. Chem. Phys. 195, 1369-1379 (1994).

Sperling, L.H.; Introduction to Physical Polymer Science, John Wiley & Sons., Inc., pp 108-115. (1992)

Styring, M.G.; Hamielec, A.E.;*Determination of Molecular Weight*, Edited: A.R. Cooper, John Wiley & Sons. Inc., 1989, Chapt. 10.

Schwank, D.; *Single-Site Metallocene Catlaysts Yield Tailor-Made Polyolefin Resins*, Modern Plastics, August, 49-50 (1993).

Sinclair, K.B.; *The New Generation Polyethylene Technologies: A Comparison*, Polyolefins XI, Society of Plastics Engineers, Houston, Texas, Feb. 21-24, 1999.

Suhm, J.; Schneider, M.J.; Mulhaupt, R.; *Temperature Dependence of Copolymerization Parameters in Ethene/1-Octene Copolymerization Using Homogeneous rac-Me$_2$Si(2-MeBenz[e]Ind)$_2$ZrCl$_2$/MAO Catalyst*, J. Polym. Sci., Part A: Polym. Chem., 35, 735-740 (1997).

Thorshaug, K.;Strovneng, J.A.;Rylter, E.;Ystenes; *Termination, Isomerization, and Propagation Reactions During Ethene Polymerization Catalyzed by Cp$_2$Zr-R$^+$ and Cp$^*_2$Zr-R$^+$. An Experimental and Theoretical Investigation*, Macromolecules, 31, 7149-7165 (1998).

Utracki, L.A.; Polymer Alloys and Blends, Thermodynamics and Rheology, Hanser Publishers, New York, 1990, pp. 1-27

Vega, J.F.; Santamaria, A.; Munoz-Escalona, A. ;Lafuente, P. ; *Comparison of the Rheological Properties of Metallocene-Catalyzed and Conventional High Density Polyethylenes*, Macromol., 31, 3639-3647 (1998).

Vega, J.F. ; Fernandez, M. ; Santamaria, A. ; Munoz-Escalona, A. ; Lafuente, P. ; *Rheological Criteria to Characterize Metallocene Catalyzed Polyethylenes*, Macromol. Chem. Phys., 200, 2257-2268 (1999).

Vela Estrada, J.M.; Hamielec, A.E.; *Modelling of Ethylene Polymerization With Cp$_2$ZrCl$_2$/MAO Catalyst*, Polymer, 35, 808-818 (1994).

Wang, S.; Kuntz, B.A.; Nistala, S.; Collins, S.; Harrison, D.; Coulter, I.; *High Activity, Supported Metallocene Catalysts for Ethylene Polymerization and Copolymerization,* Worldwide Metallocene Conference – MetCon '95, Houston, TX (1995).

Wood-Adams, P.M.;Dealy, J.M.;deGroot, A.W.; Redwine, O.D.; *Effect of Molecular Structure on the Linear Viscoelastic Behaviour of Polyethylene,* Macromolecules, 33, 7489-7499 (2000).

Xanthos, M.; Tan, V.; Ponnusamy, A.; *Measurement of Melt Viscoelastic Properties of Polyethylenes and Their Blends – A Comparison of Experimental Techniques,* Polym. Eng. Sci, 37, 1102-1112 (1997).

Xie, T.;McAuley, K.B.;Hsu, J.C.C.;Bacon,D.W.;*Gas Phase Ethylene Polymerization: Production Processes, Polymer Properties, and Reactor Modeling,* Ind. Eng. Chem. Res.; 33, 449-479 (1994).

Xu, X., Xu, J, Feng, K., Chen, W.; *Effect of Short Chain-Branching on Crystallinity and Modulus of Metallocene-Based Ethylene-Butene Copolymers,* J. Appl. Polym. Sci., 77, 1709-1715 (2000).

Ystenes, M.; *The Trigger Mechanism for Polymerization of α-Olefins with Ziegler-Natta Catalysis: A New Model Based on Interaction of Two Monomers at the Transition State and Monomer Activation of the Catalytic Centers,* J. Catal., 129, 383-401 (1991).

Zucchini, U.; Cecchin, G.; *Control of Molecular-Weight Distribution in Polyolefins Synthesized with Ziegler-Natta Catalytic Systems,* Adv. Polym. Sci., 51,101-154 (1983).

Appendix

Appendix A1 - Estimation of Monomer/Comonomer Liquid Concentrations

Bubble point calculations were performed to estimate the concentrations of ethylene and 1-hexene or 1-octene in hexane solvent at various temperatures and pressures. A modified Raoult's law was used to iterate the compositions based on an input temperature, pressure and comonomer/ethylene ratio. The Chao-Seader correlation was used to determine the pure component fugacity coefficients; Redlich-Kwong correlation for the vapour component fugacity coefficients; Scatchard-Hildebrand regular solution theory for the liquid phase activity coefficients (Smith and Van Ness, 1975).

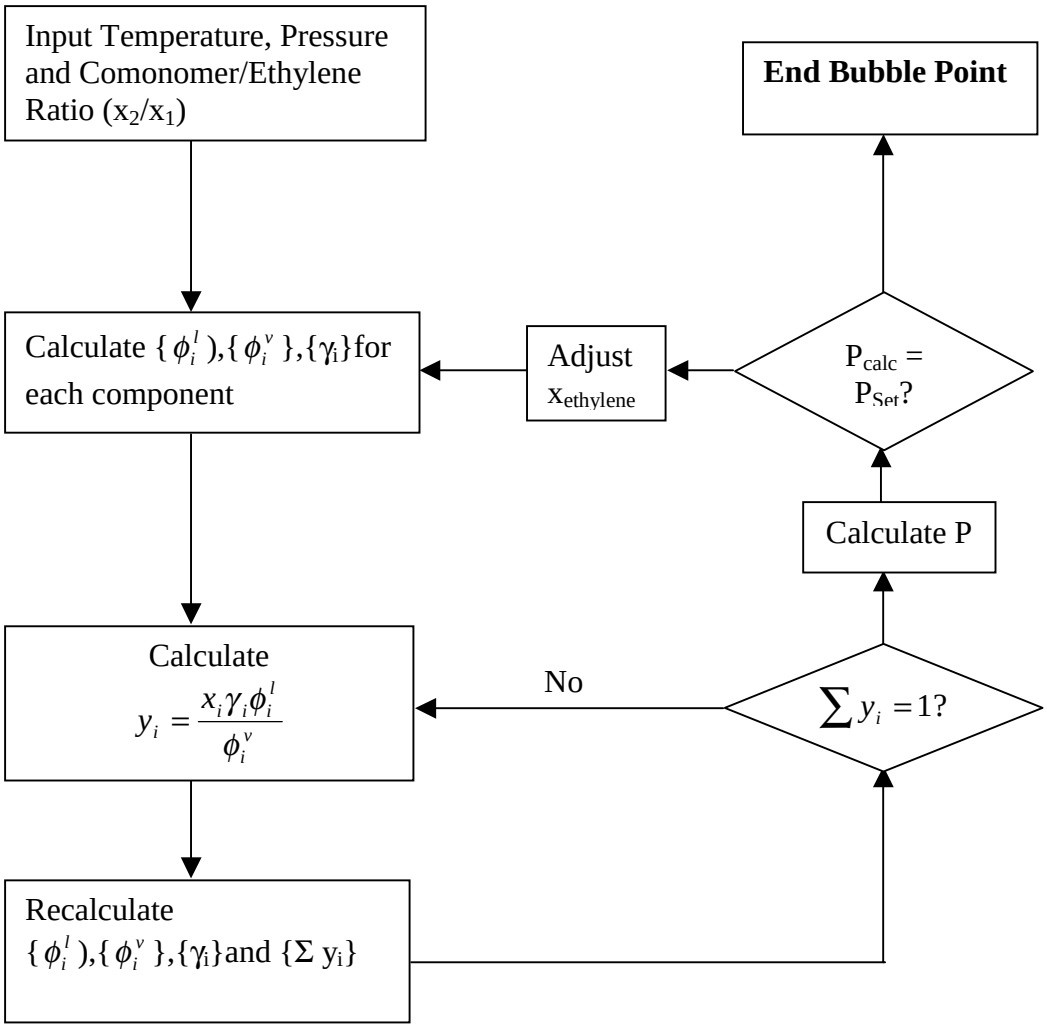

Figure A1.1 – Algorithm Used for Estimation of Monomer/Comonomer Liquid Concentrations

Appendix A2 - Fortran 77 Program: Vapour Liquid Equilibrium Ethylene α-olefin Composition Estimation

```
C*****************************************************************C
C                                                                 C
C    This   program   performs   a bubble  point   pressure       C
C    calculation for the ternary system 1-octene, ethylene  and   C
C    n-hexane using the Chao-Seader Correlation, the Redlich-Kwong C
C    Equation, and Scatchard-Hildebrand regular solution theory.  C
C                                                                 C
C*****************************************************************C
      DIMENSION X(3),Y(3),PHIL(3),PHIG(3),TC(3),PC(3),
     1VC(3),ZC(3),GAMMA(3),W(3),PL(2),S(2),XMOLV(3)

C     1-octene, ethylene, n-hexane
      DATA TC/566.6,282.4,507.4/
      DATA PC/25.9,49.7,29.3/
      DATA VC/464.,129.,370./
      DATA ZC/.260,.276,.260/
      DATA W/0.386,.0949,.296/
      WRITE(*,2)
2     FORMAT(' THIS PROGRAM PERFORMS A BUBBLE POINT PRESSURE'/
     &' CALCULATION FOR VARIOUS LIQUID PHASE COMPOSITION.'/
     &' THE CHAO SEADER CORRELATION IS USED FOR THE PURE COMPONENT'/
     &' THE REDLICH-KWONG EQUATION IS USED TO DETERMINE THE VAPOR')
      WRITE(*,6)
6     FORMAT(' FUGACITY COEFFICIENTS, WHICH DEPEND ON THE VAPOR'/
     &' COMPOSITION.  SCATCHARD-HILDEBRAND REGULAR SOLUTION THEORY'/
     &' IS USED TO DETERMINE THE LIQUID PHASE ACTIVITY COEFFICIENTS')
      WRITE(*,3)
3     FORMAT(1X/' * INPUT DATA FORM *'/
     &' *  A),  B),  C)  *'/
     &' ******************'/
     &' WHERE, <LIQUID COMPOSITION INPUT>'/
     &' a) MOL RATIO OF 1-OCTENE TO ETHYLENE'/
     &' b) THE TEMPERATURE (C)'/
     &' c) THE TOTAL PRESSURE(ATM)'/
     &' ******************'/
     &'   WRITE RATIO(C8/C2),T,P')
      READ(*,*) RATIO,T,P1
      WRITE(*,8)T
8     FORMAT(' THE CENTIGRADE TEMPERATURE IS',F10.2,'DEG C'/2X)
      WRITE(6,1)
1     FORMAT(4X,'VAPOR PHASE COMPOSITION',18X,
     1'LIQUID PHASE COMPOSITION'/7X,'(MOLE FRACTION)'9X,
     1'PRESSURE',9X,'(MOLE FRACTION)',3X,'g-mole/l'/2X,'1-HEXENE ',2X,
     1'ETHYLENE',2X,'Y(2)/Y(1)',3X,'ATM',3X,
     1'1-HEXENE ',2X,'ETHYLENE',3X,'C6MOL',3X,'C2MOL'/2X)
      T=273.16+T
      X(2)=0.
      DX=0.01
2500  X(2)=DX+X(2)
      X(1)=RATIO*X(2)
      X(3)=1.-X(1)-X(2)
```

```
      ICOUNT=1
      PL(2)=.1
      S(2)=2.
      IT=1
      CALL ACTIVITY(X,GAMMA,T)
C----estimate of P(atm)
C Antoine Equation (1-octene, ethylene, n-hexane)
      P= EXP(15.9630-3116.52/(t-60.39))*x(1)/760.
     &  +EXP(15.5368-1347.01/(T-18.15))*X(2)/760.
     &  +exp(15.8366-2697.55/(T-48.78))*x(3)/760.
C----Set vapor fugacity coefficients to unity for the first iteration
      DO 10 I=1,3
10    PHIG(I)=1.
C----Calculate liquid fugacity coefficients
20    DO 30 I=1,3
      TR=T/TC(I)
      PR=P/PC(I)
30    CALL LFUG(TR,PR,W(I),PHIL(I))
C----Calculate and SUM and Y(I)
      SUM=0.
      DO 40 I=1,3
      Y(I)=X(I)*PHIL(I)*GAMMA(I)/PHIG(I)
40    SUM=SUM+Y(I)
      IF(IT.NE.1) GO TO 50
C----first iteration
      IT=2
      GO TO 60
50    IF(SQRT((SUM-SUM1)**2) .LT. .0001) GO TO 70
60    DO 80 I=1,3
80    Y(I)=Y(I)/SUM
      SUM1=SUM
      CALL GFUG(Y,PHIG,TC,PC,VC,ZC,P,T)
      GO TO 20
70    SUM1=SUM
      IF(SUM.GT. .9995 .AND. SUM .LT. 1.0005) GO TO 90
      IT=1
      ICOUNT=ICOUNT+1
      IHALF=ICOUNT/2
      INDEX=ICOUNT-IHALF*2+1
      PL(INDEX)=P
      S(INDEX)=SUM
      P=(PL(2)-PL(1))/(S(2)-S(1))*(1.-S(1))+PL(1)
      GO TO 20
90    CALL LIQDEN(XMOLV)
c-----if(FLAG .EQ. 1.0) go to 1500
      CTOT=1./(X(1)*XMOLV(1)+X(2)*XMOLV(2)+X(3)*XMOLV(3))
      C2MOL=CTOT*X(2)*1000
      C3MOL=CTOT*X(1)*1000
      WRITE(*,95) Y(1),Y(2),Y(2)/Y(1),P,X(1),X(2),C3MOL,C2MOL
      IF(SQRT((P-P1)**2) .LT. 0.01) GO TO 3500
      IF (P .Lt. P1) GO TO 1500
      X(2)=X(2)-DX
      DX=DX*0.1
      GO TO 1500
95    FORMAT(1X,8F9.5)
1500  GO TO 2500
3500  STOP
      END
C-------------------------------------------------------------
C     Estimation of Liquid Fugacity using Chao-Seader
C-------------------------------------------------------------
      SUBROUTINE LFUG(TR,PR,W,PHIL)
      DIMENSION A(10),A1(10),A0(10)
      DATA A0/-3.01761,-4.985,2.02299,0.,.08427,
```

```
     &.26667,-.31138,-.02655,.02883,5.75748/
      DATA A1/1.02972,-.054009,.0005288,0.,
     &.008585,0.,0.,0.,1.96718/
C----SIMPLE FLUID; HEXANE
      DO 20 I=1,10
20    A(I)=A0(I)
      V0=A(10)+A(1)/TR+A(2)*TR+A(3)*TR**2+A(4)*TR**3+
     &(A(5)+A(6)*TR+A(7)*TR**2)*PR+(A(8)+A(9)*TR)*PR**2
     &-LOG10(PR)
      V1=-4.23893+8.65808*TR-1.2206/TR-3.15224*TR**3
     &-.025*(PR-.6)
      PHIL=EXP(2.302585*(V0+W*V1))
      RETURN
      END
C-------------------------------------------------------------
C     Estimation of Activity Coefficients using Scatchard-Hildebrand
C-------------------------------------------------------------
C

      SUBROUTINE ACTIVITY(X,GAMMA,T)
      DIMENSION V(3),DELTA(3),X(3),GAMMA(3)
      DATA V/156.945,61.,130.77/
      DATA DELTA/7.62,6.08,7.28/
      R=1.987
      SUM=0.
      SUM1=0.
      DO 10 I=1,3
      SUM=SUM+X(I)*V(I)*DELTA(I)
10    SUM1=SUM1+V(I)*X(I)
      DELAV=SUM/SUM1
      DO 20 I=1,3
20    GAMMA(I)=EXP(V(I)/R/T*(DELTA(I)-DELAV)**2)
      RETURN
      END
C-------------------------------------------------------------
C     Estimation of Vapour Fugacity using Redlich-Kwong Correlation
C-------------------------------------------------------------
      SUBROUTINE GFUG(Y,PHIG,TC,PC,VC,ZC,P,T)
      DIMENSION Y(3),B(3),A(3,3),PHIG(3),TC(3),PC(3),VC(3),ZC(3)
      R=82.05
      BT=0.
      AT=0.
      DO 10 I=1,3
      B(I)=.0867*R*TC(I)/PC(I)
      BT=BT+B(I)*Y(I)
      DO 10 J=1,3
      TC1=SQRT(TC(I)*TC(J))
      ZC1=(ZC(I)+ZC(J))/2.
      VC1=((VC(I)**(1./3.)+VC(J)**(1./3.))/2.)**3
      PC1=ZC1*R*TC1/VC1
      A(I,J)=.4278*R**2*TC1**2.5/PC1
10    AT=AT+A(I,J)*Y(I)*Y(J)
      ABRT=AT/BT/R/T**1.5
      H0=BT*P/R/T
      E=.0001*H0
      H=H0
30    H1=H0/(1./(1.-H)-ABRT*H/(1.+H))
      IF(SQRT((H1-H)**2) .LT. E) GO TO 20
      H=H1
      GO TO 30
20    Z=BT*P/H/R/T
      DO 40 I=1,3
      SUM=0.
      DO 50 K=1,3
```

```
50    SUM=SUM+Y(K)*A(I,K)
40    PHIG(I)=EXP(B(I)/BT*(Z-1.)-LOG(Z-Z*H)+ABRT*(B(I)/BT-
     1 2.*SUM/AT)*LOG(1.+H))
      RETURN
      END
C-------------------------------------------------------------
C     Calculation of Liquid Density of Components
C-------------------------------------------------------------
      SUBROUTINE LIQDEN(XMOLV)
      DIMENSION XMW(3),DEN(3),XMOLV(3)
      DATA DEN/0.715,0.577,0.659/
      DATA XMW/112.216,28.054,86.178/
      DO 30 I=1,3
   30 XMOLV(I)=XMW(I)/DEN(I)
      RETURN
      END
```

Appendix A3 - Thermodynamic Property Data for Common Olefins and Solvents (Reid et al., 1977)

COMPONENT	MOLE WT	FREEZE POINT K (TFP)	BOILING POINT K (TB)	CRITICAL TEMP K (TC)	CRITICAL PRESSURE ATM (PC)	CRITICAL VOLUME $CM^3/G\text{-}MOL$ (VC)	CRITICAL COMPRESS (ZC)	ACENTRIC FACTOR (OMEGA)	LIQ DEN @TDEN G/CM^3 (LIQDEN)	REF T FOR LIQDEN K (TDEN)	ANTOINE VAPOR PRESSURE EQN LN(P)=A-B/(T+C) P (mmHg), T (K) A	B	C
Monomers													
ETHYLENE	28.054	104.0	169.4	282.4	49.7	129.0	0.276	0.085	0.577	163.0	15.5368	1347.01	-18.15
PROPYLENE	42.081	87.9	225.4	365.0	45.6	181.0	0.275	0.148	0.612	223.0	15.7027	1807.53	-26.15
Solvents													
N-HEXANE	86.178	177.8	341.9	507.4	29.3	370.0	0.260	0.296	0.659	293.0	15.8366	2697.55	-48.78
TOLUENE	92.141	178.0	383.8	591.7	40.6	316.0	0.264	0.257	0.867	293.0	16.0137	3096.52	-53.67
N-OCTANE	114.232	216.4	398.8	568.8	24.5	492.0	0.259	0.394	0.703	293.0	15.9426	3120.29	-63.63
α-Olefins													
1-HEXENE	84.162	133.3	336.6	504.0	31.3	350.0	0.260	0.285	0.673	293.0	15.8089	2654.81	-47.30
1-HEPTENE	98.189	154.3	366.8	537.2	28.0	440.0	0.280	0.358	0.697	293.0	15.8894	2895.51	-53.97
1-OCTENE	112.216	171.4	394.4	566.6	25.9	464.0	0.260	0.386	0.715	293.0	15.9630	3116.52	-60.39
1-NONENE	126.243	191.8	420.0	592.0	23.1	580.0	0.280	0.430	0.745	273.0	16.0118	3305.03	-67.61
1-DECENE	140.270	206.9	443.7	615.0	21.8	650.0	0.280	0.491	0.741	293.0	16.0129	3448.18	-76.09
1-DODECENE	168.324	238.0	486.5	657.0	18.3	0.0	0.000	0.558	0.758	293.0	16.0610	3729.87	-90.88
1-HEXADECENE	224.432	277.3	558.0	717.0	13.2	0.0	0.000	0.721	0.788	283.0	357.8500	-59.23	40.99
1-OCTADECENE	252.486	290.8	588.0	739.0	11.2	0.0	0.000	0.807	0.789	293.0	16.2221	4416.13	-127.30

Component	Solubility Parameter $(cal/cm^3)^{1/2}$	Molar Volume (g/cm^3)
N-HEXANE	7.28	130.77
TOLUENE	8.9	106.28
1-HEXENE	7.36	125.06
1-OCTENE	7.62	156.95

*Solubility parameters estimated using group contribution methods (Fedors), http://www.pirika.com/chem/TCPEE/TCPE.html